

NASA CR-152336-1

PRELIMINARY DESIGN STUDY  
OF  
ADVANCED COMPOSITE BLADE AND HUB  
AND  
NONMECHANICAL CONTROL SYSTEM  
FOR THE TILT-ROTOR AIRCRAFT  
VOLUME I - ENGINEERING STUDIES

H. R. ALEXANDER

K. E. SMITH

M. A. McVEIGH

P. G. DIXON

B. L. McMANUS

NOVEMBER 1979

PREPARED UNDER CONTRACT NO. NAS2-10160

FOR

NATIONAL AERONAUTICS AND SPACE ADMINISTRATION

AMES RESEARCH CENTER


BY

BOEING VERTOL COMPANY

P. O. BOX 16858

PHILADELPHIA, PENNSYLVANIA 19142

D210-11569-1



FOREWORD

The information presented in this document is the result of engineering design studies performed by Boeing Vertol Company for the National Aeronautics and Space Administration, Ames Research Center under Contract NAS2-10160.

Mr. D. P. Chappell was the Technical Monitor and Mr. H. R. Alexander was the Boeing Vertol Program Manager. The following personnel made significant contributions to the present study:

K. E. Smith	Blade Design
M. A. McVeigh	Aerodynamics
B. V. McManus	Flight Controls
P. G. Dixon	Hub Design
V. C. Capurso	Dynamics

ABSTRACT

Composite structures technology is applied in a preliminary design study of advanced technology blades and hubs for the XV-15 tilt-rotor research demonstrator aircraft. The study shows that significant improvements in XV-15 hover and cruise performance are available using blades designed for compatibility with the existing aircraft, i.e., blade installation would not require modification of the airframe, hub or upper controls.

Provision of a low-risk nonmechanical control system was also studied, and a development specification is given.

Program planning data for rotor and control system procurement and testing is given in Volume II of this report.

## TABLE OF CONTENTS

Sheet

FOREWORD

ABSTRACT

LIST OF TABLES

ii

LIST OF FIGURES

iii

1.0 INTRODUCTION

1

1.1 Blade Preliminary Design

1

1.2 Hub Preliminary Design

4

1.3 Nonmechanical Control System

5

2.0 TRADE-OFF ANALYSIS AND CONCEPT SELECTION

9

2.1 Performance

11

2.2 Cost

16

2.3 Inspectability, Repairability, and Maintainability

18

2.4 Strength

18

2.5 Development of a Consolidated Index of Comparison

20

2.6 Research Attributes of Selected Configuration

22

2.7 Hub Concept Selection

23

2.8 Selection of Advanced Nonmechanical Flight  
Control System Concept

33

3.0 TECHNICAL EVALUATION OF SELECTED DESIGN

39

3.1 Aerodynamic Performance

39

3.2 Strength

48

3.3 Dynamic and Aeroelastic Behavior

57

4.0 PRELIMINARY DESIGN SPECIFICATIONS

65

4.1 Blade

65

4.2 Hub

107

4.3 Inspection Maintenance and Repair Characteristics

113

4.4 Advanced Nonmechanical Flight Control System

127

5.0 REFERENCES

146

APPENDIX A - Aerodynamic Design Selection Procedure

APPENDIX B - XV-15 Fly-By-Wire Preliminary Development  
Specification



## LIST OF TABLES

<u>Table</u>		<u>Sheet</u>
1.1	Summary Blade Properties and Constants	3
2.1	Summary of Performance Characteristics	10
2.2(a)	Performance Improvement Ratios or Ranking	13
(b)	Normalized Ratios	13
(c)	Consolidated Performance Index	13
2.3	Manufacturing Costs - Comparison with 12-Blade Rectangular Planform Program	14
2.4	Preference Ratios on Basis of Cost	15
2.5	Preference Ratios on Basis of Repairability and Maintainability	15
2.6	Configuration Strength Desirability Indices	17
2.7	Weighting of Major Attributes	20
2.8	Calculation of Consolidated Merit Indices for Candidate Blades	21
3.1	Performance of X <sub>2</sub> Blade Relative to XV-15	40
3.2.1	XV-15 Advanced Composite Blade - Preliminary Design - Summary of Properties	47
4.3.1	H-46 Fiberglass Rotor Blade R&M Program Problem/Maintenance Summary	125

## LIST OF FIGURES

<u>Figure</u>		<u>Sheet</u>
1.1	X <sub>2</sub> Replacement Blade Planforms, Twist, Chord and Airfoil Distribution	2
1.2	Preliminary Design Layout of Recommended Hub Concept	6
2.1	XV-15 Candidate Replacement Blades	12
2.2	Hierarchy of Attributes and Preference Factors	19
2.3	Boeing Vertol/U.S. Army Bearingless Main Rotor	25
2.4	Bell 212 Rotor Hub	26
2.5	Aerospatiale Starflex Rotor Hub	28
2.6	Kaman Flexible Hub	28
2.7	Reversed Starflex Hub Concept	30
2.8	Recommended Concept for XV-15 Composite Replacement Hub	31
3.1	Rotor Cruise Efficiency as Function of $\mu$ and $C_p$	41
3.2	Thrust and Drag Variation with Speed X <sub>2</sub> Blade and 14" and 20" Chord Rectangular Blades	42
3.2.1	Stiffness of X <sub>2</sub> Preliminary Design Blade	44
3.2.2	Distribution of Mass and Pitching Inertia	45
3.2.3	X <sub>2</sub> Blade Flap and Chord Bending Moments - Helicopter Flight at 120 Knots	46
3.2.4	X <sub>2</sub> Blades - Spanwise Distribution of Strain 120 Knots - Helicopter Flight	49
3.2.5	Flap and Chord Bending Moments in Hover	50
3.2.6	Strain Distribution - 40 Knots Sideways Helicopter Flight	51
3.2.7	Sketch of Section Through Pin Retention Wraparound	53

## LIST OF FIGURES

<u>Figure</u>	<u>Sheet</u>
3.3.1 XV-15 Replacement Blade Frequencies	58
3.3.2 Variation of Damping with Airspeed in Critical Modes	59
3.3.3 Variation of Flutter Speed and Design Dive Speeds with Altitude	60
3.3.4 Variation of Critical Speed with RPM	61
3.3.5 Root Loci for XV-15 with Composite Replacement Blade	62
4.1.1 XV-15 Composite Blade Assembly/Geometry Drawing	67
4.1.2 XV-15 Blade-End View of Stacked Twisted Contours	69
4.1.3 XV-15 Blade-Root L/O (1st Iteration Concept)	71-81
4.1.4 XV-15 Blade-Tip L/O (1st Iteration Concept)	83-95
4.1.5 Lightning Protection and Other Design Features CH-46 Composite Blade	97
4.1.6 Photo of CH-46 Blade Cross Section Illustrating Fiberglass-Graphite Mixed Spar (Neg. #C31400)	98
4.1.7 Manufacturing Process with Major Tools	100
4.1.8 Automatic Tape Layup of Hairpin Wraps	102
4.1.9 Spar Assembly	103
4.2.1 XV-15 Advanced Rotor Hub-Conceptual Layout	105
4.3.1 Design Features of CH-46 Composite Blade	116
4.4.1 Fly-by-Wire Flight Control System	128
4.4.2 Dual Driver Actuator	130
4.4.3 Primary Flight Control System Functions and Interfaces	131
4.4.4. Redundancy Management of Primary Flight Control System	134
4.4.5 Dual Path Primary Flight Control Channel	136

## LIST OF FIGURES

<u>Figure</u>		<u>Sheet</u>
4.4.6	Dual Driver Servoloop and Failure Detection	137
4.4.7	Collective Actuator Driver Installation	141
4.4.8	Longitudinal Cyclic Driver Installation	142
4.4.9	Lateral Cyclic Actuator	143
4.4.10	Primary Flight Control Single Channel Interconnect	145
A-1	Geometric Properties of Existing Bell XV-15 Rotor Blade	A3
A-2	$C_l, \alpha$ Data Used in Evaluation of XV-15 Steel Blade	A4
A-3	$C_d$ , Mach Data in XV-15 Steel Blade Evaluation	A5
A-4	$C_d$ , Mach Data Used in XV-15 Steel Blade Evaluation	A6
A-5	$C_d$ , Mach Data Used in XV-15 Steel Blade Evaluation	A7
A-6	Computed Performance of Baseline XV-15 Rotor	A9
A-7	Comparison of Advanced Airfoil Performance With Existing XV-15 Airfoil Performance	A11
A-8	Criteria Used to Select Position of Blade Airfoil	A12
A-9	Family of Blade Twist Distributions Selected for Study	A14
A-10	Variation of Cruise and Hover Efficiencies With Position of Start Taper for Various Levels of Twist	A15
A-11	Variation of Lift Coefficient for Maximum L/D for the VR-7 and VR-8 Airfoil With Mach Number	A17
A-12	Determination of Optimal Twist and Planform For the Replacement Blade	A18
A-13	Candidate Blade Properties	A20
A-14	Comparative Performance of Candidate Configuration	A21
A-15	Hover Stall Margin Comparison	A23

## LIST OF FIGURES

<u>Figure</u>		<u>Sheet</u>
B-1	Fly By Wire Flight Control System	B3
B-2	Primary Flight Control System Functions and Interfaces	B4
B-3	Rotor Cyclic Controls	B15
B-4	Airplane Surface Controls	B16
B-5	Rotor Cyclic Controls Mixing and Cumulative Limits - Right Rotor	B17
B-6	Thrust Management System	B19
B-7	Primary Flight Control Signal Channel Interconnect	B20
B-8	Dual Driver Actuator	B26
B-9	Dual Driver Actuator Schematic	B27
B-10	Longitudinal SCAS	B33
B-11	Lateral SCAS	B34
B-12	Directional SCAS	B35
B-13	Lateral Directional SCAS	B37
B-14	Typical Gust Alleviation Configuration	B38

## 1.0 INTRODUCTION

### 1.1 Blade Preliminary Design

This document reports results of a preliminary investigation of the preliminary design of a composite rotor blade hub and non-mechanical control system for the XV-15 tilt-rotor aircraft. The purpose of the proposed program is to provide replacement blades and spares for the XV-15 aircraft while, at the same time, improving the hover and cruise performance, and rotor stall margins of the aircraft. The RFP envisions the use of advanced composite materials and a fatigue life not less than 3600 hours. The study involved selection of an optimal concept subject to the restrictions of interfacing with an existing aircraft. These restrictions included limitations on rotor diameter and operating rpm, and strength considerations in the support structure and power train impose additional restraints which effectively defined the dynamic properties required from the rotor system.

In the case of the blades, planform configuration, twist, and airfoil type were the only properties which could be varied in the process of optimizing against the performance objectives.

This, combined with the performance requirements of the RFP, led to active consideration of tapered blade planforms, and to the selection of a planform with linear taper of approximately 2:1 starting at the 47% and ending at the 77% radius station, with additional 2:1 taper from 95% to the tip. The planform is illustrated in Figure 1.1 along with the blade twist selected as the best compromise between hover and cruise performance objectives, and the airfoil section and thickness distribution.

XV15 ADVANCED COMPOSITE BLADE PRELIMINARY DESIGN

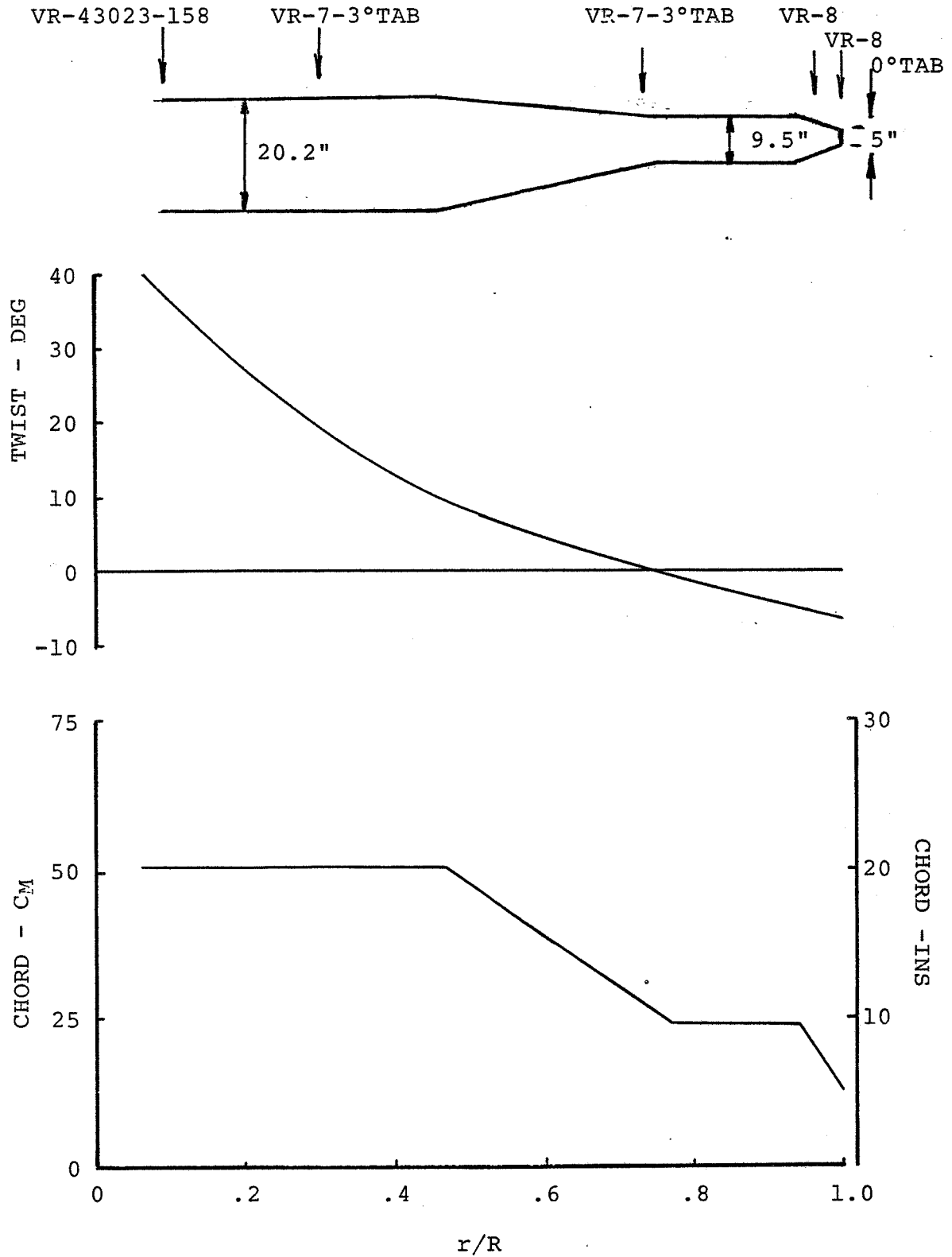


FIGURE 1.1. X<sub>2</sub> REPLACEMENT BLADE PLANFORMS, TWIST, CHORD AND AIRFOIL DISTRIBUTION

TABLE 1.1. SUMMARY BLADE PROPERTIES AND CONSTANTS

DIMENSIONS	% RADIUS	S. I.	U.S.	
		Kg.M.	IN.LB.	SLUGS.FT.
RADIUS		3.81 M	150 IN	12.5 FT
LOCATION OF PIN RETENTION	.167		24 IN	2 FT
CHORDS:				
ROOT - .3 r	.135	.508 M	20.2 IN	1.68 FT
.77R - .95	.063	.241 M	9.5 IN	.792 FT
TIP	.036	.137 M	5.4 IN	.45 FT
MASS (CARRY-AWAY BLADE)		22.01 Kg	48.54 LB	1.51 SLUG.
MASS MOMENT (ABOUT DRIVE SYSTEM)		44.2 KgM	3,834 IN LB	9.94 SLUG.FT
INERTIA (ABOUT DRIVE SHAFT)		106.9 KgM <sup>2</sup>	365,400 LB IN <sup>2</sup>	78.8 SLUG.FT <sup>2</sup>
MASS (BLADE + 1/3 BELL HUB)		47.48 Kg	104.7 LB	3.25 SLUG.
MASS MOMENT		52 KgM	4,514 LB IN	11.69 SLUG.FT
INERTIA (I <sub>b</sub> )		109.89 KgM <sup>2</sup>	375,000 KgM <sup>2</sup>	81.07 SLUG.FT <sup>2</sup>
PITCHING INERTIA		.229 KgM <sup>2</sup>	780 LB IN <sup>2</sup>	.169 SLUG.FT <sup>2</sup>
SOLIDITY (THRUST WEIGHTED)		.076	.076	.076
(GEOMETRICAL)		.091	.091	.091
GAMMA $\rho_0 a \bar{c} R^4 / I_b$		4.06	4.06	4.06
DELTA 3 (PITCH FLAP COUPLING)	.268	- 15.0 DEG.	- 15.0 DEG.	-15.0 DEG.
DISC LOADING (13,000 LB. GROSS WT.)		64.64 KgM <sup>-2</sup>	.0917 LB IN <sup>-2</sup>	.411 SLUG.FT <sup>-2</sup>
ROTOR BLADE AREA (3 BLADES)		1.3851 M <sup>2</sup>	6,441.12 IN <sup>2</sup>	44.73 FT <sup>2</sup>
ROTOR DISC AREA		45.60 M <sup>2</sup>	70,685.28 IN <sup>2</sup>	490.87 FT <sup>2</sup>

3



The selection of blade aerodynamic characteristics is not significantly influenced by other design objectives with the exception of cost. Thus the selected structural design concept, (D spar with Nomex core trailing edge and mix of uni- and cross-ply material to provide desired strength and stiffness), is suitable for all envisioned aerodynamic options. In the case of cost, a study of the relative costs of the various planforms was made and these were taken into account in the trade study analysis.

While the tapered blade planform noted above had a higher cost than the other configurations, this was more than outweighed by its performance and strength advantages. An engineering evaluation of the proposed design was made with respect to performance, structural integrity, dynamics, aeroelastic stability, also manufacturing methodology, and maintainability, repairability, and inspectability. The selection rationale is discussed in Section 2, and Engineering Evaluation in Section 3.

## 1.2 Hub Preliminary Design

A second objective of the subject contract was to identify a composite hub design suitable for replacement of the XV-15 metal gimbaled hub. In this context, the first impression was that an integrated hub-blade design, of the flex-strap type used in the Boeing Vertol Bearingless Main Rotor, would be ideal. However, examination of this concept showed that the dynamics of the XV-15 rotor system could not be matched while retaining adequate strength. The requirement for a very low-hinge offset

implies very short lengths of the flexing member, and therefore, high values of curvature at the flapping excursions which are required for trim and control. This in turn implies unacceptably high strain levels because the flexing member in the B.M.R. concept must be sized to sustain centrifugal force. In practice, the blade geometry constrains the width of flexure material, and to sustain the centrifugal forces, the flexing member would be of such thickness that flapping motions would result in early fatigue failure.

This has led to an approach being adopted which permits a phased introduction of new blades and hubs. Since an integrated blade/hub design does not appear to be possible under the current ground rules, it is proposed that a new hub should be interchangeable with the existing hub, and hub replacement should not require modification to the new composite blade. Blade and hub programs can then proceed independently. This requires a hub which is dimensionally compact with the radial location of blade attachment the same as that of the XV-15 hub with modified pitch housing. A review of available hub concepts using composite material technology led to the rejection of all except one using the Starflex principle (Figure 1.2). This is discussed in Section 2 along with the design of a proposed replacement hub.

### 1.3 Nonmechanical Control System

The tilt-rotor research aircraft can benefit to a substantial degree from the versatility, in control scheduling and mixing

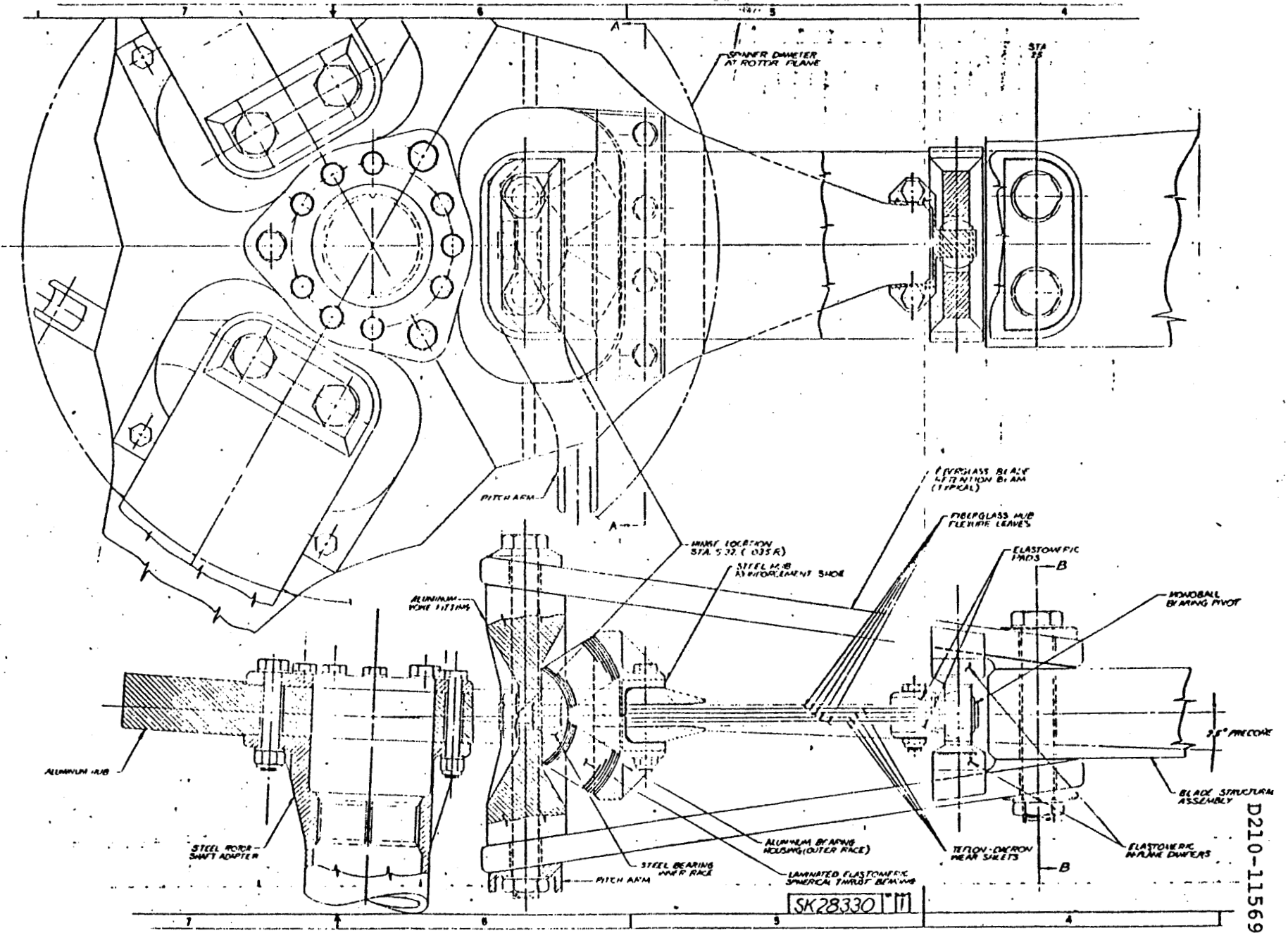


FIGURE 1.2. PRELIMINARY DESIGN LAYOUT OF RECOMMENDED HUB CONCEPT

ORIGINAL PAGE IS OF POOR QUALITY

and adaptation to advanced control concepts, such as, gust alleviation and automatic landing, that can be provided by a fly-by-wire system. In the present study, a system is defined requiring minimum changes to the existing aircraft. The nacelle power actuators, swashplate, and upper controls are unchanged and actuator inputs are provided by separate driver actuators which accept electrical signals from a digital or analog computer stage which, in turn, accepts inputs generated by the pilot and the conditions of flight.

## 2.0 TRADE-OFF ANALYSIS AND CONCEPT SELECTION

Trade-off analyses of different blade concepts were conducted in accordance with the requirement of the Statement of Work. The prime areas of consideration were Cost, Structural Integrity and Dynamic Stability, Reliability, Inspectability and Maintainability, Performance and Noise, Weight, Failsafety Characteristics, Impact and Foreign Object Damage Tolerance, aeroelastics and vibration were also considered. The full range of composite materials were considered. The hierarchy method for decision making in the face of multiple objectives was used, Ref. 1, suitably modified to accept objective calculated data when available in place of subjective pair-wise comparison data. An early decision was made to retain the structural design concept of the CH-46 composite blade because this was already the outcome of extensive in-depth trade study analyses. The same outcome would be expected from a repeat investigation of materials and structural design concepts and construction methods, and this also has the advantage of benefiting from developed and proven technology. This still leaves the designer with a wide choice of structural design parameters, and the ability to meet strength and stiffness criteria with combinations of uni- and cross-ply materials, while still retaining the basic D spar and Nomex core trailing edge concept developed for earlier applications.

The trade study then becomes a matter of choosing between various blade geometrical configurations (planform, twist, airfoil

TABLE 2.1. SUMMARY OF PERFORMANCE CHARACTERISTICS

BLADE TYPE	FIGURE OF MERIT <sup>(1)</sup>	% IMPROVEMENT	CRUISE EFFICIENCY <sup>(2)</sup>	% IMPROVEMENT	MAXIMUM <sup>(3)</sup> GROSS WEIGHT	$\Delta$ PAYLOAD LB.
XV-15 Steel Rectangular	.691	0	.735	0	15245	0
$\left. \begin{array}{l} X_1 \\ X_2 \\ X_4 \end{array} \right\}$ Composite Tapered Planform	.722	4.5	.820	11.56	15364 <sup>(4)</sup>	119
	.752	8.83	.798	8.6	16191	946
	.737	6.7	.802	9.1	15836	591
$\left. \begin{array}{l} X_{03} \\ X_{02} \end{array} \right\}$ Composite Rectangular Planform	.706	2.2	.797	8.4	15482	237
	.720	4.2	.776	5.7	15777	532

- NOTE: (1) Sea Level 13,000 lb. gross weight  
 (2) 200 Knots at 10,000 ft.  
 (3) At torque limit in hover with 7% download OGE  
 (4) Insipient stall is present at this thrust level

section) and the basis of cost, performance, strength, dynamics, and aeroelasticity, and other attributes of lesser importance.

## 2.1 Performance

The blade characteristics which result in significant improvements in both hover and cruise performance (e.g., taper and airfoil variation) tend to increase cost so a group of five alternate planforms were studied to provide a choice of blade performance characteristics which could be evaluated against cost. These are shown in Figure 2.1. The process of identifying these as candidate blades is discussed in Appendix A, along with the estimates of these relative performance characteristics. The performance of the recommended blade is discussed in additional detail in Section 3.

The comparative performance data for the five candidate blades are summarized in Table 2.1. This shows the improvements that may be achieved in each of three categories, hover performance, cruise efficiency, and total lifting capability. No single blade is ahead in all three categories, and this required construction of a consolidated index taking account of the relative importance attached to performance in each category. The Contract Work Statement gives the order of importance as being, first, hover efficiency; second, stall margin; and third, cruise efficiency. However, specific quantitative goals are defined for cruise efficiency which requires significant improvements in the index. Therefore, in quantifying the relative importance

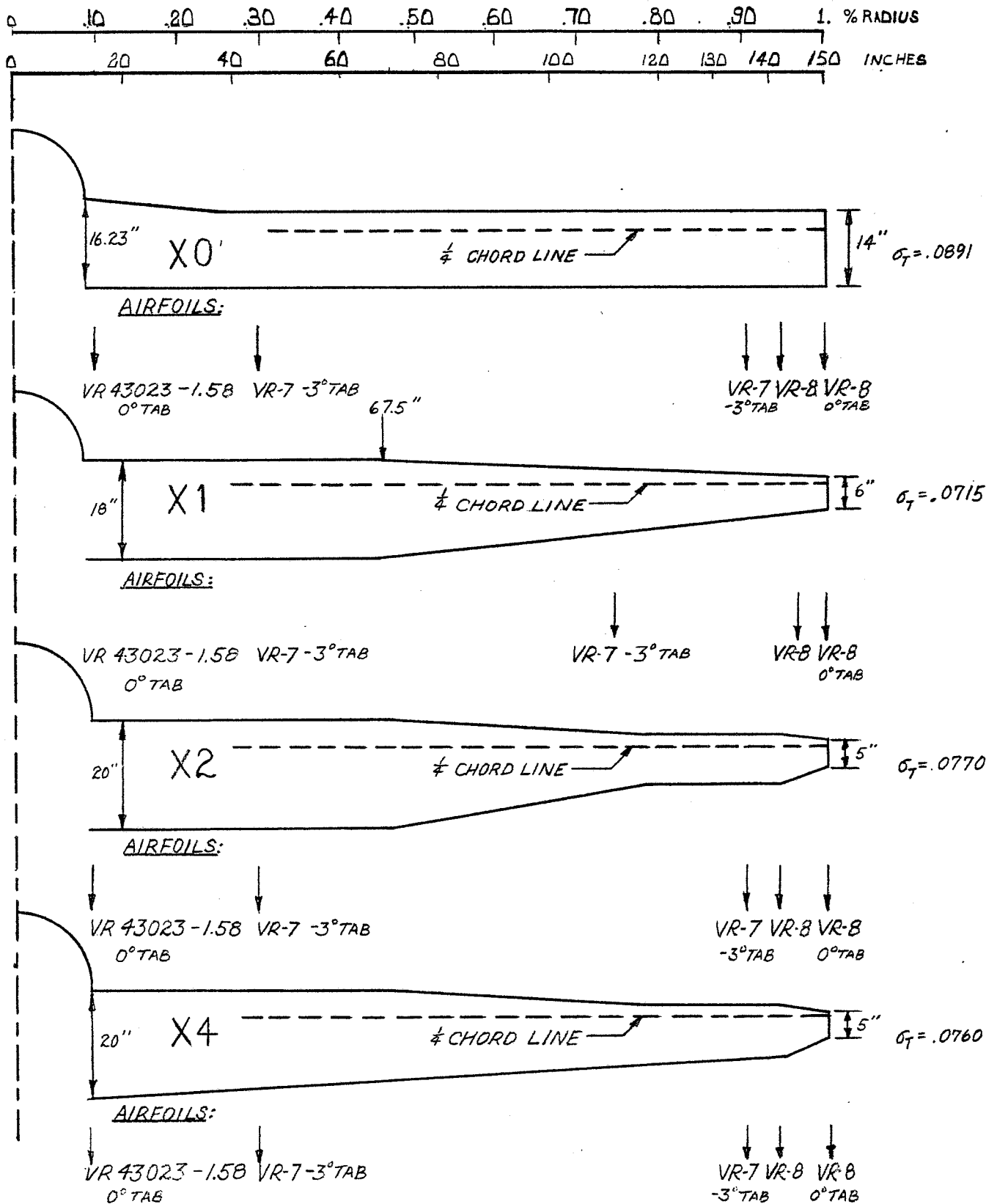


FIGURE 2.1 XV-15 CANDIDATE REPLACEMENT BLADES



TABLE 2.2. (a) PERFORMANCE IMPROVEMENT RATIOS OR RANKING

BLADE	FM	$\eta_c$	TOTAL LIFT
X <sub>1</sub>	.508	1.00	.126
X <sub>2</sub>	1.0	.746	1.00
X <sub>4</sub>	.754	.788	.625
X <sub>03</sub>	.246	.729	.251
X <sub>02</sub>	.476	.482	.562

TABLE 2.2. (b) NORMALIZED RATIOS

BLADE	FM	$\eta_c$	TOTAL LIFT
X <sub>1</sub>	.17	.27	.05
X <sub>2</sub>	.33	.20	.39
X <sub>4</sub>	.25	.21	.24
X <sub>03</sub>	.09	.19	.10
X <sub>02</sub>	.16	.13	.22
ASSUMED WEIGHTING {FM: $\eta_c$ : LIFT} = {1.0: .8: .9}			

TABLE 2.2. (c) CONSOLIDATED PERFORMANCE INDEX

BLADE	NET INDEX.
X <sub>1</sub>	.16
X <sub>2</sub>	.31
X <sub>4</sub>	.24
X <sub>03</sub>	.12
X <sub>04</sub>	.17

TABLE 2.3. MANUFACTURING COSTS  
COMPARISON WITH 12-BLADE RECTANGULAR PLANFORM PROGRAM

BLADE	TYPE	12-BLADE PROGRAM	18-BLADE PROGRAM
$x_1, x_4$ } $x_2$ }	TAPERED	1.08	1.155
		1.10	1.177
$x_{03,2}$	UNTAPERED	1.0	1.070

NOTE:

Above ratios include costs of tooling - Design and fabrication, blade and socket fabrication and assembly, bench testing of specimens, and full-scale validation testing in AMES' 40' x 80' tunnel.

Not included: Material costs and engineering.

These will increase totals by similar amounts and reduce differential.

TABLE 2.4. PREFERENCE RATIOS ON BASIS OF COST \*

BLADE	COST RATIO	PREFERENCE RATIO	NORMALIZED RATIO
X <sub>1</sub>	1.08	.926	.194
X <sub>2</sub>	1.10	.909	.190
X <sub>4</sub>	1.08	.926	.194
X <sub>03</sub>	1.00	1.0	.210
X <sub>02</sub>	1.00	1.0	.210

\* 12-BLADE PROGRAM

TABLE 2.5. PREFERENCE RATIOS ON BASIS OF REPAIRABILITY AND MAINTAINABILITY

BLADE	COMPARISON RATIO	NORMALIZED INDEX
X <sub>1</sub>	1.0	.2
X <sub>2</sub>	1.0	.2
X <sub>4</sub>	1.0	.2
X <sub>03</sub>	1.0	.2
X <sub>02</sub>	1.0	.2

of the performance characteristics, we have assumed that on a scale of ten, with hover efficiency ranking at 10, lift capability would merit 9, and cruise efficiency 8. These may be interpreted directly as weighting factors and applied to individual normalized performance indices as shown in Table II (a), (b) and (c). It is seen that on performance taken alone, the  $X_2$  configuration is ahead of the others with the  $X_4$  blade in second place.

## 2.2 Cost

A study of the relative costs of manufacturing the five candidate blades was made and the results referenced to the costs of a 12-blade program for the rectangular planform blades. The results of this study shown in Table 2.3 indicate that the tapered blades require up to 10% more manhours to produce. The incremental cost of an 18-blade relative to a 12-blade program is approximately 7% reflecting the fact that tooling and set up costs are a major component of overall cost.

The differential in cost ratios between blade types is smaller than had been originally expected. When the overall program is considered, the differential in cost ratios will be reduced because of the inclusion of other costs, such as engineering which do not vary significantly from one blade configuration to another. Thus, we are implicitly placing additional weighting on cost as an attribute to be considered in the decision process.

Table 2.4 shows the cost ratios converted to normalized preference ratios.

TABLE 2.6. CONFIGURATION STRENGTH DESIRABILITY INDICES

DESIGN	$\mu$	$\mu \text{ MAX} / \mu$	STRENGTH INDEX
$X_1$	940	1.868	.207
$X_2$	600	2.432	.327
$X_4$	800	2.195	.244
$X_{02}$	1756	1.000	.111
$X_{03}$	1756	1.000	.111

APPROACH: STRAINS AT 0.3 R FOR AN ARBITRARY HOVER  $10^0$  CYCLIC CONDITION

### 2.3 Inspectability, Repairability, and Maintainability

Differences in these attributes would be expected from the use of a variety of structural design concepts. Since we are proposing to use the structural design concept developed for the CH-46 blade in all of the candidate blade configurations, we would expect substantially the same IR and M characteristics. This results in the indices shown for these attributes in Table 2.5.

### 2.4 Strength

Comparative strengths of the candidate blades were assessed on the basis of strain levels generated by the same flight conditions. Strain levels from the root end to 0.5 R are considerably lower for the X<sub>2</sub> blade, and out to .45 R the X<sub>4</sub> strains are lower than X<sub>1</sub>. From .7 R to .90, the X<sub>2</sub> strains were about 25% higher than X<sub>4</sub> levels over the region where the X<sub>2</sub> blade taper ends. This was based on bending moments for the 120-knot helicopter flight condition obtained from the XV-15 published data. (Note: In the strength evaluation of the X<sub>2</sub> blade reported in Section 3, loads are calculated for the specific X<sub>2</sub> properties and substantially confirm loads used in comparison study.)

The strain level for the rectangular planform blades is very much higher. This could be considered a direct result of the lower values of chord and EI over the inboard sections of the rectangular blades. However, it should be noted that the dynamic properties of rectangular blades of this solidity and

19

DESIGN CONFIGURATION

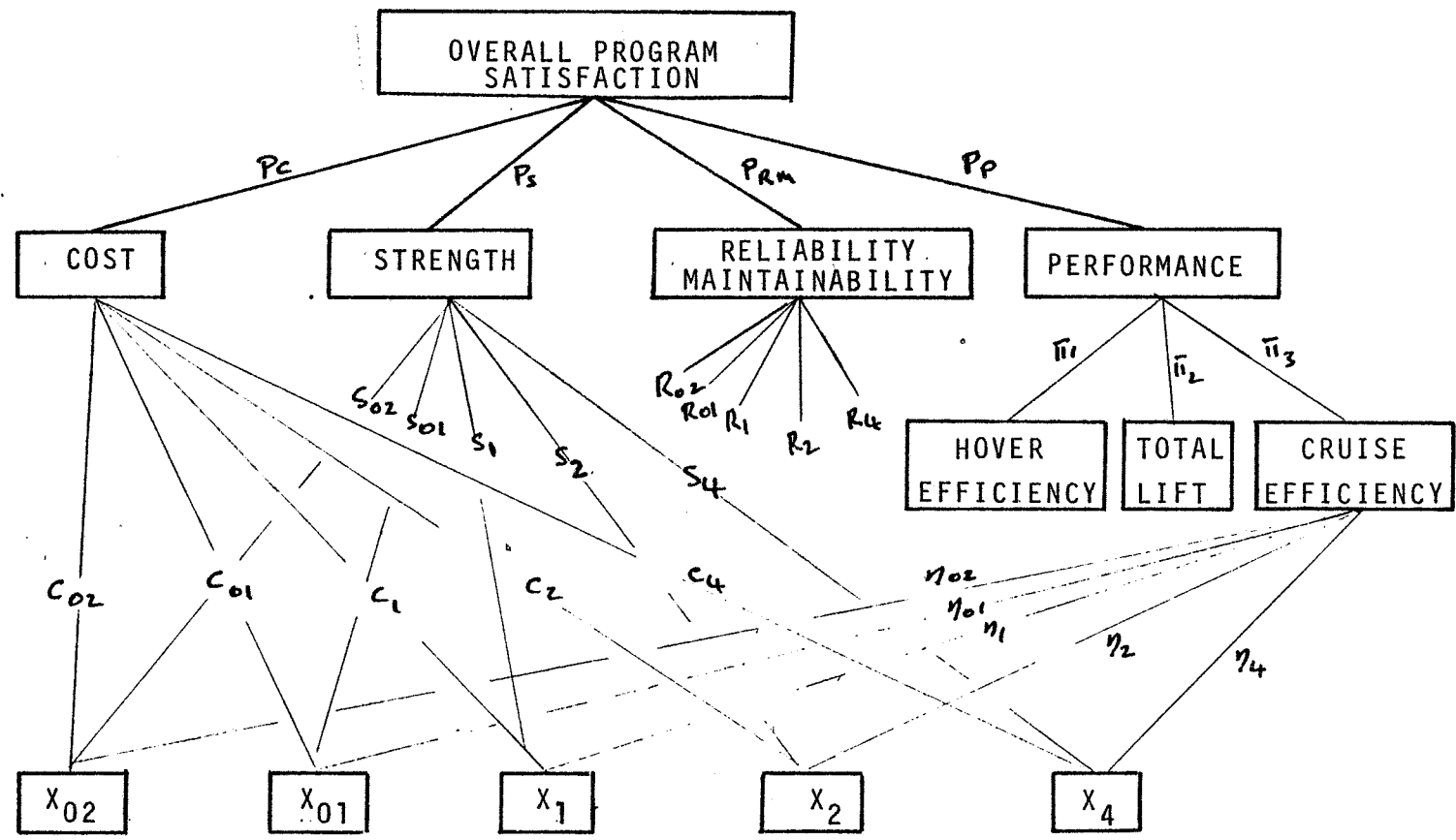


FIGURE 2.2. HIERARCHY OF ATTRIBUTES AND PREFERENCE FACTORS

structural design are such that bending moments are actually much higher than assumed. It is estimated that the chords would have to be increased to around 17 inches to provide adequate stiffness and strength characteristics. This would severely penalize cruise efficiency.

With these reservations, the comparative strength characteristics are listed in Table 2.6.

### 2.5 Development of a Consolidated Index of Comparison

Figure 2.2 indicates the hierarchy of attributes and the manner in which those for a candidate blade are summed according to the relative preference weightings to construct an index of how the multiple objectives are met.

On a scale of 10, it was decided that the major attributes would rank as shown in Table 2.7, and these rankings become the normalized weighting factors shown.

TABLE 2.7. WEIGHTING OF MAJOR ATTRIBUTES

ATTRIBUTE	IMPORTANCE RANKING	NORMALIZED WEIGHTING FACTOR
COST	10	.40
STRENGTH	7	.28
R,M&I	5	.20
PERFORMANCE	3	.12



CALCULATION OF CONSOLIDATED MERIT

<u>BLADE</u>	<u>COST</u>	<u>STRENGTH</u>	<u>R&amp;M</u>	<u>PERFORMANCE</u>	<u>PI</u>
X <sub>1</sub>	.194	.207	.2	.16	} .40 .28 .20 .12
X <sub>2</sub>	.190	.327	.2	.31	
X <sub>4</sub>	.194	.244	.2	.24	
X <sub>03</sub>	.210	.111	.2	.12	
X <sub>02</sub>	.210	.111	.2	.17	

CONSOLIDATED INDEX

<u>BLADE</u>	<u>RANKING</u>	<u>RANKING ON SCALE OF 10</u>
X <sub>1</sub>	.195	8.0
X <sub>2</sub>	.246	10.0
X <sub>4</sub>	.214	8.7
X <sub>03</sub>	.169	6.9
X <sub>02</sub>	.176	7.1

TABLE 2.8. CALCULATION OF CONSOLIDATED MERIT INDICES FOR CANDIDATE BLADES

The operation of the normalized weighting factors over the individual attribute indices is summarized in Table 2.8. This shows that on a consolidated basis, the  $X_2$  blade ranks significantly higher than the other configurations.

It was, therefore, recommended that the further preliminary design activity under the contract should focus on the  $X_2$  blade configuration.

#### 2.6 Research Attributes of Selected Configuration

It is relevant to note that a development program for a blade of tapered planform would have intangible merits which may nevertheless be important. The most important of these is the research content of such a program. While blade taper has been recognized to be beneficial in a number of contexts and the technology well understood, until the advent of composite materials the cost of fabrication was considered to outweigh the potential benefits. With composite materials, this is no longer the case as illustrated by the preceding discussion. The successful development of high performance blades of tapered planform would be a milestone in blade technology in addition to providing higher strength and performance replacements for the current XV-15 blades.

## 2.7 Hub Concept Selection

We have been successful in identifying a hub configuration design which interfaces with the existing XV-15 drive shaft, power train, transmission casing, conversion spindle and actuator. The choice is limited by the requirement of not modifying the existing aircraft to any significant extent, and to date, only one acceptable solution using composite materials technology has been identified.

### 2.7.1 Hub Selection Criteria

The following objectives and criteria are defined for a replacement hub.

- Simplification - a replacement hub should result in an overall simplification by elimination of the gymbal mechanism and lubricated pitch bearings.
- Failsafe qualities should be improved - in this regard, the properties of composite materials (e.g., high allowable fatigue strain, soft failure mode, slow defect propagation and high-damage tolerance) should be exploited. However, alternating strains of  $\pm 2000 \mu$  in/in should not be exceeded in any flight condition.
- The total pitch range, including cyclic, will be -12 to +60 degrees.

- The equivalent radial flap hinge offset shall be such that the hub moment per degree of cyclic flapping shall not exceed that developed by the XV-15 gymballed rotor with its elastomeric centering spring. This places a maximum limit of approximately 5% radius on the equivalent flap hinge offset.
- The design should take account of the need to minimize drag in the cruise mode and should lend itself to fairing within existing contours.
- Endurance limits should not be exceeded in 7.5 degrees of cyclic flapping in hover.

#### 2.7.2 Review of Candidate Hub Designs

##### Boeing Vertol/U. S. Army Bearingless Main Rotor, Figure 2.3

A CF loaded blade root flexure accommodates the flap, lag and torsional excursions of the rotor blade. Twenty-five percent of the blade radius is used up for this flexure which currently provides an equivalent flap hinge at 15 percent radius; however, this could be reduced to 5 percent. The BMR is essentially a single rotor aircraft system since it is designed to accommodate a pitch range of  $-12^{\circ}$  to  $25^{\circ}$  only and a maximum flapping angle of  $\pm 3^{\circ}$ . Preliminary attempts at reducing flap hinge offset and increasing allowable torsional and flapping excursions resulted in a much increased flexure length and an impractically large flexure width.

ORIGINAL PAGE IS  
OF POOR QUALITY

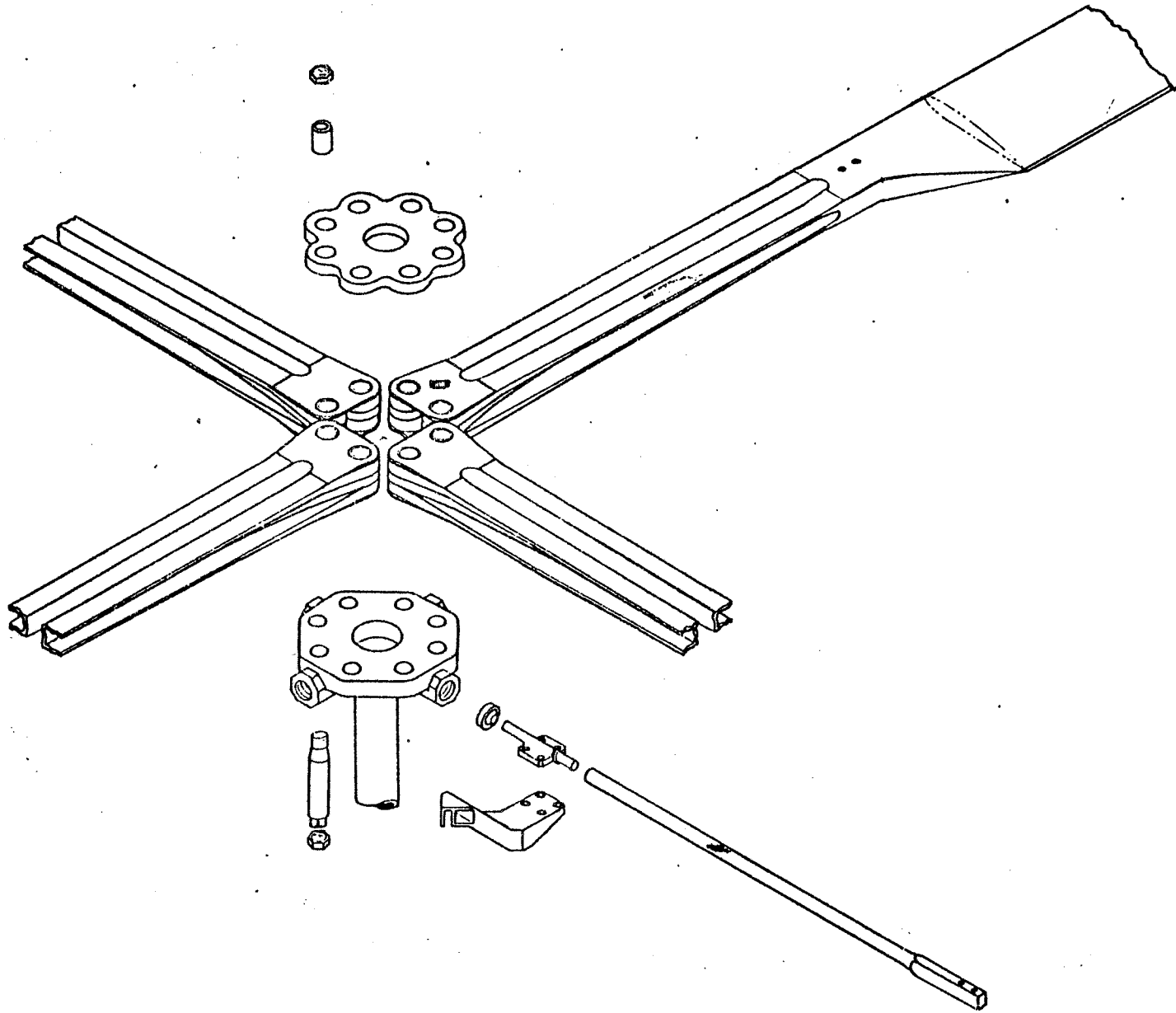


FIGURE 2.3. BOEING VERTOL/U.S. ARMY BEARINGLESS MAIN ROTOR

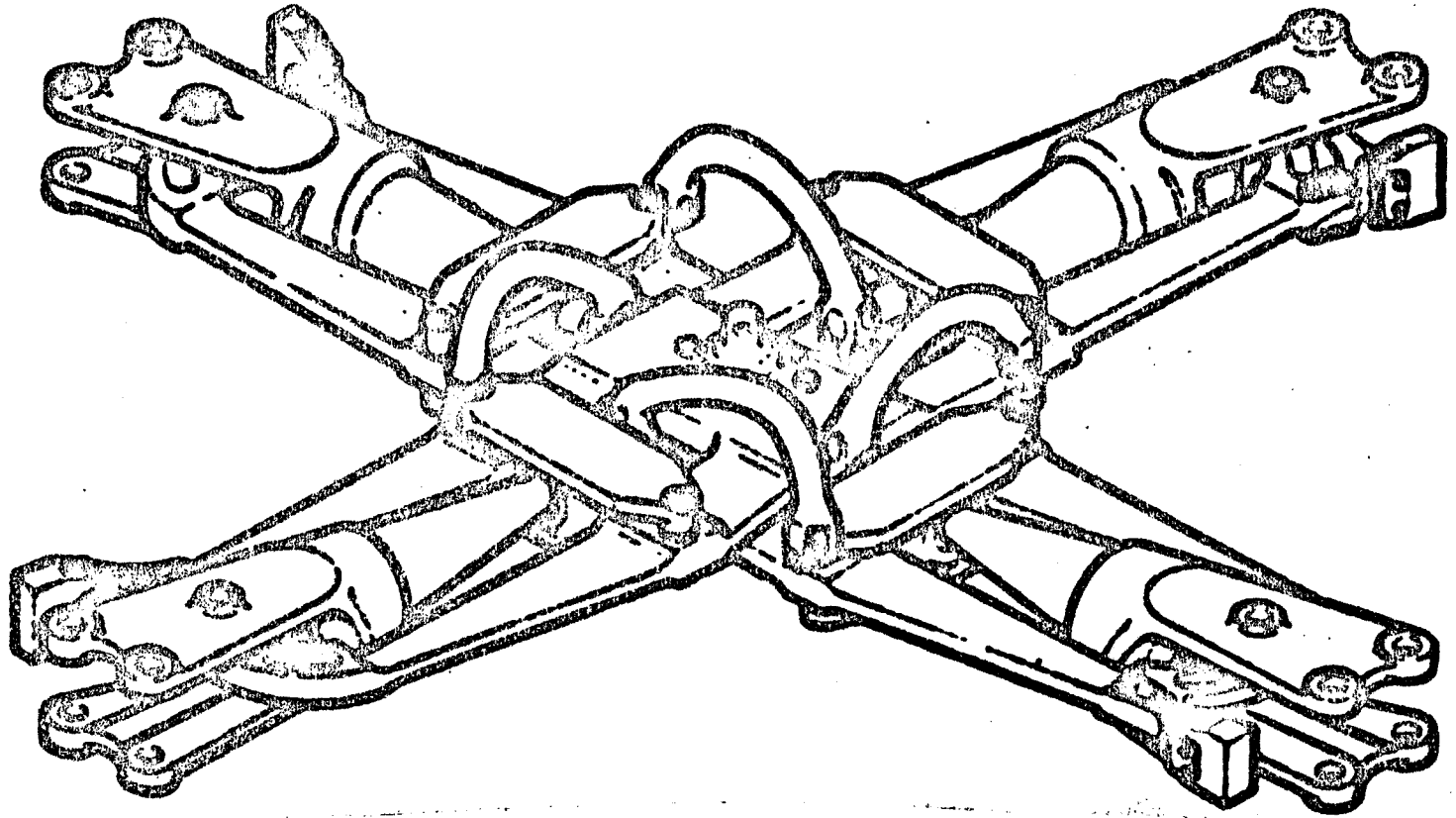


FIGURE 2.4. BELL 212 ROTOR HUB

Bell 212 Rotor Hub, Figure 2.4

A single-rotor helicopter rotor hub in which the flapping motions only are accommodated by a metal CF loaded flexure and the lead/lag and torsional excursions are obtained through elastomeric bearings. Due to its application, flapping and pitching motions are within the  $\pm 3$  degrees and -12 to 25 degree range, although a low-hinge offset of 5 percent radius or less could be expected.

A preliminary redesign of this system to increase the allowable flapping motions and replacement of the titanium flexure with fiberglass still resulted in an impractically large flexure width when the fiber strains are reduced to acceptable proportions.

Aerospatiale Starflex Rotor Hub, Figure 2.5

A single rotor helicopter rotor hub with a fiberglass blade root flapping flexure which is notably unloaded from CF forces. Elastomeric bearings are used to accommodate torsional and lagging motions. Typical of a single-rotor helicopter system, flapping and pitching are confined within the ranges  $\pm 5$  and -12 to +25 degrees, respectively. A redesign of this system to increase the allowable flapping motions is eased by the lack of CF forces in the flexure, however, the resultant width once again became impractically large when the thickness of the flexure was reduced to accommodate the direct fiber strains associated with  $\pm 7\frac{1}{2}$  degrees of flapping.

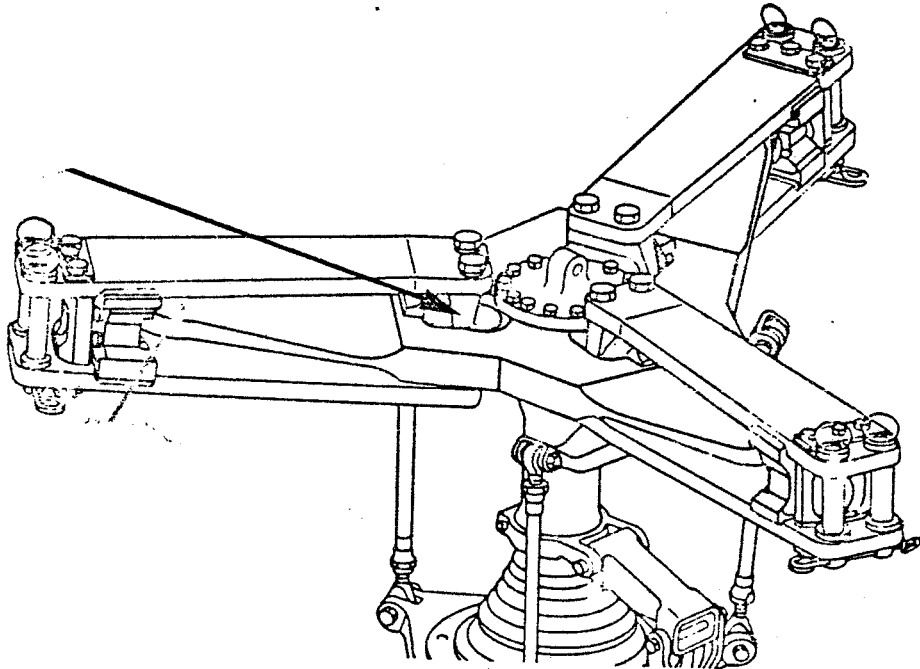


FIGURE 2.5. AEROSPATIALE STARFLEX ROTOR HUB

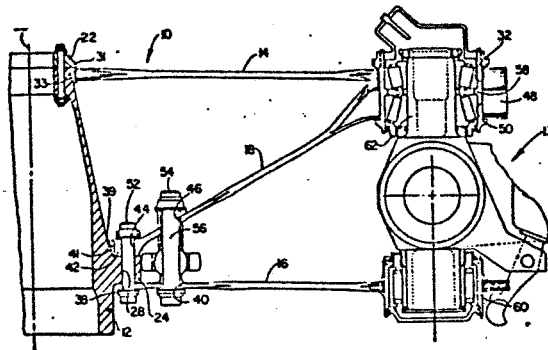


FIGURE 2.6. KAMAN FLEXIBLE HUB



The purpose of the flapping flexure in the Starflex is not for blade retention but as a lead/lag and flapping (droop stop) restraint. Increasing the allowable 4g static droop to -15 degrees through reduction of the flexure stiffness still resulted in a large flexure width.

This configuration appeared to be the most promising candidate for further exploration.

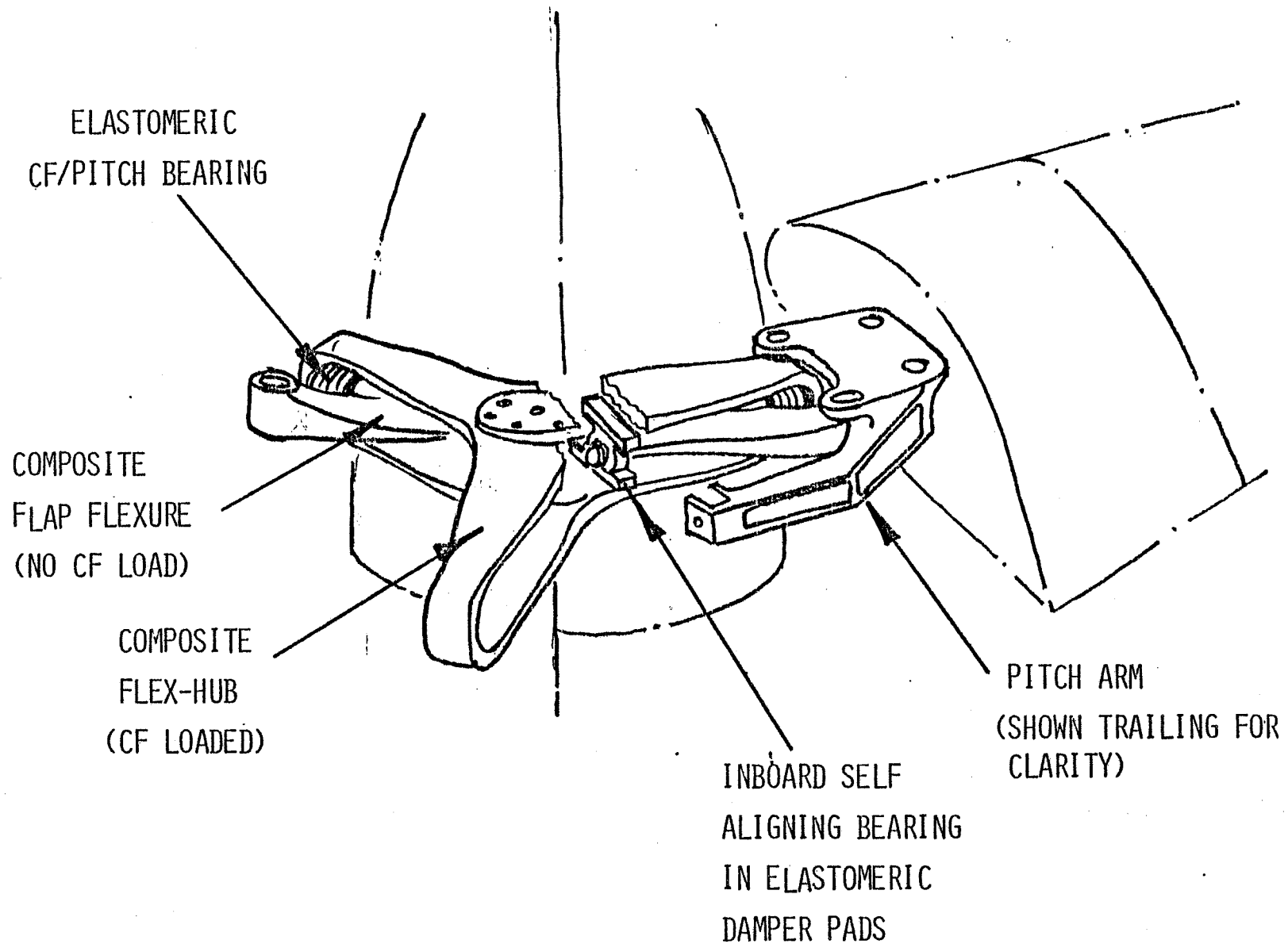
#### Kaman Flexible Hub, Figure 2.6

Another interesting concept studied was this unique hub of upper and lower flexible fiberglass plates which allow some vertical freedom for the blade root attachment. It was thought that this characteristic could be added to the Starflex system such that only a portion of the required flapping was accommodated by the flexure and the remainder through flexible hub plates.

#### Reversed Starflex, Figure 2.7

By reversing each arm of the Starflex hub such that the CF carrying elastomeric bearings were outboard instead of inboard, and the upper and lower yoke plates which transmitted the CF from the blade root to the bearing were again reversed such that the CF is transmitted from the blade, through the bearing, then through the yoke plates to the shaft centerline; thereby making the yoke plates a flexible hub, the Kaman concept could be introduced.  $\pm 7\frac{1}{2}$  degrees of flapping motion was then accommodated. The elastomeric CF/torsion bearing, now located

FIGURE 2.7. REVERSED STARFLEX HUB CONCEPT



30

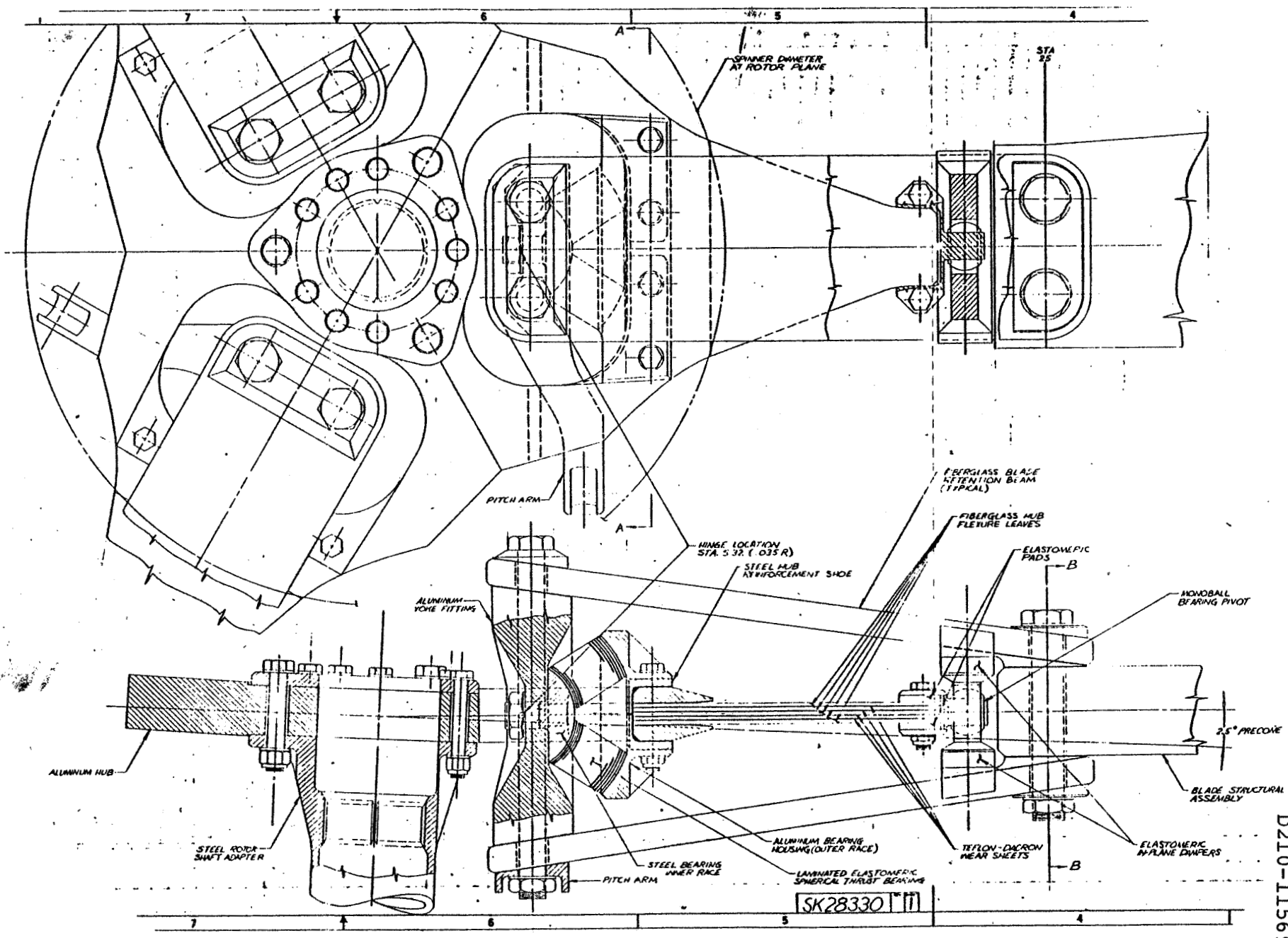


FIGURE 2.8. RECOMMENDED CONCEPT FOR XV-15 COMPOSITE REPLACEMENT HUB

outside the spinner, becomes large when redesigned to cope with the required pitch excursions. The concept, therefore, becomes less attractive because of the impact on aerodynamic performance caused by the blade envelope necessary to fair the fittings surrounding the elastomeric beading.

#### Starflex with Leaf-Spring Flexure

A modification of the Starflex design was defined using multiple layers of composite material for the flexure and with the elastomeric bearing oriented to provide the lowest hinge offset. This configuration seemed to provide the functional and strength characteristics necessary for XV-15 application, and was, therefore, selected for further work. The preliminary design layout is shown in Figure 2.8, and the concept is discussed in detail in later sections of the report.

## 2.8 Selection of Advanced Non-mechanical Flight Control System Concept

### 2.8.1 Description of Recommended Design

For the advanced non-mechanical flight control system, Boeing recommends a triplex, inline monitored dual fail operative primary flight control system (PFCS) interfaced with a triplex cross-channel monitored, fail operative/fail safe stability and control augmentation system (SCAS).

The recommended system will interface with the existing XV-15 cockpit controls at the point where the force feel system is tied in. All system control and computation will be accomplished in a single line replaceable unit LRU, the flight control processor. This unit will be configured with dualized digital micro-processors performing the primary control function interfaced with a third digital processor performing the SCAS function. This arrangement will be functionally analogous to that used on the Heavy Lift Helicopter (HLH) except that digital rather than analog computation will be used in the primary control path. As in HLH the interface between the SCAS and PFCS will be designed to limit PFCS response for SCAS failures and provide a minimum necessary time delay even for triplex SCAS failures such as could occur with programming errors.

The recommended approach includes use of driver actuators to position the existing XV-15 boost actuators, and the incorporation of electrical control for the engines in place of the mechanical throttle controls now fitted in the XV-15.

The recommended approach for signalling is dedicated wiring for in-channel communication and fiber optic signalling using dedicated fiber optic links for cross-channel exchange of digital information. The specification for this system are given in Appendix B. Details on this approach are given in Section 4.5.

#### 2.8.2 Rationale for Selection of Recommended Design

The primary issues considered in configuring the recommended system were 1) the computational approach, 2) the actuator configuration. With the former being of most importance; the latter being primary related to the constraints imposed by the existing airframe.

##### 2.8.2.1 Computation

For the computational configuration three options were considered:

- a) The use of an inline monitored analog primary linkage similar to that used on HLH, proposed for XV-15 in an earlier study (Reference 2 ) and discussed in Boeing's proposal for this study (reference 3). In this approach the analog computation could be interfaced with a separate SCAS. For minimum weight and cost these functions could be integrated in a single LRU. The SCAS functions could be either analog or digital. This configuration is certainly still viable and represents a virtually no-risk approach as far as safety is concerned. It may be limited in its flexibility and potential for growth in the primary system and certainly does not advance the vehicle toward a production configuration which would clearly

be more along the lines of the recommended approach.

b) A second configuration considered, and one proposed by two suppliers in the original XV-15 study, was a single digital processor performing both the PFCS and SCAS functions. Honeywell Inc. proposed a triplex arrangement based on their HDP-5301 Bit-Slice Processor wherein first PFCS failures were detected by cross-channel comparison and second PFCS failures were detected by in-channel self-checks. This configuration includes a fail operative/fail safe SCAS. The General Electric Company proposed as an alternate to the analog approach (which was used by Boeing in the final system proposed to NASA) a quadruplex cross-channel monitored digital arrangement based on their MCP-701A Processor. This processor is used in the F-18 Flight Control Computer. This system provided dual SCAS sensing with Quadruplex SCAS computation. The digital systems were 1-1/2 to 2 times higher in cost reflecting 1) cost for software development, 2) experience with the analog hardware which had been through refinement in the two HLH hardware programs and a UTTAS study.

These digital systems have two disadvantages in comparison to that recommended for XV-15 and that used on HLH. 1) By use of a single processor, they do not bound the flight safety risk to the primary control path. Each change of software even if it be in some mundane function of the SCAS can affect the PFCS because there is one memory, one processor, etc. Under these conditions, each software change must be treated as affecting flight safety. The cost of this approach is being seen on the F-18 program. 2) These approaches make use of cross-channel signalling

to detect some (or all) of the failures in the primary path which can allow propagation of failures from channel-to-channel. In-channel self-monitoring provided, may not be adequate coverage of latent failures without extensive pre-flight built-in-test.

The limitations discussed above may be justified if a fully integrated system requiring full-time, large-authority, high-rate, stabilization as required, and reversion to a PFCS is not feasible. Both fixed wing and helicopter designers have traditionally resisted this approach.

Fixed wing designs have tended to strong static and dynamic stability and are only now finding the benefits of relaxed static stability and are configuring systems with full time augmentation (i.e., F-16). Helicopter designers have been working with control configured vehicles (CCV) for years, but have adapted an approach of providing adequate stability for degraded flight with augmentation off and using the technique of frequency splitting where low authority is allowed at high rate and high authority is allowed at low rate. This approach will be used to bound the response of the XV-15 PFCS to SCAS failures.

- c) The selected approach overcomes the limitations of the system discussed above. The primary computation and SCAS interface is handled in a single microprocessor (such as the 16 Bit INTEL 8086). Within the limitations of cycle time and to a lesser extent memory, functions may be added to the primary path. This flexibility comes at the price of revalidation of the program.



With the proposed approach only the PFCS portion is affected however. All monitoring for the primary function is accomplished in-channel by simple comparison of the computed results of the two PFCS processors. The recommended approach will give fail operational SCAS within the same LRU if the needed sensors are provided. If only dual sensing is provided the SCAS will be fail-safe like the current XV-15 configuration.

#### 2.8.2.2 Actuation

Both integrated and driver actuators were considered. The choice was made based on space availability in the existing XV-15 airframe. With the assistance of NASA and Bell personnel, Boeing reviewed the space available for installation of integrated actuators and boost-driver actuators, of two different types.

Based on this review, a driver actuator was selected. Installation of an integrated design in the collective pitch position was not possible. Installation of an integrated actuator in the flaperon position would have major impact on adjacent equipment. In other locations installation of a driver or integrated design was possible without major impact on adjacent equipment or structure.

A dual driver having triplex electrical interfaces is recommended. It allows operation with a dual hydraulic supply (the same as required by the boost actuator) while providing for interface with the triplex flight control processors via current summing in the electro-hydraulic valve. This scheme is described in more detail in Section 4.

### 3.0 TECHNICAL EVALUATION OF SELECTED DESIGN

A summary evaluation of the selected candidate blade was made for those areas which are considered to be most critical to the development and successful application of an advanced composite blade. In some instances, this evaluation has been required as part of the comparison process, and the results will be used if appropriate.

#### 3.1 Aerodynamic Performance

The selected blade effects a compromise between hover and cruise performance objectives.

Blade performance objectives included an improvement in hover performance of unspecified amount; for cruise a 6% improvement in specific range is desired. These objectives are interpreted as follows:

- o HOVER - Gross Weight = 13000 lb @ sea level std.  
           Tip Speed = 740 ft/sec  
           Download = 7%  
           Diameter = 25 ft
- o Cruise - Gross Weight = 13000 lb  
           Tip Speed = 600 ft/sec      $\mu = .563$   
           Velocity = 200 kts

<u>Altitude</u>	<u>C<sub>T</sub></u>	<u><math>\eta_{Goal}</math></u>
0	.00131	.767
10000	.00177	.804
16000	.00222	.839

As discussed in Section 2, the selected blade will provide the comparative rotor performance shown in Table 3.1 with respect to the current XV-15 blade.

Table 3.1. Performance of X<sub>2</sub> Blade Relative to Current XV-15

Performance Index	Current XV-15	X <sub>2</sub> Blade	% Improvement
Hover Figure of Merit	.691	.752	8.8
Cruise Efficiency	.735	.798	8.6
Lift Capability Kg(lb)	6929(15245)	7359(16191)	6.2

The Figure of Merit is given at sea level std, O.G.E. at a gross weight of 13000 pounds with 7% download. Cruise efficiency is computed for 200 knots TAS at 10,000 feet.

The lift capability is evaluated for a maximum continuous shaft torque of 130,000 in-lbs.

The rotor efficiency as a function of  $\mu$  and power coefficient is mapped in Figure 3.1. Figure 3.2 shows the line of maximum thrust (derived from Figure 3.1) as a function of speed for maximum continuous torque at 456 (cruise) rpm. This is superimposed on estimates of aircraft drag versus speed for a range of values of  $f_e$  from 7 to 14 square feet.

The estimated thrust variation of the current blades is also shown and confirms the published XV-15 cruise speed of 280 knots at 10,000 feet.

XV-15 COMPOSITE REPLACEMENT BLADE

X<sub>2</sub> BLADE CRUISE PERFORMANCE

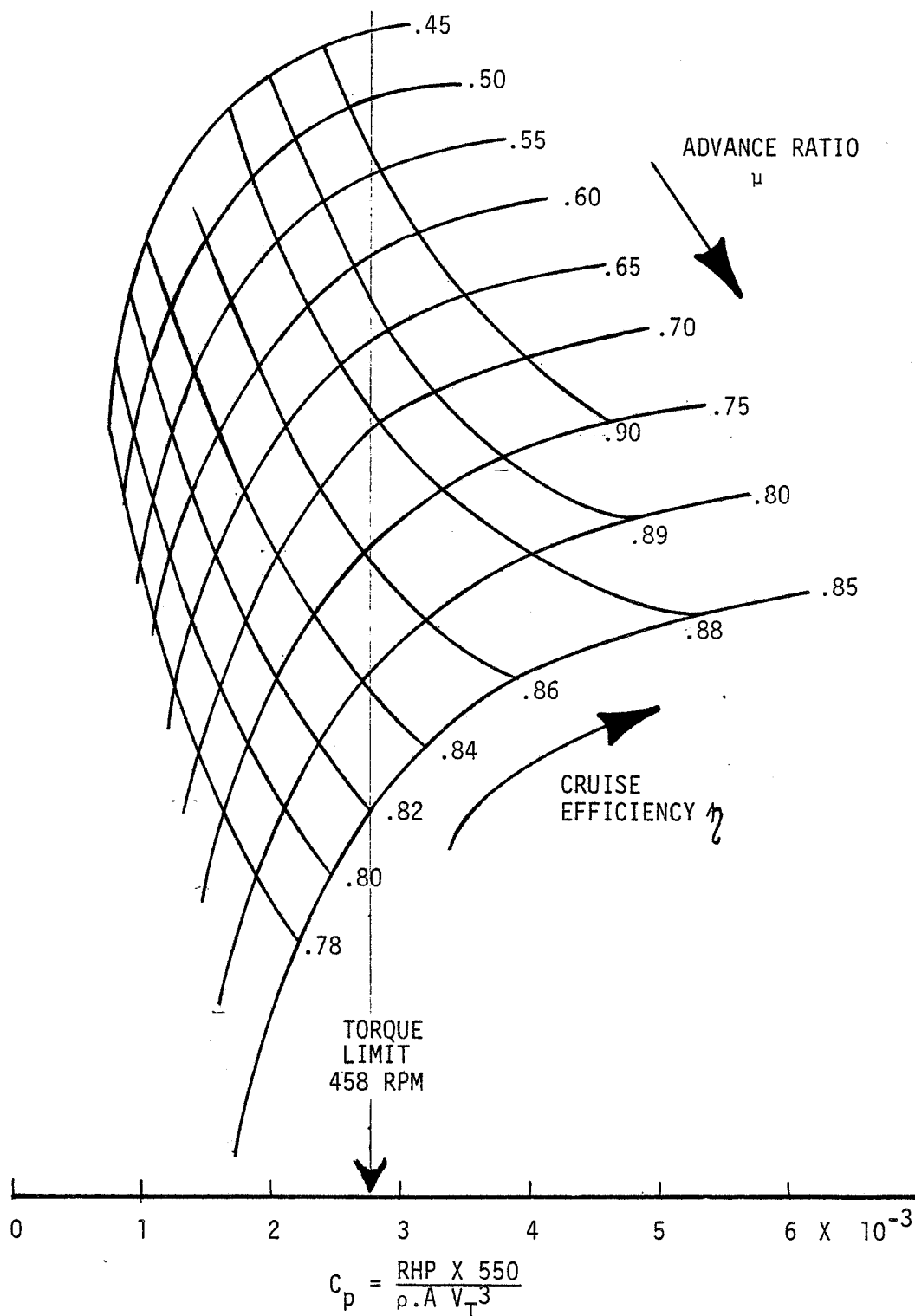


FIGURE 3.1. ROTOR CRUISE EFFICIENCY AS FUNCTION OF  $\mu$  AND  $C_p$

XV-15 AIRCRAFT WITH X<sub>2</sub> REPLACEMENT BLADE

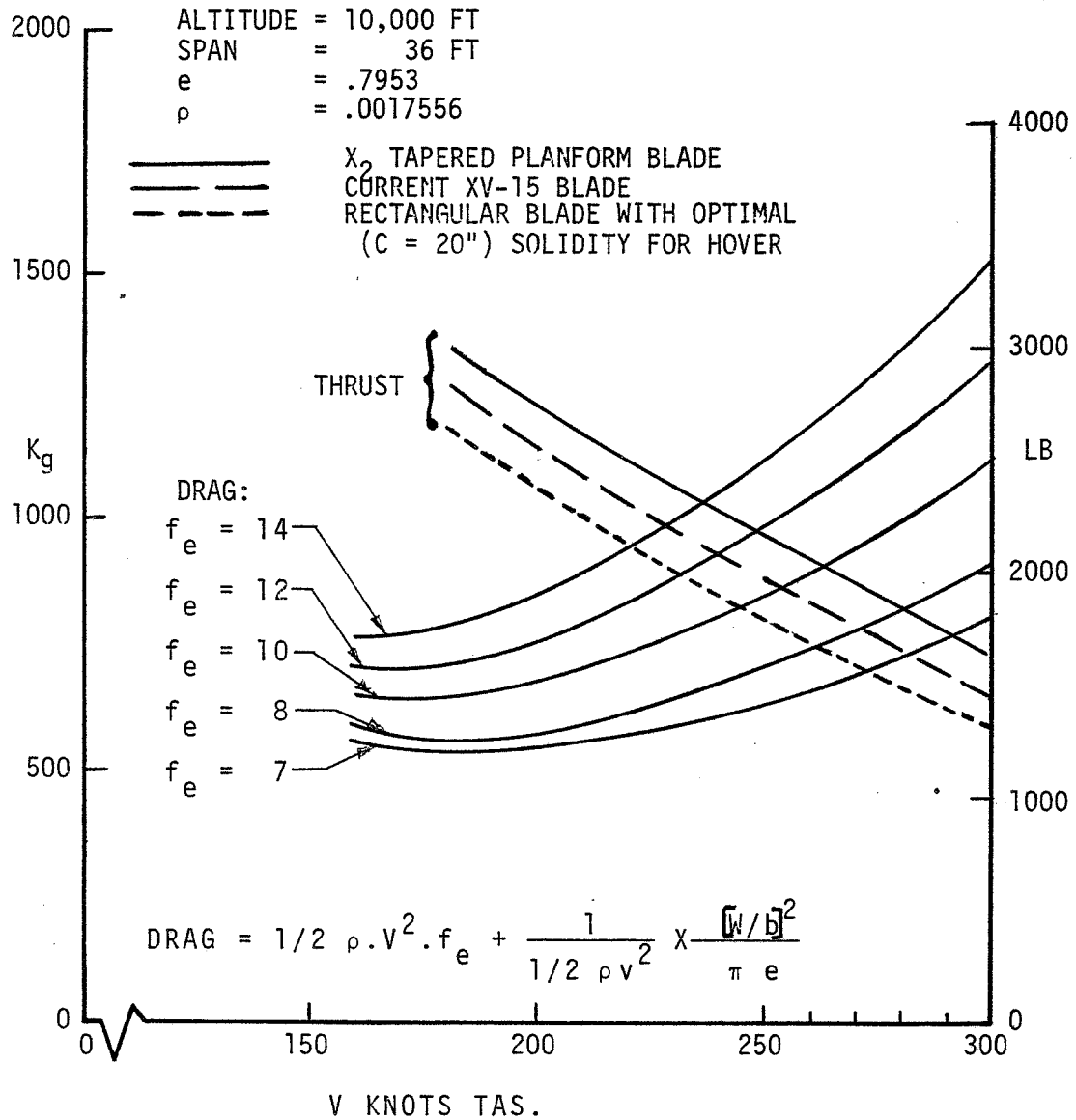


FIGURE 3.2. THRUST AND DRAG VARIATION WITH SPEED X<sub>2</sub> BLADE AND 14" AND 20" CHORD RECTANGULAR BLADES

The proposed rotor is seen to give an additional 7 to 8 knots in maximum cruise speed over the range of possible  $f_e$  values. The improvement is due in large part to the reduced solidity of the  $X_2$  blade relative to the current XV-15 blades.

An increase in solidity to maximize hover efficiency at the design gross weight would degrade cruise efficiency and results in a reduction in available thrust. Figure 3.2 shows the thrust that would be obtainable with a 20" chord rectangular blade which operates close to the maximum figure of merit at a gross weight of 13,000 pounds. The decrease in maximum cruise speed is 10 knots relative to the current system, or 18 knots when compared with the advanced configuration blade.

XV15 ADVANCED COMPOSITE BLADE PRELIMINARY DESIGN

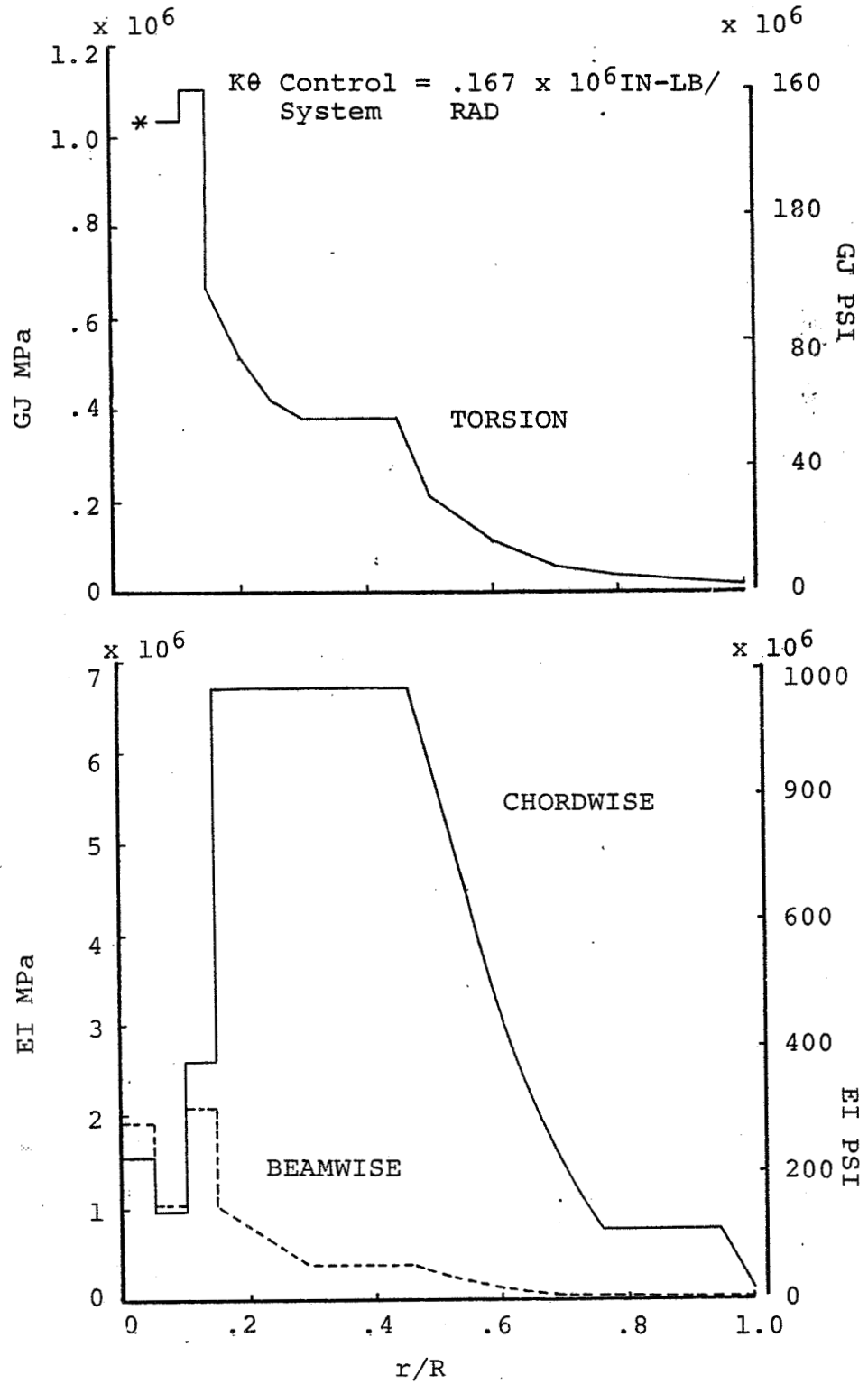


FIGURE 3.2.1. STIFFNESS OF  $X_2$  PRELIMINARY DESIGN BLADE

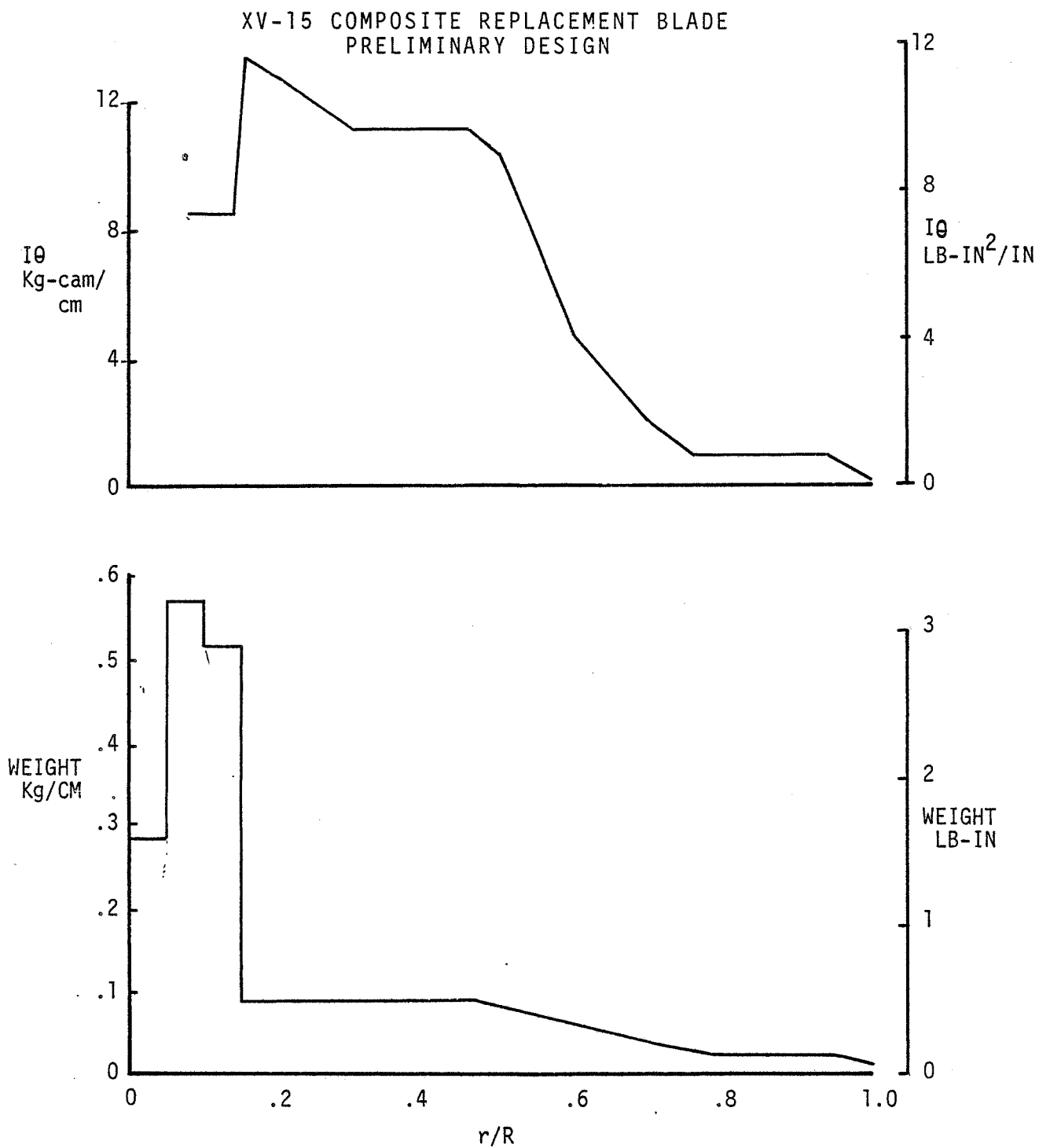


FIGURE 3.2.2. DISTRIBUTION OF MASS AND PITCHING INERTIA



XV-15 COMPOSITE REPLACEMENT BLADE

FLAP - CHORD BENDING  
MOMENT DISTRIBUTION

HELICOPTER FLIGHT: 120 KNOTS

$A_1 = -4.0^\circ$   $B_1 = -6.11^\circ$

NET GIMBAL ANGLE =  $5^\circ$

13,000 LB. GROSS WT.

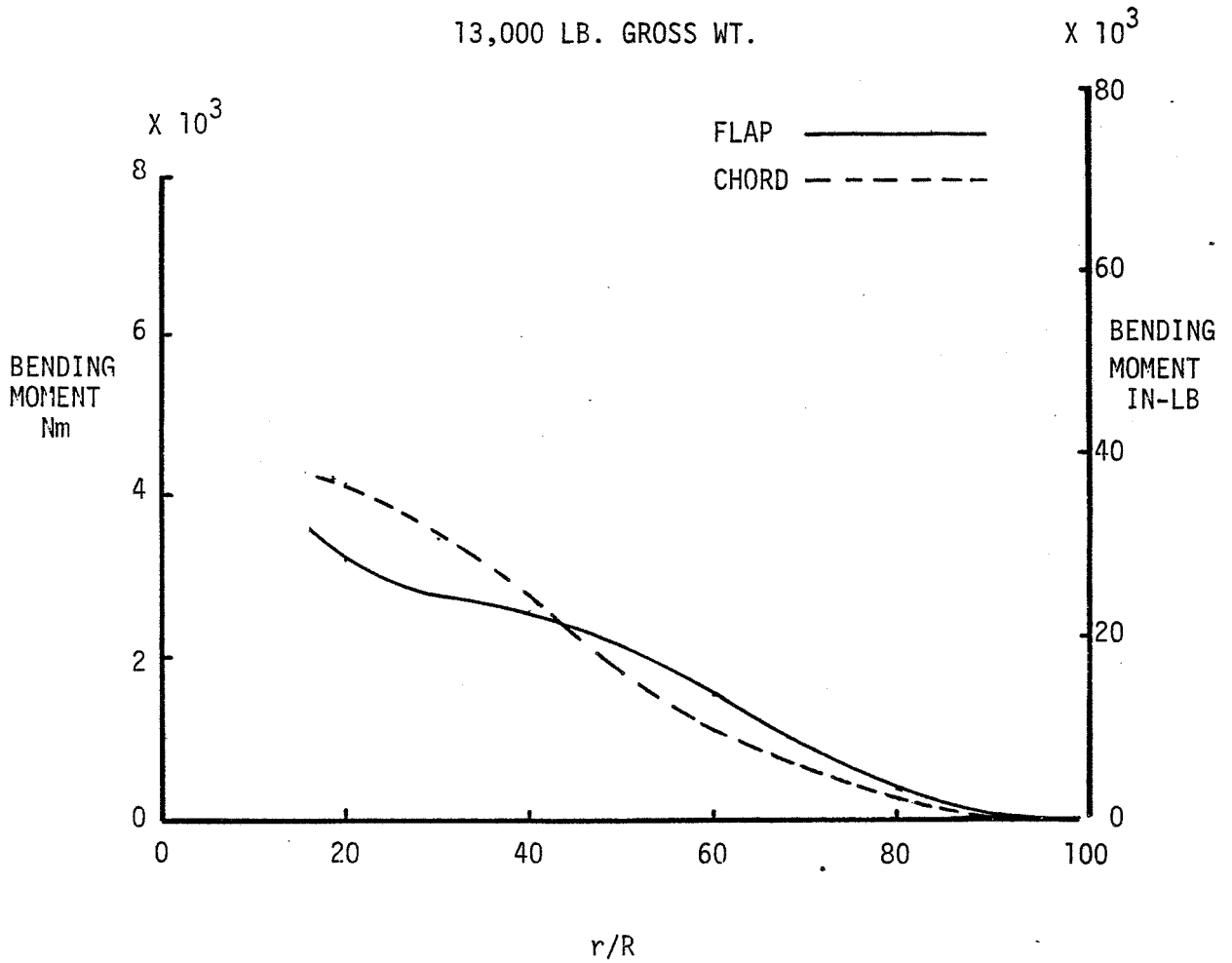


FIGURE 3.2.3.  $X_2$  BLADE FLAP AND CHORD BENDING MOMENTS - HELICOPTER FLIGHT AT 120 KNOTS

**TABLE 3.2.1. XV-15 ADVANCED COMPOSITE BLADE PRELIMINARY DESIGN**  
**SUMMARY OF PROPERTIES**

X/R	EI FLAP		EI CHORD		GJ		MASS PER UNIT LENGTH		PITCH INERTIA PER UNIT LENGTH		CHORD	
	PSI x 10 <sup>6</sup>	MPa x 10 <sup>6</sup>	PSI x 10 <sup>6</sup>	MPa x 10 <sup>6</sup>	PSI x 10 <sup>6</sup>	MPa x 10 <sup>6</sup>	Kg/cm	lb/in	lb-in <sup>2</sup> /in	Kg-cm <sup>2</sup> /cm	in	cm
.15	152.7	1.05	990.	6.82	97.2	.670	.231	1.296	9.51	10.94	20.2	51.3
.20	116.8	.80	990.	6.82	74.4	.513	.088	.492	11.01	12.67	20.2	51.3
.30	55.24	.38	990.	6.82	35.	.241	.088	.492	9.65	11.10	20.2	51.3
.40	55.24	.38	990.	6.82	35.	.241	.088	.492	9.65	11.10	20.2	51.3
.50	42.3	.29	840.	5.79	29.1	.200	.086	.480	8.35	9.61	19.02	48.3
.60	17.3	.119	460.9	3.17	15.8	.109	.062	.349	4.08	4.69	15.49	39.34
.62	14.6	.101	391.7	2.70	13.3	.091	.058	.326	3.48	4.01	14.78	37.54
.64	11.95	.082	337.9	2.33	11.8	.081	.054	.303	2.93	3.37	14.07	35.73
.66	9.35	.064	289.9	1.99	10.1	.069	.050	.278	2.40	2.76	13.37	33.95
.68	7.42	.051	246.	1.69	8.6	.059	.046	.256	1.97	2.27	12.66	32.15
.70	5.99	.041	207.	1.42	7.2	.049	.042	.237	1.64	1.89	11.95	30.35
.72	5.25	.036	172.7	1.19	6.0	.041	.039	.216	1.30	1.50	11.25	28.57
.74	4.75	.033	136.4	.94	4.9	.033	.035	.195	1.01	1.16	10.5	26.67
.76	4.25	.029	102.4	.706	3.58	.024	.031	.172	.740	.85	9.6	24.38
.78	4.00	.027	102.4	.706	3.58	.024	.031	.172	.740	.85	9.6	24.38
.80	3.75	.025	102.4	.706	3.58	.024	.031	.172	.740	.85	9.6	24.38
.90	2.40	.016	102.4	.706	3.58	.024	.031	.172	.740	.85	9.6	24.38
1.0	1.11	.007	15.1	.104	.24	.001	.015	.085	.095	.11	5.7	14.47

NOTE: BALANCE WEIGHTS NOT INCLUDED IN ABOVE. PROVISION IS MADE FOR ADDING UP TO 1.8 KG (4 LB) BETWEEN 0.90 AND 0.95 RADIUS.

47

D210-11569-1

### 3.2 Strength

There has been no attempt at this stage to optimize blade weight so that the strength exceeds stated goals. However, it should be noted that this reflects desirable features in the selected design which may permit weight reduction when we enter the detailed design phase. Two regions are the subject of detailed attention at this phase. The first is the .77R span location where the taper ends and a constant chord section continues outboard. The other is the twin-pin retention; here stress concentrations were expected to cause strain levels which would require special attention.

#### 3.2.1 Outer Blade Strain Levels

Figure 3.2.1 shows flap and chord EI and GJ distribution for the X2 blade. The mass and pitching inertia distributions are given in Figure 3.2.2 and the properties of the blade are tabulated in Table 3.2.1. Blade bending moment distributions are given for two nominal conditions. The loads in helicopter flight at 120 knots are expected to provide design oscillatory loads over the outer sections of the blade. Also to be examined is the sideways flight condition in hover with the C.G. in the most forward location. This condition is known from past experience to generate larger flapping excursions and possibly governing conditions.

#### 120 Knots Helicopter Flight

Flight in the helicopter mode at 120 knots requires a nose down attitude of  $15^\circ$ , or a mast angle of  $75^\circ$  and control application of  $A_1 = .4$  degrees and  $B_1 = -6.11$  degrees, resulting in a net rotor gimbal angle of  $5^\circ$ . Figure 3.2.3

XV-15 COMPOSITE REPLACEMENT BLADE  
PRELIMINARY DESIGN

STRAIN AT CRITICAL STATION COMPARES WITH ENDURANCE LIMITS

$V = 120$  KNOTS

$i_n = 90^\circ$

$\alpha_{fus} = -15^\circ$

GIMBAL ANGLE =  $5^\circ$

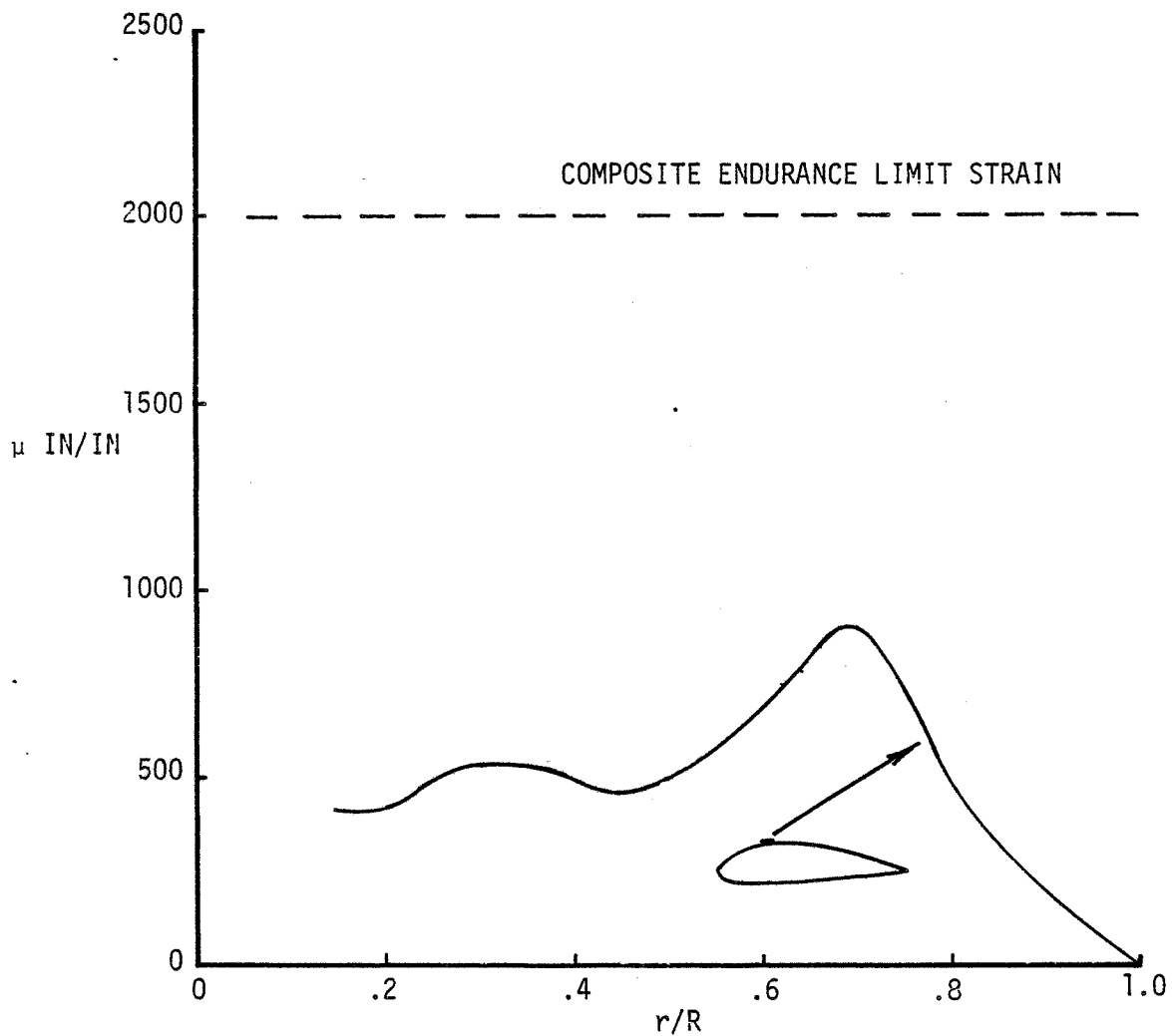


FIGURE 3.2.4.  $X_2$  BLADE - SPANWISE DISTRIBUTION OF STRAIN  
120 KNOTS - HELICOPTER FLIGHT

## XV15 COMPOSITE REPLACEMENT BLADE

FLAP AND CHORD BENDING  
 MOMENT DISTRIBUTION  
 HOVER  $A_1 = 0$ ,  $B_1 = 4.5$   
 NET GIMBAL ANGLE =  $5^\circ$

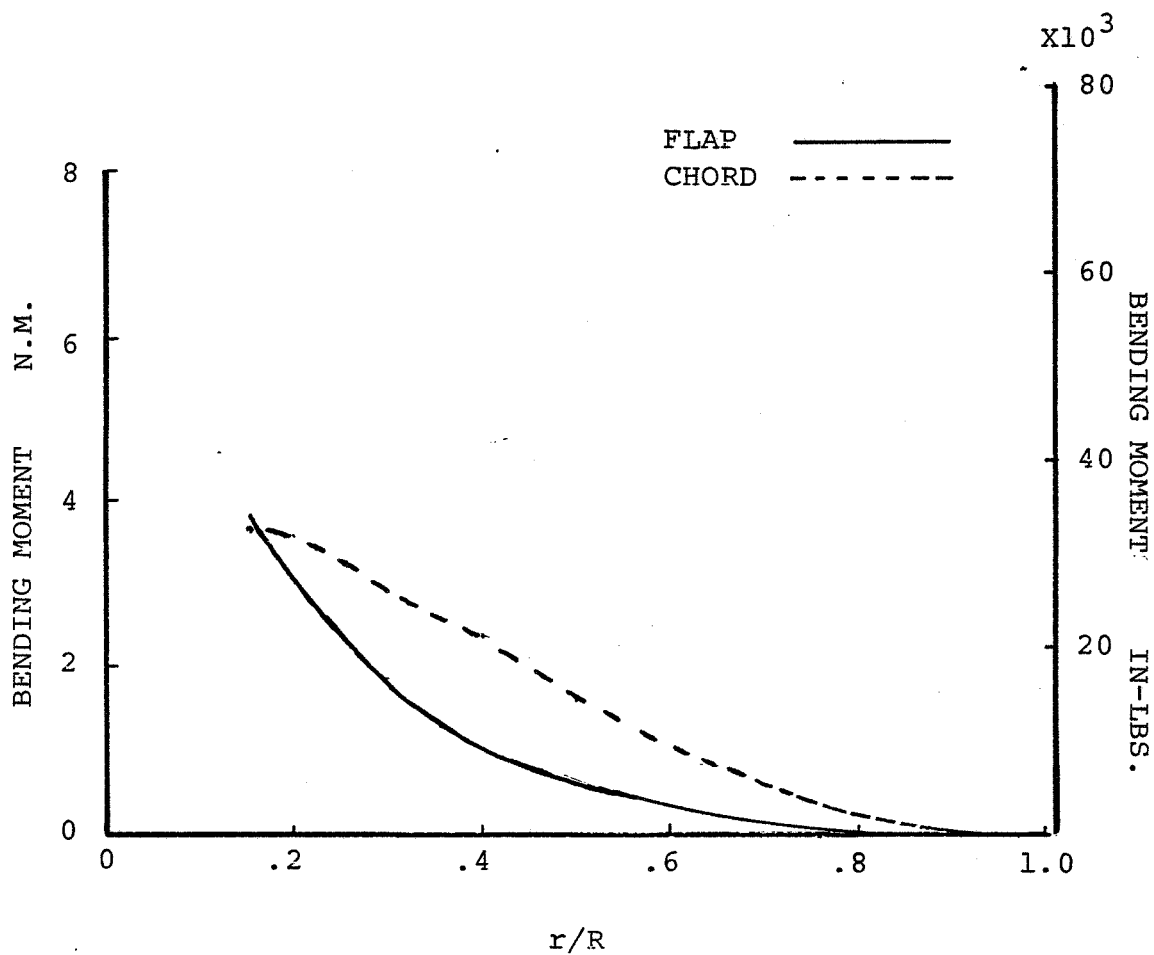


FIGURE 3.2.5 FLAP AND CHORD BENDING MOMENTS IN HOVER

XV-15 COMPOSITE REPLACEMENT BLADE  
PRELIMINARY DESIGN

13,000 LB GROSS WEIGHT

$i_n = 90^\circ$

40 KNOTS SIDEWAYS

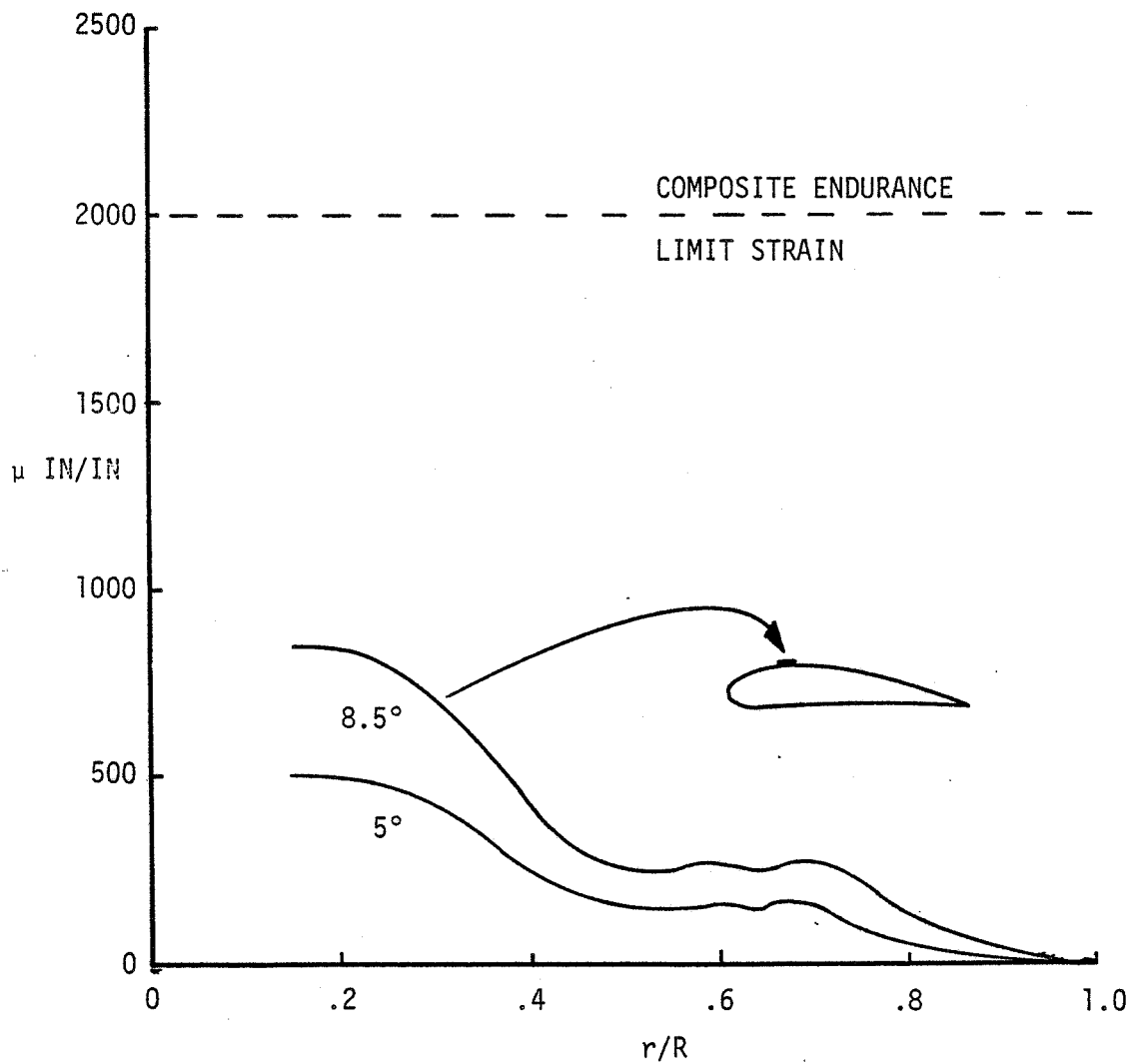


FIGURE 3.2.6. STRAIN DISTRIBUTION - 40 KNOTS SIDEWAYS HELICOPTER FLIGHT

shows the calculated bending moments in the beam and chord-wise directions, and Figure 3.2.4 shows the distribution of strain in the upper skin at the point of maximum strain. It is noted that the strain does not anywhere approach the endurance limit in the extreme flight condition.

#### 40 Knots Sideways Flight

This is a particularly severe sustained flight condition because the rotor not only provides moments to trim in pitch, but must also provide the yawing moment to maintain direction. At 13,000 lb. gross weight with the C.G. at the forward limit, the control requirement to trim results in  $4.5^\circ$  of gimbal angle. At 40 knots sideways, approximately full pedal travel is required to hold direction so that an additional  $4^\circ$  of differential gimbal angle is imposed. This results in loads equivalent to  $8.5^\circ$  of gimbal displacement on the more severely loaded rotor.

Figure 3.2.5 shows the distribution of flap and chord bending moment in low speed helicopter flight for a nominal gimbal angle of  $5^\circ$ . Figure 3.2.6 shows the strain distribution which results from this bending moment distribution, and the distribution estimated for  $8.5^\circ$  of gimbal flapping. Here again, comfortable margins are in evidence over the outer sections of the blade.

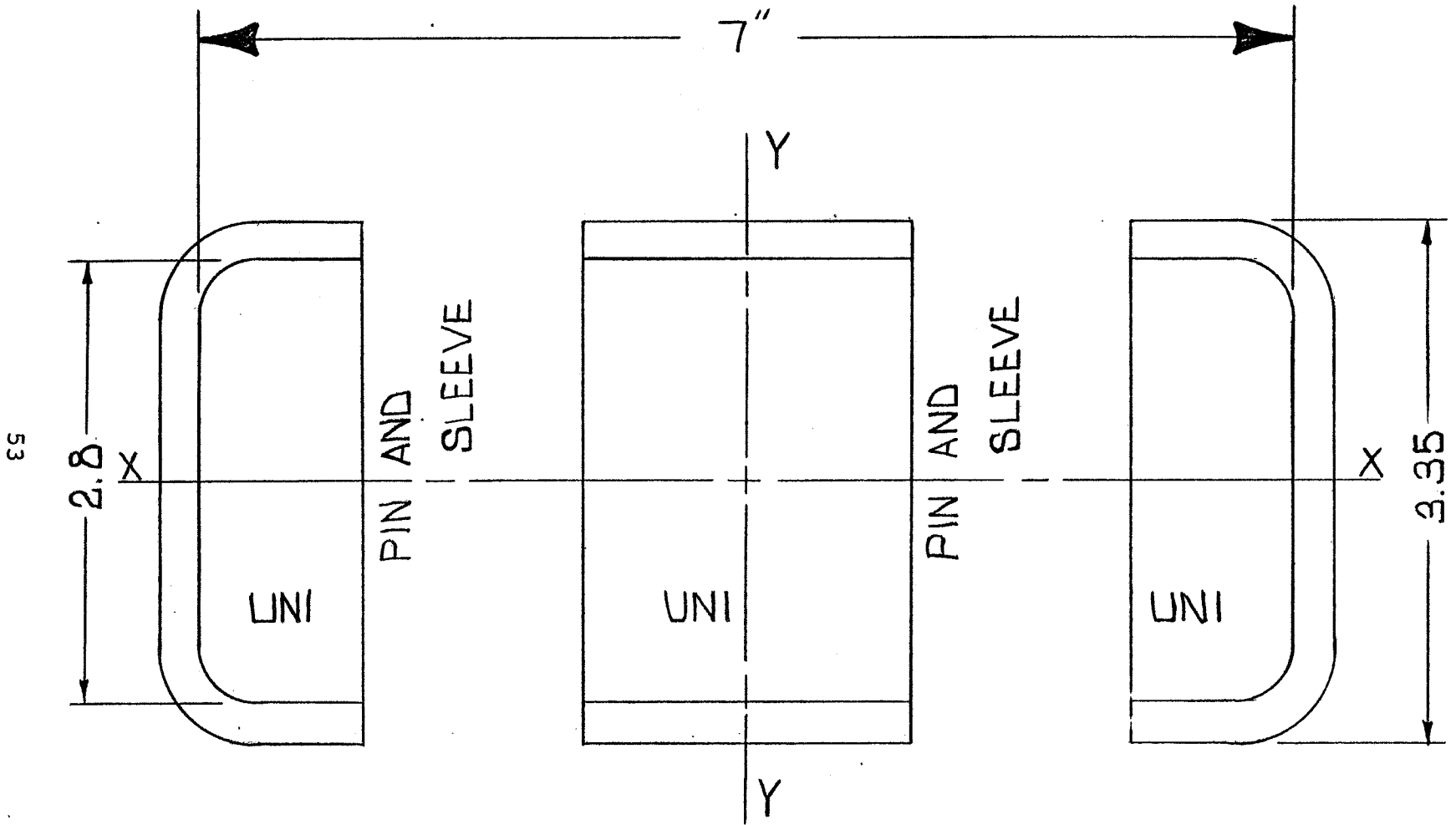


FIGURE 3.27 SKETCH OF SECTION THROUGH PIN RETENTION WRAPAROUND.



### 3.2.2. Strains at Pin Retention

Figure 3.2.7 is a sketch of section through the retention pins as illustrated in SK28304, Sheet 3 (see Section 4).

The section properties are:

$$EI_{\text{flap}} = 150.5 \times 10^6$$

$$EI_{\text{chord}} = 1030.0 \times 10^6$$

For a nominal gimballed condition of  $5^\circ$  flapping moments at the pin station are:

$$M_F = 38,000 \text{ in. lb.}$$

$$M_C = 38,750 \text{ in. lb.}$$

The strains at the surface of the outer torsion wrap would therefore be

$$\epsilon_f = \frac{38,000 \times 1.675}{150.5 \times 10^6} = 423 \mu \text{ in/in}$$

$$\epsilon_c = \frac{38,750 \times 3.5}{1030 \times 10^6} = 132 \mu \text{ in/in}$$

$$\text{Corner strain} = 555 \mu \text{ in/in}$$

Assuming a stress concentration factor of 2.0, this becomes

$$1110 \mu \text{ in/in}$$

For an  $8.5^\circ$  gimballed angle, this scales to  $1887 \mu \text{ in/in}$

Thus the endurance limit shown is not exceeded even at the very severe condition of sideways flight at the limit of directional pedal control with the C.G. at the most forward position. In the above calculation, the modulus of graphite has been used. If it were decided to use uniglass instead of graphite, the strain level would increase by a factor of approximately 3, and this would necessitate resizing to provide additional flap

moment of area. However, it is also noted that more endurance limit exceedances would be acceptable in fiberglass and no difficulty is envisioned in achieving a satisfactory design within a similar envelope.

### 3.2.3 Spindle Fatigue Strength

The titanium main rotor yoke spindle is the other initial component which must be evaluated at this stage. Fatigue testing established an endurance limit stress of 30,000 psi at the critical section. (Source: Bell Helicopter Company Report No. 301-199-003).

The oscillatory bending moments for the worst sustained flight condition are quoted as  $M_{\text{BEAM}} = \pm 16,500$  in-lb and  $M_{\text{CHORD}} = \pm 44,000$  in-lb. These loads resulted in a resultant oscillatory stress of  $\pm 10,800$  psi which was well below the endurance limit for the spindle.

Boeing Vertol estimates higher loads at the critical section (6% radius); these are partly due to blade differences but some increase comes from the continued rise in bending moment inboard of 10% radius where Bell assumes a constant level of bending moment.

At 120 knots in the helicopter mode, the bending moments in plane and out of plane at 6% radius are estimated to be:

$\pm 12,000$  out of plane

$\pm 58,000$  in plane

The resultant oscillatory stress is:

$$10800 \times \left\{ \frac{58^2 + 12^2}{44^2 + 16.5^2} \right\}^{\frac{1}{2}} \text{ psi} = \pm 13612 \text{ psi}$$

In 40 knots sideways flight, the stresses are higher and are caused by oscillatory bending moments.

$$103,360 = 60,800 \times \frac{8.5}{5.0} \text{ in plane}$$

$$14,960 = 8,800 \times \frac{8.5}{5.0} \text{ out of plane}$$

Hence, resultant stress equals

$$10,800 \times \left\{ \frac{103^2 + 14.8^2}{44^2 + 16.5^2} \right\}^{\frac{1}{2}} = 10,800 \times 2.215 = 23,918 \text{ psi}$$

Thus, in this case, we estimate that the spindle stresses approach 80% of the endurance limit stress.

#### 3.2.4 Strength Conclusions

It is seen that endurance limits are not exceeded at the very severe conditions selected for examination. Hence, we can deduce that satisfactory fatigue life conditions exist even at this very preliminary stage of design, and that detailed evaluation may permit reduction of structural weight in the final design while still providing 3600 hours of life.

### 3.3 Dynamic and Aeroelastic Behavior

Since the rotor hub configuration remains the same, or in the case of a replacement hub steps are taken to ensure the same kinematic and dynamic properties, we would not expect any major changes in the dynamics of the aircraft. Changes in blade mass and stiffness distributions were, however, expected to cause frequency shifts relative to the basic XV-15 blades. Also, these changes, along with the redistribution of spanwise thrust loading, were expected to have an effect on blade deflections under flight loads which would in turn modify the pitch-lag and pitch-flap coupling which is a determining factor on high-speed aeroelastic stability.

#### 3.3.1 Frequencies

Figure 3.3.1 shows collective and cyclic mode blade frequencies over the range of operating rpm and collective pitch. In detail design, we would attempt to tune the first collective mode away from  $2p$ . This would also reduce the frequency of the first cyclic mode which is also slightly higher than the current XV-15 equivalent.

It is, therefore, concluded that we have acceptable blade frequency characteristics at this preliminary design stage.

#### 3.3.2 Aeroelastic Stability

The aeroelastic stability of the aircraft with the replacement composite blades installed was investigated using advanced aeroelastic methodology developed at AMES Research Center (Reference NASA TN D 8515). This indicated that instability occurs at

X<sub>2</sub> CANDIDATE BLADE FREQUENCIES

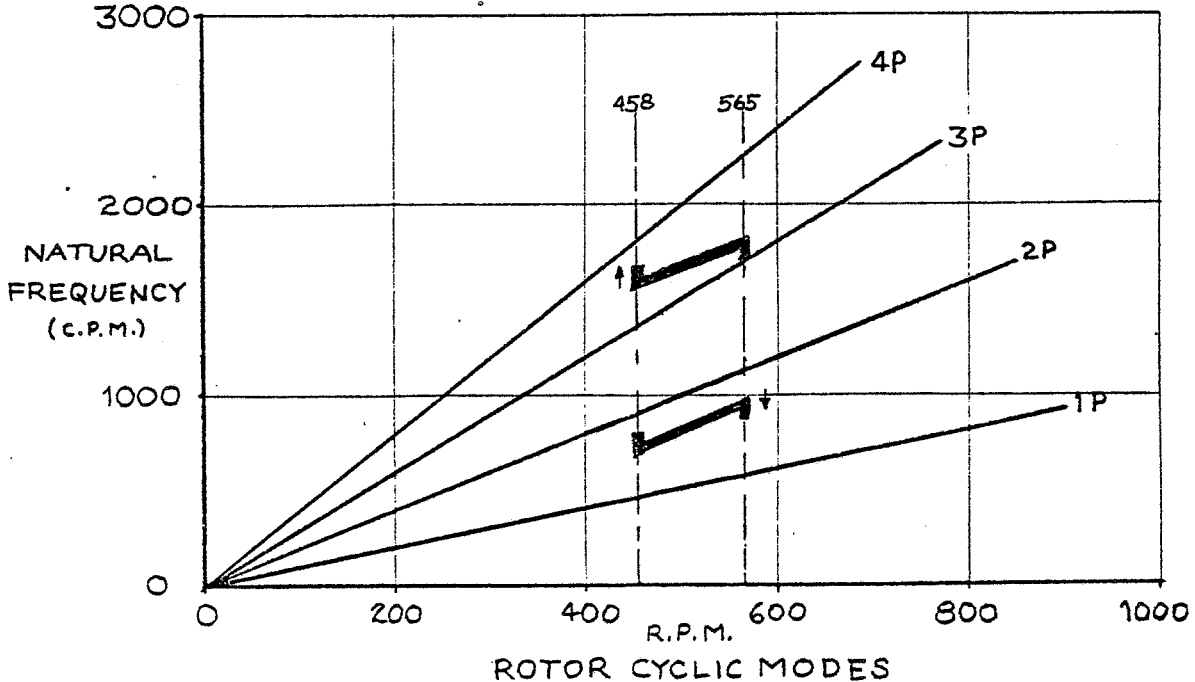
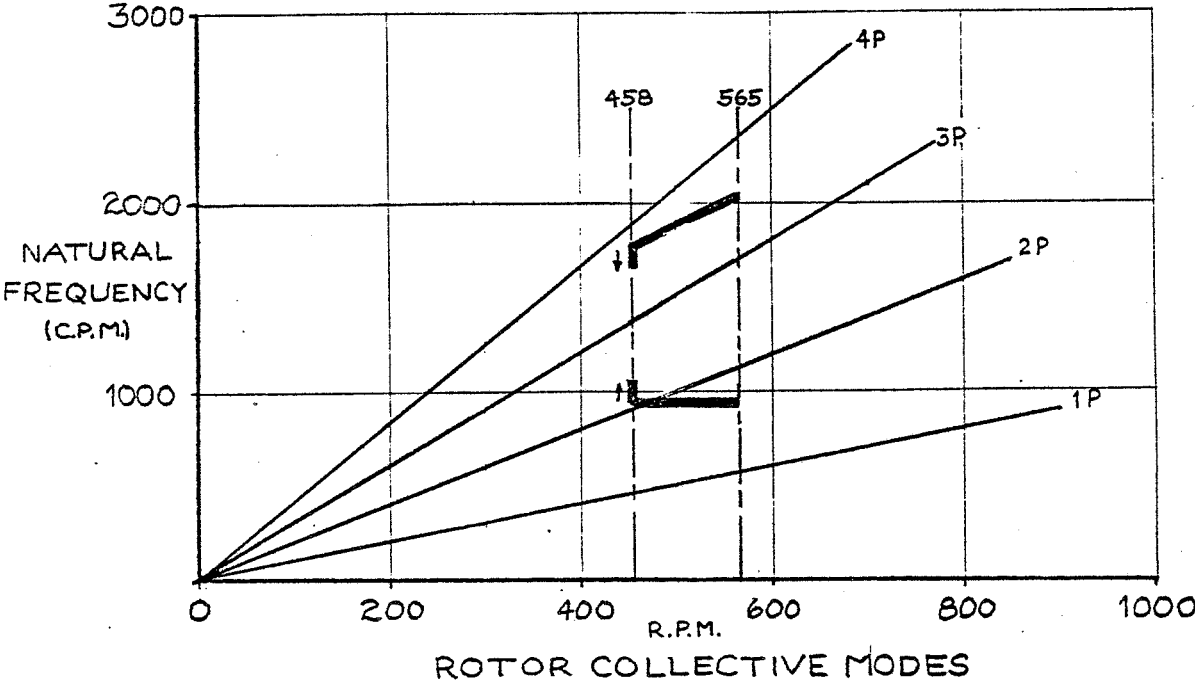


FIGURE 3.3.1. XV-15 REPLACEMENT BLADE FREQUENCIES

## XV-15 WITH COMPOSITE REPLACEMENT BLADE

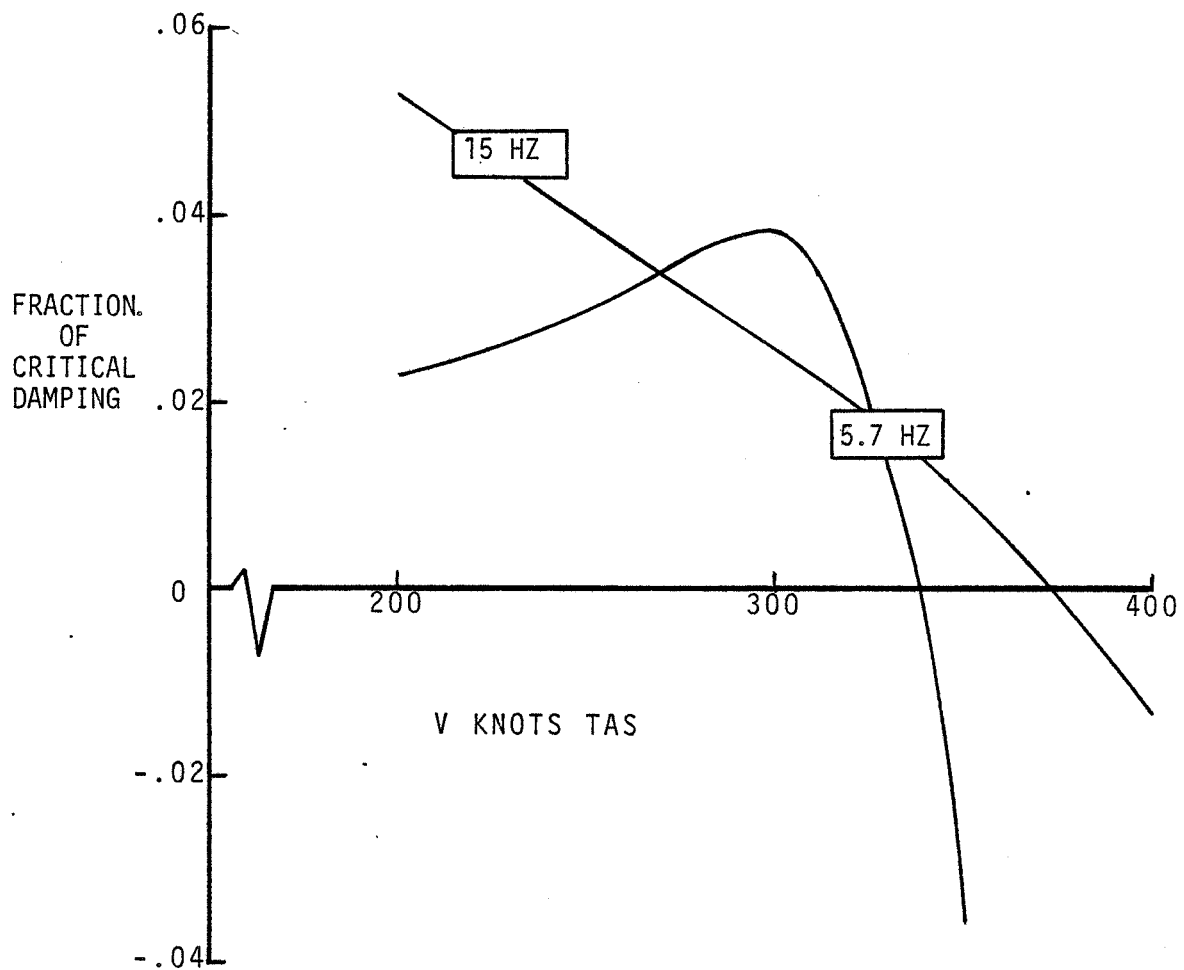
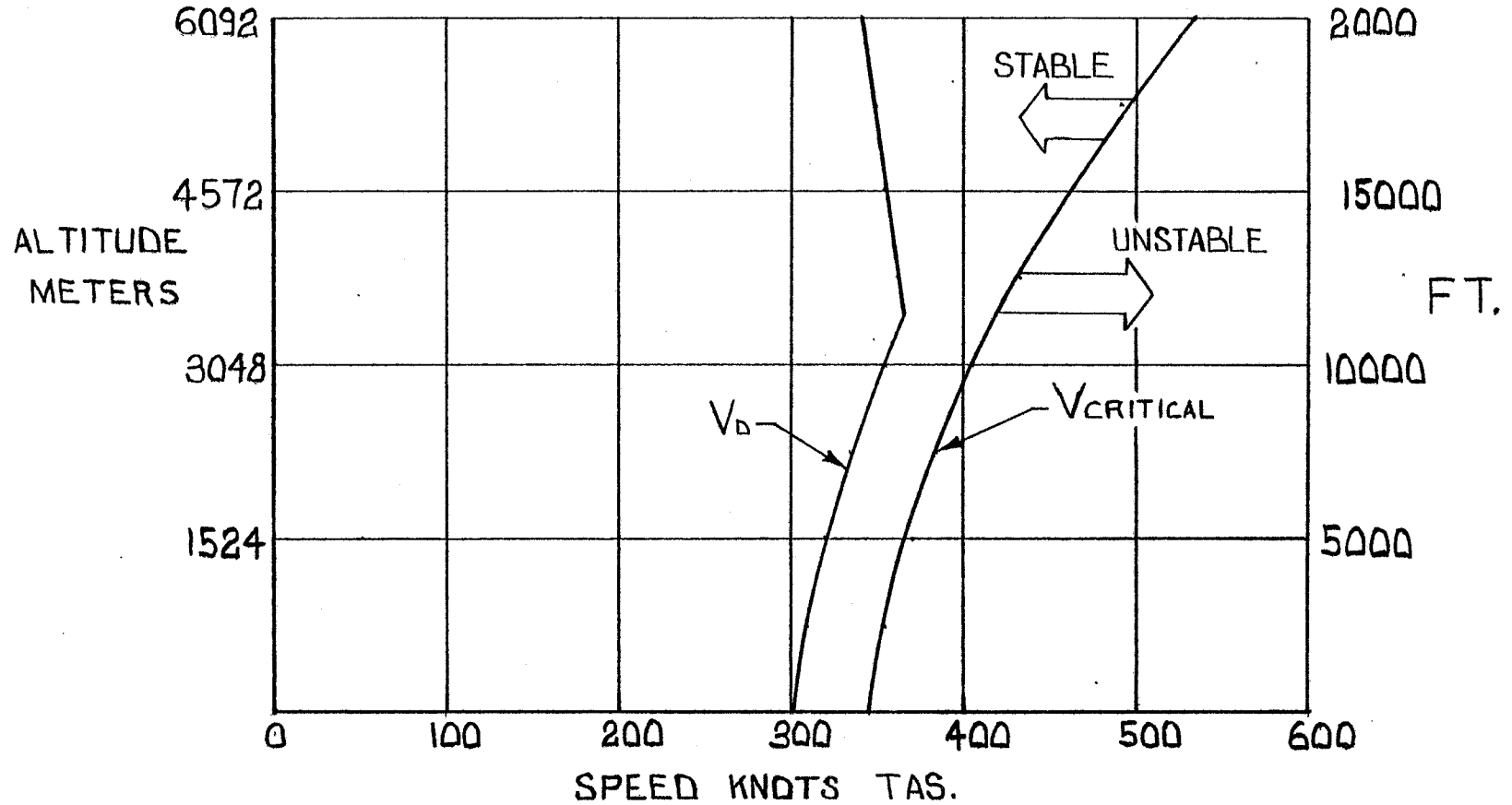


FIGURE 3.3.2. VARIATION OF DAMPING WITH AIRSPEED IN CRITICAL MODES

# XV15 AIRCRAFT AEROELASTIC STABILITY WITH X2 REPLACEMENT BLADE

GROSS WEIGHT = 13000 LB

458 RPM



60

FIG. 3.3.3 VARIATION OF FLUTTER SPEED AND DESIGN DIVE SPEEDS WITH ALTITUDE.

XV-15 WITH COMPOSITE REPLACEMENT BLADE

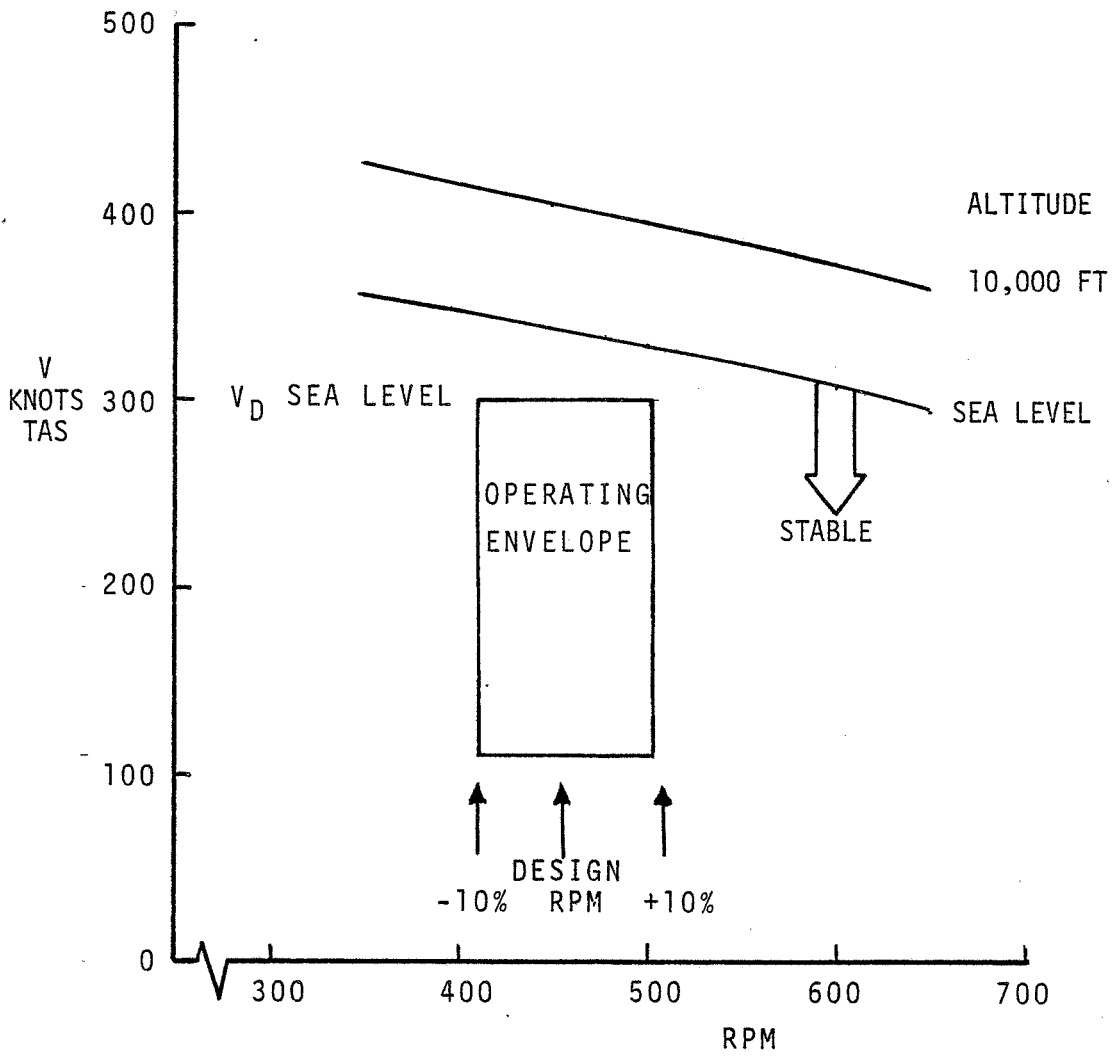


FIGURE 3.3.4. VARIATION OF CRITICAL SPEED WITH RPM



XV-15 WITH COMPOSITE REPLACEMENT BLADE

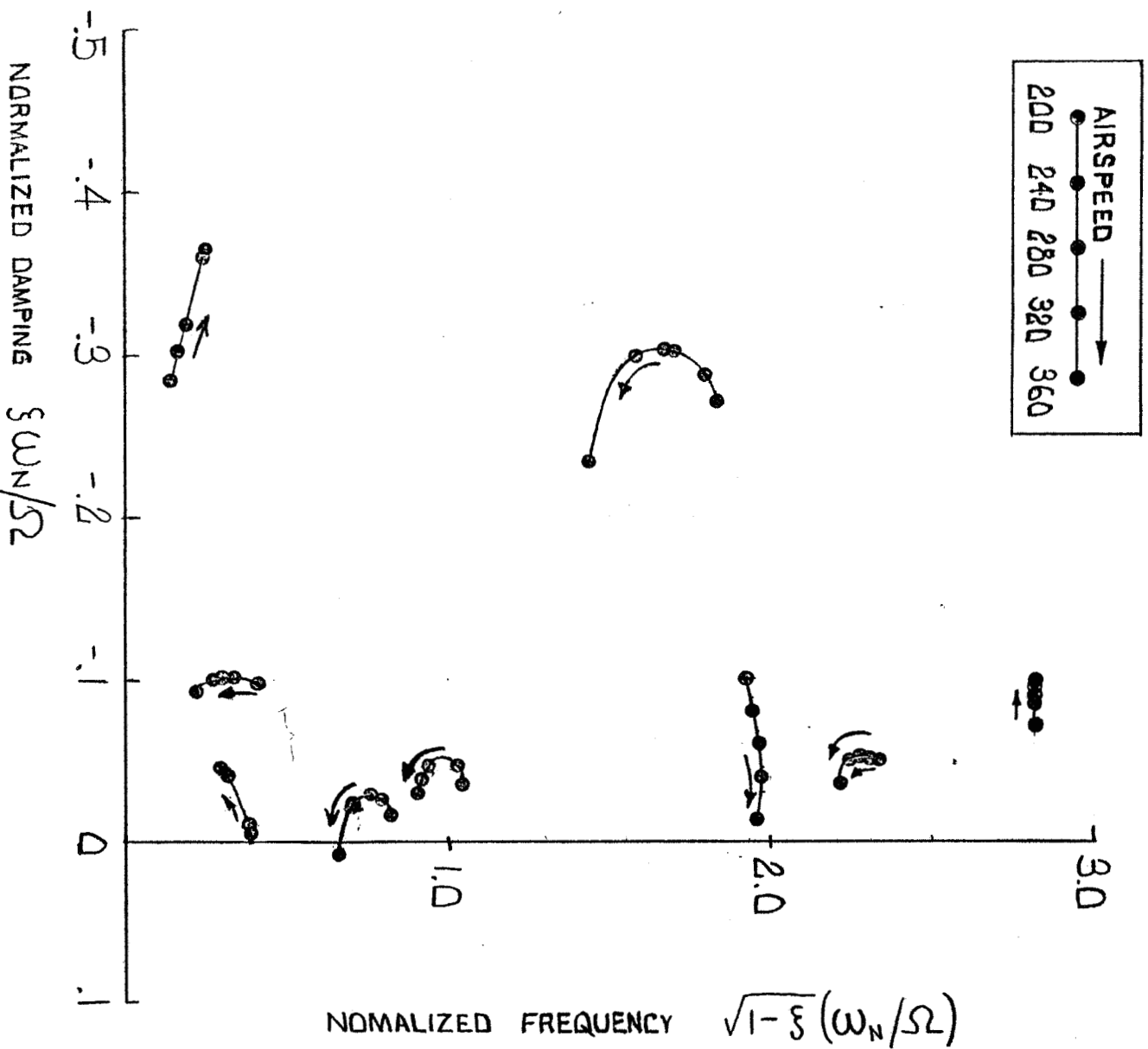


FIGURE 3.3.5 ROOT LOCI FOR XV-15 WITH COMPOSITE REPLACEMENT BLADE.

338 knots at sea level, in a mode associated with wing chord bending. The variation of damping with airspeed is shown in Figure 3.3.2 and the relation of critical speed and  $V_D$  over a range of altitude is shown in Figure 3.3.3. The onset of flutter occurs at  $1.15 V_D$  at sea level and the margin increases with altitude. Figure 3.3.4 shows the variation of critical speed as a function of rpm. Figure 3.3.5 is a root locus plot showing the migration of the lower frequency roots of the system as airspeed is increased incrementally from 200 knots to 500 knots. Overall a satisfactory stability situation is evident at this stage of preliminary design.

#### 4.0 PRELIMINARY DESIGN SPECIFICATIONS

##### 4.1 Blade

###### 4.1.1 Blade Design Concept

The selected blade concept is based upon Boeing Vertol state-of-the-art manufacturing techniques presently being employed in the production of CH-46 and CH-47 composite blades. This approach guarantees least program cost, least development time, and least risk. The blade geometry, presented in Figure 4.1.1 (SK 28311), has been developed to achieve the best trade between performance and cost. Figure 4.1.2 (SK 28312) illustrates the twist distribution of the contour control stations.

The blade is composed of a blade structural assembly, an inboard aerodynamic fairing cuff, a removable tip shell assembly, and incorporates a two-pin root attachment fitting/pitch change housing. Details of the root configuration of the structural assembly, installation of the root fitting/pitch change housing, and illustration of the fairing cuff are illustrated in Figure 4.1.3 (SK 28304, 6 sheets). Details of the tip configuration including the installation of tip weight fittings, weights and tip shell are illustrated in Figure 4.1.4 (SK 28279, 7 sheets).

###### 4.1.2 Erosion Protection

Leading edge erosion protection is provided as follows:

- a. Inboard end to Sta. 45 (.3R) - .03 thick polyurethane sheet with solvent activated adhesive backing.

- b. Station 45 to Station 115.95 (.773R) - .04 thick formed 6 AL-4V titanium sheet or polyurethane sheet as in a. above.
- c. Station 115.95 to Station 135 (.9R) - .04 thick formed nickel 200 (1/4 hard) sheet.
- d. Station 135 to tip - electroformed nickel cap.

Additional studies should be performed to evaluate extending the polyurethane coverage outboard in lieu of the titanium erosion caps. If the titanium is not needed to provide structural stiffness, polyurethane protection could be used out to Station 115.95 (.773R). This change would reduce the cost of tooling and blade fabrication significantly.

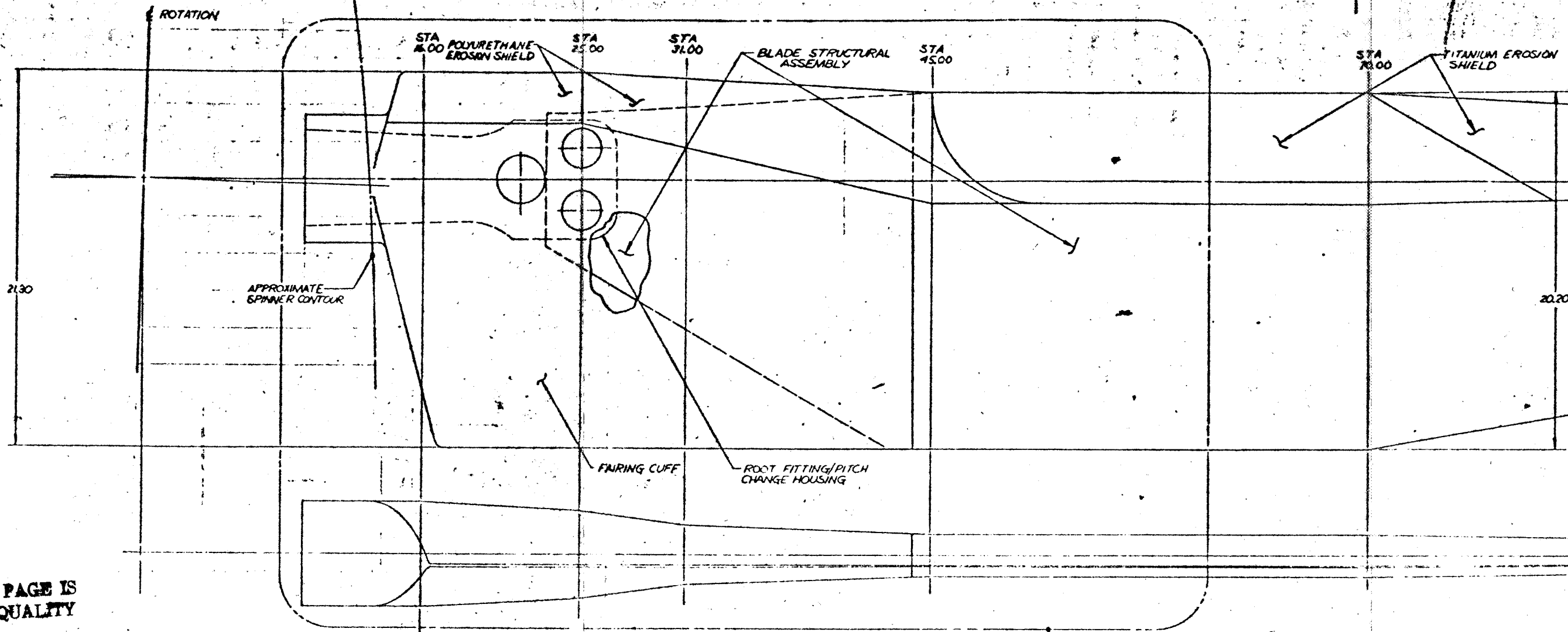
#### 4.1.3 Lightning Protection

Lightning protection will be provided in the same manner as employed on the CH-46 composite blade, illustrated in Figure 4.1.5.

#### 4.1.4 Blade Structural Assembly

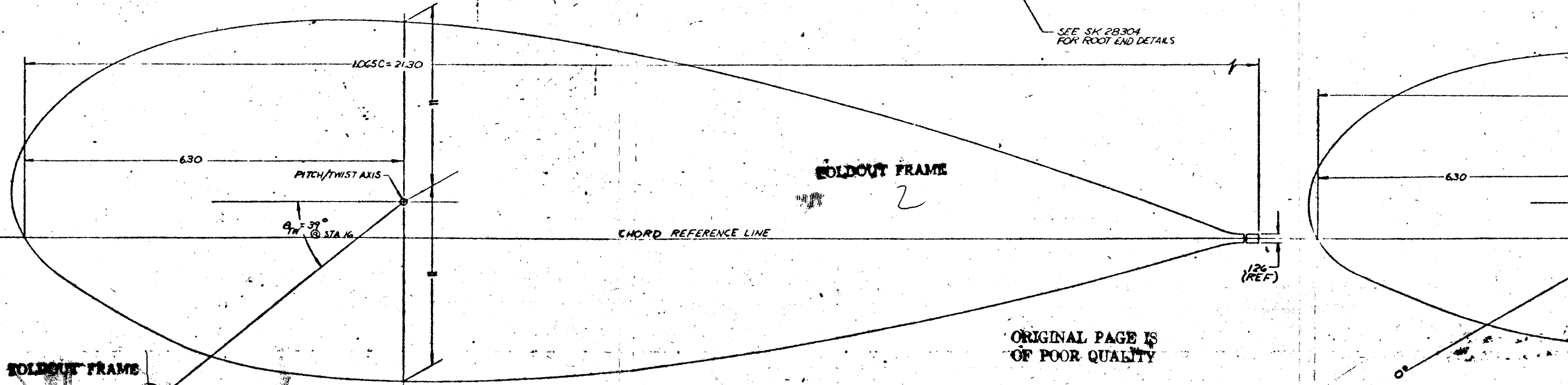
The nominal blade section (see Figure 4.1.3, Sheet 5) consists of a graphite-epoxy D-spar (unidirectional straps and fillers, bias plied outer torsion wrap), segmented balance weights, erosion caps, bias plied fiberglass-epoxy skins, Nomex honeycomb core and unidirectional fiberglass-epoxy trailing edge filler. The nominal inboard blade section (Station 45 to Station 70) was designed to match the stiffness to weight ratio of the present XV-15 blade. This required an all-graphite/epoxy spar. Additional studies should be performed to evaluate the use of fiberglass in lieu of graphite or a mix of graphite and fiberglass. Figure 4.1.6 illustrates a cross section of the

12 11 10 9 8



ORIGINAL PAGE IS OF POOR QUALITY

SEE SK 28304 FOR ROOT END DETAILS



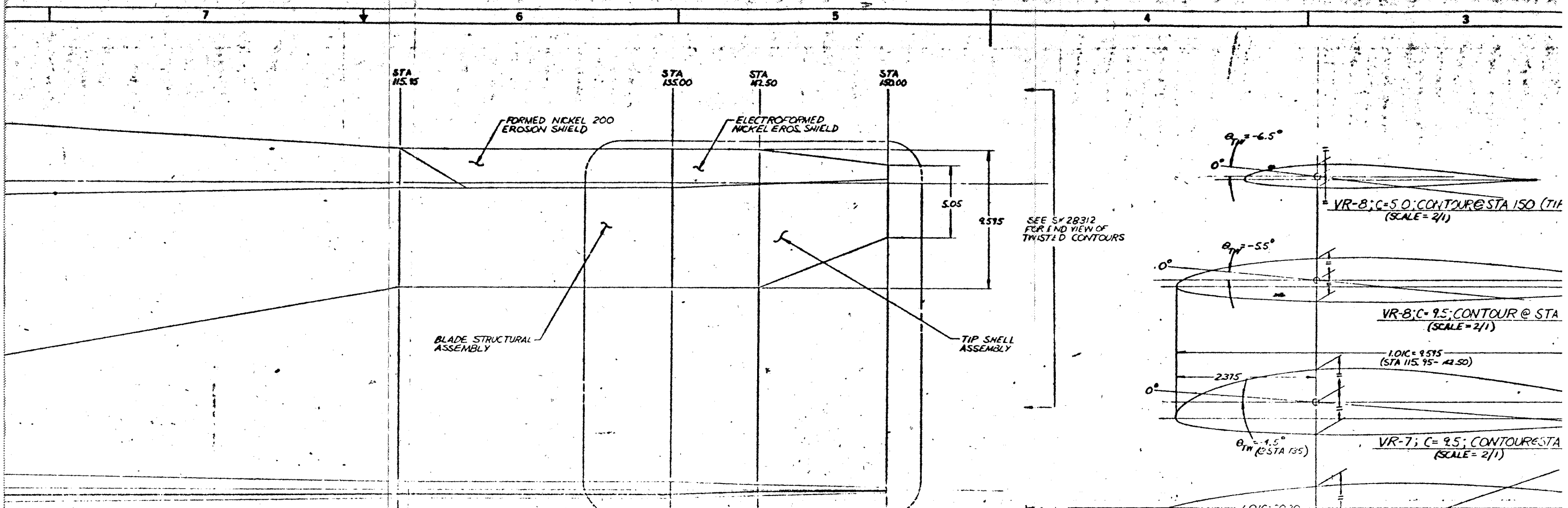
FOLDOUT FRAME

ORIGINAL PAGE IS OF POOR QUALITY

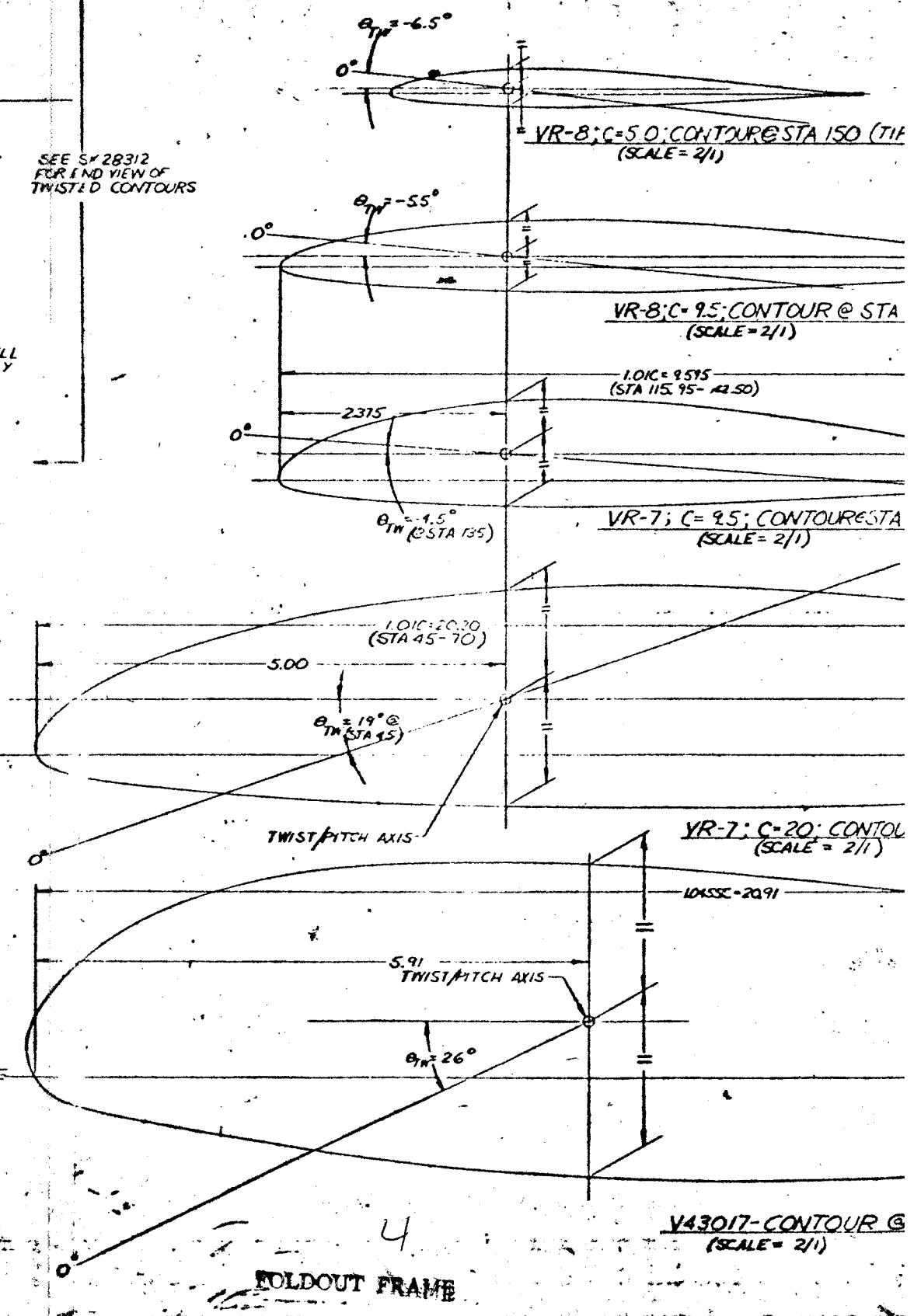
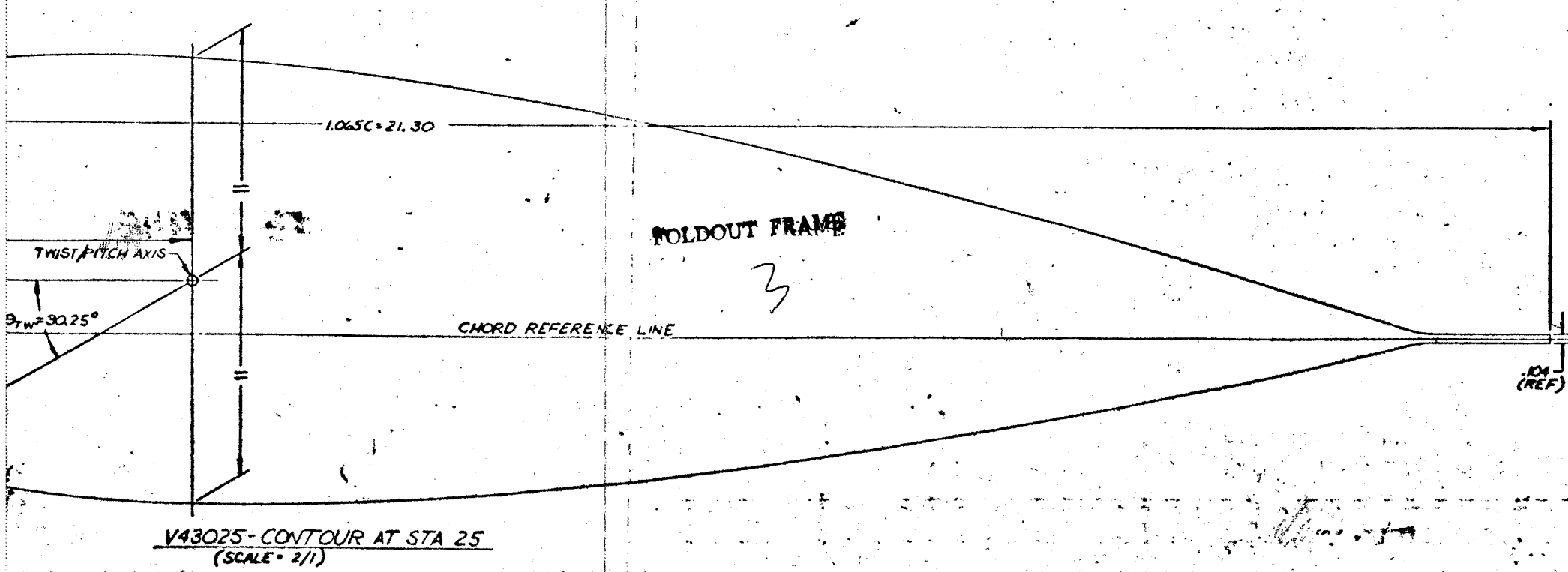
V43030 - CONTOUR @ STA. 16 (SCALE = 2/1)

SK28311

10 9 8



XV-15 COMPOSITE BLADE ASSEMBLY  
 (DRAWN WITHOUT TWIST, SCALE = 1/2)



SK 28311

D210-11569-1

ORIGINAL PAGE IS  
OF POOR QUALITY

FOLDOUT FRAME

B; C=5.0; CONTOUR @ STA 150 (TIP)  
(SCALE = 2/1)

VR-8; C=9.5; CONTOUR @ STA 142.50  
(SCALE = 2/1)

1.01C = 9.515  
(STA 115.95 - 142.50)

VR-7; C=9.5; CONTOUR @ STA 115.95-135  
(SCALE = 2/1)

VR-7; C=20; CONTOUR @ STA 45-70  
(SCALE = 2/1)

104SSC-2091

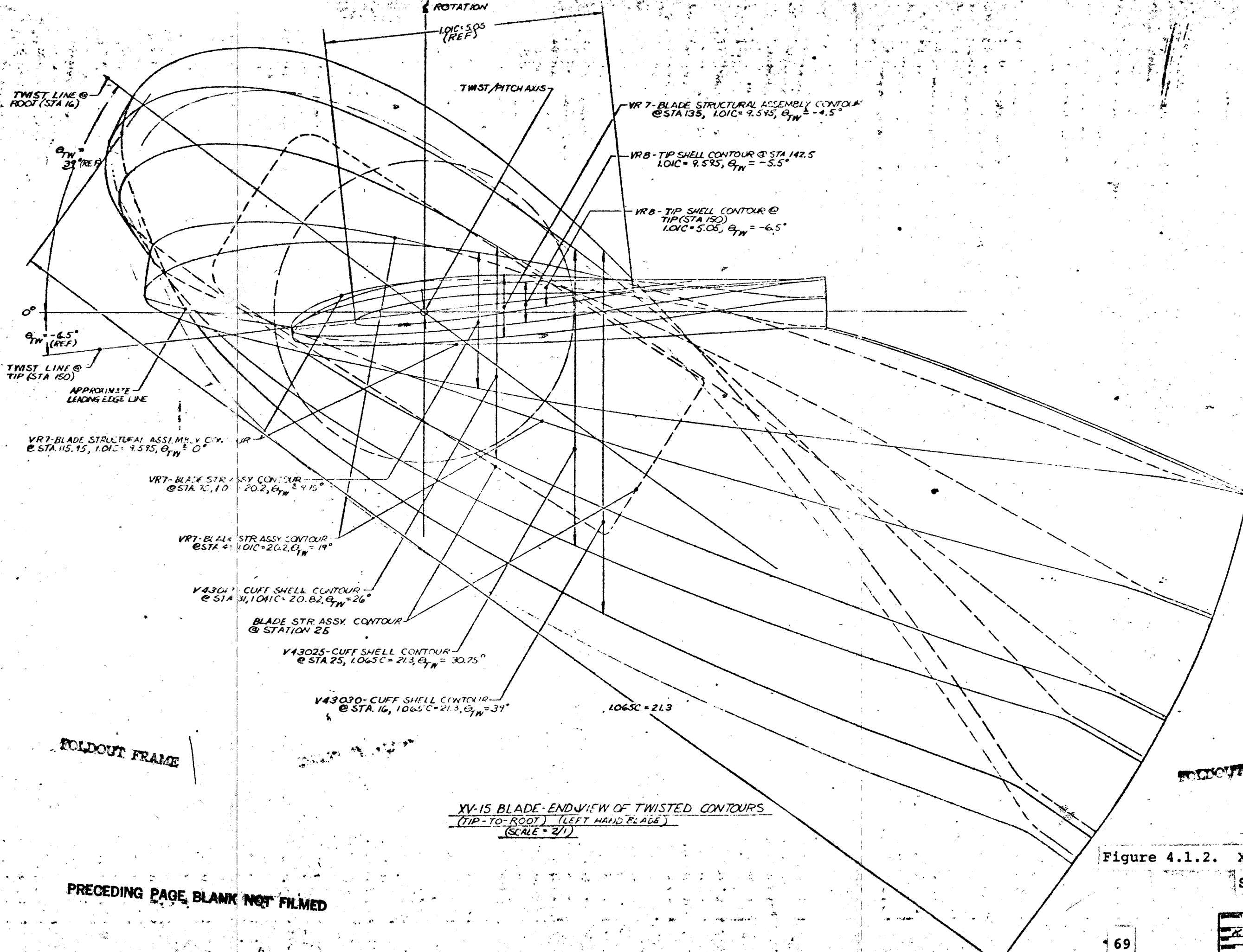
V43017-CONTOUR @ STA 31  
(SCALE = 2/1)

Figure 4.1.1. XV-15 Composite Blade

Assembly/Geometry Drawing

DATE: 12/15/87		DRAWN BY: KSM:TH		CHECKED BY:	
SCALE: 2/1	DATE: 12/15/87	DESIGN: XV-15	PROJECT: XV-15	FIG. NO: 77272	REV: SK28311
67					

D  
C  
B  
A



ORIGINAL PAGE IS OF POOR QUALITY

XV-15 BLADE-ENDVIEW OF TWISTED CONTOURS (TIP-TO-ROOT) (LEFT HAND BLADE) (SCALE = 2/1)

Figure 4.1.2. XV-15 Blade-End View of Stacked Twisted Contours

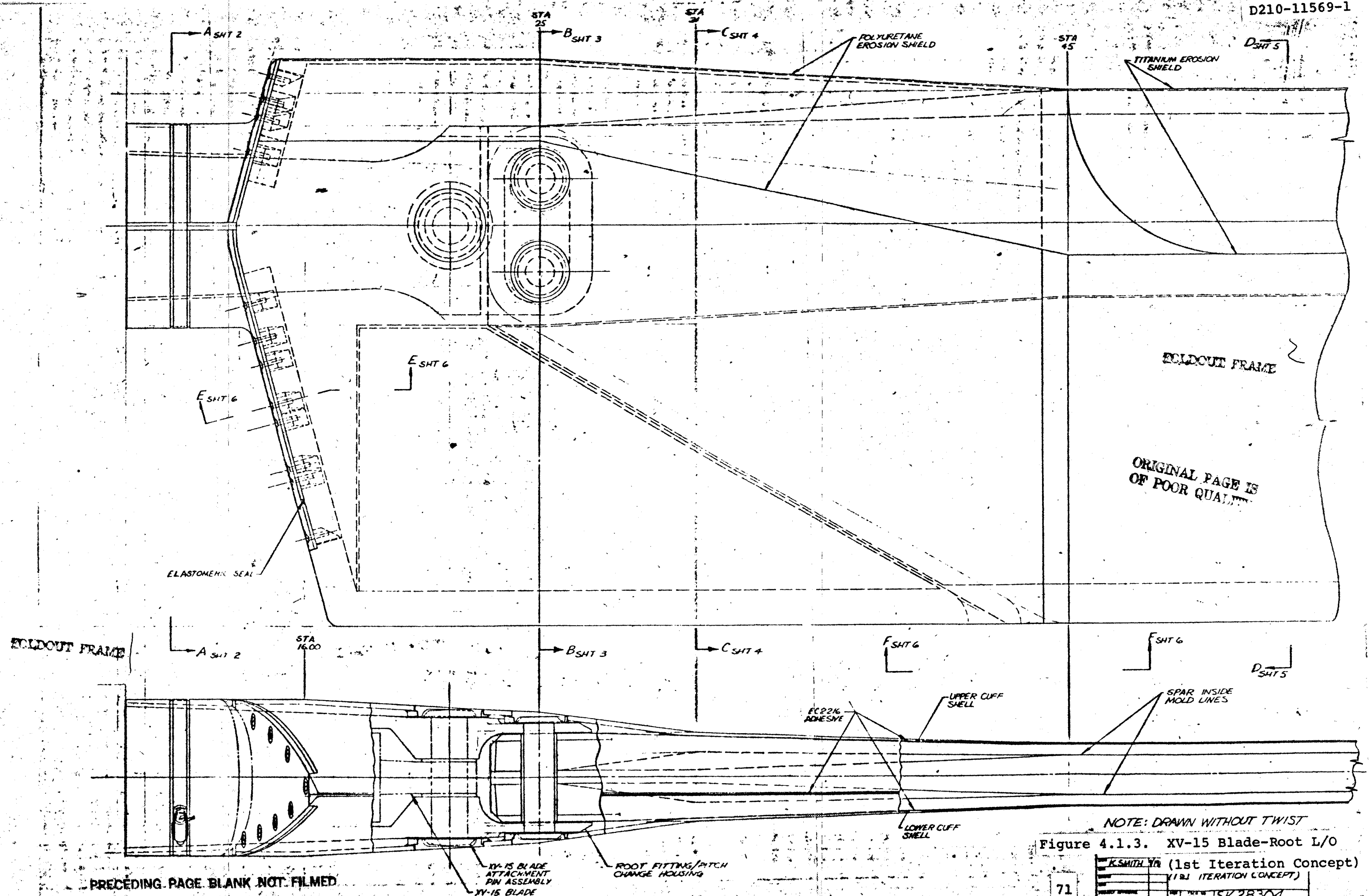
FOLDOUT FRAME

FOLDOUT FRAME

PRECEDING PAGE BLANK NOT FILMED

BOEING AIRCRAFT COMPANY	
PHILADELPHIA, PENNSYLVANIA 19134	
DESIGNED BY K. SMITH 9-4-47	PROJECT XV-15 BLADE-END VIEW OF STACKED TWISTED CONTOURS
DATE 10-1-47	BY L. K. 22310

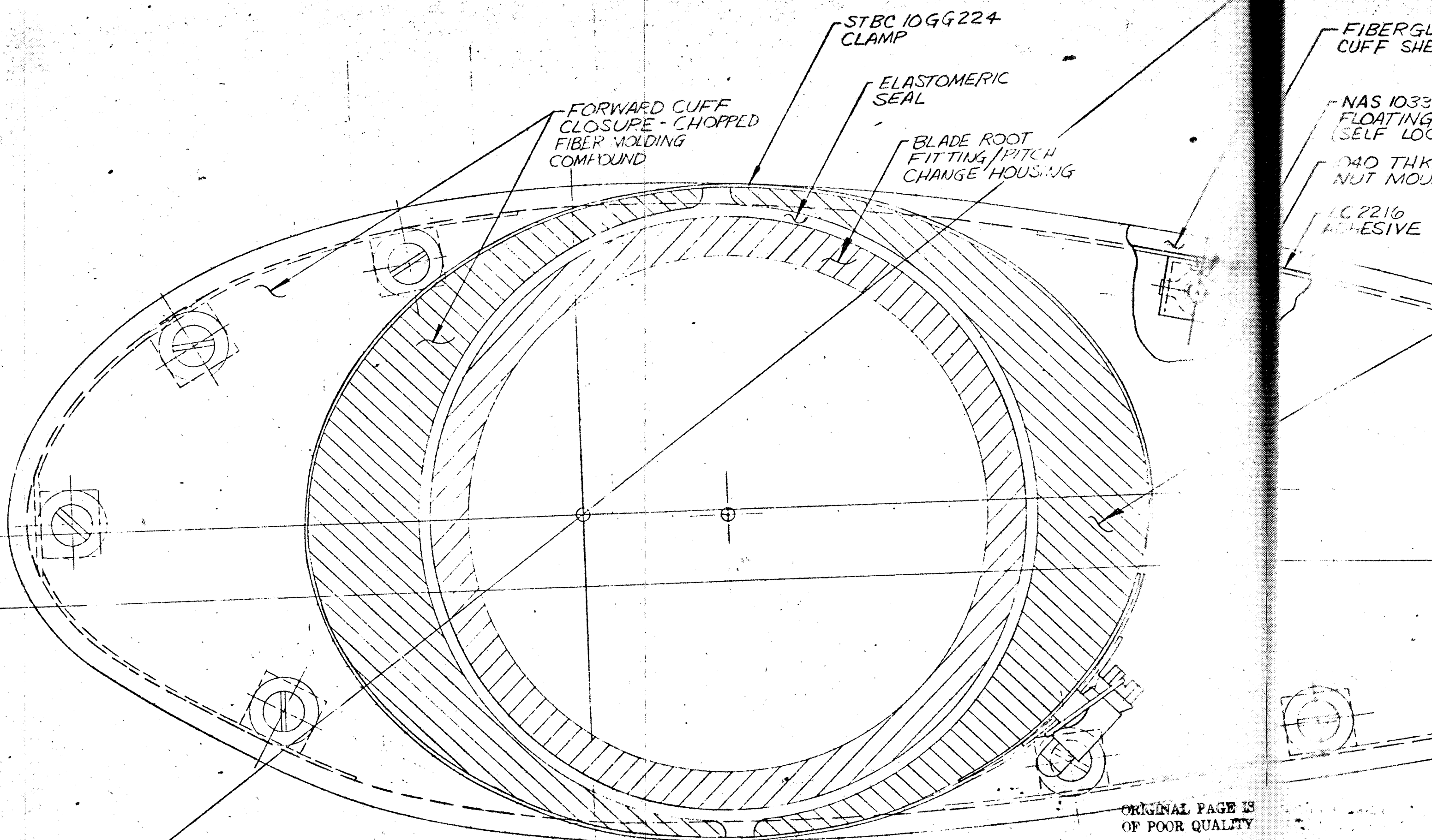




NOTE: DRAWN WITHOUT TWIST

Figure 4.1.3. XV-15 Blade-Root L/O

K. SMITH	YR	(1st Iteration Concept)
		(1st Iteration Concept)



STBC 10GG224  
CLAMP

ELASTOMERIC  
SEAL

BLADE ROOT  
FITTING/PITCH  
CHANGE HOUSING

FORWARD CUFF  
CLOSURE - CHOPPED  
FIBER MOLDING  
COMPOUND

FIBERGLASS  
CUFF SHELL

NAS 10330  
FLOATING  
SELF LOCKING

040 THK.  
NUT MOUNT

AC2216  
ADHESIVE

FOLDOUT FRAME

FOLDOUT FRAME

ORIGINAL PAGE IS  
OF POOR QUALITY

XV-15 BLADE-ROOT FITTING/PITCH CHANGE HOUSING/CUFF/CUP  
ARRANGEMENT - 1<sup>ST</sup> ITERATION: 43030  
(SCALE = 2/1)

PRECEDING PAGE BLANK NOT FILLED

FIBERGLASS  
CUFF SHELL

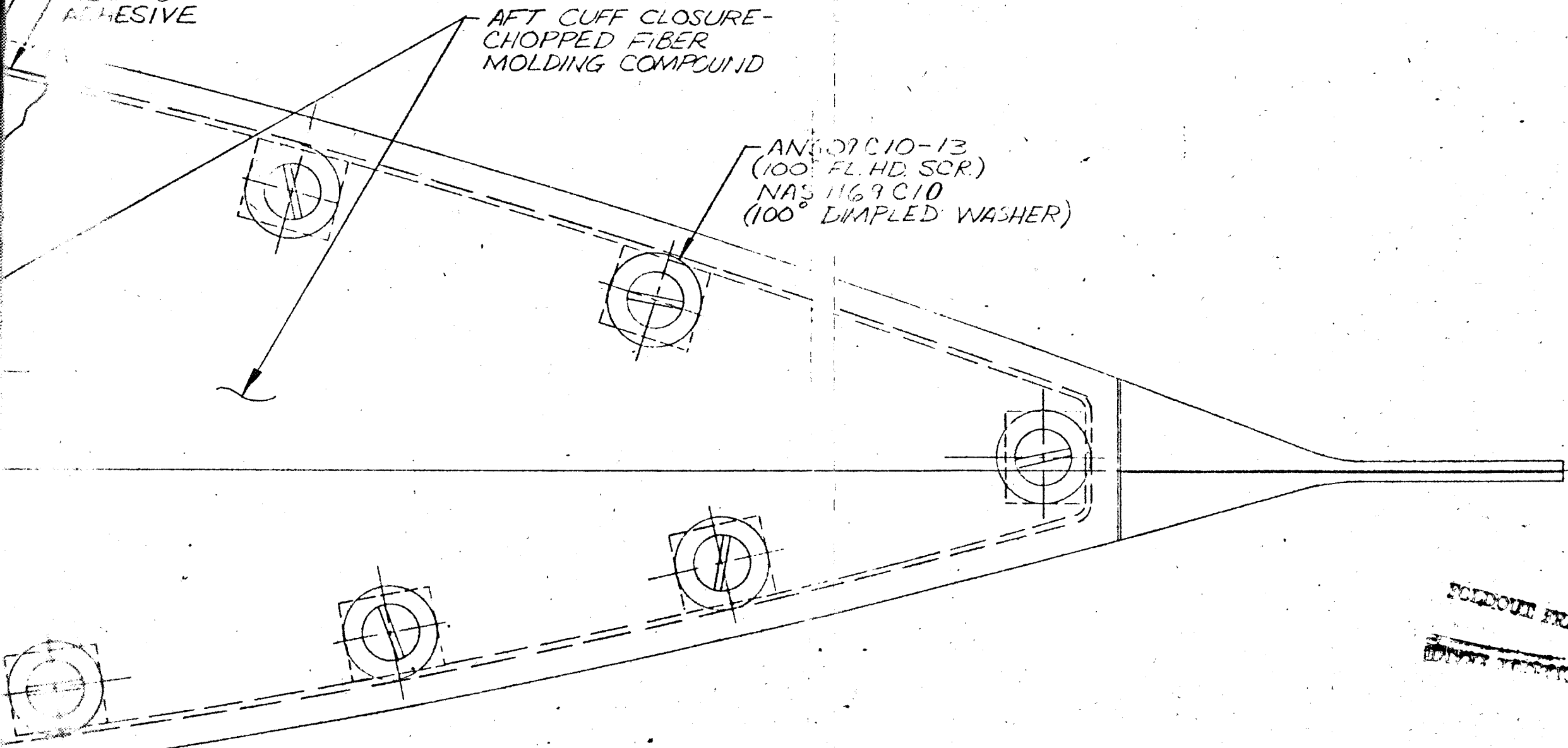
NAS 1033C3 RIGHT ANGLE  
FLOATING ANCHOR NUT  
(SELF LOCKING)

040 THK. ALUMINUM  
NUT MOUNTING STRIP

EC 2216  
ADHESIVE

AFT CUFF CLOSURE-  
CHOPPED FIBER  
MOLDING COMPOUND

ANG 07C10-13  
(100 FL. HD. SCR.)  
NAS 1169C10  
(100° DIMPLED WASHER)



FOLDOUT FRAME

~~DATE~~

FOLDOUT FRAME 3

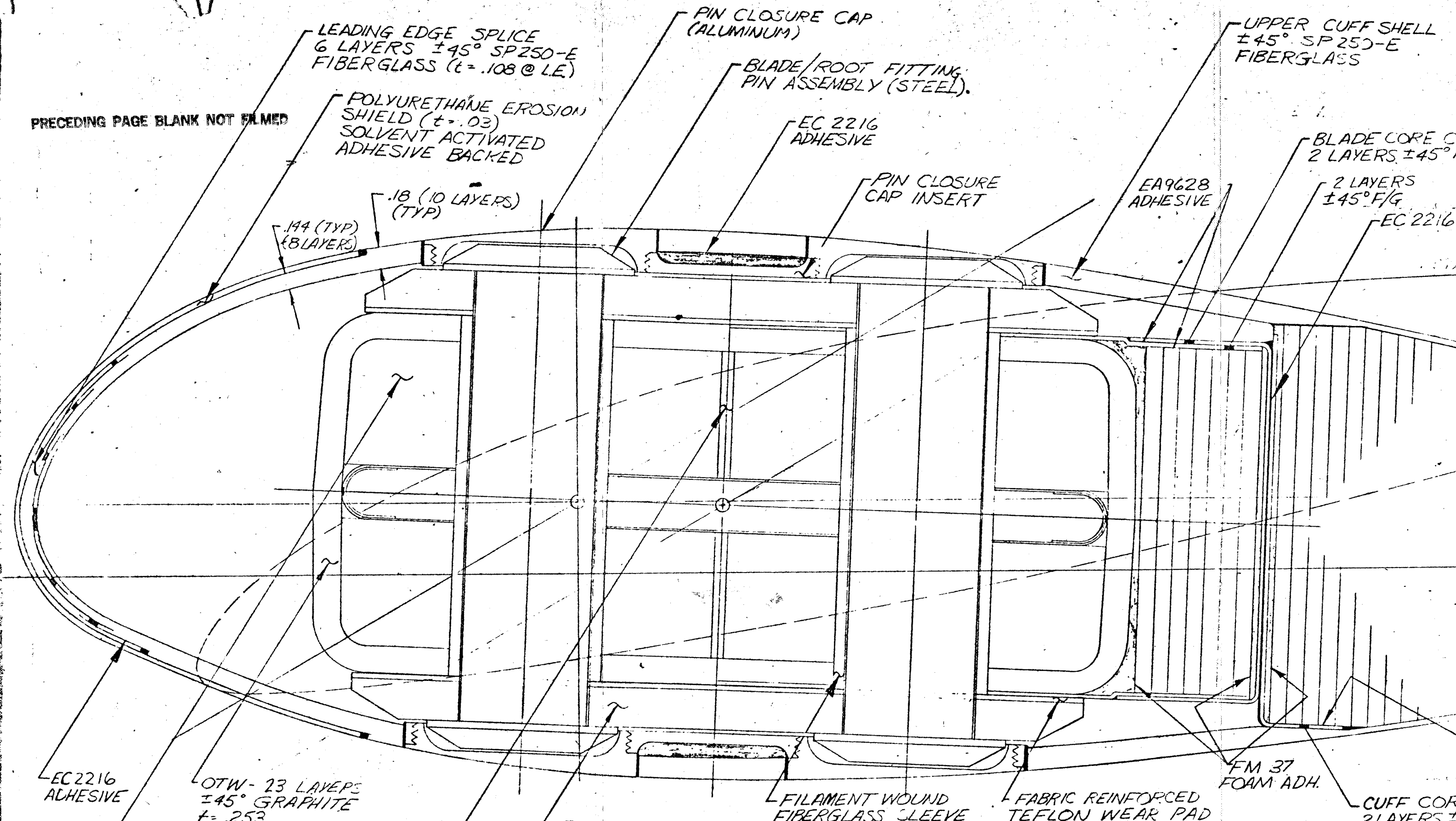
ORIGINAL PAGE IS  
OF QUALITY

SECTION A-A

CUFF/CUFF CLOSURE  
43030, C-20

SK 28304  
SHEET 2 OF 6

Figure 4.1.3 (continued)



PRECEDING PAGE BLANK NOT FILMED

XV-15 BLADE - ROOT END/FITTING/CUFF  
ARRANGEMENT - 1 ST. ITERATION

V43025, C=20, STA. 25

(SCALE = 2/1)

ROOT FRAME

ORIGINAL PAGE IS  
 OF POOR QUALITY

ROOT FRAME

2

UPPER CUFF SHELL  
±45° SP 250-E  
FIBERGLASS

BLADE CONTOUR  
@ STA. 45 (VR-7)

BLADE CORE CLOSURE  
2 LAYERS ±45° F/G

2 LAYERS  
±45° F/G

EC 2216 ADHESIVE

2 PCF NOMEX CORE

EC2216  
ADHESIVE

.036 (2 LAYERS)  
(TYP)

EA 9628  
ADHESIVE

FM 37  
FOAM ADH.

CUFF CORE RIB  
2 LAYERS, ±45° F/G (t=.036)

LOWER CUFF SHELL

FITTING/CUFF  
SECTION

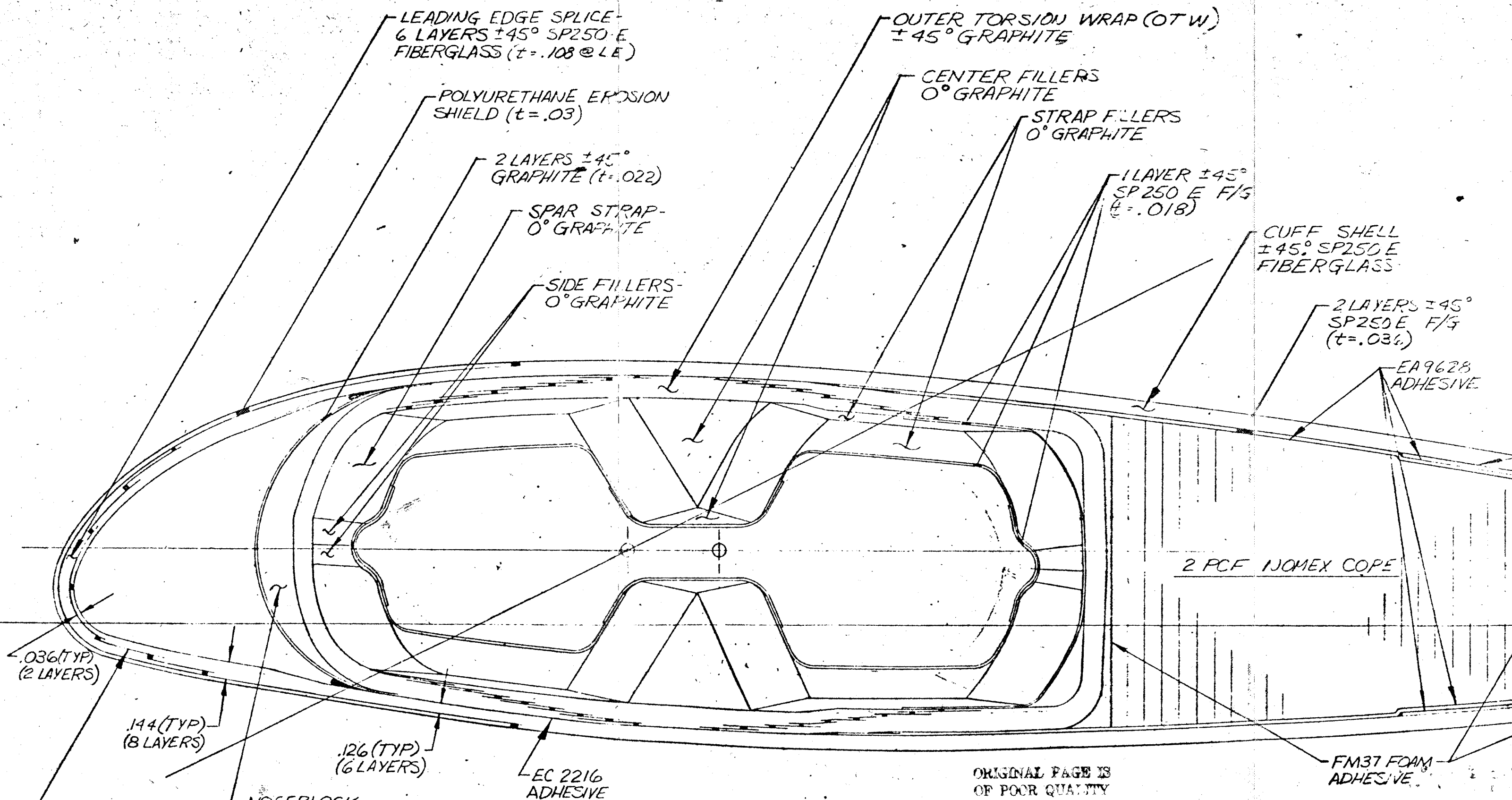
SECTION B-B

FOLDOUT FRAME

FOLDOUT FRAME

SK 28304 Figure 4.1.3 (continued)

SHEET 3 OF 6



XV-15 BLADE - SPAR ROOT TRANSITION/CUFF  
 ARRANGEMENT - 1<sup>ST</sup> ITERATION  
 V43017, C=20, STA. 31  
 (SCALE = 2/1)

PRECEDING PAGE BLANK NOT FILMED

FOLDOUT FRAME

FOLDOUT FRAME 2

ORIGINAL PAGE IS  
 OF POOR QUALITY

CUFF SHELL  
± 45° SP250 E  
FIBERGLASS

2 LAYERS ± 45°  
SP250 E F/G  
(t=.034)

EA9628  
ADHESIVE

EC2216  
ADHESIVE

NOMEX CORE

2 PCF NOMEX CORE

FM37 FOAM  
ADHESIVE

EA9628  
ADHESIVE

.036 (TYP)  
(2 LAYERS)

4  
FOLDOUT FRAME

SECTION C-C

SK 28304  
SHEET 4 OF 6

Figure 4.1.3 (continued)

FOLDOUT FRAME 3



18.7 EOP CORE & TE FILLER

1 LAYER EA 9628  
ADHESIVE (.045 PSF)

2 PCF NOMEX CORE

.073

-3°

1 LAYER ±45° SP250E  
t=.018

2 LAYERS ±45° SP250E  
t=.036

3 PLIES 0° SP250E  
t=.027

23 PLIES 0° GRAPHITE  
t=.127

1 LAYER ±45° SP250E  
t=.018

ORIGINAL PAGE IS  
OF POOR QUALITY

PRECEDING PAGE BLANK NOT FILMED

WALLOUT FRAME

2

NOMINAL XV-15  
BLADE SECTION (.3R - .45R)  
(1ST ITERATION)  
(SCALE = 2/1)

WALLOUT FRAME



20.20 = 1.01 C

14.00 = .7 C

6.20

.040 TITANIUM  
LEADING EDGE CAP

OTW - 8 LAYERS  
±45° GRAPHITE  
t = .088

1 LAYER AF-30  
ADHESIVE t = .010

NOMEX CORE

19° @ STA 45 (.3R)

0°

46 PLYS 0° GRAPHITE  
t = .253

23 PLYS 0° GRAPHITE  
t = .127

1 LAYER ±45° SP250E  
t = .018

.375 DIA STEEL  
BALANCE WEIGHT

FOLDOUT FRAME

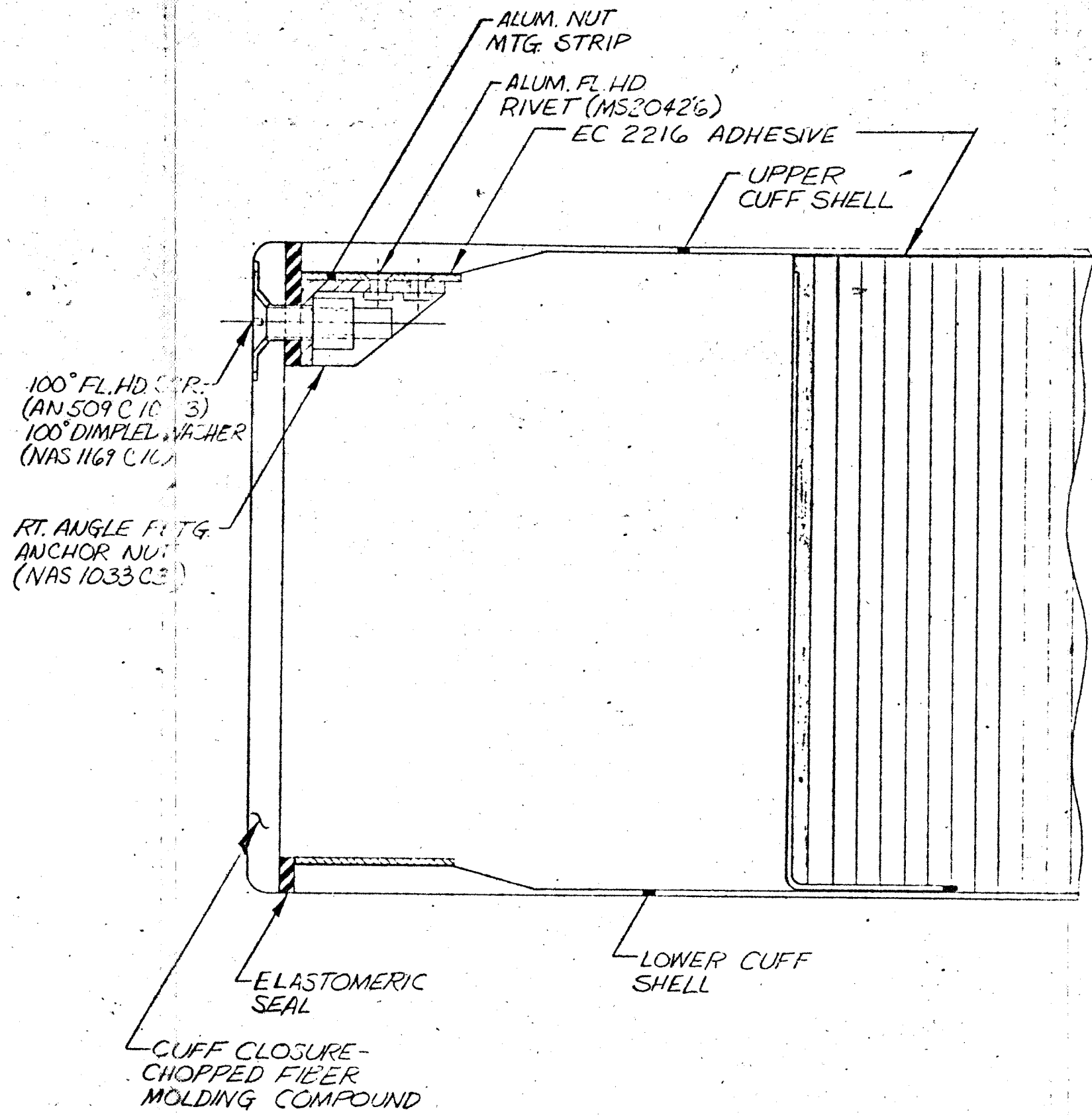
SECTION D-D

SK 28304  
SHEET 5 OF 6

MINAL XV-15  
E SECTION (.3R - .45R)  
ITERATION)

SCALE = 2/1

Figure 4.1.3 (continued)



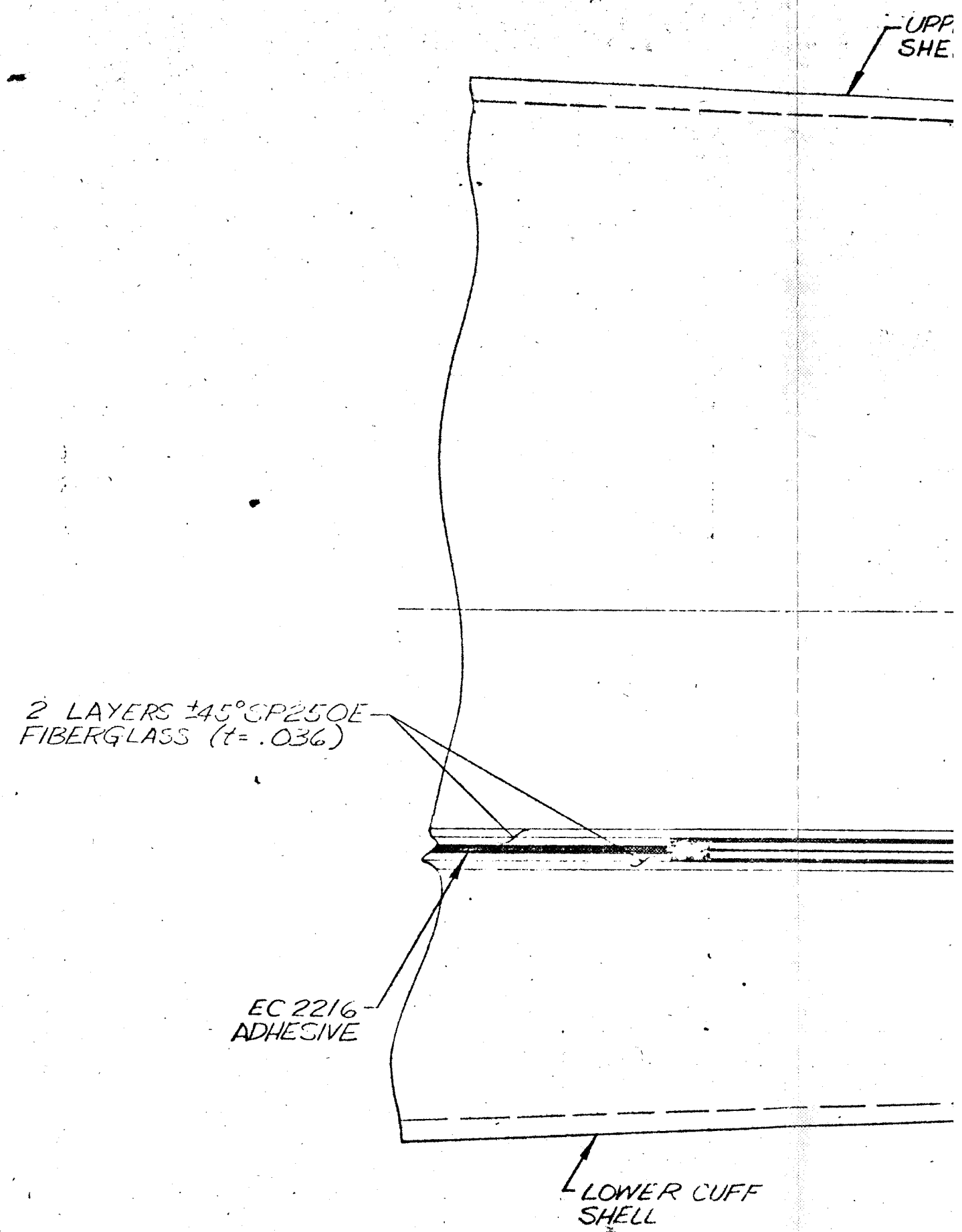
100° FL. HD S.P.R.  
(AN 509 C 10 3)  
100° DIMPLED WASHER  
(NAS 1169 C 10)

RT. ANGLE FIBER  
ANCHOR NUT  
(NAS 1033 C 3)

SECTION E-E  
(SCALE = 2/1)

PRECEDING PAGE BLANK NOT FILMED

ORIGINAL PAGE IS  
OF POOR QUALITY



2 LAYERS ±45° SP250E  
FIBERGLASS (t = .036)

EC 2216  
ADHESIVE

FOLDDOUT FRAME 2

STA  
45

UPPER CUFF  
SHELL

BLADE STRUCTURAL  
ASSEMBLY

1 LAYER  $\pm 45^\circ$  SP250 E  
FIBERGLASS (t=.018)

EA 9628  
ADHESIVE

5 PLYS  $0^\circ$  SP250 E  
FIBERGLASS T.E.  
FILLER (REF.)  
(t=.045)

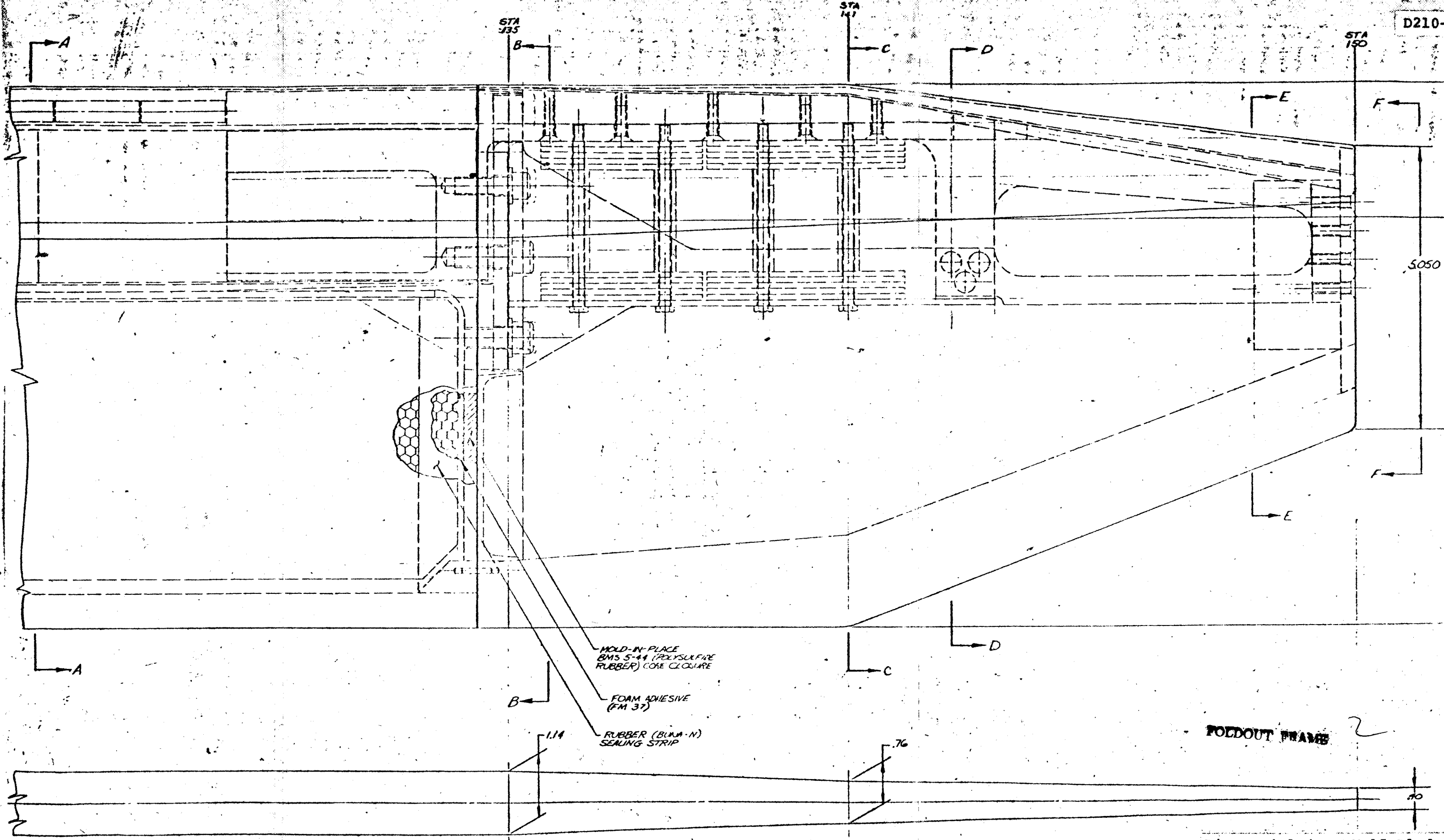
FOLDOUT FRAME 4

VIEW F-F  
(SCALE = 5/1)

EC 2216 ADHESIVE  
SQUEEZOUT FAIRED  
TO FEATHER EDGE

SK 28304  
SHEET 6 OF 6

FOLDOUT FRAME 3



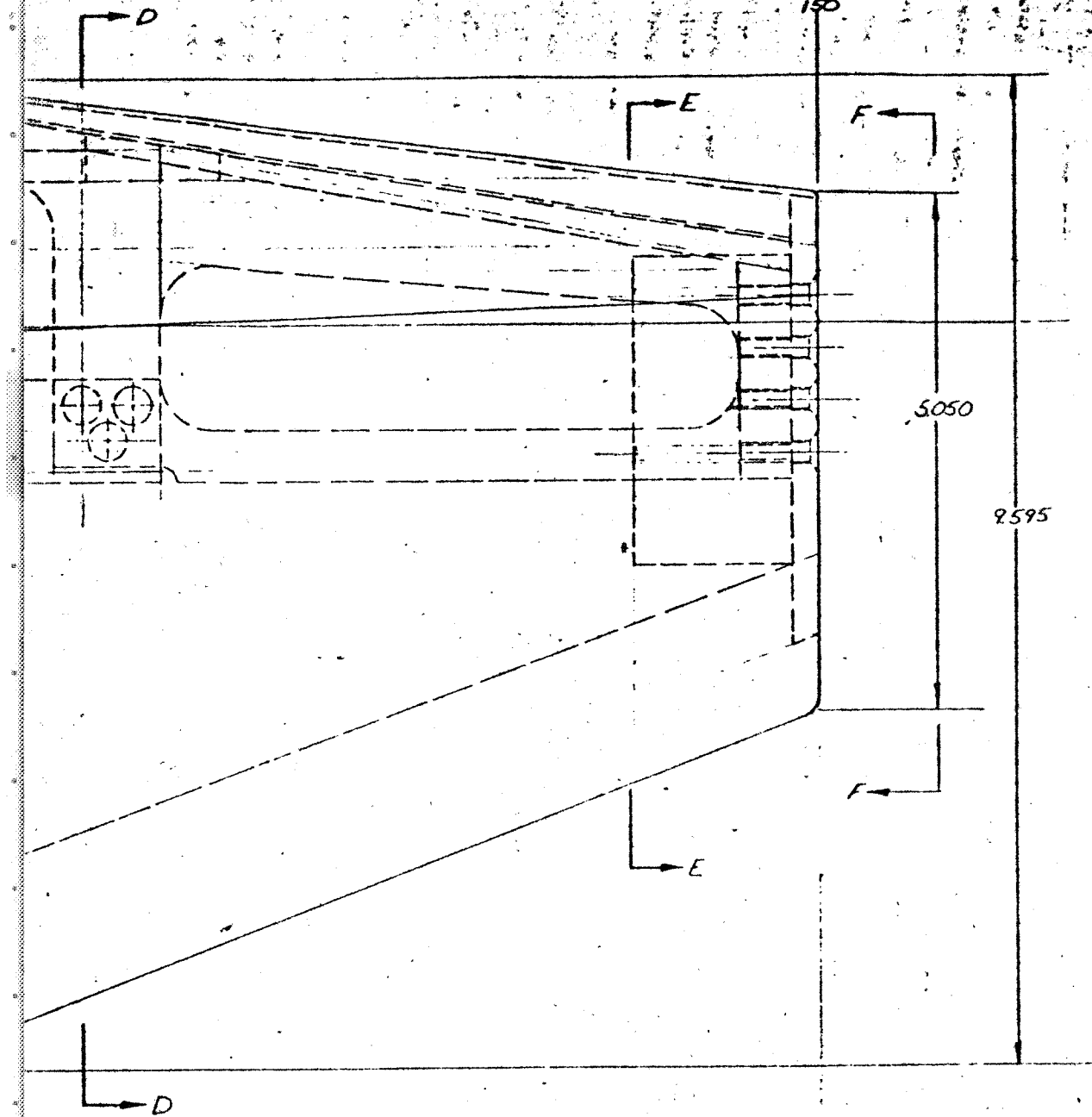
NOTE: DRAWN WITHOUT TWIST

Figure 4.1.4. XV-15 Blade (1st Iteration)

PRECEDING PAGE BLANK NOT FILMED

DESIGN COMPANY		BRUNNEN ENGINEERING COMPANY	
DESIGNER		K. Smith 4/77	
PROJECT		XV-15 BLADE - TIP LK	
ITERATION		(1st ITERATION CON)	
SCALE		1:1	
DATE		2/77	
DRAWN BY		SK 28279	

STA 150

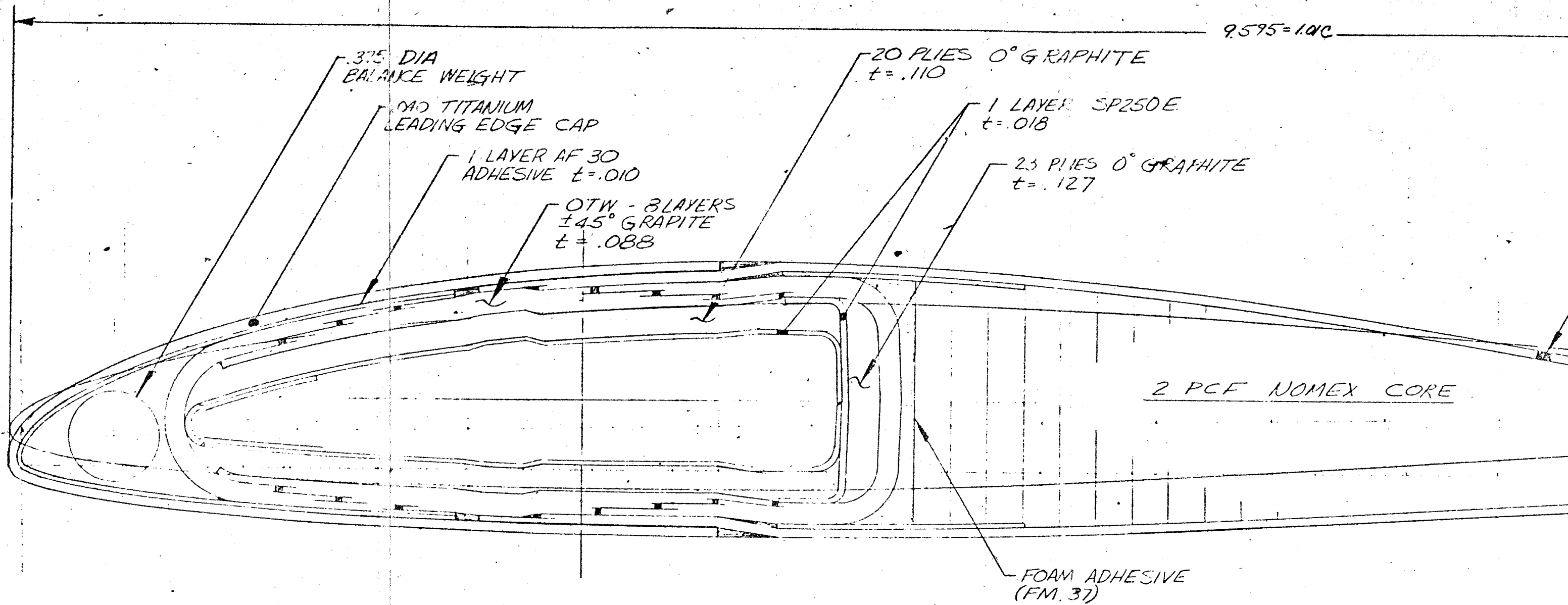


FOLDOUT FRAME

NOTE: DRAWN WITHOUT TWIST

Figure 4.1.4. XV-15 Blade-Tip L/O (1st Iteration Concept)

DESIGNER K. Smith W77		BRUNNEN COMPANY PHILADELPHIA, PENNSYLVANIA 19102	
TITLE XV-15 BLADE-TIP L/O (1st ITERATION CONCEPT)		FILE NO. SK 28279	
PROJECT NO. 21		DATE 1-77	



9.595 = 1.00

.375 DIA  
BALANCE WEIGHT

TITANIUM  
LEADING EDGE CAP

1 LAYER AF 30  
ADHESIVE t=.010

OTW - 3 LAYERS  
±45° GRAPHITE  
t=.088

20 PLYES 0° GRAPHITE  
t=.110

1 LAYER SP250E  
t=.018

23 PLYES 0° GRAPHITE  
t=.127

2 PCF NOMEX CORE

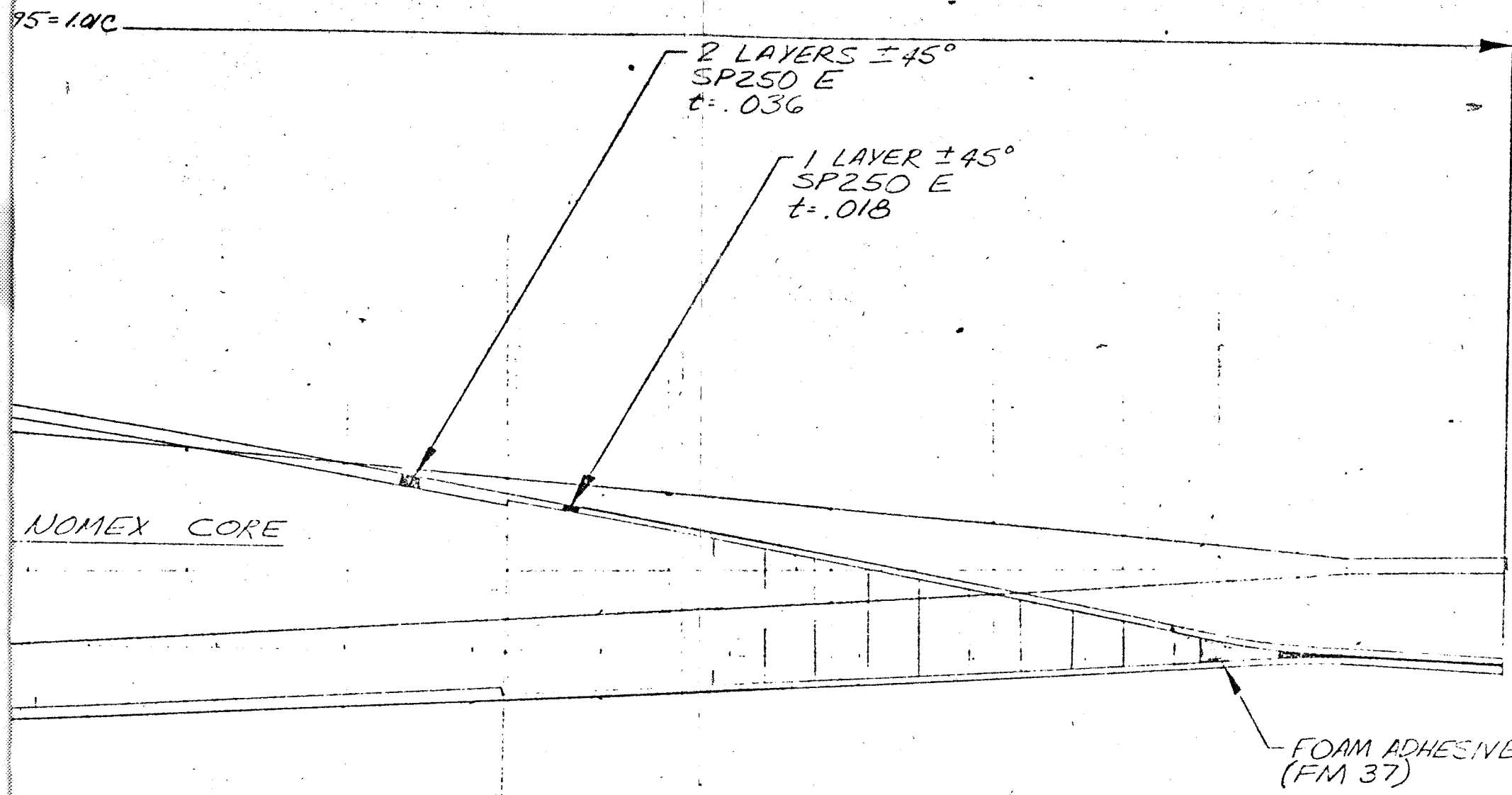
FOAM ADHESIVE  
(FM. 37)

SECTION A-A  
OUTBOARD XV-15  
BLADE SECTION (.773R-.9R)  
(1ST ITERATION)  
(SCALE = 4/1)

PRECEDING PAGE BLANK NOT FILLED

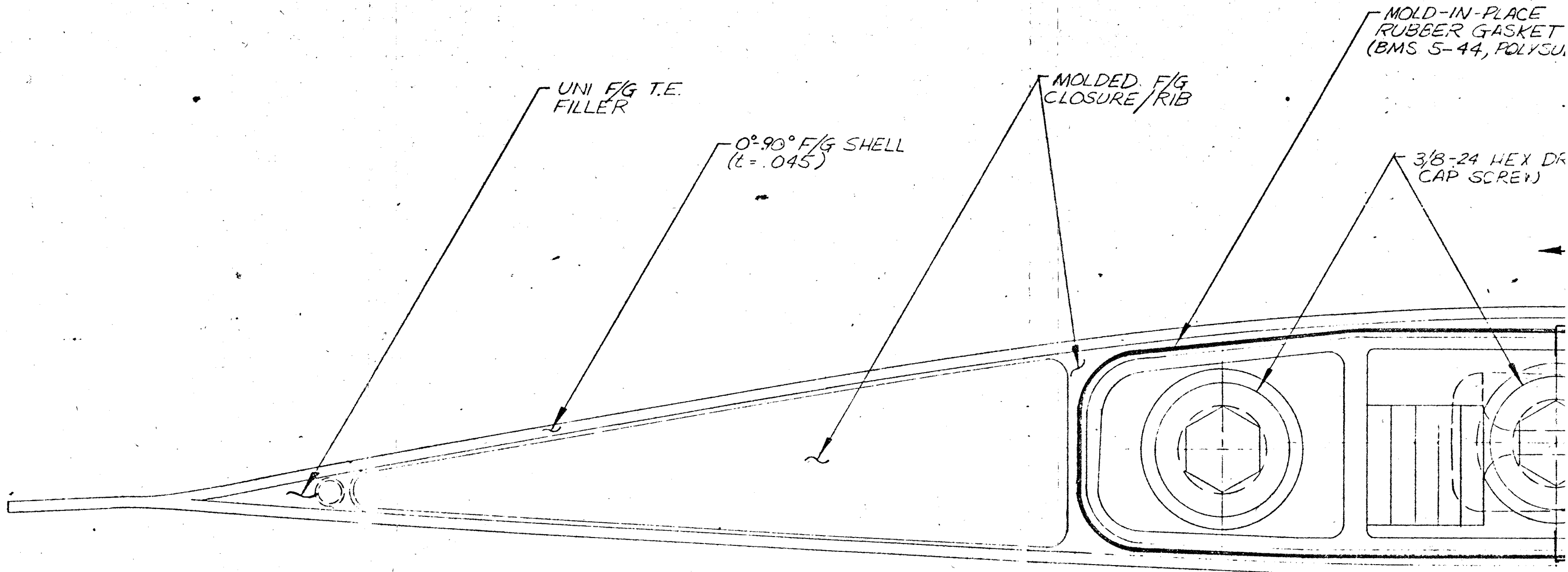
FOLDOUT FRAME

FOLDOUT FRAME



FOLDOUT FRAME

SK 28279  
SHT 2 OF 7



FOLDOUT FRAME

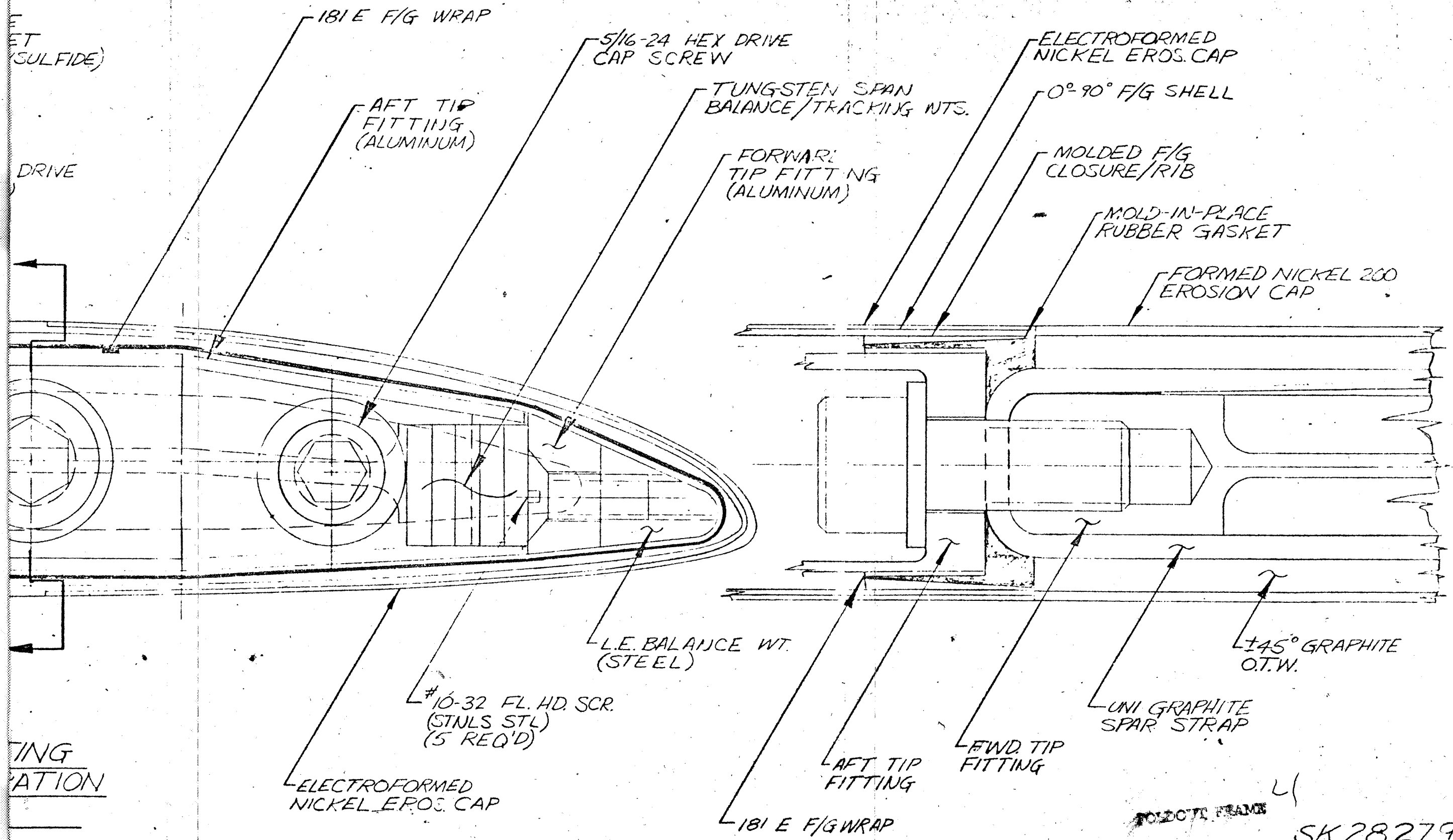
PRECEDING PAGE BLANK NOT FILMED

FOLDOUT FRAME

SECTION B-B

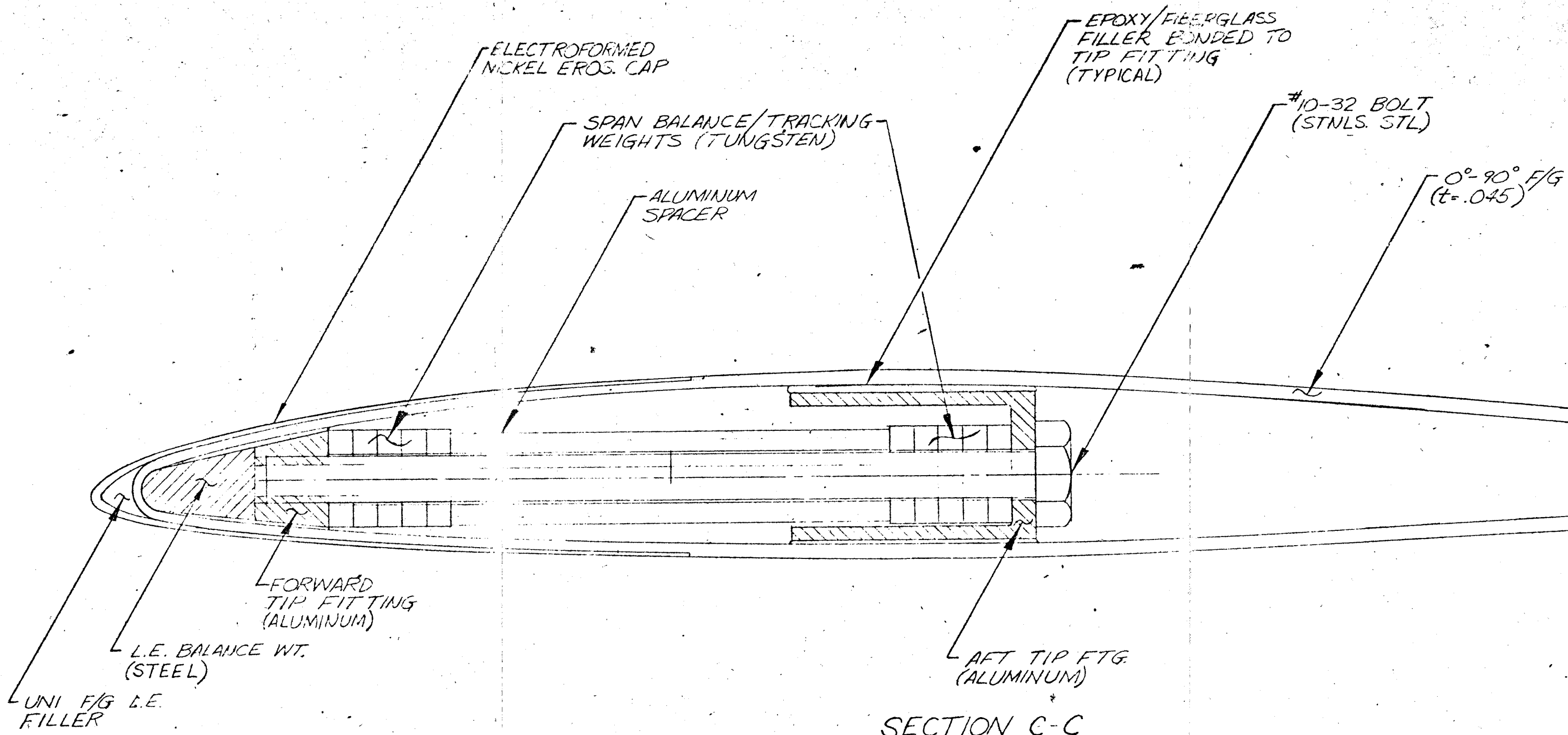
XV-15 BLADE-TIP FITTING  
ARRANGEMENT - 1ST ITERATION  
VR-7, C = 9.50, STA 135.75  
 (SCALE = 4/1)





SK 28279  
(SHT 3 OF 7)

Figure 4.1.4 (continued)



ELECTROFORMED NICKEL EROS. CAP

SPAN BALANCE/TRACKING WEIGHTS (TUNGSTEN)

ALUMINUM SPACER

EPOXY/FIBERGLASS FILLER BONDED TO TIP FITTING (TYPICAL)

#10-32 BOLT (STNLS. STL)

0°-90° F/G (t=.045)

FORWARD TIP FITTING (ALUMINUM)

L.E. BALANCE WT. (STEEL)

AFT TIP FTG. (ALUMINUM)

UNI F/G L.E. FILLER

SECTION C-C

XV-15 BLADE - TIP COVER / WEIGHT ARRANGEMENT - 1<sup>ST</sup> ITERATION.

VR-8, C = 9.5 @ STA. 141

(SCALE = 4/1)

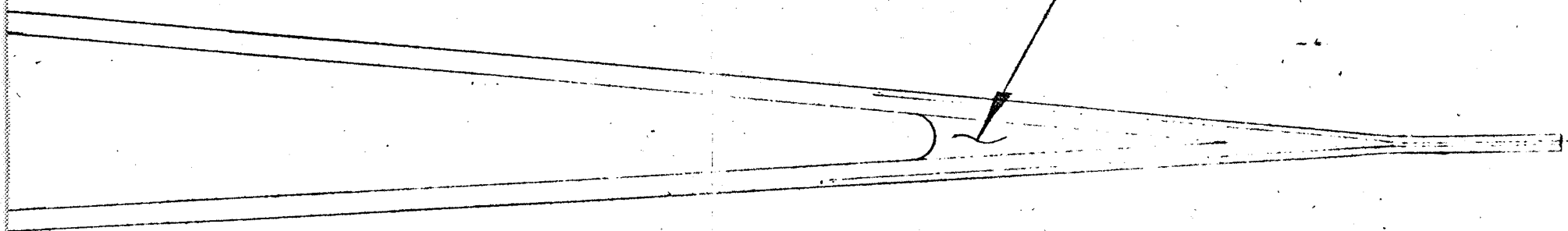
ORIGINAL PAGE IS OF POOR QUALITY

PODDOTT FRAME

PODDOTT FRAME

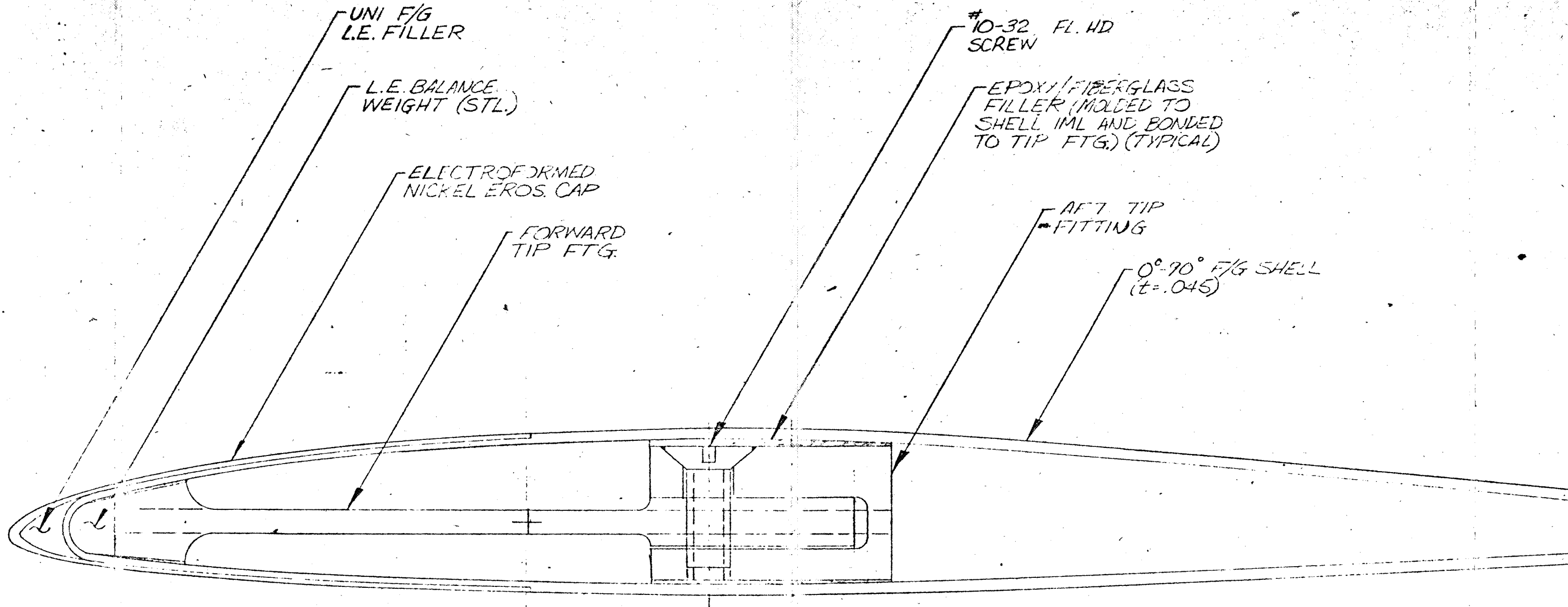
3  
0°-90° F/G SHELL  
(t=.045)

UNI F/G  
T.E. FILLER



EXCISE FRAME 3

SK 28279  
SHT 4 OF 7



SECTION D-D

XV-15 BLADE TIP COVER/FITTING  
ARRANGEMENT - 1ST ITERATION

VR-8, C=8.59, STA 42.825

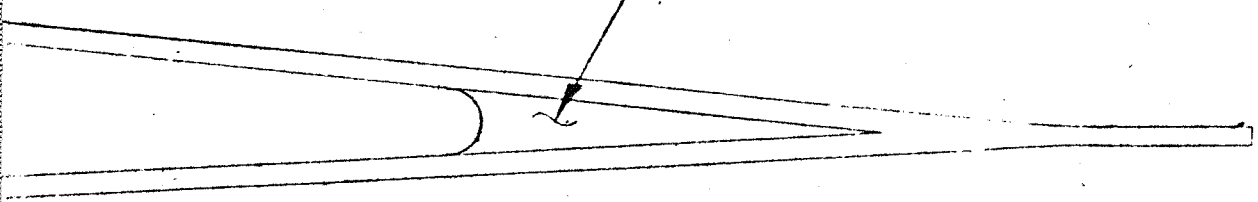
(SCALE = 4/1)

FOLDOUT FRAME 1

FOLDOUT FRAME 2

PRECEDING PAGE BLANK NOT FILMED

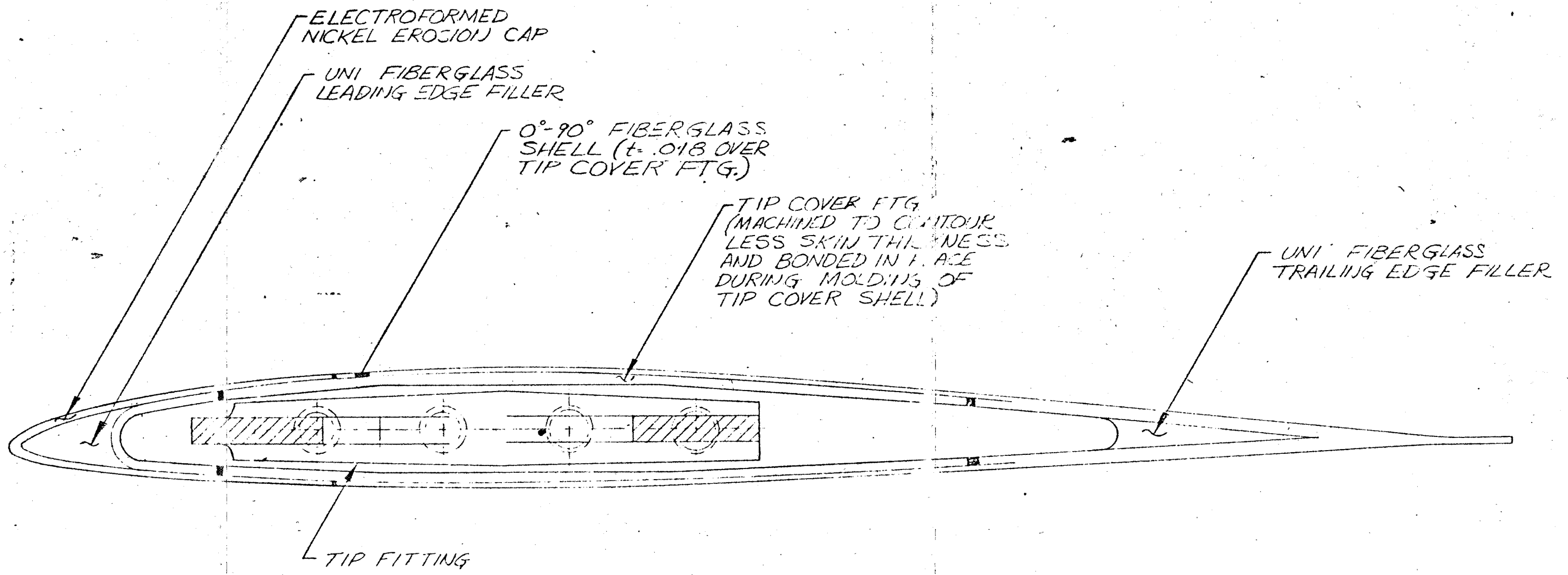
UNI F/G  
T.E. FILLER



**HOLDOUT AREA** →

SK 28 279

SHT 5 OF 7



SECTION E-E

TIP COVER-XV-15 BLADE (1<sup>ST</sup> ITERATION)

VR-8, C=5.89 @ STA 148.22

(SCALE = 4/1)

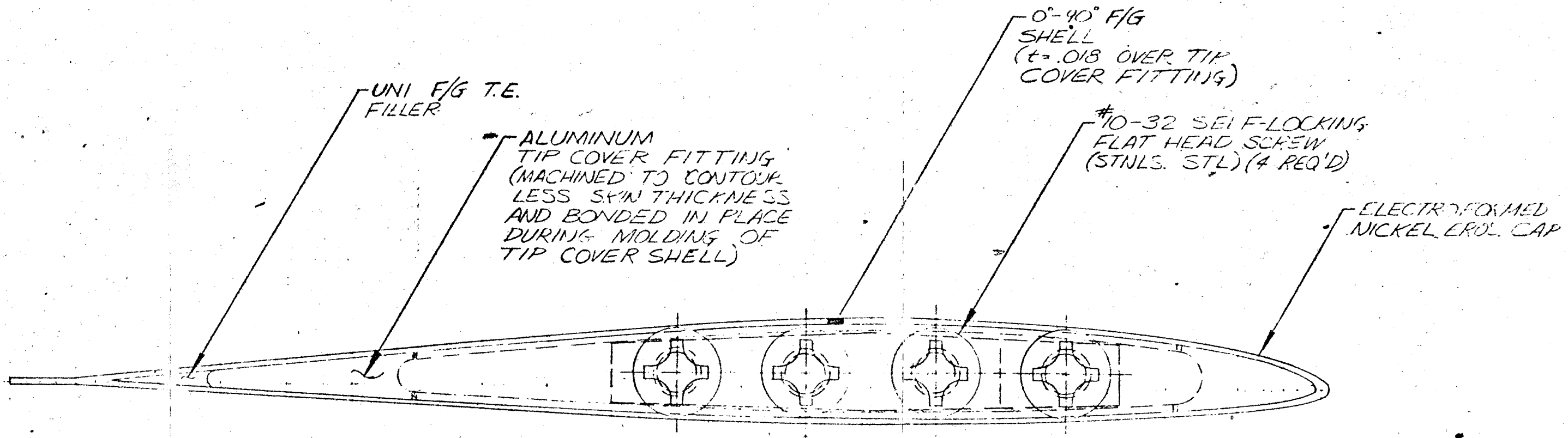
FOLDOUT FRAME

FOLDOUT FRAME 2

SK 28279  
(SHT 6 OF 7)

PRECEDING PAGE BLANK NOT FILMED

Figure 4.1.4 (continued)



VIEW F-F  
TIP COVER INSTALLATION  
XV-15 BLADE (1<sup>ST</sup> ITERATION)  
VR-8, C=5.00 (STA 150)  
 (SCALE 4/1)

ORIGINAL PAGE IS  
 OF POOR QUALITY

PRECEDING PAGE BLANK NOT FILMED

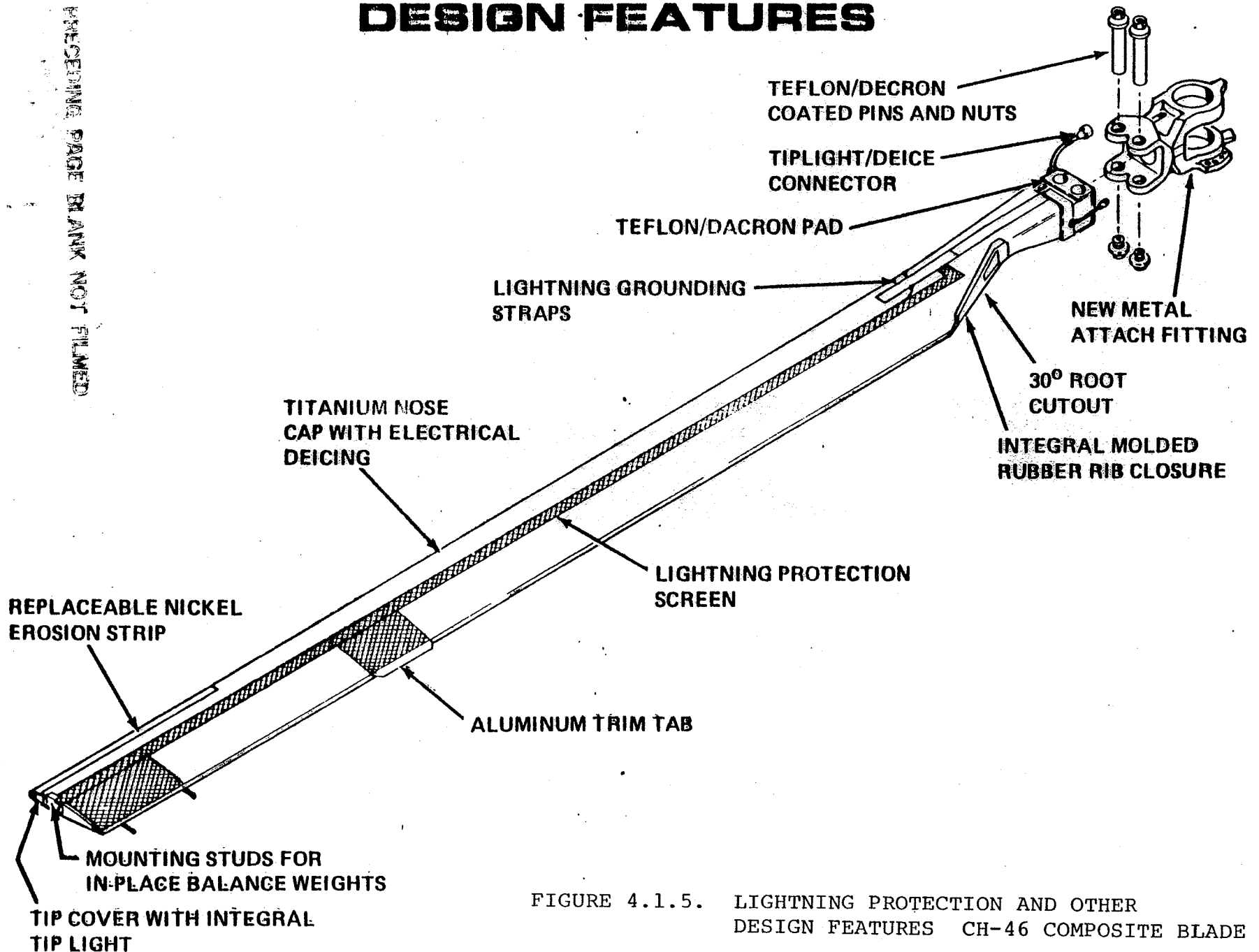
EXCISE FRAME

EXCISE FRAME

SK 28279  
 (SHT 7 OF 7)

# H-46 COMPOSITE ROTOR BLADE

## DESIGN FEATURES



97

FIGURE 4.1.5. LIGHTNING PROTECTION AND OTHER DESIGN FEATURES CH-46 COMPOSITE BLADE

D210-11569-1



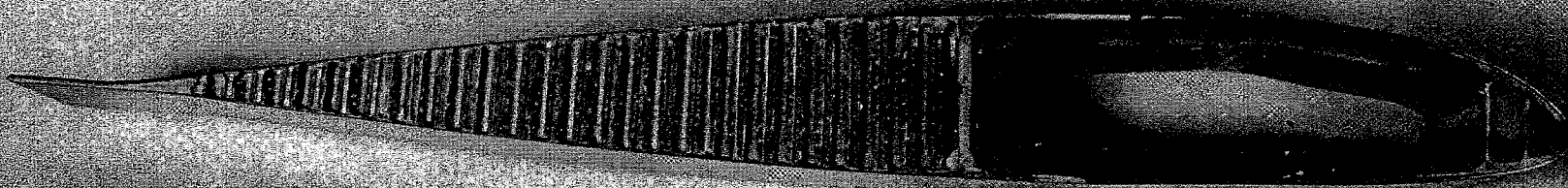


FIGURE 4.1.6. PHOTO OF CH-46 BLADE CROSS SECTION ILLUSTRATING  
FIBERGLASS-GRAPHITE MIXED SPAR (NEG. #C31400)

SHEET

98

ORIGINAL PAGE IS  
OF POOR QUALITY

D210-11569-3

CH-46 composite blade which incorporates a mixed fiberglass-graphite spar.

The spar configuration employs a two-pin root wraparound retention system. The attachment pin holes are lined with replaceable filament wound fiberglass sleeves (see Figure 4.1.3, Sheet 3). Figure 4.1.3, Sheet 4, a typical transition section, illustrates how the vertical spar strap wraparound at the root section rotates into the chordal packs in the nominal blade section and also shows the structural fillers needed because of the strap rotation. At the outboard end of the spar, the unidirectional strap wraps around the tip weight fitting as shown in Figure 4.1.4, Sheet 3.

#### 4.1.5 Blade Manufacturing Process

The state-of-the-art manufacturing process for the Blade Structural Assembly starts with three components which are fabricated in parallel. These components are:

- a. Uncured spar layup.
- b. Cured leading edge assembly.
- c. Cured fairing assembly.

Upon completion of each, the components are assembled with the required adhesives, placed in a mold, and the spar is cured and the cured components are bonded to the spar with one cure cycle.

The CH-46 blade manufacturing process is illustrated in Figure 4.1.7.

# MANUFACTURING CONCEPT

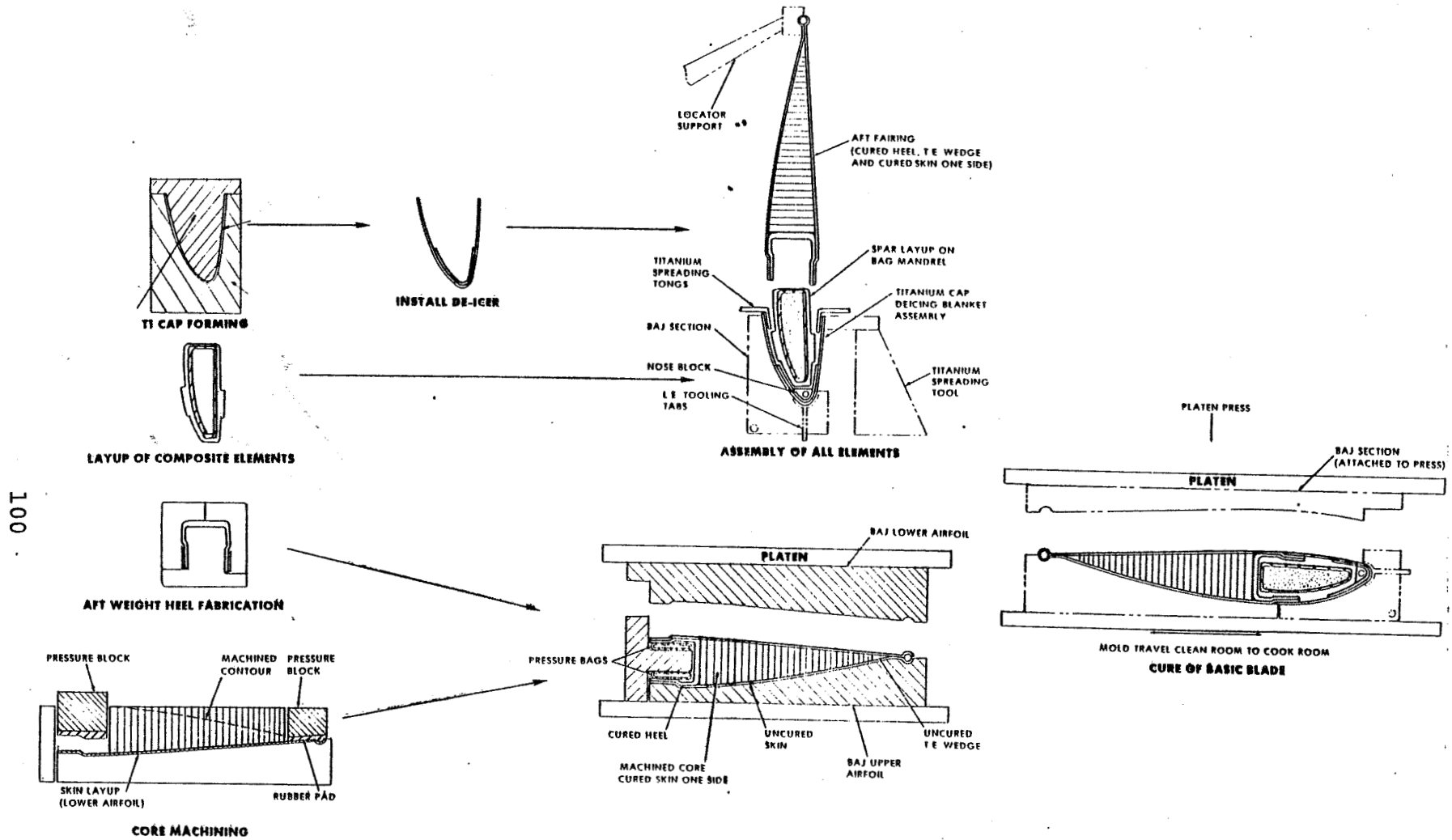


FIGURE 4.1.7. MANUFACTURING PROCESS WITH MAJOR TOOLS

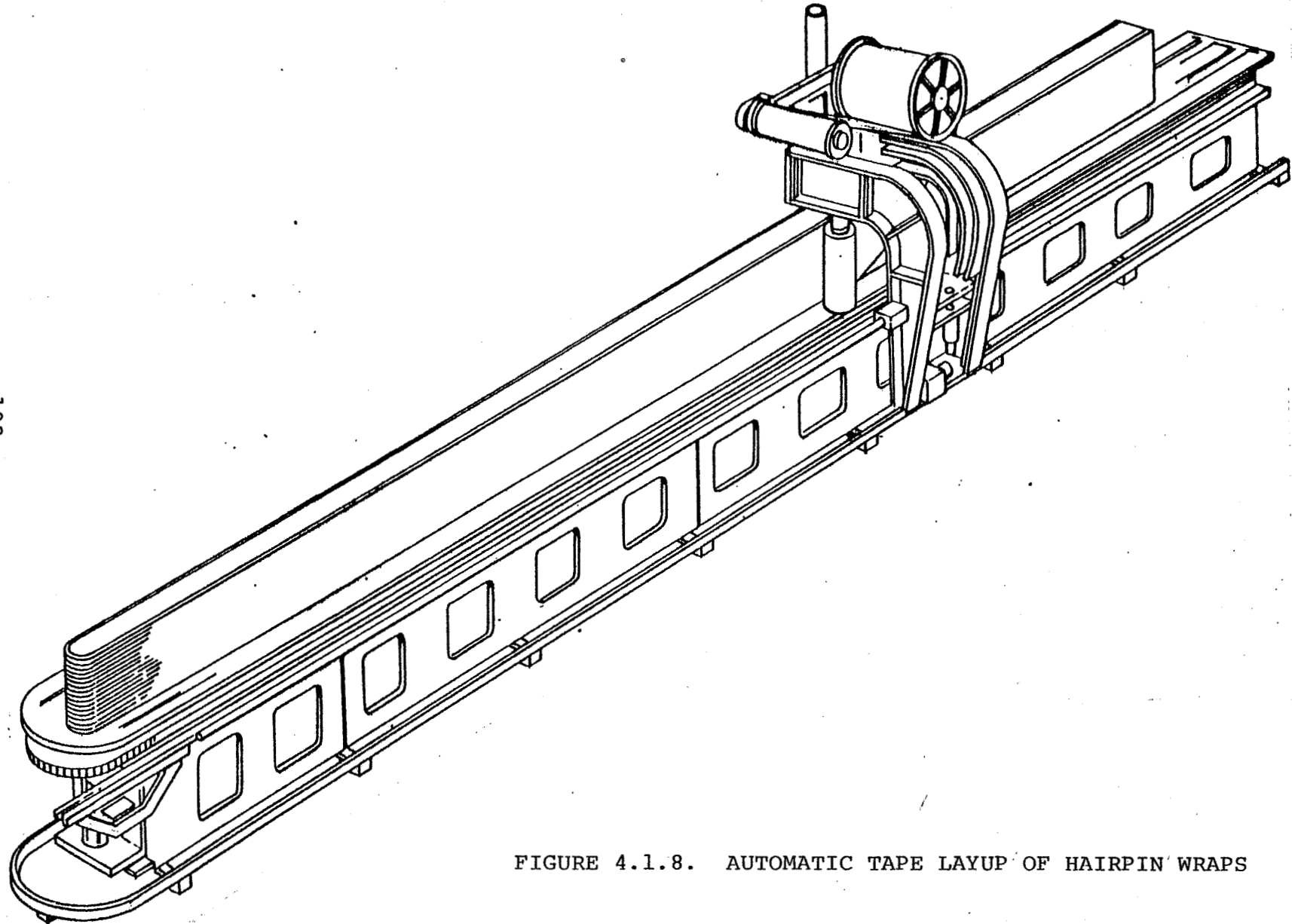
#### 4.1.6 Spar Layup Process

The unidirectional spar straps are laid up in hairpin shaped wraps using a tape layup machine as shown in Figure 4.1.8. As the tapes are laied up, the machine automatically starts laying the tape at a given station, running inboard, around the root loop, and returns outboard to the required station. These start and stop stations are specified to produce the required spar strap thickness distribution. The unidirectional spar fillers are laid up and coined to their required shape in a mold. The inner and outer torsion wrap layers are cut out of sheets of bias plied material to their required flat patterns. The individual spar components are then transferred to their respective layup mandrels where they are shaped and assembled as illustrated in Figure 4.1.9. This spar layup assembly is completed on an elastomeric bag which is rigidized with a foam mandrel. This bag is used during the final assembly cure to provide the required laminating and bonding pressure internally.

#### 4.1.7 Leading Edge Assembly

The leading edge erosion caps are formed to the required contours, trimmed, chemically treated, coated with a layer of adhesive and cured in preparation for subsequent bonding. This coating of adhesive prevents the formation of oxides and other contaminants on the faying surface of the caps. The bias plied layers of outer torsion wrap that go into the leading edge assembly are laid up on a contoured elastomeric internal mandrel, overlaid with film adhesive, and the erosion caps are installed

# AUTOMATED SPAR-STRAP-LAYUP MACHINE



102

FIGURE 4.1.8. AUTOMATIC TAPE LAYUP OF HAIRPIN WRAPS

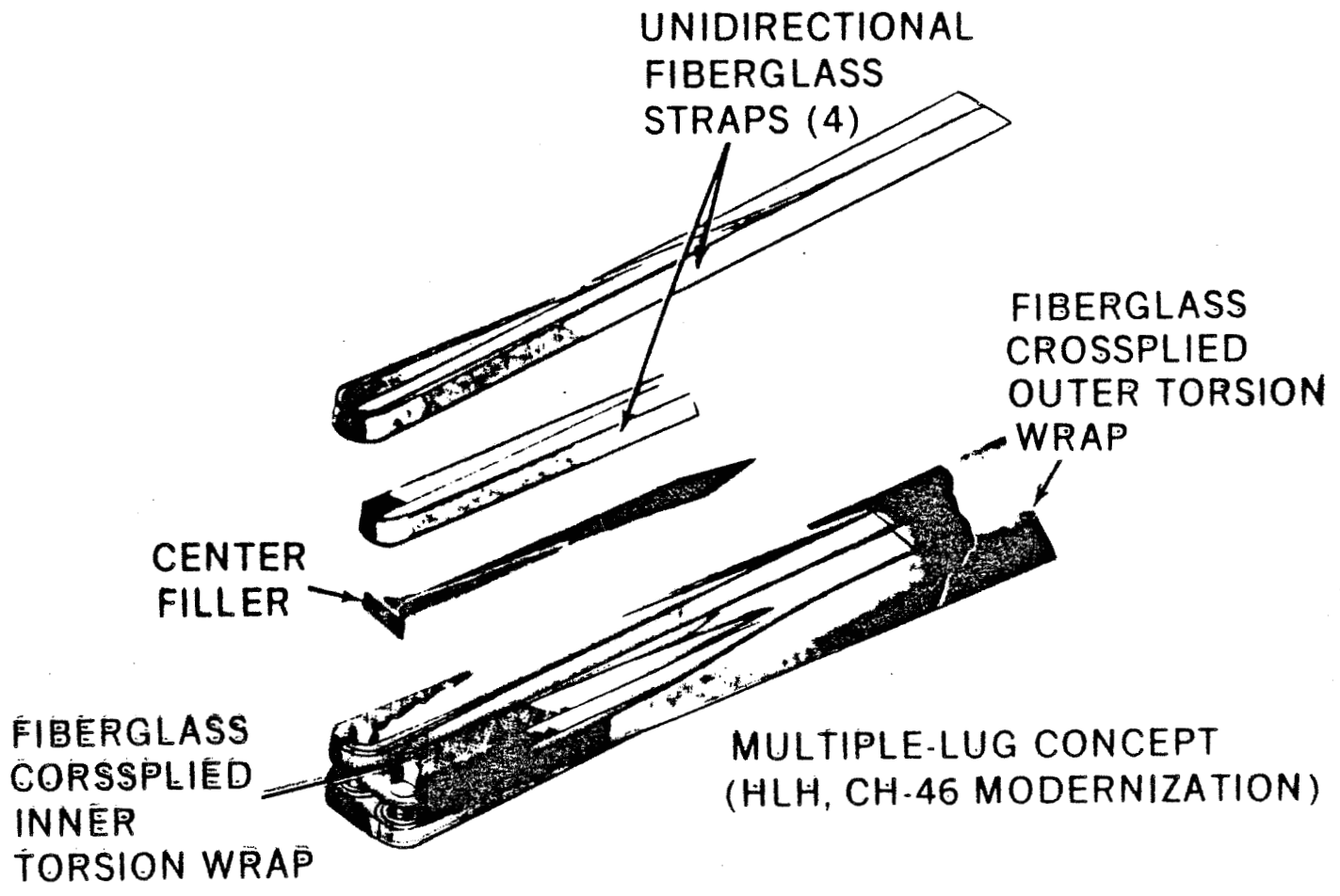


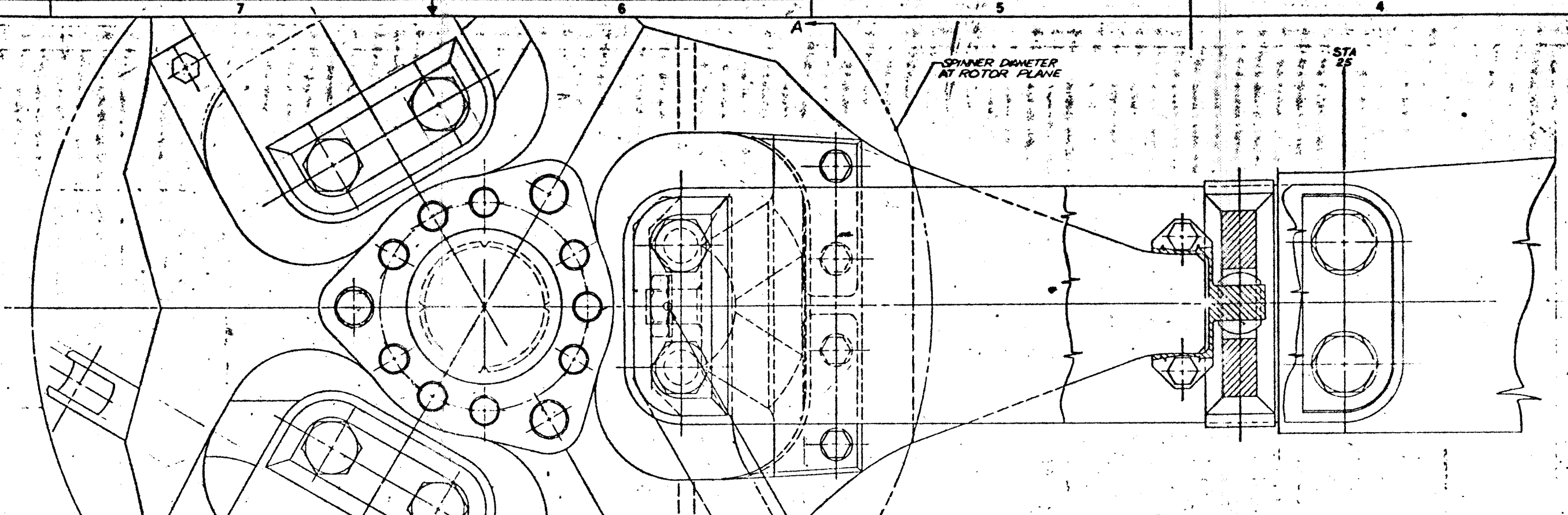
FIGURE 4.1.9. SPAR ASSEMBLY

over the layup. The contoured outer metal die is closed on the total layup, and the assembly is cured under pressure applied by compressing the elastomeric internal mandrel.

#### 4.1.9 Aft Fairing Assembly

The aft fairing assembly consists of two precured components fabricated in parallel, the spar heel (aft outer torsion wrap member) and the fairing subassembly. The spar heel is fabricated in a manner similar to that used for the leading edge assembly. The bias plied layers are laid up on a contoured elastomeric internal mandrel, the outer metal die is closed, and the layup is cured. The fairing subassembly is fabricated by laying up the lower bias plied skin and doubler layers in the lower contoured mold cavity, applying film adhesive, installing the flexible Nomex core blocks, and curing under pressure. The upper contour is then machined slightly oversize. This feature allows the Nomex to provide the required pressure during the fairing assembly cure as the material compresses to conform to the exact dimensions of the mold. The upper bias plied skin and doubler layers and unidirectional trailing edge filler are laid up in the upper contoured mold cavity and overlaid with film adhesive. The heel assembly is installed and the fairing subassembly is installed with foam adhesive between the heel and core face. The fairing assembly is placed in the platten press and the lower mold section is closed. The assembly is cured with pressure from the compression of the Nomex core and pressure bags as shown in Figure 4.1.7. The

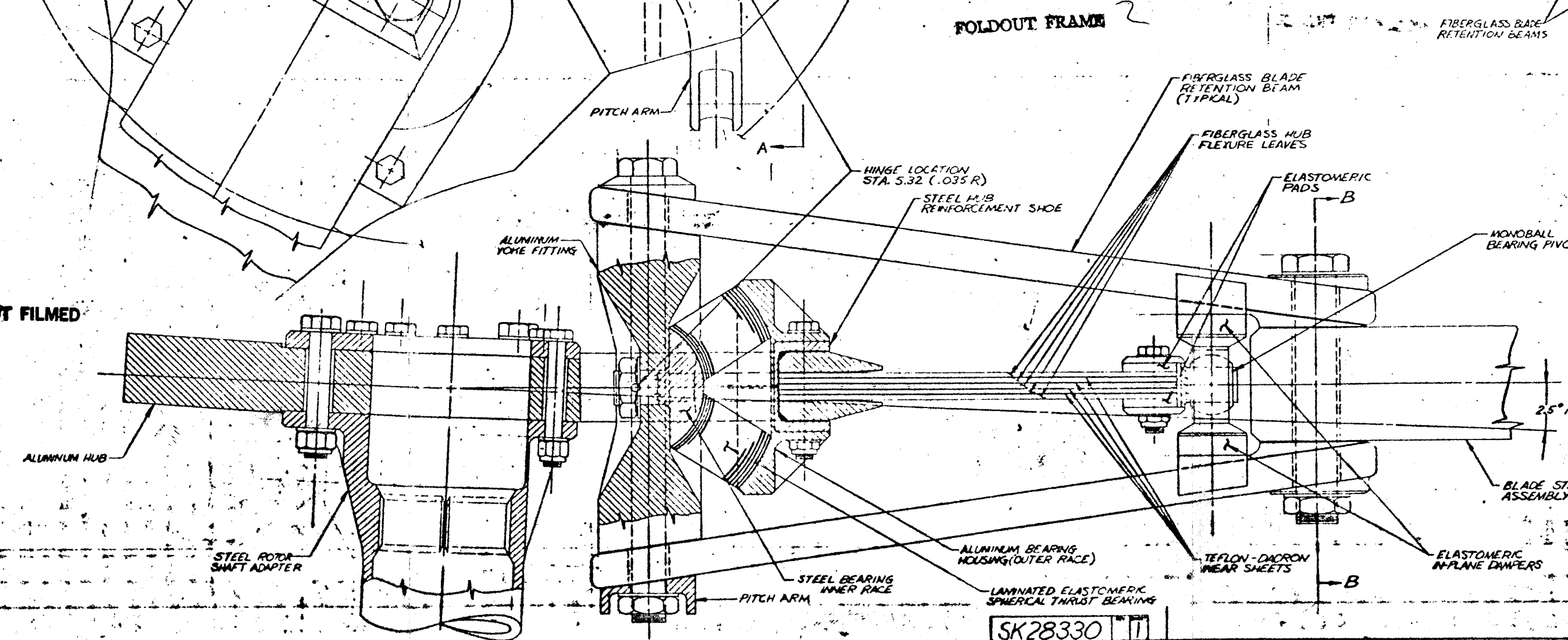




FOLDOUT FRAME

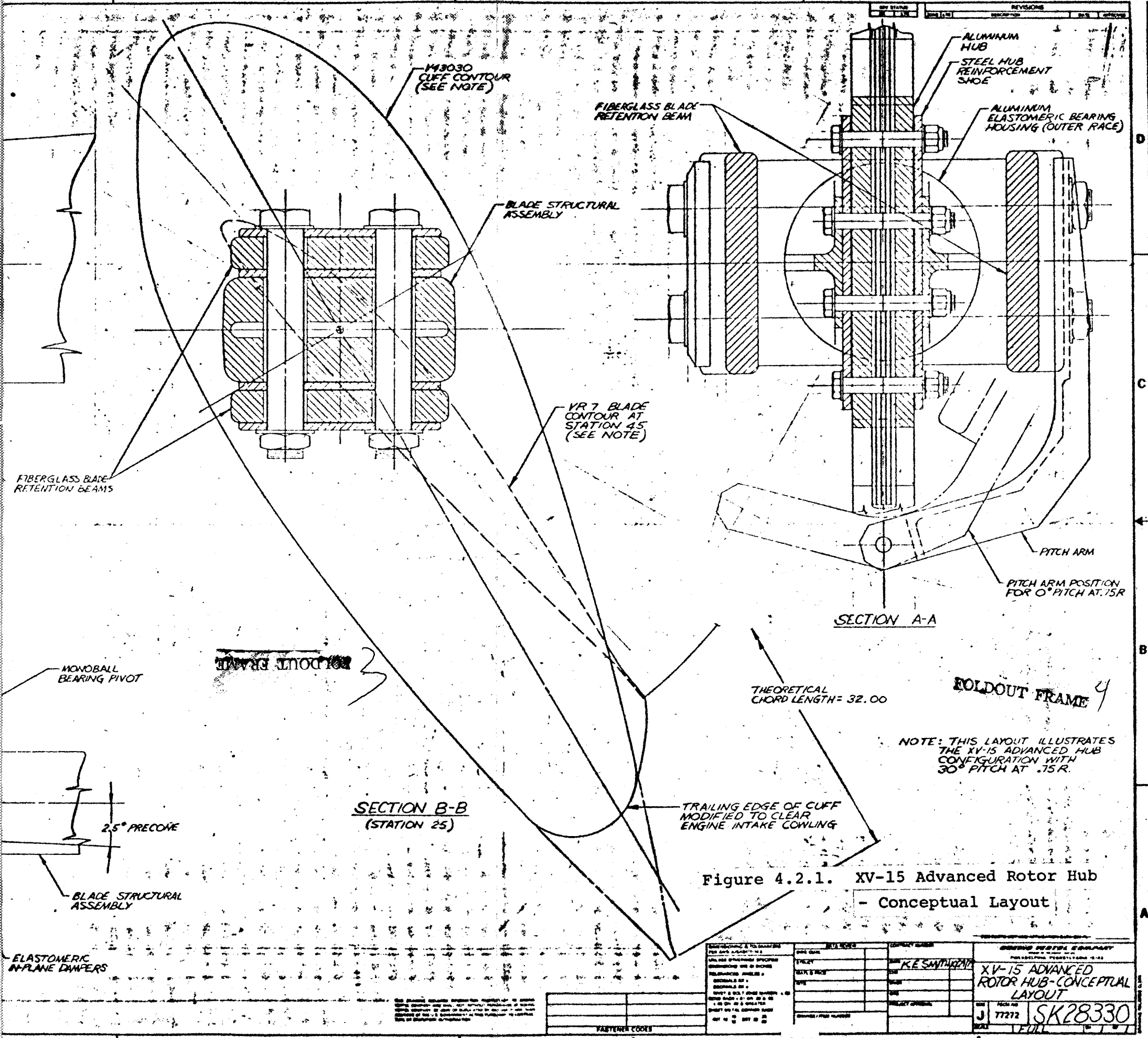
PRECEDING PAGE BLANK NOT FILMED

ORIGINAL PAGE IS OF POOR QUALITY



SK28330





NOTE: THIS LAYOUT ILLUSTRATES THE XV-15 ADVANCED HUB CONFIGURATION WITH 30° PITCH AT .15R.

Figure 4.2.1. XV-15 Advanced Rotor Hub - Conceptual Layout

SK28330

PREPARED BY: CHECKED BY: DESIGNED BY: DRAWN BY: DATE:		REVISIONS:		DRAWING NUMBER:	
AUTHORITY:		DATE:		PROJECT:	
FASTENER CODES:		SCALE:		SHEET NO. OF SHEETS:	
105		1		11	

XV-15 ADVANCED ROTOR HUB-CONCEPTUAL LAYOUT  
 SK28330

manufacturing process for the fairing assembly may be further simplified by machining both sides of the Nomex core block to the required contours laying up the skins, assembling and curing the entire assembly with one cycle.

#### 4.1.10 Assembly of Blade Structural Components

The structural assembly is prepared for final cure as follows:

- a. The leading edge assembly is spread open.
- b. The preformed nose block and balance weights are assembled, wrapped with film adhesive and installed into the leading edge assembly.
- c. The spar layup is wrapped with film adhesive and installed into the leading edge assembly.
- d. The aft fairing assembly is installed over the spar with the forward edges of the skins under the erosion cap.
- e. The leading edge assembly is closed.

The assembled elements are transferred to the mold, installed in the platen press and cured and bonded with internal pressure. The foam mandrel shrinks to allow removal of the internal pressure bag through the opening in the root end of the spar after cure.

## 4.2 Hub

### 4.2.1 Advanced Composite Hubs Design Concept

The articulated elastomeric hub concept illustrated in Figure 4.2.1 (SK 28330) was selected based on the following rationale:

- a. Concept allows the out-of-plane (flap) hinge to be located at inboard location to most nearly duplicate the dynamic properties of the present XV-15 rotor system.
- b. Concept eliminates oil lubricated pitch change and gimbal bearings, increasing reliability and reducing maintenance requirements.
- c. Concept offers least risk and least cost approach for a new advanced rotor hub concept.
- d. Concept allows for interface with an advanced replacement XV-15 composite blade with 2-pin attachment at Station 25.
- e. Concept offers low torsional stiffness for pitch control through the elastomeric spherical bearing.

Although the selected concept is very similar to the Aero-spatiale Starflex rotor, it possesses several unique advantageous features as follows:

- a. Center of spherical elastomeric thrust bearing is reversed locating the out-of-plane hinge inboard, therefore allowing for a good match with the dynamic properties of the present XV-15 rotor.
- b. The basic hub member is aluminum, offering a least cost, least risk approach for this member.
- c. The out-of-plane (flap) flexure is made up of multiple leaves insuring infinite life.
- d. The flexure leaves may be removed from the hub for inspection and replacement of the wear sheets, if required, and/or replacement of a damaged leaf or leaves at minimal cost without resulting in replacement of the entire hub.

#### 4.2.2 Functional Description

The rotor blade is attached at the outboard end of a yoke assembly. The inboard end of the yoke is attached to the hub through a laminated spherical elastomeric thrust bearing which transfers the centrifugal forces carried by upper and lower fiberglass blade retention beams into the aluminum hub. The elastomeric bearing also permits out-of-plane, in-plane, and pitching motions. Pitch control is provided by an arm at the inboard end of the hub arm flexure. Out-of-plane motion results in deflection of the flexure, while in-plane motions deform elastomeric dampers. This rotor configuration has coincident flap and lag hinges at approximately 3.5 percent offset. The resulting low lag frequency would require the use of inplane dampers to avoid mechanical instability.

#### 4.2.3 Description of Primary Elements

##### 4.2.3.1 Center Block

The aluminum center block is a machined plate which is attached to the rotor shaft through an internally splined steel adapter. The steel adapter also transfers control loads through bearings into a rigid metal member which is needed to replace the elastomeric hub spring. Further studies are needed to determine the detail design requirements for replacing the hub spring.

The outboard corners of the hub arm cutouts are reinforced with steel shoes to distribute centrifugal forces entering through the elastomeric thrust bearing and to accommodate concentrations. The outboard end of the hub arms are slotted

to allow for rigid clamp-up of the hub arm flexure leaves. Also, the outboard inside surfaces of the slots are curved to the minimum radius of curvature required for the flexure leaves. These surfaces are covered with bonded teflon-dacron wear sheets.

#### 4.2.3.2 Flexure

The fiberglass flexure leaves are flat plates made up of span-wise unidirectional material overlaid with one layer of bias plied material. The leaves are rigidly clamped in the hub arm and clamped at the outboard end with elastomeric pads. The leaves are separated with teflon-dacron wear sheets. This arrangement allows each leaf to shift relative to the others as the flexure is deflected. The monoball bearing pivot essentially makes the arrangement a cantilevered-pinned beam flexure. The thickness of each leaf was determined to insure infinite life with  $\pm 7.5^\circ$  of out-of-plane deflection of the blade about the hinge location. The number of leaves was determined to allow a maximum of  $15^\circ$  deflection under a 4 G static loading of the rotor system.

#### 4.2.3.3 Elastomeric Spherical Thrust Bearing

The bearing is fabricated by vulcanizing and bonding thin elastomeric layers and cup shaped stainless steel shims with the metal inner and outer members (races). Typically, natural rubber is the most commonly used elastomer. Natural rubber can operate in an ambient temperature from  $-65^\circ$  to  $160^\circ\text{F}$  without adverse effects on service life or bearing performance.

This bearing is particularly suited for this application because it accommodates high compressive loads induced by centrifugal forces and oscillating torsional and cocking motions in shear. The bearing exhibits high compressive stiffness but low torsional or shear stiffness. This bearing was sized to have a 3000-5000 hour service life dependent on actual total mission profile. Because these bearings wear gradually, they require only occasional inspection.

#### 4.2.3.4 Fiberglass Blade Retention Beams

The fiberglass blade retention beams are fabricated using a wet filament winding technique. Each beam is made up of two spanwise unidirectional windings which are wound around the attachment bushings. The spanwise windings are overwound with one layer of  $+45^{\circ}$  fibers. The wet layup is placed in a mold and heat cured.

#### 4.2.3.5 Elastomeric In-Plane Dampers

The total damper area shown is approximately 28 sq.in. and the damper thickness is approximately .75 in. Further studies should be performed to select a material having the damping characteristics required to provide the damping necessary to prevent ground resonance. Hydraulic or friction dampers have commonly been used to provide the required energy dissipation. Both of these types of dampers have a history of poor service due to leakage and wear. The use of a highly damped elastomer to perform this function offers significant advantages in terms of eliminating maintenance and improving reliability.

Elastomeric dampers have been employed in the Aerospatiale aircraft and in the Hughes YAH-64(AAH) and their Model 500D. Since elastomers are visco elastic materials, they exhibit both spring and damper characteristics. The spring restraint of the blade provided by the elastomeric damper will be advantageous. Lag motions due to steady loads, such as aerodynamic drag, are reduced significantly. By increasing the in-plane natural frequency, the spring restraint reduces the amount of damping required for mechanical stability.

#### 4.3 INSPECTION MAINTENANCE AND REPAIR CHARACTERISTICS

##### 4.3.1 General Comments on Composite Blade Characteristics

Composite blades provide major gains in reliability, maintainability and inspectability over metal blades and have reduced vulnerability and increased survivability.

Reliability, safety, and cost are improved by elimination of corrosion and by reduced sensitivity to scratches, dents, and cracks. A series of tests were performed to compare damage tolerance of UTTAS fiberglass blades with aluminum blades. Tests were conducted by dropping a 1.92 pound tungsten ball, a 3/4 pound plumb bob with a sharp point, and a 2.6 pound axe from various heights (2 to 10 feet) on to the skin of each blade. Results of the tests showed that the aluminum blade sustained considerable damage in all tests, whereas the fiberglass blade sustained only minor damage from the high level drop made by the plumb bob and axe. Additional tests were made by dropping the same tungsten ball from heights of 18 and 29 feet respectively. The 18-foot drop caused a dent in the aluminum blade .28 inches deep and 2.50 inches in diameter. The 29-foot drop caused a dent in the aluminum blade .38 inches deep and 3.25 inches in diameter. In both cases, there was no visible damage when the identical drops were made on the fiberglass blade. These tests indicated strongly that the fiberglass skin nomex honeycomb is considerably more damage-tolerant than the aluminum skin and aluminum honeycomb.

Maintainability is improved because many types of damage that are irreparable or require depot overhaul on metal blades can



be easily repaired in the field on composite blades. In the H-46 program, with over 18,000 blade flight hours (see Table 4.3.1) a total of 24 problem reports were submitted. All reported problems were repaired in the field with no returns to depot required and no blades scrapped. UH-61A history shows that a total of 3400 aircraft hours, which amounts to 13,600 blade hours, were accumulated in flight and on the ground test vehicle. All blades were repairable even though considerable damage was done to several blades. No blades were scrapped. Inspectability is improved over that of metal blades. Inherent to composite blades is the slow propagation of damage which generates long failure progression intervals. No special inspection equipment is required for composite blades. The reliability of visual inspection has been demonstrated on the H-46 fiberglass blades as well as other Boeing Vertol fiberglass blades such as BO-105, UH-61A and HLH.

Our most recent experience has been with the H-46 fiberglass rotor blade currently undergoing a fleet wide retrofit on the H-46 helicopter. Due to the similarity in design, materials, and manufacturing techniques between the H-46 and the proposed XV15 replacement blade, a brief discussion of the H-46 blade development programs follows.

#### 4.3.2 Experience with H-46 Fiberglass Rotor Blade

##### Objective

This blade was designed and developed by Boeing Vertol for use on the H-46 helicopter. The primary reason for this effort was to provide a rotor blade of improved reliability and maintainability over that of the metal rotor blades. At the time of writing (October 1979) this composite rotor blade is in production (Phase III) and over 200 blades have been delivered to the U.S. Navy.

##### Blade Design (See Figure 4.3.1)

The rotor blade consists of a fiberglass "D" spar, stiffened with graphite, terminating in a two-pin, four-lug root end retention. The tip weight fittings are simply threaded tubes which are surrounded by fiberglass and integrally cured in place during the spar cure. All fiberglass elements of the spar are assembled and cured directly to the titanium nose cap to ensure a high quality, nonporous bond between metal and laminate. In addition, an electro-formed nickel cap 46 inches long is bonded to the outboard end of the titanium cap to provide erosion protection.

The spar consists of four tension straps that run from the blade tip, loop around a blade retaining pin sleeve, and back to the tip. Each strap is composed of many layers of uni-directional fiberglass. The four straps are covered by multiple layers of crossply fiberglass to provide torsional stiffness and graphite filament for flap bending stiffness. The number of layers in the tension and torsion wraps decrease as they progress from the root end toward the tip.

# CH-46 COMPOSITE ROTOR BLADE

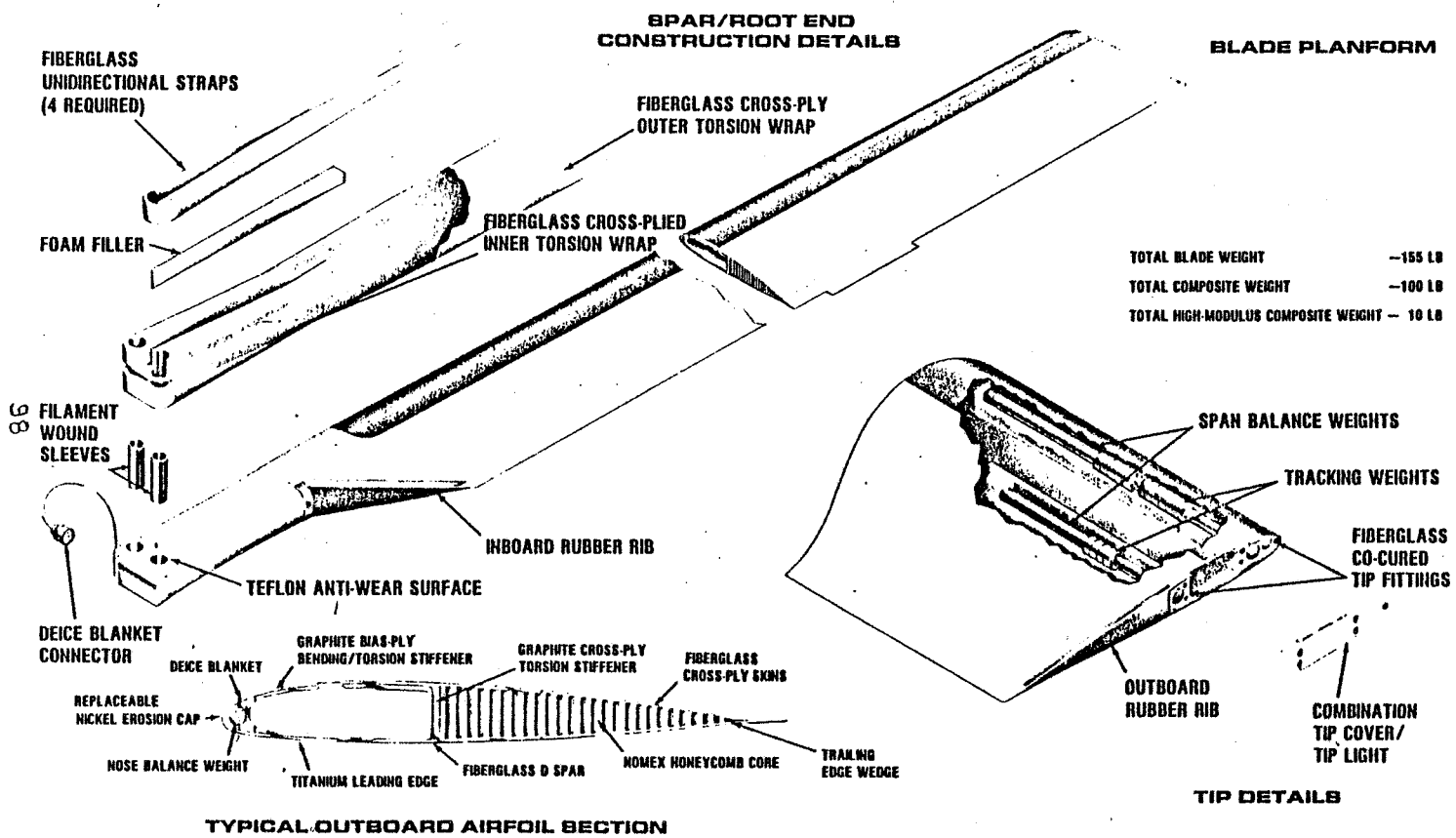


FIGURE 4.3.1. DESIGN FEATURES OF CH-46 COMPOSITE BLADE

116

D210-11569-1

The aft fairing consists of fiberglass crossply skins over a Nomex honeycomb core. The trailing edge is an integral part of this subassembly and is formed by bonding a fiberglass trailing edge wedge between the two skins. This fairing is fabricated as a unit with the fiberglass heel portion of the "D" spar and aft tip weight fitting which in turn is bonded to the spar during the basic blade cure. In this way, the aft fairing skins are bonded in place under the titanium leading edge. This provides a fail-safe attachment to fairing-to-spar.

Lightning protection is provided by an aluminum wire mesh diverter bonded to portions of the upper fairing skin. A three inch wide strip of mesh runs spanwise just aft of the nose cap and chordwise from the nose cap to the trim tab. The outboard 22 inches of the fairing is also covered. The entire blade is painted with a conductive coating and connected to the rotor head by a bonding jumper to dissipate static electricity.

#### Repairability

An integral part of the blade development was the validation of a Maintenance Engineering Analysis Record (MEAR) repair program conducted during Phase II of the program.

This effort addressed all aspects of Integrated Logistic Support (ILS) for the blade from establishing a maintenance concept to identifying maintenance requirements, maintenance levels, personnel requirements, GSE and spare parts provisioning. The program included, in addition to the above, validation of the repairs procedures and prototype GSE as well as fatigue testing of representative repairs.

A summary of the repair program follows:

The objective of the CH-46 Fiberglass Rotor Blade Phase II MEAR Validation Program was to develop and validate maximum repair capability for the CH-46 fiberglass rotor blade at the lowest practical maintenance levels using minimum Ground Support Equipment (GSE) and minimal skills.

Maintenance concepts were established and repairs were then made on blade samples to validate the maintenance tasks and develop and validate the GSE. Selected repairs were then tested on the fatigue test specimens to prove the structural integrity of the repairs. The results of the fatigue test prove the service life of the blade is unaffected by repairs since the endurance limits of the repairs are as good as the endurance limit of the basic blade. Approximately 30 Organizational and Intermediate repairs were developed and evaluated. The repair procedures have been documented in the MEARS and have been included in the CH-46 Maintenance Instruction Manuals and Training Programs which were also prepared and implemented during this program. All necessary logistics support elements were considered and evaluated. These included materials, publications, training, spares, GSE, personnel, and limited packaging and storage requirements.

The results of the program prove that all authorized blade repairs can be accomplished in either Organization or Intermediate Level maintenance. Damage in excess of establish limits does not necessarily require that the blade be

scrapped. In those circumstances, operating activities should request assistance from the Cognizant Field Activity (CFA) for engineering evaluation, identification of the necessary repair and instructions for the performance of the repairs. Under these circumstances, the repair limits can be continually updated.

Although no specific goals were established for Mean Time to Repair (MTTR), the following MTTRs were determined using demonstrated repair times and failure frequencies from the Failure Mode and Effects Analysis (FMEA):

MTTR Organization	=	1.98 manhours
MTTR Intermediate	=	2.88 manhours

These items include the standard Marine/Navy Operational Adjustment Factor (OAF) of 1.8. They do not include track and balance if required, or adhesive cure times.

#### RELIABILITY DEMONSTRATION

This effort was conducted during Phase II of the program by U.S. Navy and Marine operating activities. Its purpose was to determine the operational suitability of the fiberglass rotor blade. It included an extensive evaluation of repair procedures, materials, and GSE published in NAVAIR 01-250-HDA-2-4.5, "Organizational and Intermediate Maintenance with Illustrated Parts Breakdown, Fiberglass Rotor Blade (A02R1702)."

A flight test program of 2925 flight hours using ten aircraft was established. The primary objective was to demonstrate a Mean Time Between Return to Depot (MTBRD) of 2500 hours for the fiberglass blade.

In summary, the reliability demonstration clearly indicated that the H-46 fiberglass rotor blades are operationally acceptable and reliability and maintainability goals have been met or exceeded. A total of 3109 aircraft hours were flown during the demonstration.

Final achieved reliability numbers are as follows:

	<u>Goal</u>	<u>Achieved</u>
Mean Blade Flight Hours between Maintenance Action (MBFHBMA)	56	720
Mean Blade Flight Hours between Return to Depot (MBFHBRD)	2500	No removals for Depot repair
Mean Blade Flight Hours between Failure (MBFHBF) from all causes	280	947
4.3.3 Inspection Maintenance and Repair of the Composite XV15 Blade		

Since the replacement XV15 blade follows the same general design philosophy as the H-46 blade, the following observations may be made:

Advantages of the XV15 composite rotor blade are:

1. Elimination of corrosion.
2. Simple repair procedures.
3. Most failures repairable in the field.
4. Minimum GSE required for repairs.
5. Simple visual inspection procedures.
6. No inspection equipment required.
7. Slow propagation of damage.

8. Root end fitting removable for inspection or replacement.
9. Easy access to balance/tracking weights.
10. High damage-tolerant in normal field operations.

Risk Areas:

1. Use of graphite material in the XV15 blade. Boeing Vertol has limited experience with graphite. Only a small amount of graphite is used in the H-46 blade spar. Failure analysis did not reveal a need to repair and no repairs were made. However, graphite repair procedures have been developed at Boeing and other aerospace companies, and this technology is available for application to the XV15 blade.
2. Skin delamination in tapered areas of the blade. Skin is susceptible to delamination in areas where the blade tapers. The XV15 blade has several such taper areas. Design improvements to reduce or eliminate the potential problems are being considered. However, these tapered areas are similar in load transfer to the H-46 composite blade root end transition area, and no problems have been experienced to date. The key to insuring the delamination will not occur is smooth interlaminar load transfer, proof by realistic fatigue test simulation, repeatable process control and effective Q.C., which Boeing Vertol has achieved in production blades.



3. Use of polyurethane on leading edge. Polyurethane is highly effective in resistance to particle abrasion and is being considered as a material for leading edge erosion protection. However, under certain conditions of precipitation (large rain drops), it undergoes rapid deterioration/unbonding. This undesirable feature is overcome in part by its ease of repair. For developmental purposes on the XV15, where very little flying will be done in sand, dust and rain, polyurethane should be adequate.

#### 4.3.4 Description of Current XV15 Rotor Hub

The hub consists of a titanium yoke with three spindles and a universal joint assembly that is spline to the mast. A non-rotating, elastometric hub-moment spring is attached to the yoke through a bearing. The lower end of the hub-moment spring is attached to the transmission case.

The universal joint assembly consists of a steel cross with bearings mounted in aluminum pillow blocks on two opposing spindles and a steel fork with bearings on the other two spindles. These four roller bearings are not provided with inner races, but roll on the case-hardened journals of the steel cross member. A common oil reservoir is created by oil passages drilled within the cross member. Oil level sight gages are installed on the pillow block housings. The bearing housings contain thrust bearings to carry the prop-rotor H-forces, and seals to retain the oil.

The inboard and outboard pitch-change roller bearings assemble in the blade's integral root fitting. The inner race of these bearings assemble on the spindles of the yoke. A stainless steel liner is bonded to the spindle to prevent fretting between the inner race and the titanium spindle. The pitch-change bearings are oil lubricated from a reservoir located in the pitch horn.

The three wire-wound blade-retention straps have an integral steel fitting which seats at the inboard end of each spindle of the yoke. The outboard fitting, of the retention strap, is attached to the blade by a steel bolt through the blade root fitting, spar and doublers.

#### 4.3.5 Description of Replacement Elastomeric Hub

The proposed replacement hub design shown in Figure 4.2.1 is similar in concept to the Aerospatiale AS350 Astar or Starflex hub. The rotor blades are attached at the outboard end of the yoke which twists about a fiberglass hub arm. The inboard end of the yoke is attached to a spherical elastomeric bearing which transfers centrifugal forces to the hub arm close to the center of rotation. The elastomeric bearing also permits flapping, lead-lag, and pitching motions. Pitch control is provided by an arm at the inboard end of the yoke. A spherical metal bearing centers the yoke at the outboard end of the hub arm. Flapping motion results in flexing the the hub arm, while lead-lag motion deforms an elastomeric damper.

This rotor configuration has coincident flap and lag hinges at approximately a 5% offset. The resulting low lag frequency necessitates the use of dampers to avoid ground and air resonance. It employs metal hardware at the rotor shaft attachment and around the elastomeric components. There is no elastic coupling between pitch and flap or pitch and lag motions. The location of the pitch arm may be chosen to provide a controlled amount of  $\delta_3$ . An aerodynamic cuff may be fitted around the yoke and attached at both the inboard and outboard ends. This type of rotor is capable of providing the high collective and cyclic motions required in the XV15. The direct retrofit blade may be used with this rotor without modification.

#### 4.3.6 Reliability and Maintainability Analysis of Replacement Hub

A significant improvement in R&M can be expected through use of the Boeing Vertol Articulated Elastomeric Hub for the following reasons:

1. Elimination of all bearings and oil seals in the universal joint assembly plus the inboard and outboard pitch changing components. Bearings and seals are the cause of approximately 85% of the reliability and maintainability problems on the CH-46 rotor heads.
2. Servicing requirements of bearings and oil seal leaks will be eliminated.
3. Inspection requirements will be greatly simplified.

TABLE 4.3.1 H-46 FIBERGLASS ROTOR BLADE R&M PROGRAM  
PROBLEM/MAINTENANCE SUMMARY

<u>NO.</u>	<u>PROBLEM DESCRIPTION</u>	<u>OCCURANCES</u>	<u>NOT PART OF BLADE</u>
1.	L.E. of blade root end surface scratched (electrical connector came loose and hit blade)	2	
2.	Harness adapter tabs broken - sheetmetal	3	
3.	Rubber tip closure unbonded	4	
4.	Data plate partially unbonded (root end transition area)	1	
5.	Harness adapter has crack in housing - overtorqued	1	
6.	Blade fold harness failure (internal)		5
7.	Aerodynamic filler at inboard end of nickel erosion cap peeling off	2	
8.	Water entrapped in the inboard rubber blade closure rib	1	
9.	Water entrapped in fairing skin (Sta. 133) - local area	1	
10.	2" long piece of fiberglass skin flaked off top surface outboard fairing	1	
11.	Rubber inboard rib closure unbonding	1	
12.	Surface corrosion blade retaining pin		1
13.	Surface corrosion on tip cover retaining screws	1	
	TOTAL	18	6

4. Repair procedures will be reduced both in number and complexity. Some repair techniques and materials developed and validated for the H-46 fiberglass rotor blade can be used to develop repairs to the elastomeric hub.
5. GSE requirements will be reduced.
6. Total parts count between the two hubs will be reduced by an estimated 75% and will result in a reliability improvement, since reliability is approximately proportionate to parts count.
7. Overall Integrated Logistic Support will be much less due to the improved R&M features of the elastomeric hub and reduced number of parts.

#### 4.4 Advanced Nonmechanical Flight Control System

The following paragraphs give some detailed information on the recommended system (Reference paragraph 2.3) with emphasis on the primary flight control function. The complete flight control system includes a fail operative/fail-safe Stability and Control Augmentation System (SCAS) which is defined here only in terms of its interaction with the primary system. As noted previously, paragraph 2.3, the computations for the SCAS are accomplished within the flight control processor which also includes the primary computations. The PFCS and SCAS computations are isolated in the recommended multi-processor architecture.

##### 4.4.1 Overall System Description

The fly-by-wire primary flight control system controls the rotors, engines, flaperons, rudder, and elevator. It is composed of the existing XV-15 conventional dual pilot station cockpit controls, a triple redundant electrical link between cockpit controls and actuators, and redundant driver actuators which control the existing XV-15 flight control boost actuators. The system is powered by a dual hydraulic supply with a third-channel backup and a triple electrical supply which is derived from the existing XV-15 dual electrical supply and a third-channel battery supply charged from one of the existing supplies. Figure 4.4.1 is a simplified diagram of the system.

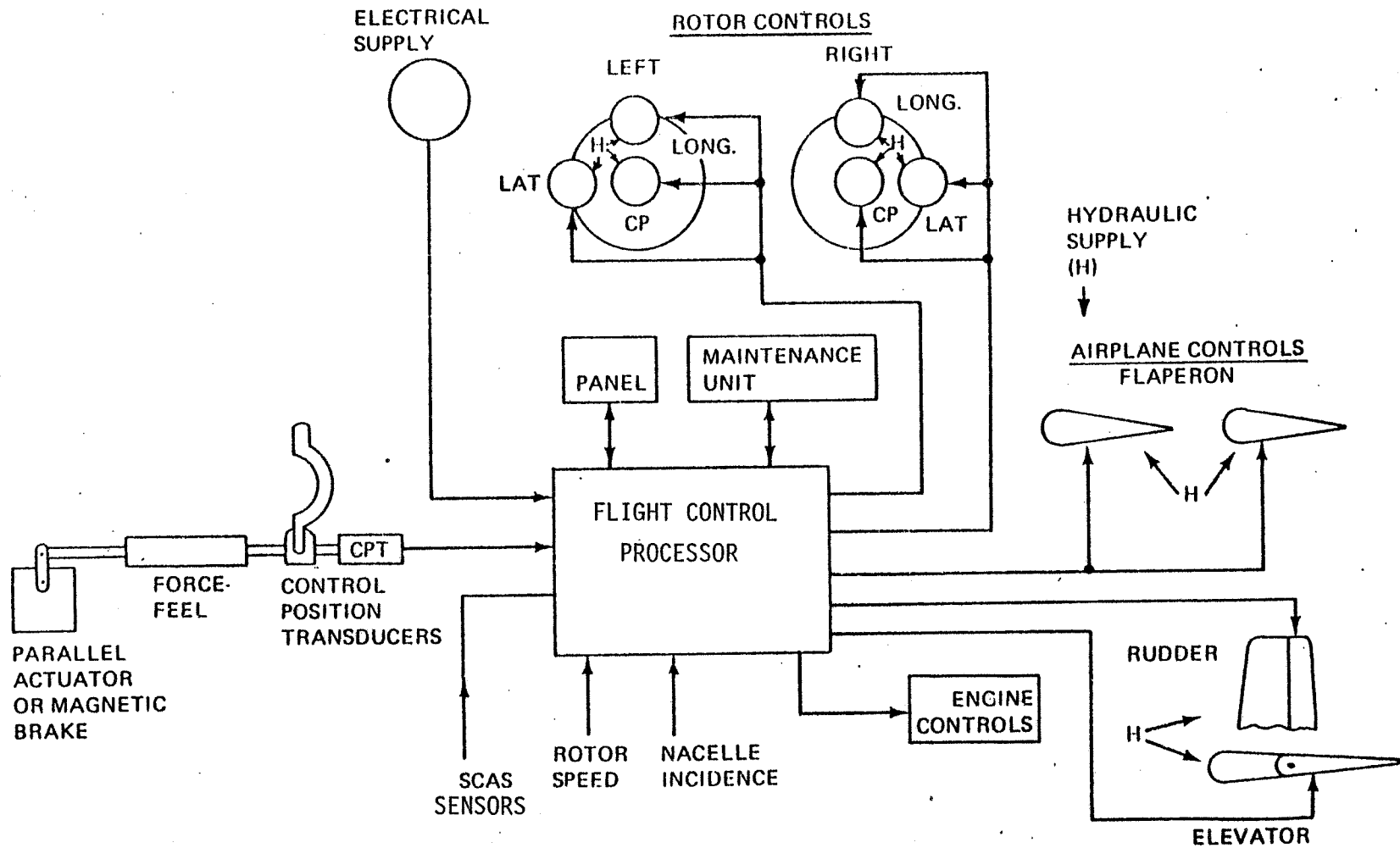


FIGURE 4.4.1 FLY-BY-WIRE FLIGHT CONTROL SYSTEM

- (a) Cockpit Controls - Cockpit controls at each pilot station consist of the existing XV-15 controls which are cyclic stick providing longitudinal and lateral control, pedals for directional control, and a throttle control lever.
- (b) Electrical Link - The electrical link is triplex to meet safety and reliability goals. Each channel of the electrical link includes control position transducers (CPT), a flight control processor, a junction box, and associated electrical cables.

The control position transducers translate cockpit control motions into electrical analog signals which, in turn, are transmitted to the flight control processor. The processor performs the equivalent functions of the mechanical flight control linkage; specifically, control signal mixing, limiting and gain scheduling with nacelle position. The processor also provides SCAS signal integration into the primary flight control system, redundancy management, fault isolation, and control of engine performance.

The proposed redundancy management scheme provides independent in-line self-monitoring of each primary control channel. This approach permits the triplex system to be dual-fail-functional because each channel detects its own failures independently of the others. Independence of control channels permits considerable simplification of the control logic and prevents any possible failure propagation or electrical interference between channels.

The cables connecting the system elements are performed and shielded multiconductor type, providing point-to-point connection at rugged self-locking threaded connectors with strain relief. Each cable is a line-replaceable unit.



130

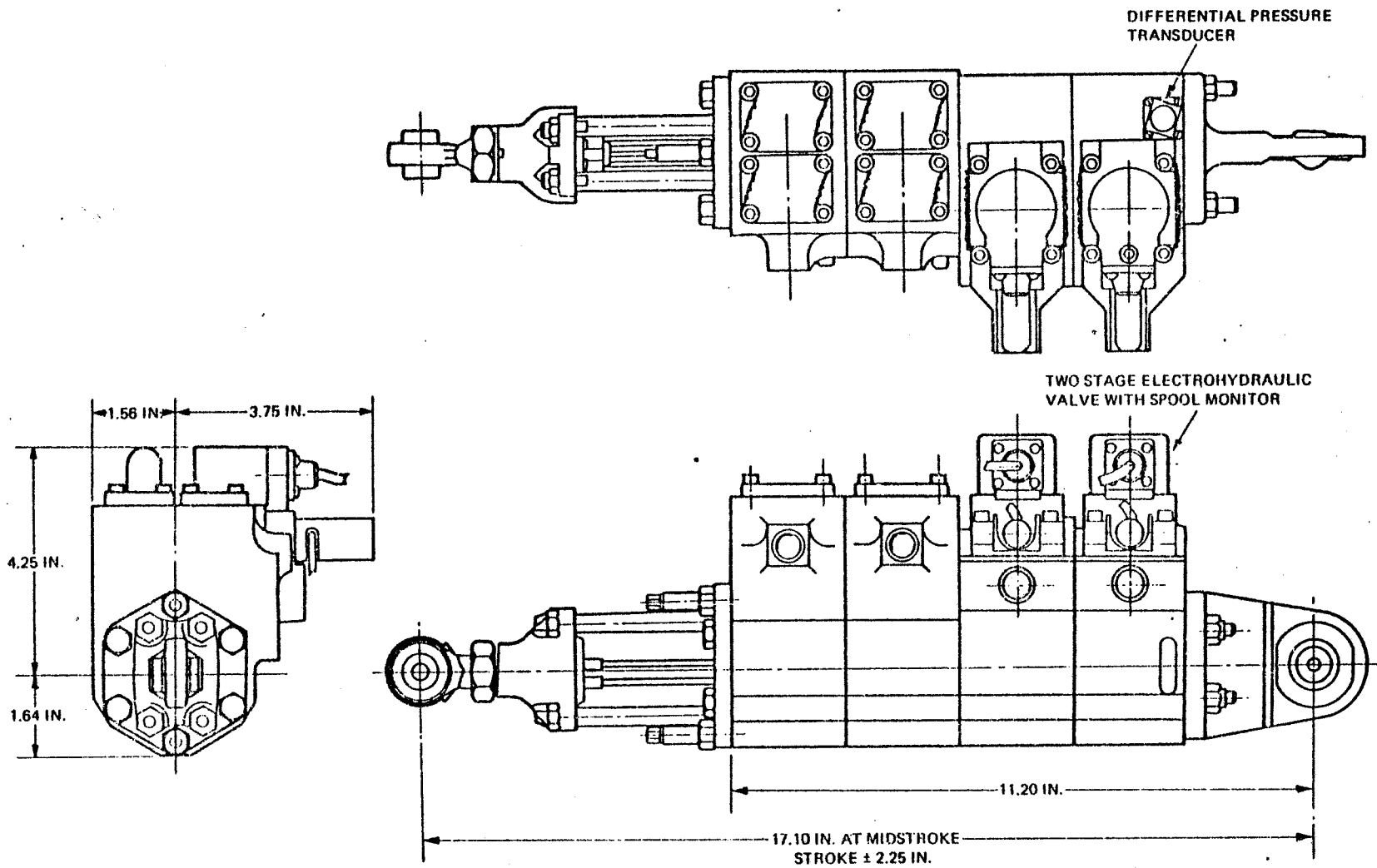


FIGURE 4.4.2 DUAL DRIVER ACTUATOR

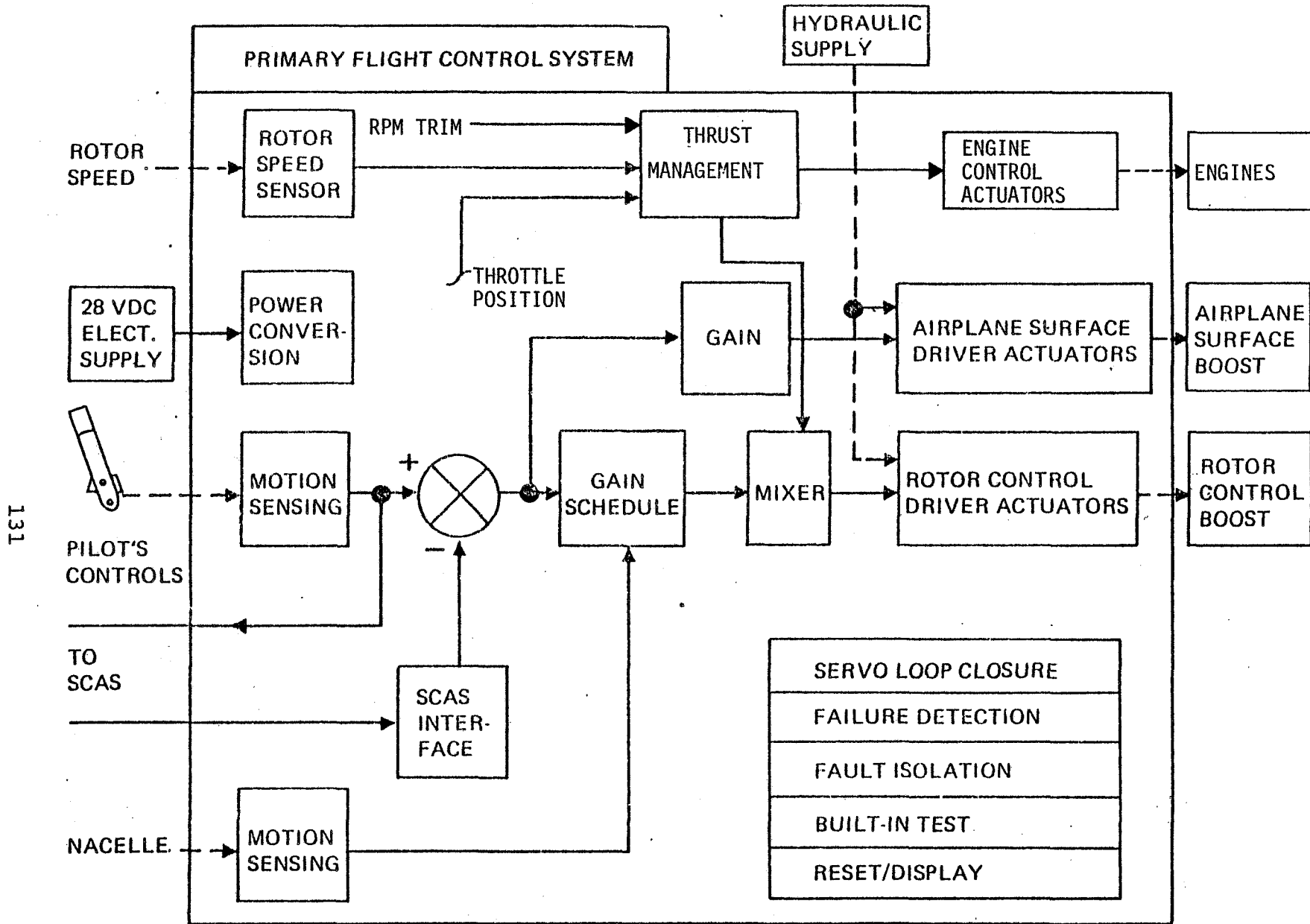


Figure 4.4.3 Primary Flight Control System Functions and Interfaces

131

Fiber optic links are provided to interface SCAS sensor signals and maintenance unit with the processor and to provide for inter-channel communications.

The maintenance unit provides automated checkout of the entire system in approximately 2 minutes; if a failure is detected, it provides the necessary failure information to quickly locate the failed line-replaceable unit. Interface is fiber optic.

Provision for adjusting rotor rpm, rotor torque balance, resetting a channel in flight, and clearing stored channel failure information is made at the primary flight control system panel.

- (c) Driver Actuators - The electrical link controls use identical electrohydraulic driver actuators at each location (Figure 4.4.2). These actuators accept commands from the flight control processor and position the existing XV-15 rotor and airplane surface boost actuators.

#### 4.4.2 System Transfer Functions/Interface

System transfer functions and performance characteristics are defined in the system specification, Appendix B. Major primary flight control system functions are shown in Figure 4.4.3, as described in the following paragraphs.

Motion sensing - The control position transducers convert pilot stick and pedal motions to equivalent electrical signals for input to the digital microprocessor.

SCAS interface - The dualized primary microprocessor accept SCAS command from the SCAS processor via authority and rate-limit functions. The limited signals shall be summed with the control position signals before mixing.

Gain scheduling - Axis command signals (summation of pilot control and SCAS command) are scheduled as a function of nacelle angle. In general, pilot inputs to the rotor are phased out as the nacelle is brought to the horizontal position (zero degrees).

Thrust management - Provides for control of rotor rpm via inputs to rotor collective pitch and engine N1 controls. The system responds to pilot throttle setting and rotor rpm. Direct pilot control of collective pitch is phased out at zero degrees nacelle incidence. Manual trim of rotor rpm and differential collective pitch is provided on the system control panel.

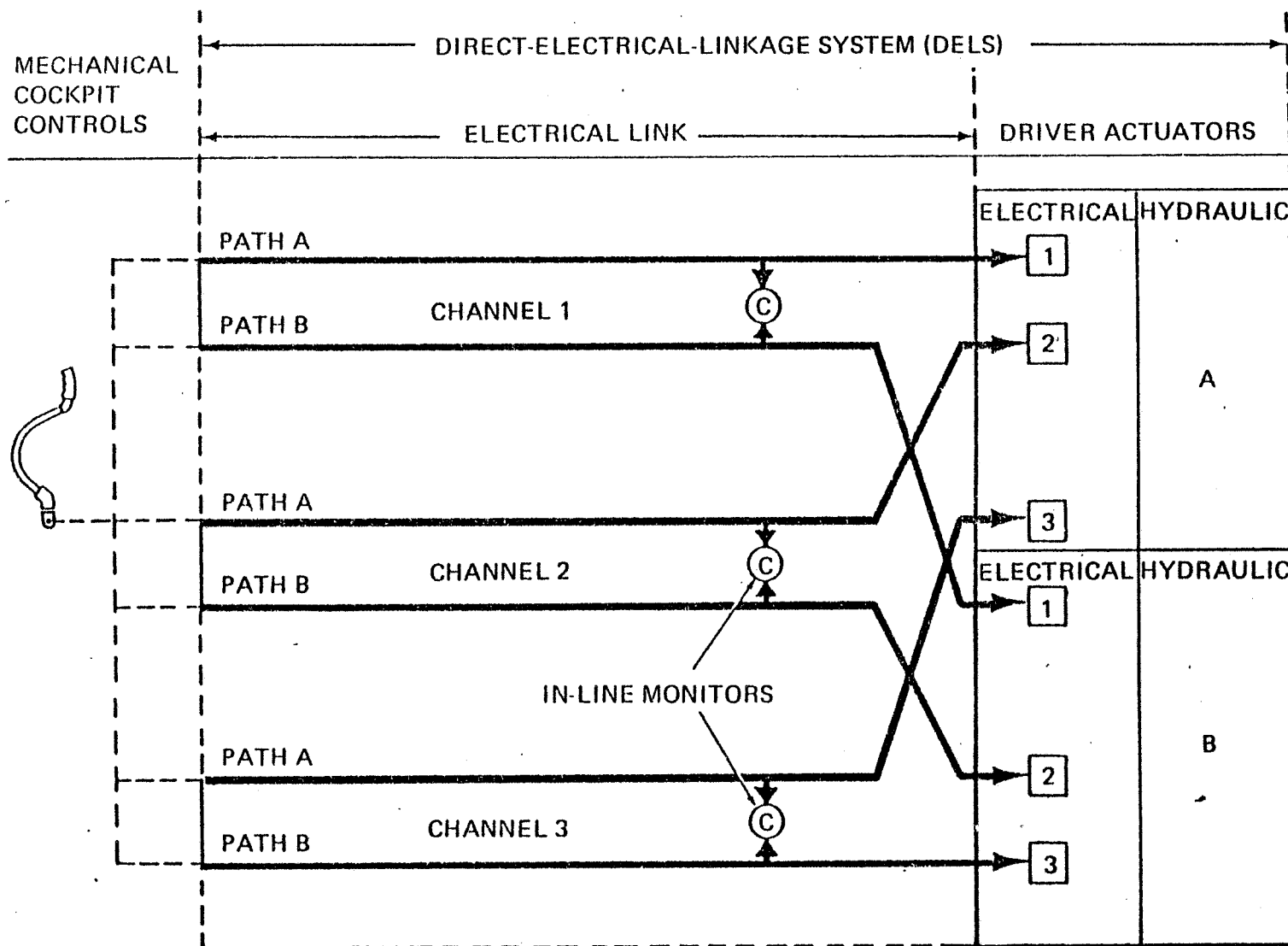
Airplane surface control - Axis commands are processed via appropriate gains and actuation to position the flaperons, rudder, and elevator.

Mixing - The processor mixes scheduled axis commands and governor outputs via appropriate gains to position the rotor control actuators.

Servo loop closure - The processor includes the electronics to control rotor and airplane surface driver actuators which in turn control boost actuators.

Rotor actuation - The rotor control boost converts the mixer outputs to equivalent rotor swashplate motion.

Power conversion - The processor converts the 28vdc supply to ac for sensor excitation and dc supplies as needed to operate electronic devices used in the system.



134

Figure 4.4.4 Redundancy Management of Primary Flight Control System

Failure detection - Each flight control processor processes all failure detection within its channel and, upon detecting a failure, shuts down the channel inputs to the affected actuators and transmits failure information to the PFCS panel and maintenance unit.

#### 4.4.3 Redundancy Management

The Primary Flight Control System is a triple redundant, self-monitored electrical link controlling dual redundant electrohydraulic driver actuators. This system is interfaced with a triplex cross-channel monitored SCAS.

As shown in Figure 4.4.4 the self-monitored concept of redundancy management for each channel involves the use of two identical control paths in each channel between the cockpit controls and the actuator input. These paths are mechanized using digital microprocessors. If a discrepancy occurs which is greater than a pre-established tolerance level, that channel is considered to have failed and is shut down. The electro-hydraulic driver actuators have dual hydraulic sections and triplex electrical sections. Thus, the mechanical linkage of the present control system is replaced with a triplex electrical link, while the present dual hydraulic power section is maintained in the fly-by-wire mechanization. Each channel of the electrical link is powered by an independent electrical supply. Tracking of three channels is maintained by control of overall gain tolerances. Channel inputs to the actuator are summed magnetically in the electro-hydraulic valves of the actuator. Inherent failsafety without time-critical switching is maintained for first failures by use of magnetic summing.

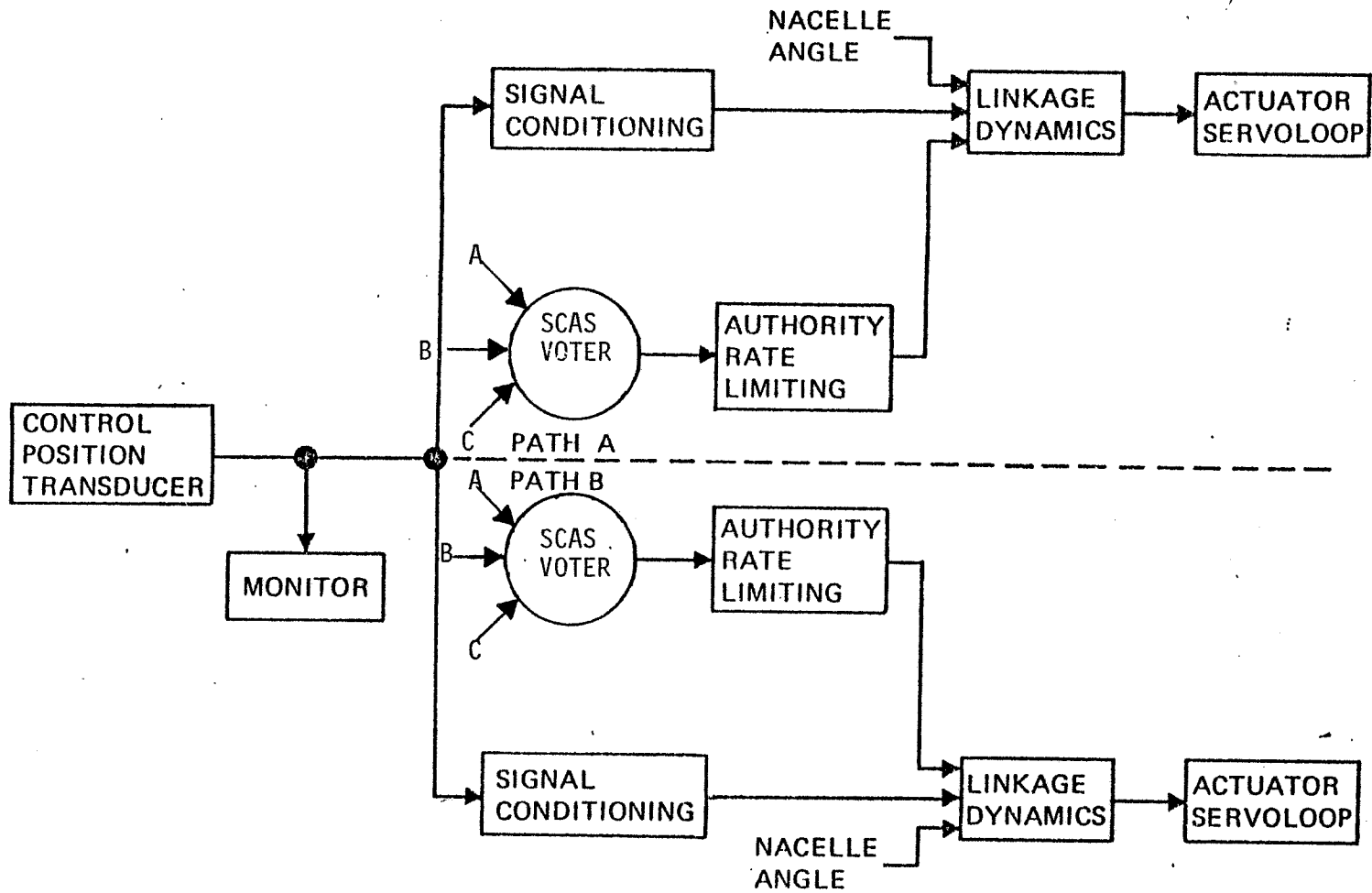


Figure 4.4.5 Dual Path Primary Flight Control Channel

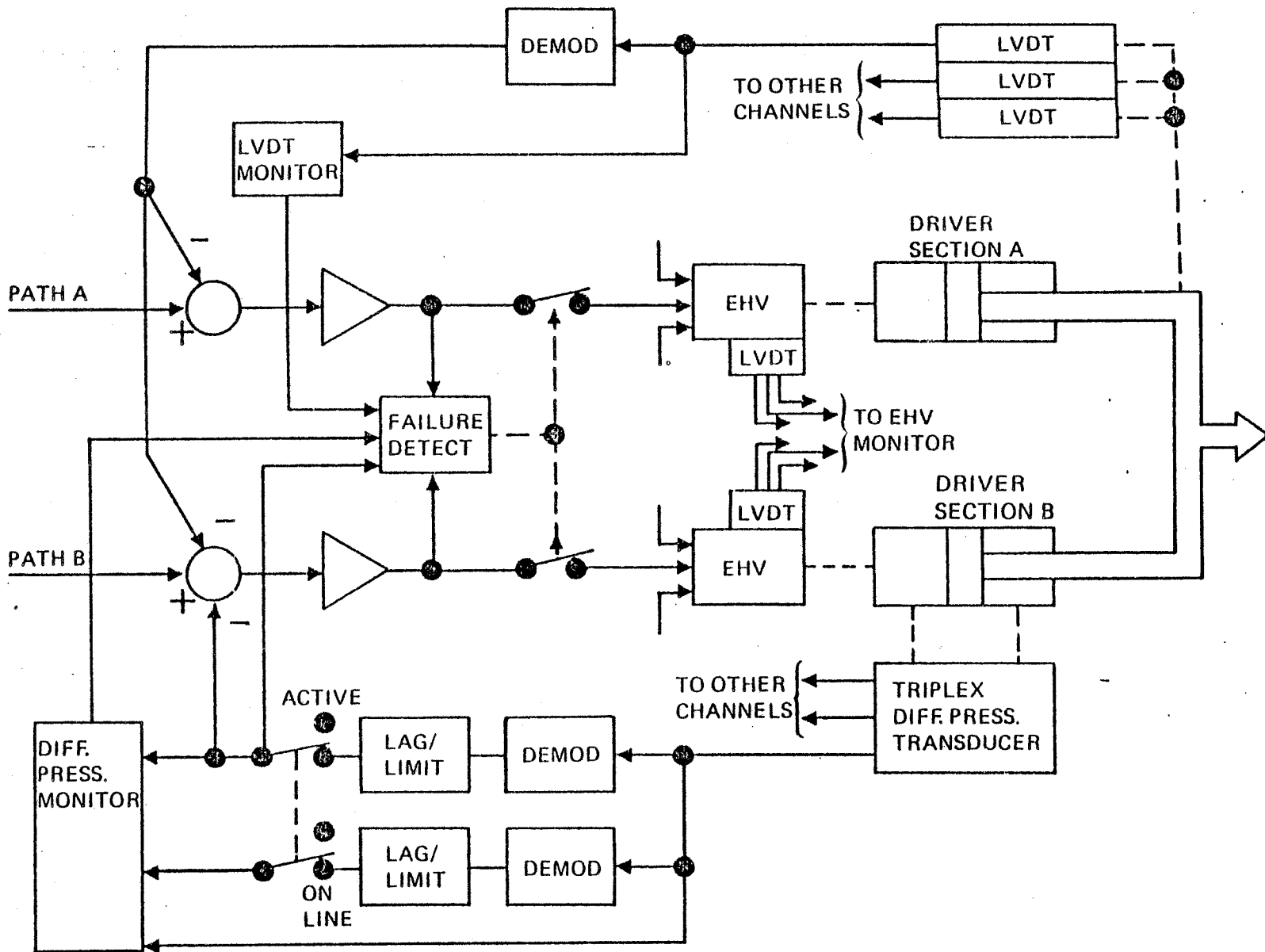


Figure 4.4.6 Dual Driver Servoloop and Failure Detection



The electrical link inputs are the cockpit controls, the SCAS, and nacelle position. Each channel receives the same signal from the self-monitored cockpit control position transducers. Figure 4.4.5 shows a typical one-axis channel of the triplex electrical link up to the actuator servo loop.

As noted previously, SCAS commands are distributed to all three channels via dedicated fiber optic links. Signals are processed to convert them to digital format. They are next voted and passed through authority/rate limiters in the primary control microprocessors and summed with the primary control commands. With this approach, SCAS failures cannot cause primary system channel shutdowns. Therefore, the primary control system reliability becomes independent of SCAS. Pilot warning without shutdown will be provided if the channel outputs differ. The pilot can then shut down these inputs, if necessary.

Figure 4.4.6 shows the mechanization of the driver actuator servo loop with details on interchannel compensation and failure detection. As noted previously, each channel provides inputs to both driver section EHV, and the tracking to the two driver sections is maintained using the active/on-line approach. When both sections are operating, the B section has a lagged limited-authority differential pressure feedback as shown in Figure 4.4.6. This feedback cancels the static offset between the sections and prevents force fights and hysteresis.

Failures of the servo path are detected as follows:

- Drive piston LVDT and differential pressure transducer - By monitoring the common-mode secondary voltage. The transducers are designed so that the common-mode voltage is essentially constant over the stroke. If excitation is lost or the coil opens, the voltage will decrease; if a secondary shorts to power, the output will increase. Either condition will cause the monitor to trip. Mechanical failures of the transducers are detected by a periodic check of channel tracking during built-in test.
- Differential pressure transducer electronics - By comparison of dual processing in differential pressure monitor.
- Input command, feedback control electronics, EHV wiring, and coils - By comparison of servo amplifier output current. This comparison includes subtraction of differential pressure input from the Path B output.
- Electrohydraulic valve mechanical failures - By comparison of EHV second spool position with input current. A mechanical failure of the EHV has a remote probability. The EHV monitor provides for a three-way vote by the channels. If all vote failure, the pressure supply to that actuator section is shut down.

#### 4.4.4 Equipment Physical Characteristics

Flight Control Processor: Configuration similar to a 3/4 ATR short case (i.e. 7.88" high x 7.50" wide x 12.52" long -740 in<sup>3</sup>). Weight 21 lbs.

Driver Actuator: Envelope per Figure 4.4.2 Weight: 22 lbs.

PFCS Control Panel: Size 5.75" wide x 5.63" high x 3.66" deep.  
Weight: 3.5 lbs

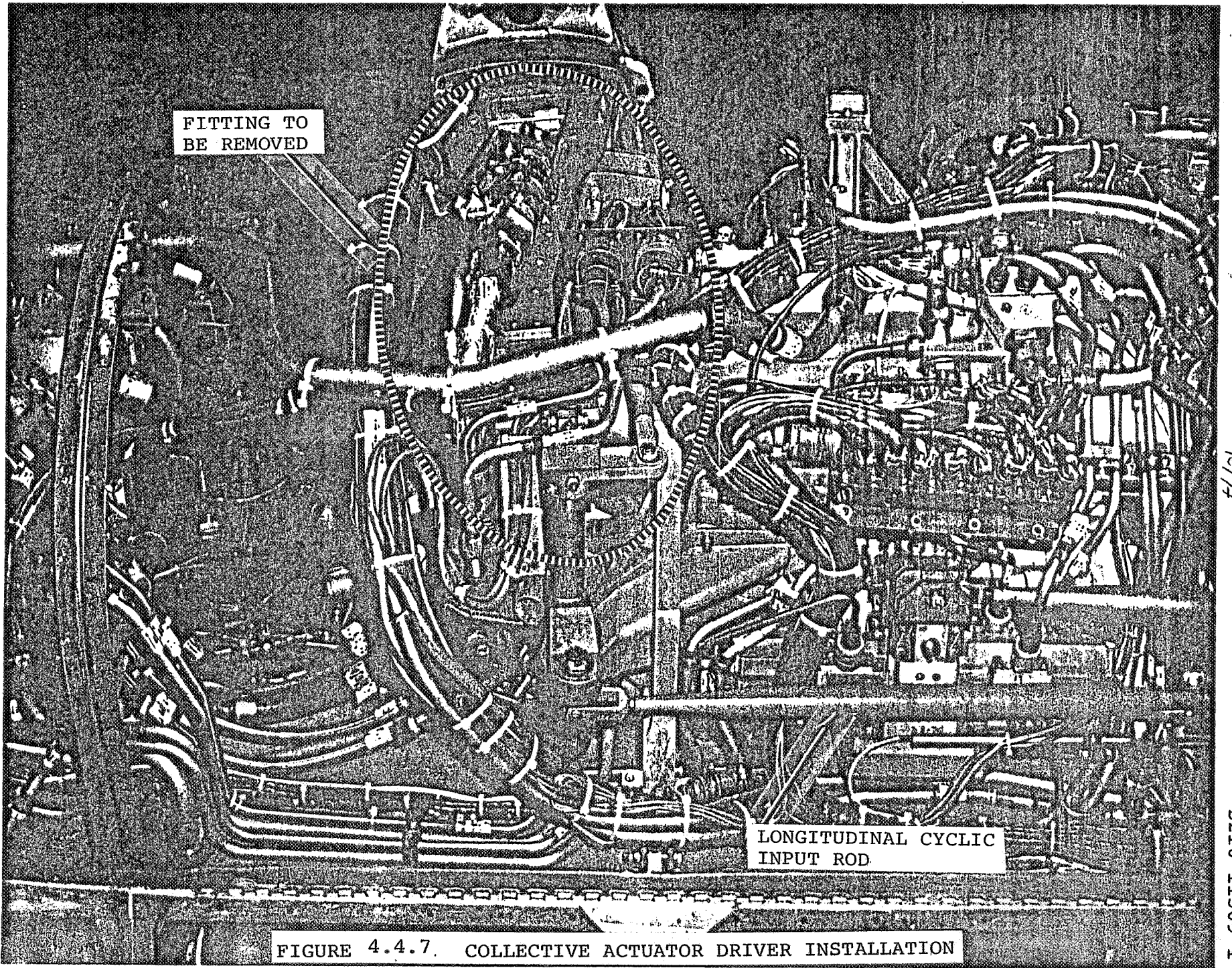
Maintenance Unit: Size 6.00" wide x 6.00" deep x 4.75 in. high.  
Weight: 4.5 lbs.

Junction Box: 7.5" long x 4.5" wide x 1.5" deep. Weight 5.0 lbs.

#### 4.5.5 Installation

The following paragraphs discuss a possible equipment installation arrangement within the XV-15.

- (a) Cockpit Area - Mechanical control runs will be disconnected and pilot's controls linked to multi-redundant LVDT packages. Existing force feel and trim provisions retained. The PFCS panel will be located in the center instrument console. An electrical input engine control quadrant will replace the existing mechanical input quadrant.
- (b) Avionics Bay - Maintenance unit will be installed.
- (c) Under Cabin Floor - Junction boxes will be installed to collect signals from cockpit/avionics bay for transmittal to the Flight Control Processor.
- (d) Flight Control Processor Installation - The units will be installed wherever a suitable space is available. The space aft of the wing, presently housing the mechanical mixer is a candidate.



FITTING TO  
BE REMOVED

LONGITUDINAL CYCLIC  
INPUT ROD

FIGURE 4.4.7. COLLECTIVE ACTUATOR DRIVER INSTALLATION

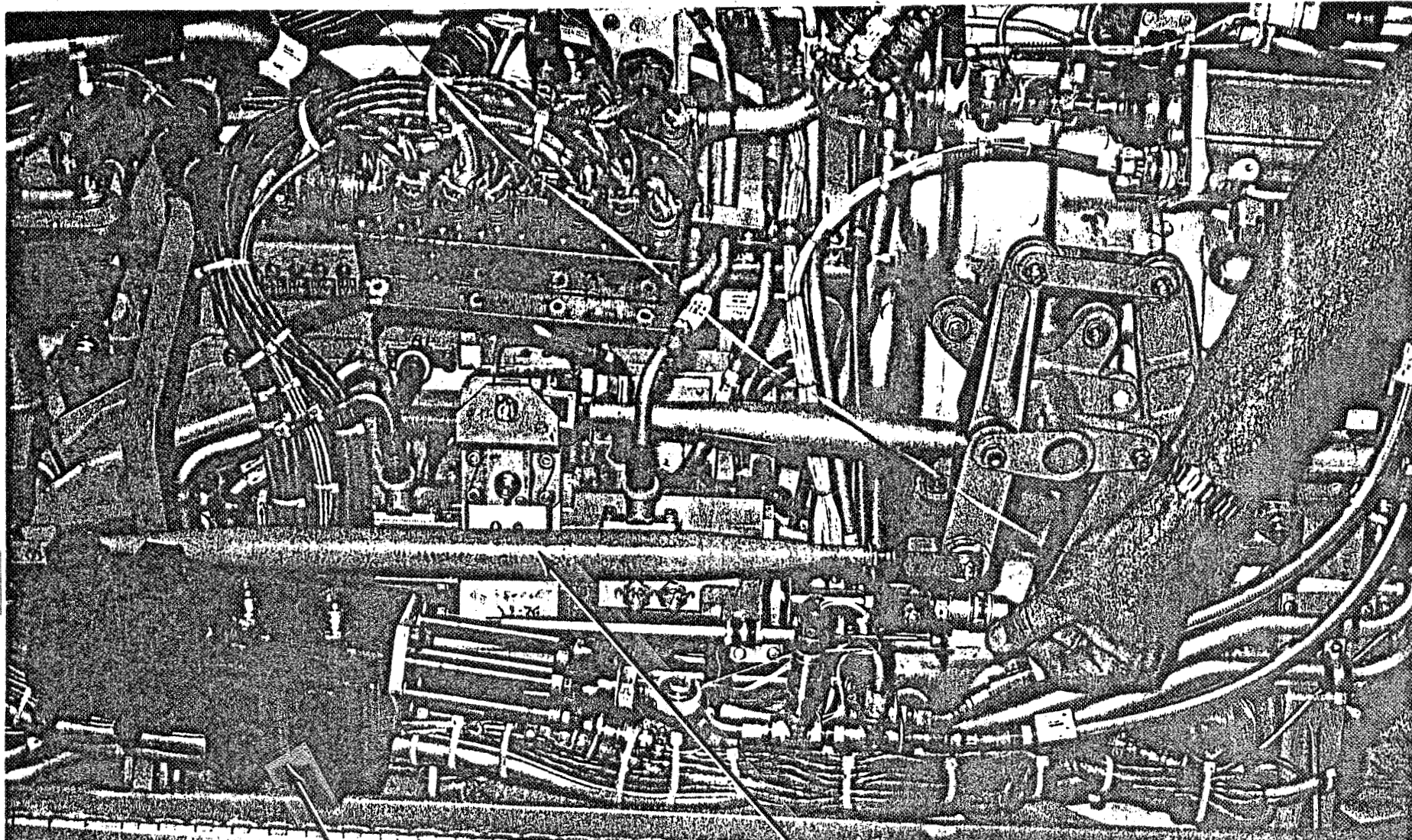
141

ORIGINAL PAGE IS  
OF POOR QUALITY

2/4

D210-11569-1



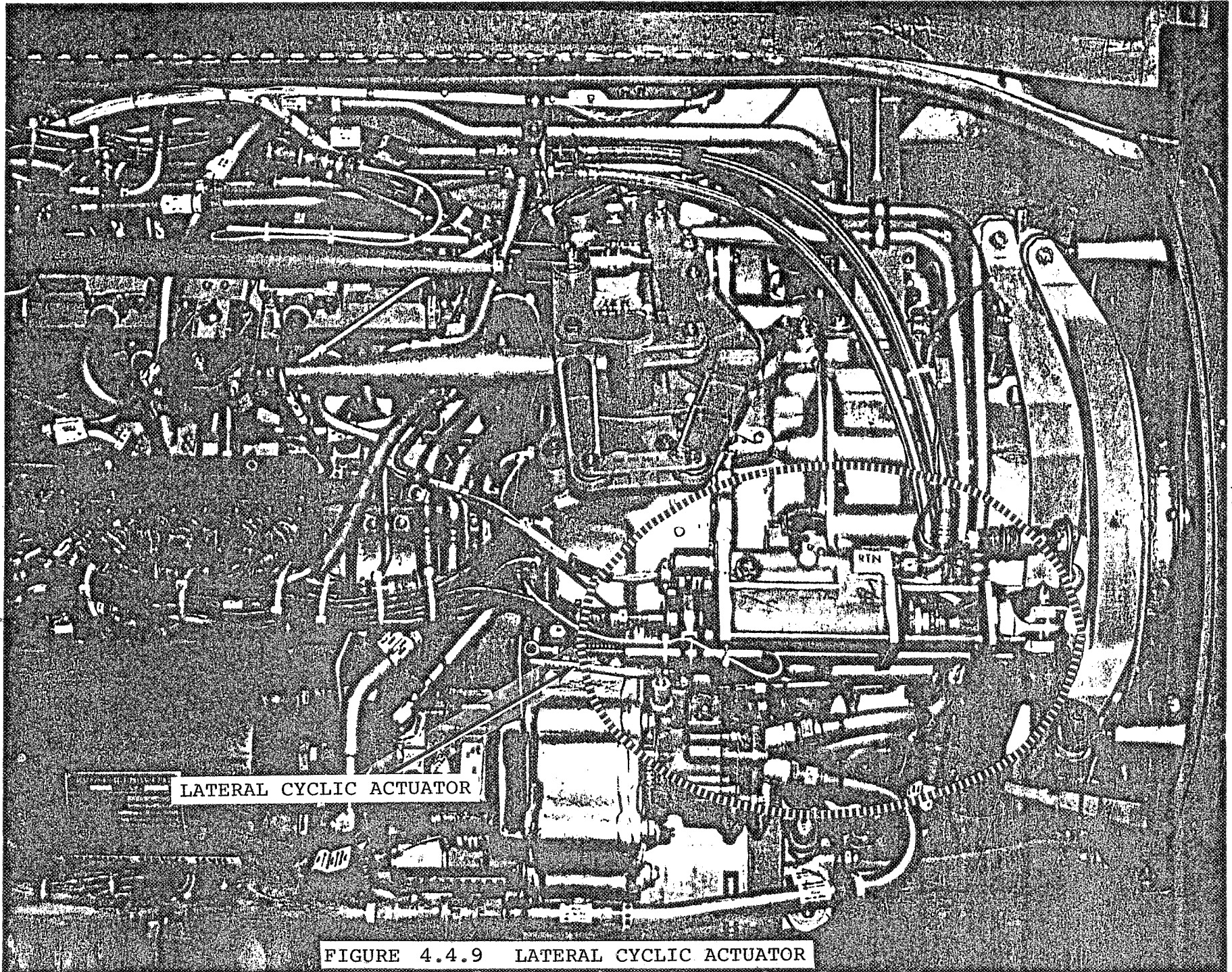


LONGITUDINAL CYCLIC  
ACTUATOR INPUT ROD

DUAL DRIVER ACTUATOR MOCKUP

FIGURE 4.4.8 LONGITUDINAL CYCLIC DRIVER INSTALLATION





LATERAL CYCLIC ACTUATOR

FIGURE 4.4.9 LATERAL CYCLIC ACTUATOR

2/14

D210-11569-1

(e) Actuators

- Collective Pitch Actuator: A dual driver will be installed and linked to the existing boost by removing the structural fitting which supports the collective and longitudinal cyclic bellcranks at the input to the nacelle (see Figure 4.4.7). The driver actuator will be tied to available nacelle structure with a new support.
- Longitudinal Cyclic: The existing push rod at the input to the longitudinal cyclic boost actuator would be removed and the driver actuator tied between the boost input and a new structural support (see Figure 4.4.8). The nacelle cowling would be enlarged locally to accommodate the actuator.
- Lateral Cyclic Actuator: The existing electrohydraulic actuator (Figure 4.4.9) would be interfaced with the fly-by-wire system.
- Flaperon Actuator: The driver would be mounted inboard and inline with the boost actuator.
- Rudder/Elevator Actuator: Drivers will be located at the input to the existing actuators. Space is not critical.

(f) Interconnection

Details on proposed system cabling are shown in Figure 4.4.10. All cables will be shielded multi-conductor units terminalled in self-locking threaded connector series MIL-C-83723. Shielding is included as a protection against lightning effects; analysis and test of system interface circuits indicates it is probably not required.

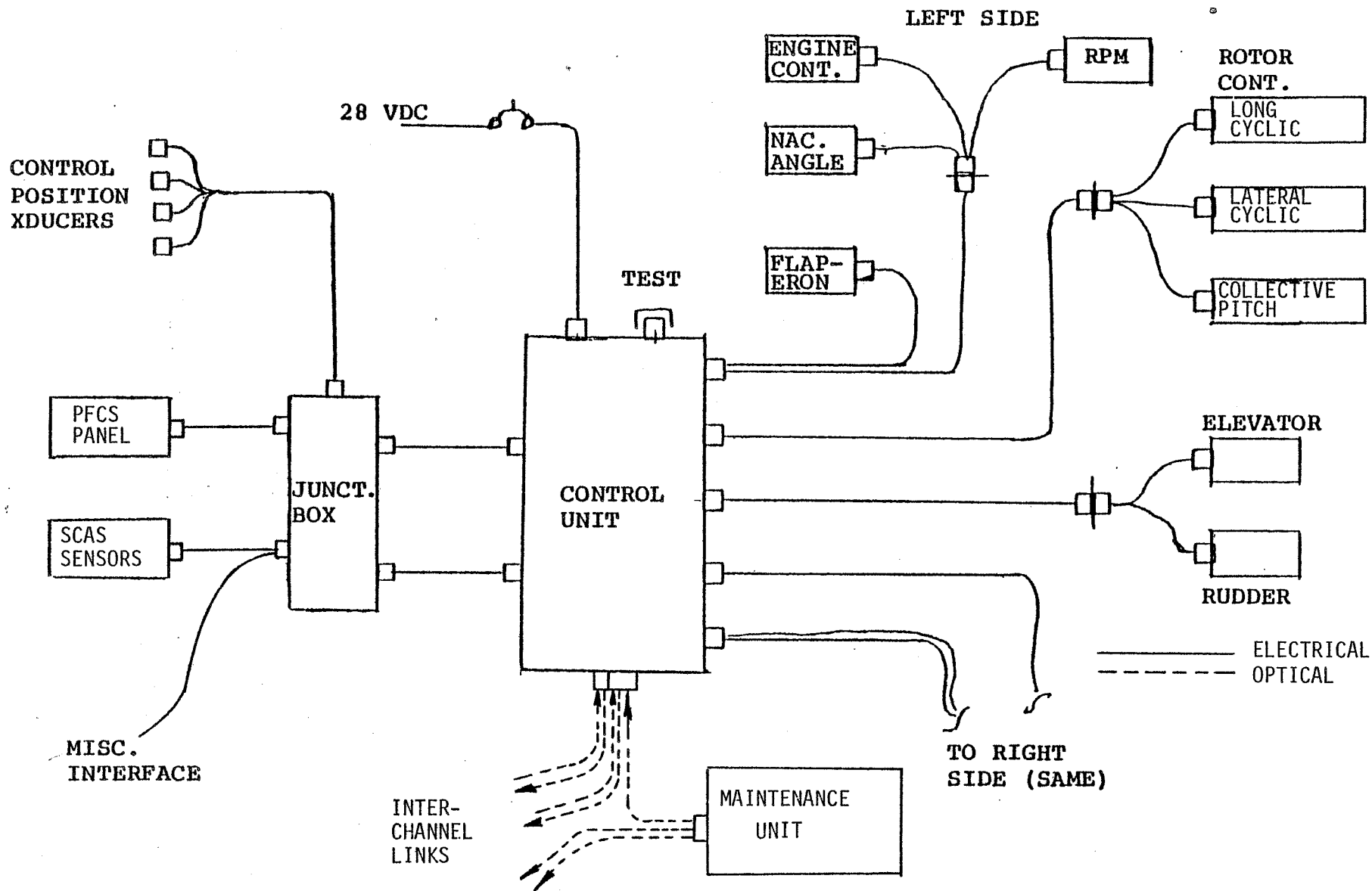


FIGURE 4.4.10 PRIMARY FLIGHT CONTROL SINGLE CHANNEL INTERCONNECT



Interchannel connectors will be via multiple conductor fiber optic bundles, which interface with conventional circular connectors similar to series MIL-C-83723.

5.0 REFERENCES

1. Saaty, T. L., "A Scaling Method for Priorities in Hierarchical Structures," Journal of Mathematical Psychology, Nov. 15, 1977
2. Magee, J. P. and Alexander, H. R., "A Hingeless Rotor XV-15 Design Integration Feasibility Study. Volume I, Engineering Design Studies," NASA CR 152310, March 1978 (Boeing Document D210-11360-1)
3. "Proposal for Preliminary Design Studies of Advanced Rotor Blades, Hubs and Control Systems for the Tilt Rotor Aircraft." Boeing Document D222-10066-1, August 1978

## APPENDIX A

## AERODYNAMIC DESIGN SELECTION PROCEDURE

A.1 Introduction

Fatigue life and performance improvements are sought for the NASA-Army XV-15 Tilt Rotor aircraft by replacing the existing metal rotor blades with blades fabricated from advanced composite materials and designed to yield increased aerodynamic efficiency in both hover and cruise flight. Design constraints on the replacement rotor are:

- (1) maintain same rotor diameter (25 feet)
- (2) maintain existing hover and cruise rpm values

The performance goals for the aircraft with the new rotors installed are stated in Reference A1 as follows:

"....to equal or improve the performance levels of the existing metal blades throughout the flight regime of the XV-15 aircraft, with emphasis on significant improvement for hover flight (increased hover thrust/horsepower and stall margin to enhance all hover performance, including single-engine operation safety margins) and range (improved cruise efficiency), in that order of preference .. the predicted performance shall be determined relative to the performance level of the XV-15 with standard metallic rotor blades installed. With the composite rotor blades installed, and at a design gross

weight and ambient conditions of 4,000 feet pressure altitude, 90°F, the stall margin as a goal shall be as much, or greater than with the metal blades. An increase of 6% in the maximum specific range in the airplane mode is desired."

In view of the design constraints on diameter and tip speeds these performance goals can only be achieved by suitably combining improvements in blade twist and planform with more efficient airfoils.

The following sections describe the steps that were taken to arrive at a candidate design rotor. These steps are

- (1) Determination of the (baseline) performance levels of the existing metal blades
- (2) Airfoil selection procedure
- (3) Twist/planform parametric studies
- (4) Blade optimization
- (5) Selection of candidate blades

#### A.2 Determination of Baseline Performance Levels for the Existing Blades

The geometric and design data on the existing blades was obtained from Reference (A2). Figure A.1 presents the planform, geometric twist and distribution of airfoil sections. Figures A.2 through A.5 show the blade section airfoil data as given in Tables 4.3 through 4.10 of Reference (A2). This data was modified as indicated to remove some inconsistencies and to bring the data more into line with trends on similar sections.

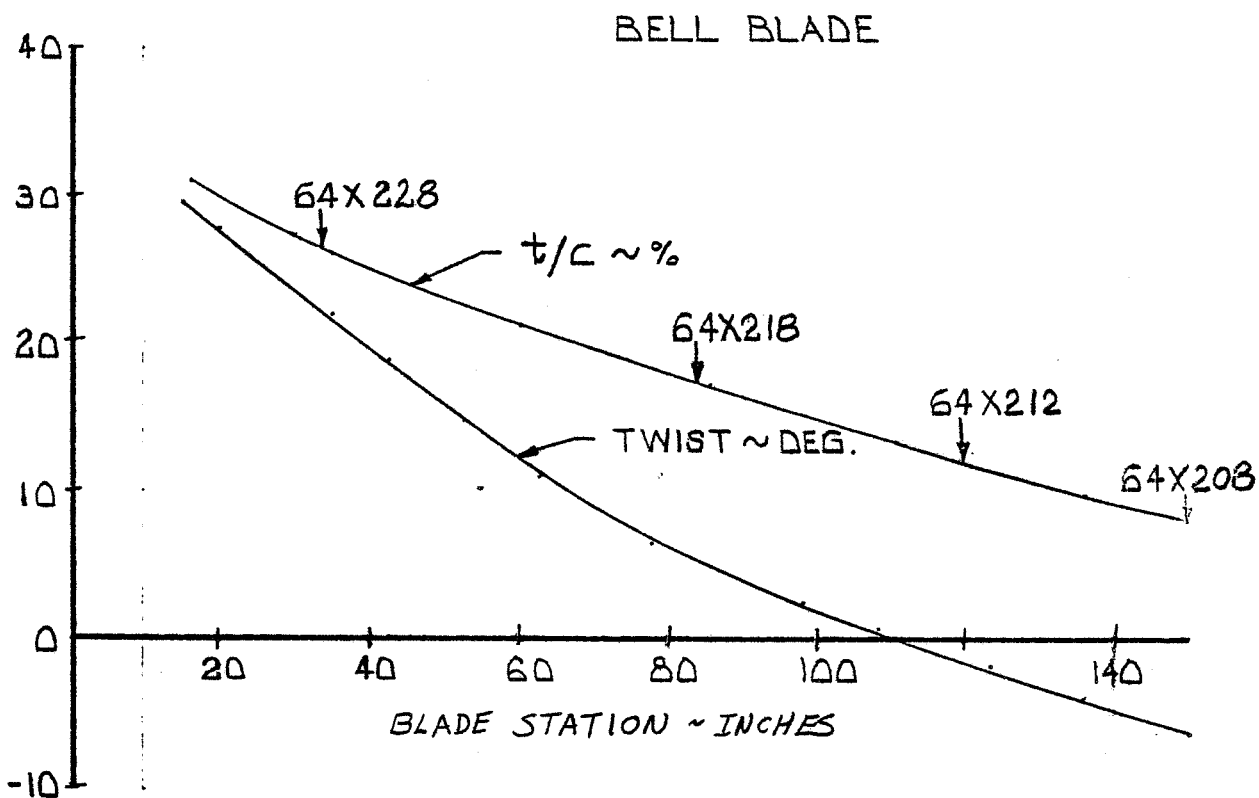
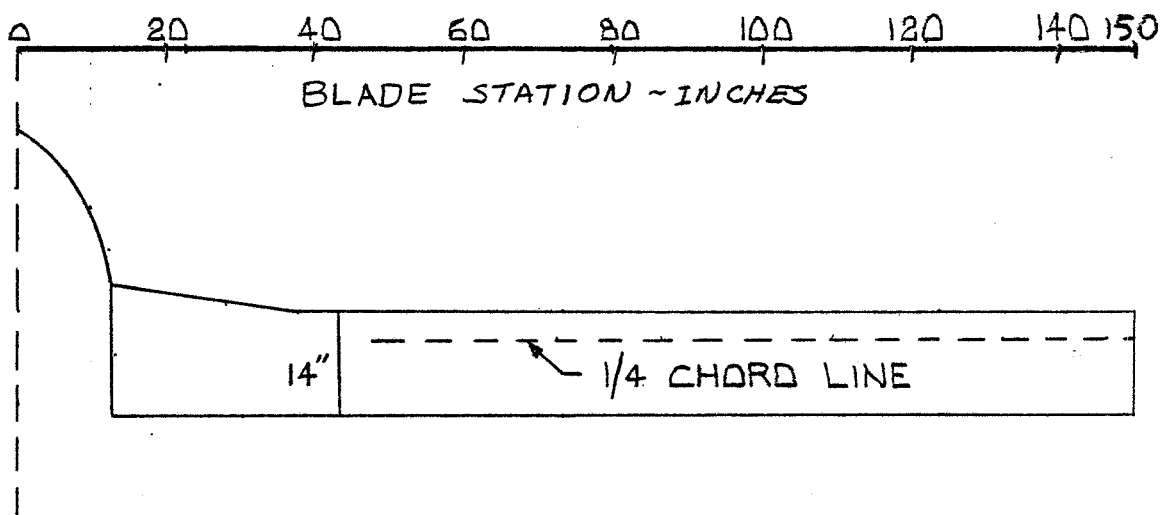
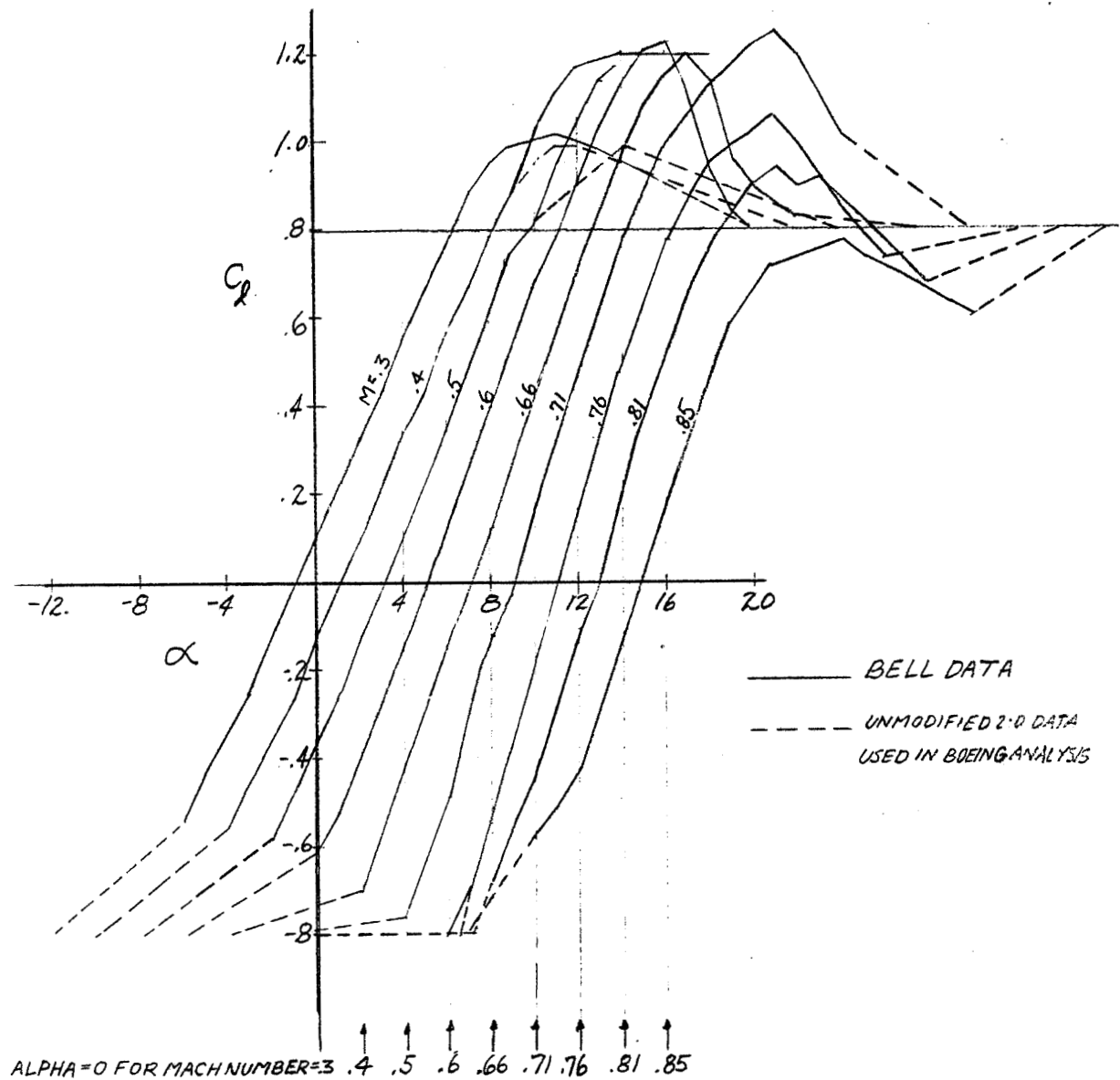


Figure A-1. Geometric Properties of Existing Bell XV-15 Rotor Blade



$C_l$  VERSUS  $\alpha$ ; 90 TO 100 PERCENT BLADE RADIUS

Figure A-2.  $C_l, \alpha$  Data Used in Evaluation of XV-15 Steel Blade

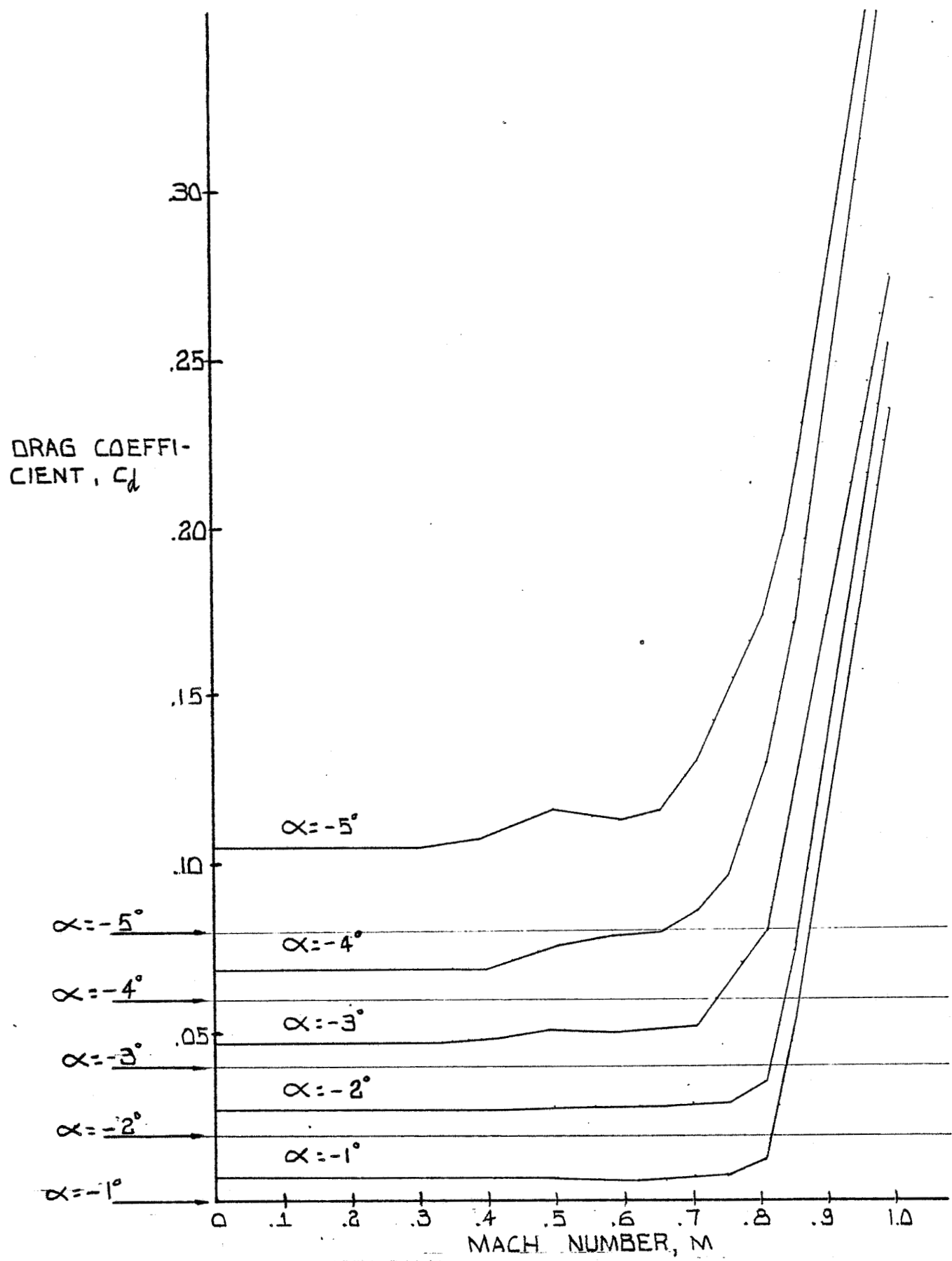


Figure A-3.  $C_d$ , Mach Data in XV-15 Steel Blade Evaluation

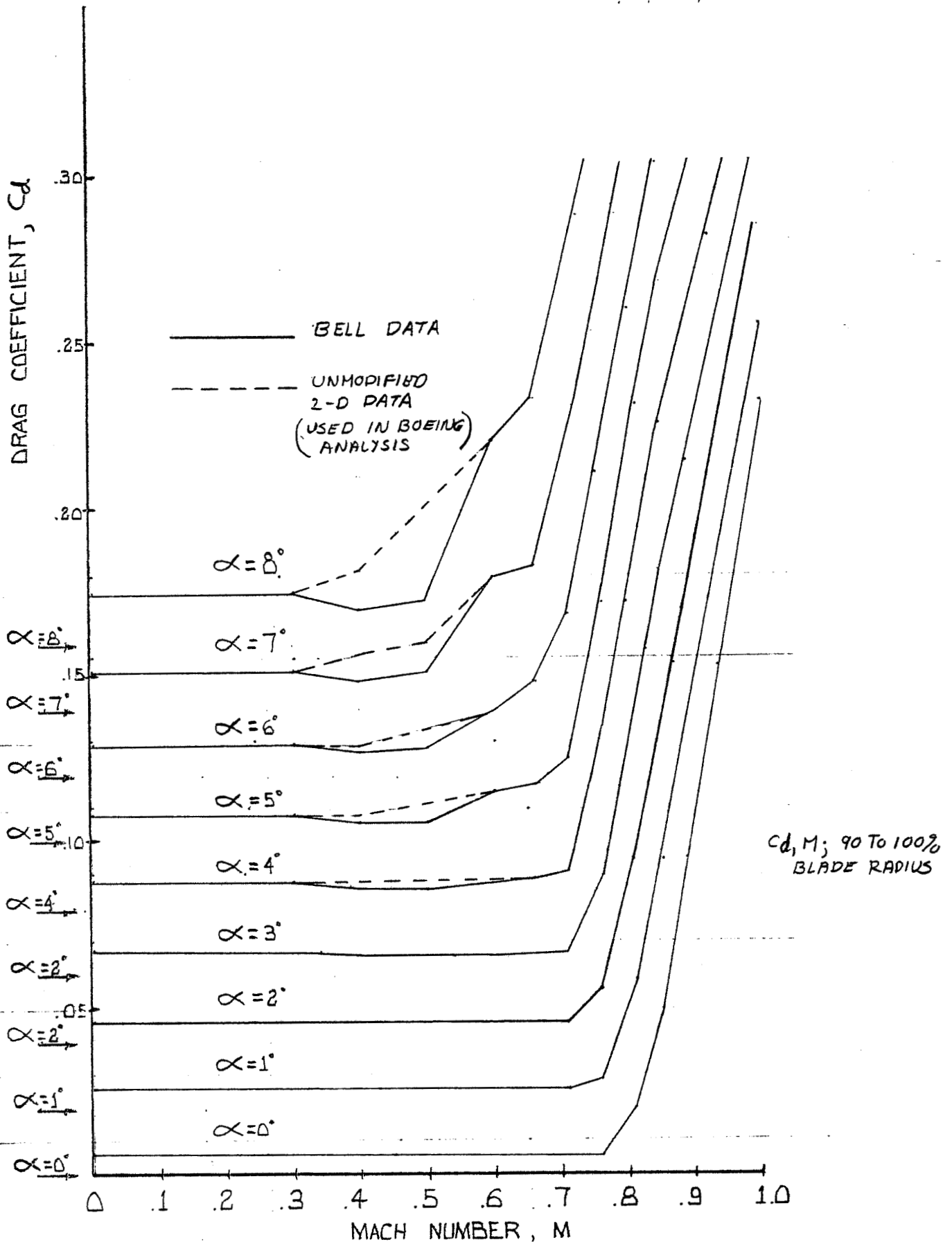


Figure A-4.  $C_d$ , Mach Data Used in XV-15 Steel Blade Evaluation



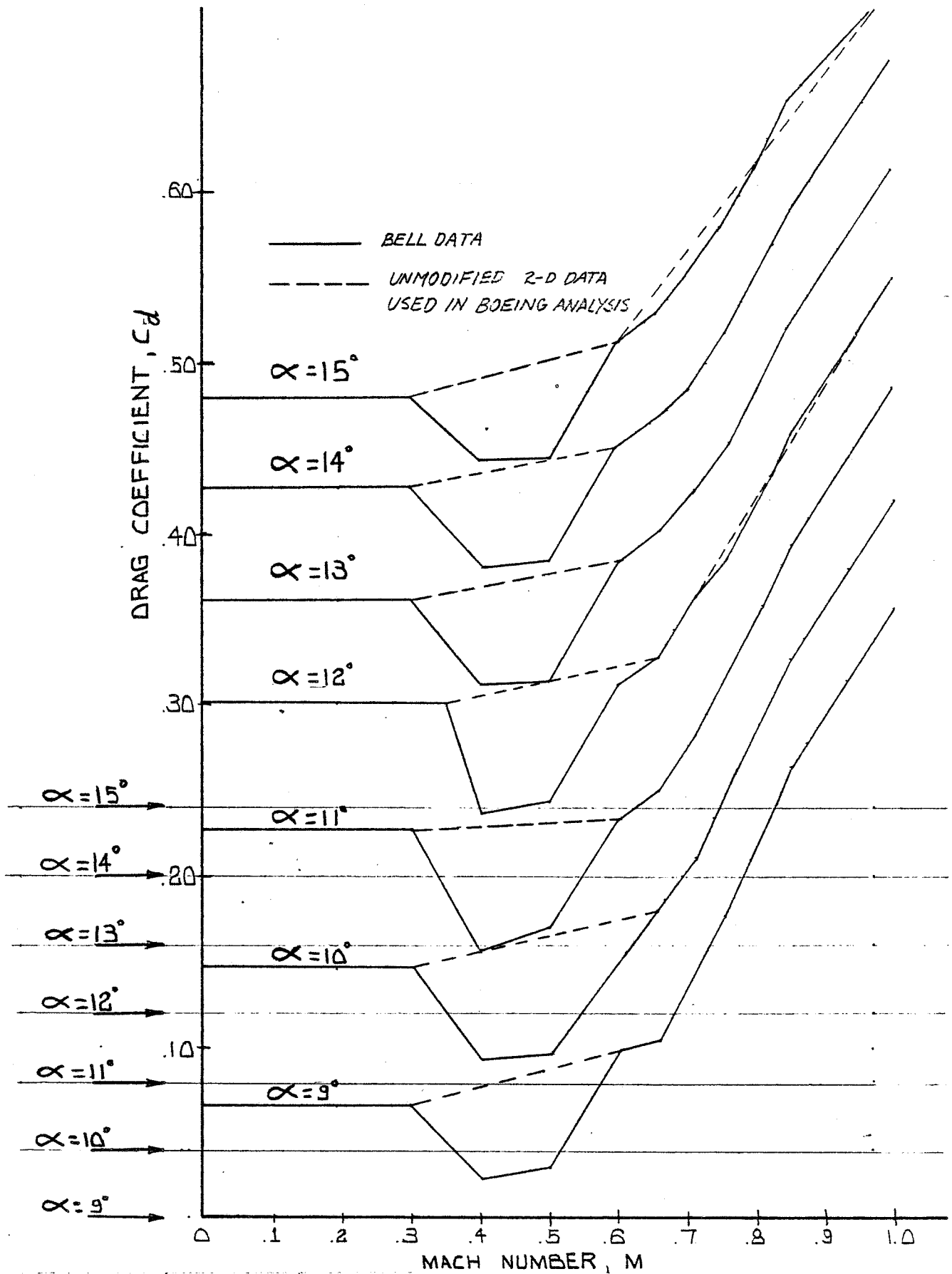


Figure A-5.  $C_d$ , Mach Data Used in XV-15 Steel Blade Evaluation

The minimum drag levels of the sections were also increased by an amount  $\Delta C_d = .002$  to represent realistic flightworthy blade airfoil conditions.

The hover and cruise performance of the rotor with the metal blades was then calculated using Boeing-developed computer program B92, Reference A3 . Figure A.6 presents the hover performance in terms of rotor figure-of-merit versus thrust coefficient and the cruise performance as a plot of cruise efficiency versus thrust coefficient at 200 knots, 10,000 feet standard.

### A.3 Target Performance Levels for the Replacement Rotor

The performance goals outlined in Reference (A1) were interpreted as follows:

1. Obtain a 6% improvement in aircraft maximum specific range.
2. Consistent with achieving (1), maximize hover figure of merit at the design gross weight
3. Maintain or exceed the existing stall margin at design gross weight and 4000'/90<sup>o</sup>F

From the data contained in Reference (A2) the speed for maximum specific range is approximately 200 KTAS. At the cruise tip speed of 600 ft/sec this represents an advance ratio of .563. Figure A.6 presents the estimated variation of cruise efficiency with thrust coefficient at this advance ratio.

Knowing the fuel flow characteristics of the LTClK-4K engines and using the transmission efficiency and aircraft drag levels

A9

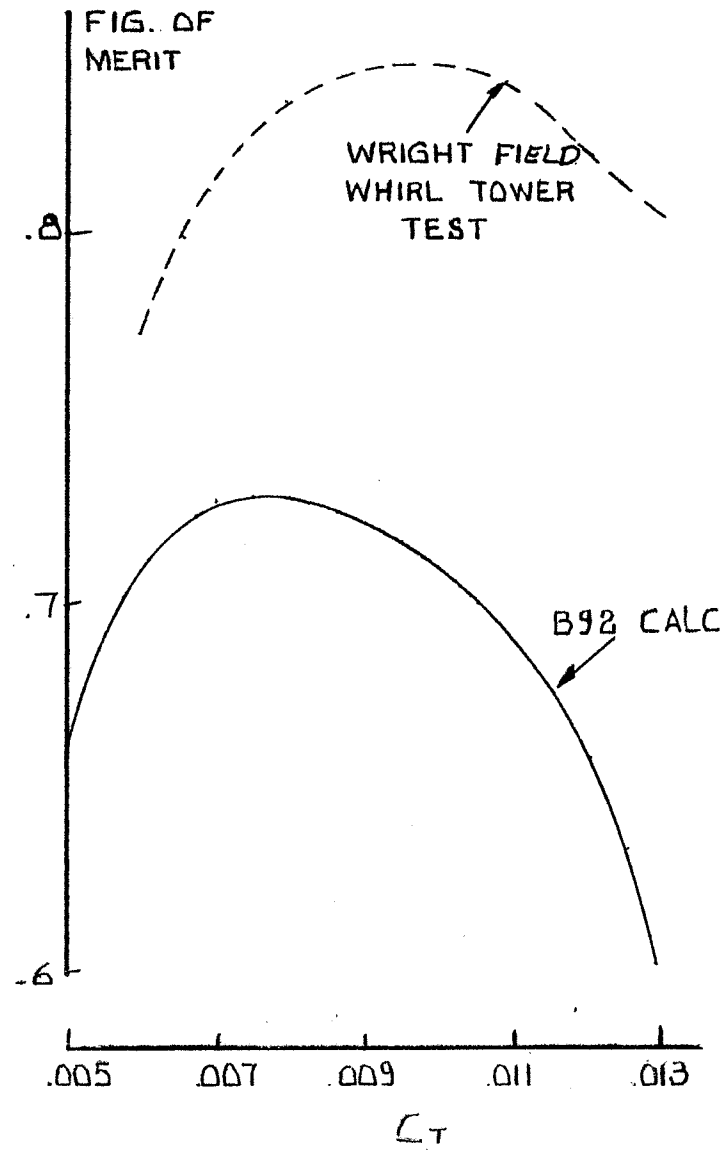
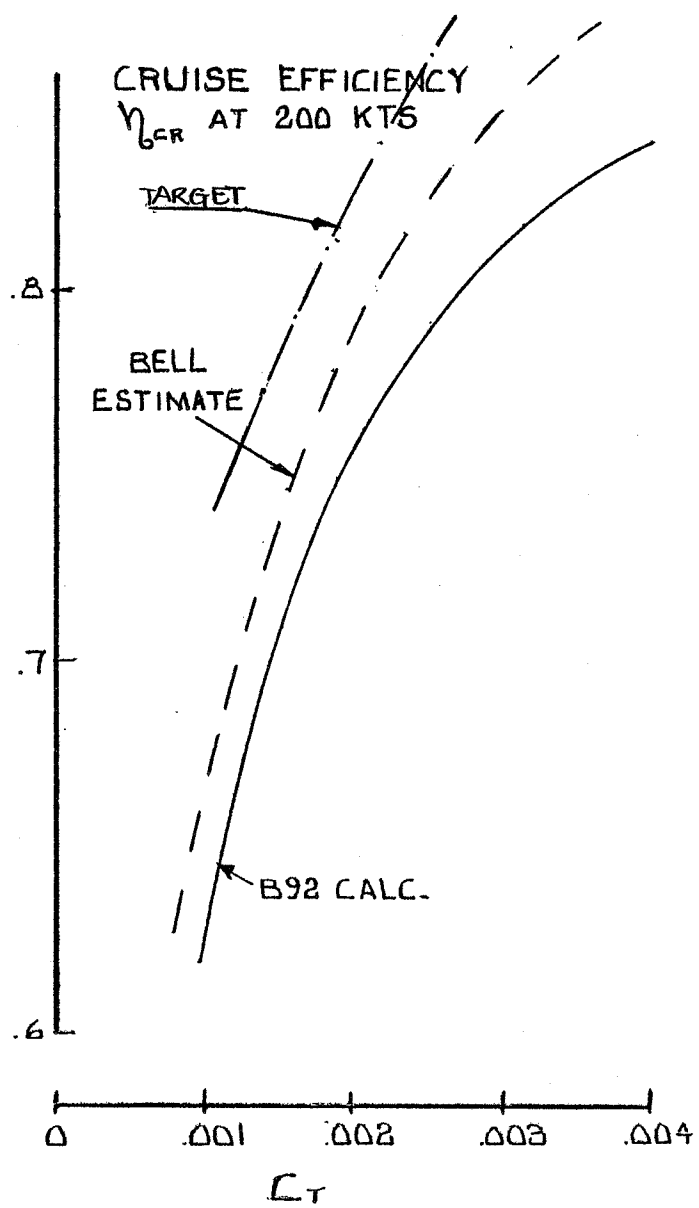


Figure A-6. Computed Performance of Baseline XV-15 Rotor

D210-11569-1

from Reference (A2) the cruise efficiencies that will be required of the new rotors to obtain the desired 6% improvement in airplane maximum specific range were calculated. The results (Figure A.6) show that in order to meet the target, the current rotor cruise efficiencies must be increased by as much as 10%.

#### A.4 Airfoil Selection

The principal airfoils chosen for the replacement blades are the Boeing Vertol-developed VR-7 for the working section and VR-8 for the tip section. These airfoils exhibit lower drag at the operating range of lift coefficients than the existing sections. Figure A.7 presents lift-drag polars for the VR-8 and VR-9 at  $M = .6$  and compares them to the 64X212 and 64X208 section employed on the existing rotor blades. As can be seen, the lift-dependent profile drag rise is delayed to higher lift coefficients with the VR series sections.

Initial selection of the radial positions of the airfoils on the blade was based on the blade Mach number environment and airfoil drag divergence characteristics. Figure A.8 presents this data and shows that in order to remain clear of drag divergence at moderate lift coefficients ( $C_l = 0.3$ ) on the advancing blade ( $\psi = 90^\circ$ ) at 120 knots in helicopter flight, the VR-7 airfoil should begin to transition to the VR-8 at  $X = 0.75$  with transition being completed before  $X = 0.90$  in order to avoid drag divergence on the VR-8 airfoil.

111

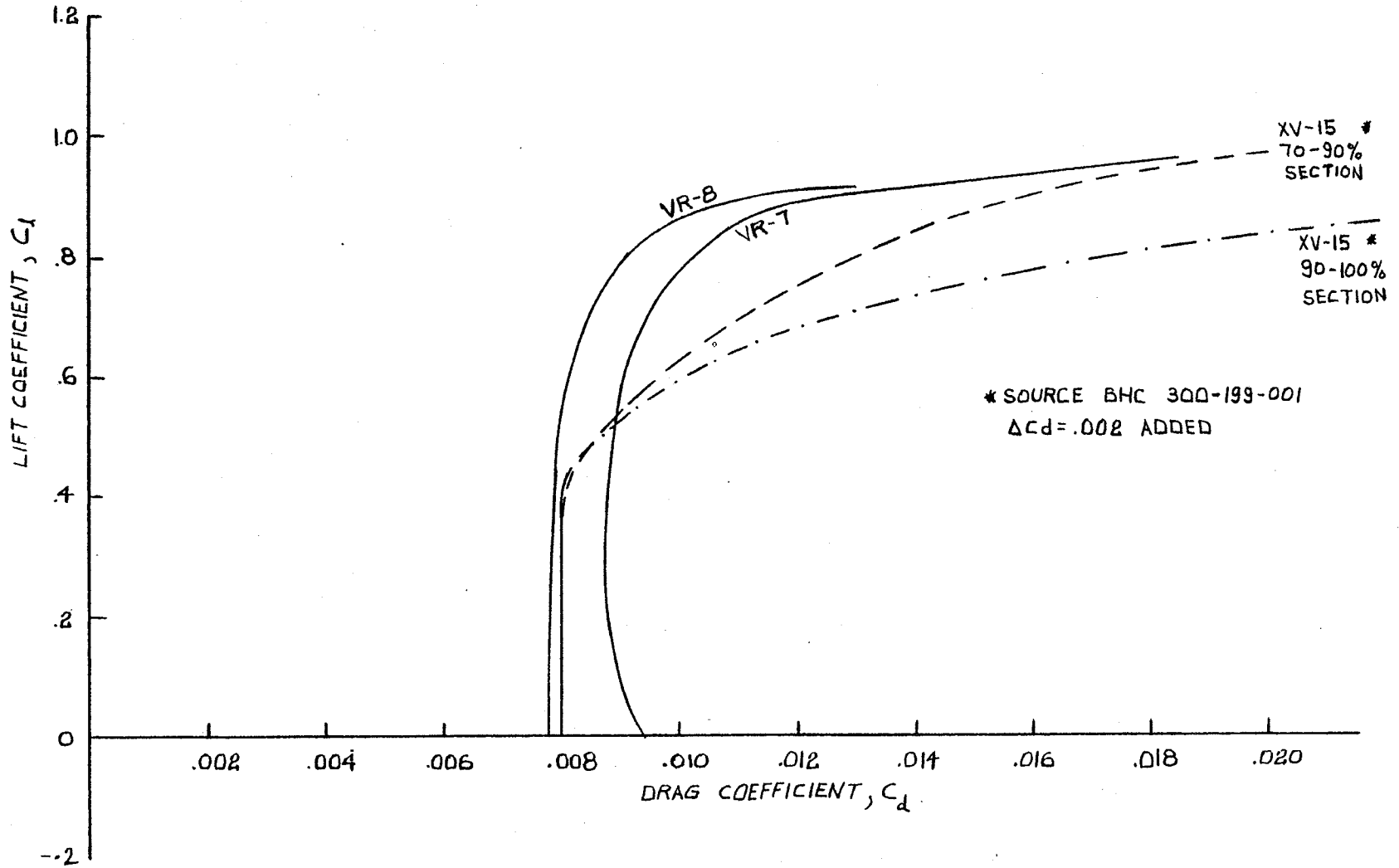


Figure A-7. Comparison of Advanced Airfoil Performance with Existing XV-15 Airfoil Performance

D210-11569-1

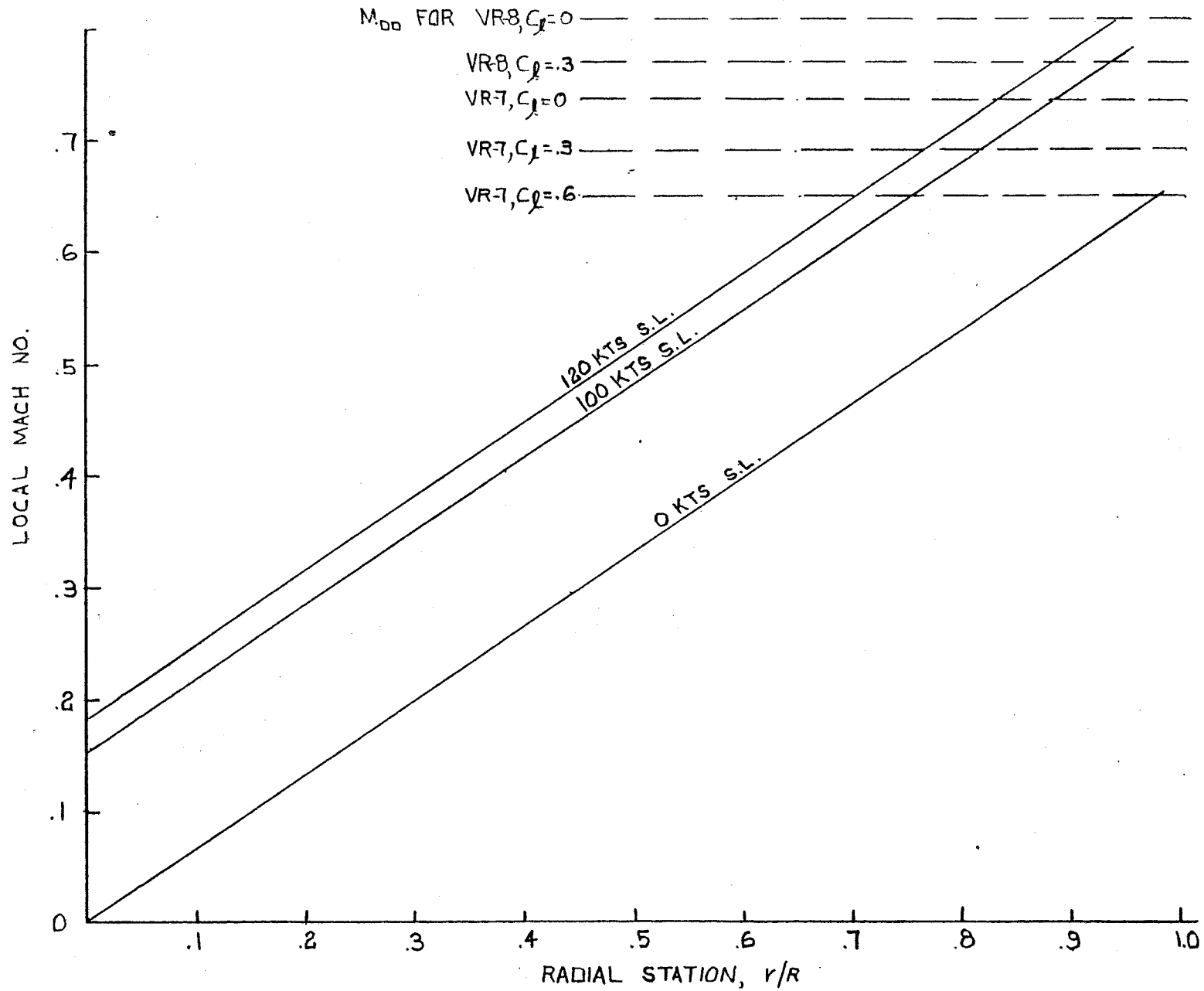


Figure A-8. Criteria Used to Select Position of Blade Airfoils

### A.5 Exploratory Parametric Studies

A series of systematic calculations was made to assess the feasibility of reaching the target performance levels and to establish the sensitivities of hover figure-of-merit and cruise efficiency to changes in twist and planform. The family of blade twists selected for study is presented in Figure A.9. Twist was varied from that distribution required to give good hover performance to that which yielded improved cruise efficiency.

Blade chords of 14, 18 and 20 inches were selected for study. At each twist and blade chord, performance calculations were made for a taper ratio of 3:1 ( $C_{\text{root}}/C_{\text{tip}}$ ) starting at various radial stations along the blade. A maximum taper ratio of 3:1 was selected because tip chords of much less than 6 inches were believed to be structurally impractical.

Figure A.10 presents typical results showing the variation of hover and cruise performance with twist and taper position for a blade having a root chord of 18 inches. The current performance levels and the target (cruise) performance level are indicated. The plot shows that the desired cruise efficiency is achievable with an 18" blade having 3:1 taper ratio starting at 45% radius and utilizing  $48^\circ$  of twist. An increase in hover figure-of-merit from .69 to .71 is obtained. Corresponding figures for the 20" chord blade are: taper from 35% radius and  $48^\circ$  twist yielding a hover figure-of-merit of .71. For the 14" chord the target cruise efficiency

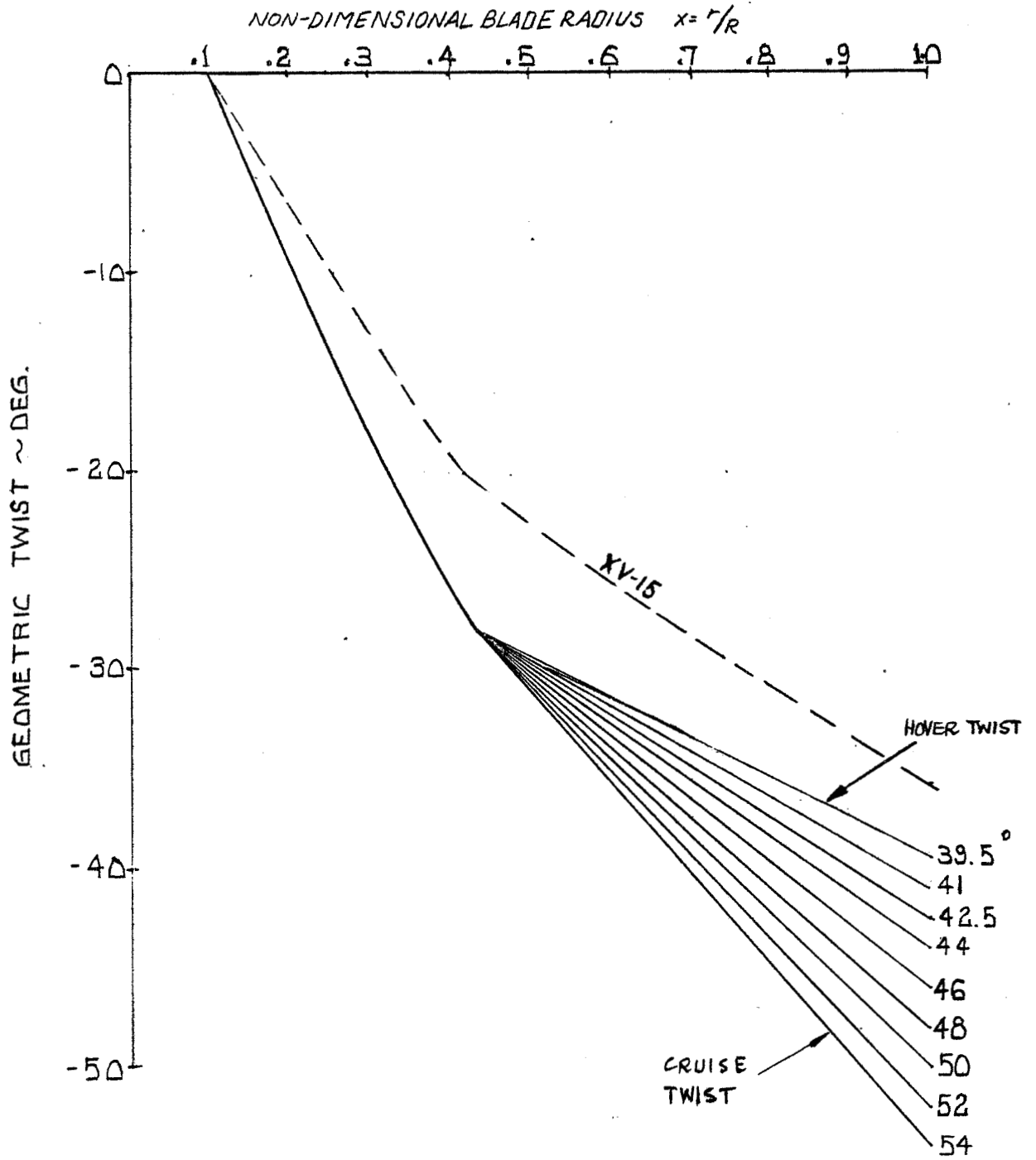


Figure A-9. Family of Blade Twist Distributions Selected for Study



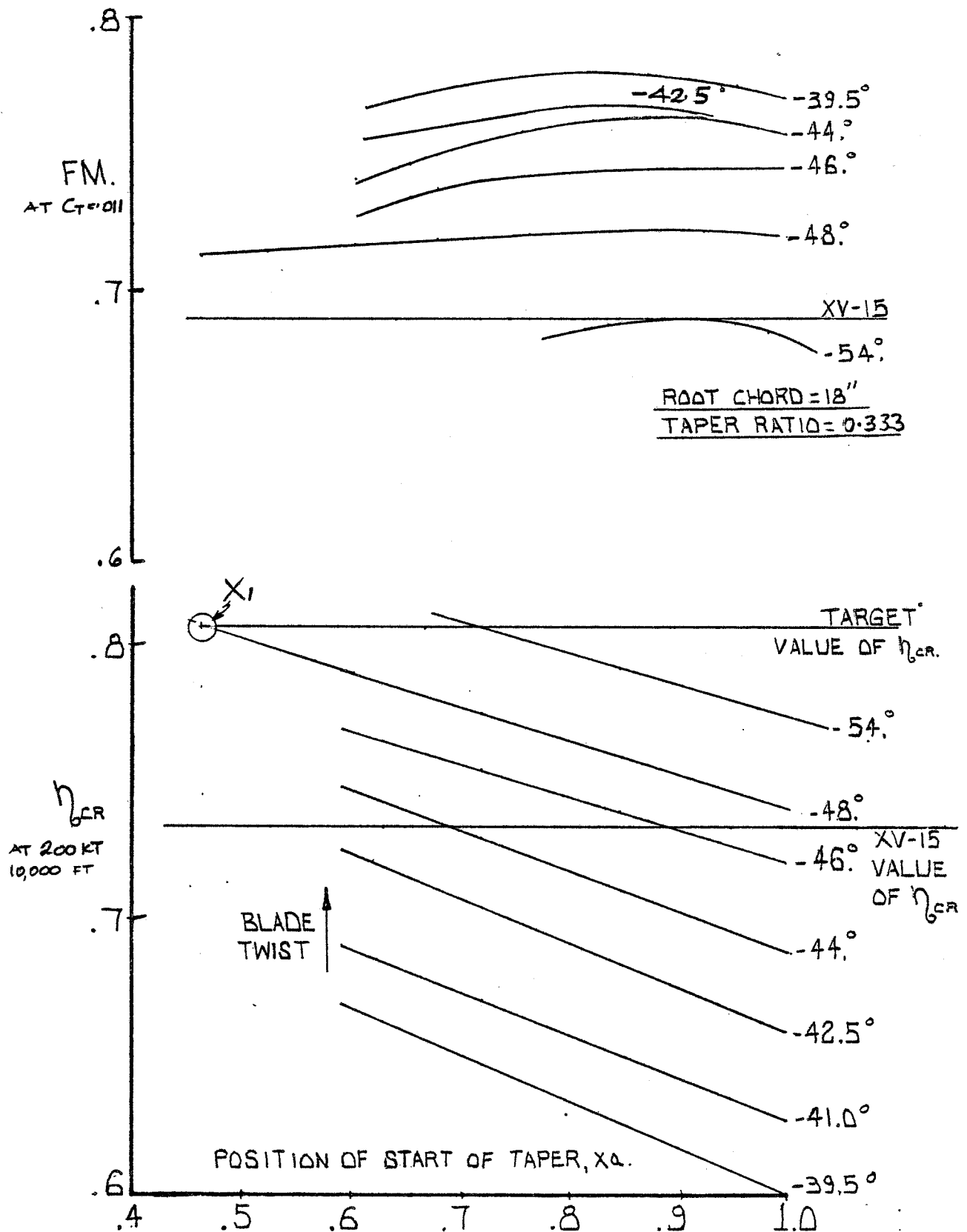


Figure A-10. Variation of Cruise and Hover Efficiencies with Position of Start of Taper for Various Levels of Twist

could be reached by tapering from 70% with  $48^\circ$  of twist. The hover figure-of-merit was not improved, however.

The 18-inch chord blade was designated configuration  $X_1$  and served as a point of departure for further optimization using the more rigorous techniques described below.

## A.6 Blade Optimization Procedure

### A.6.1 Planform Selection

Blade configurations for best hover or cruise performance are ones in which the twist and planform are selected so as to ensure that the rotor induced inflow is as uniform as possible over the disc and that each blade airfoil section operates at its angle of attack for maximum L/D. Figure A.11 presents plots of  $C_\ell$  at maximum L/D versus Mach number for the selected advanced airfoils, the VR-7 and VR-8, at Reynolds numbers corresponding to a 14-inch chord which is representative of the Reynolds number environment for the XV-15 rotor. The curves suggest changing from a VR-7 to a VR-8 between 90 and 95% in order to keep operating at optimum L/D.

Based on this required radial variation of  $C_\ell$  for optimum L/D and being able to calculate the blade circulation distribution ( $\Gamma$ ) required to provide uniform induced inflow, it is possible to compute the radial distribution of chord and blade twist. Figure A.12 shows the ideal hover planform computed in this way. Also shown is the practical interpretation of this planform derived by linearizing the curved portions, since they might prove difficult to manufacture.

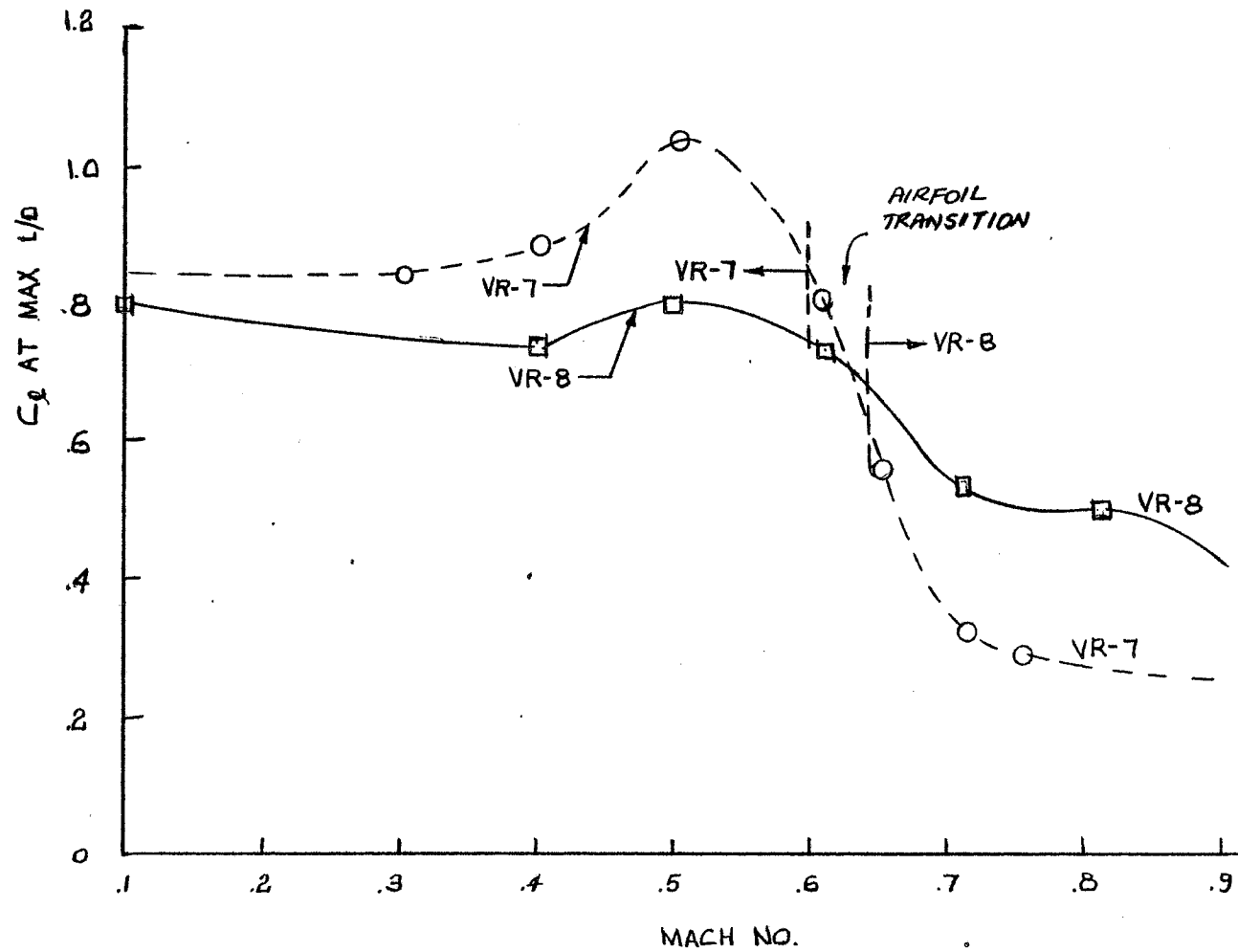


Figure A-11. Variation of Lift Coefficient for Maximum L/D for the VR-7 and VR-8 Airfoil with Mach Number

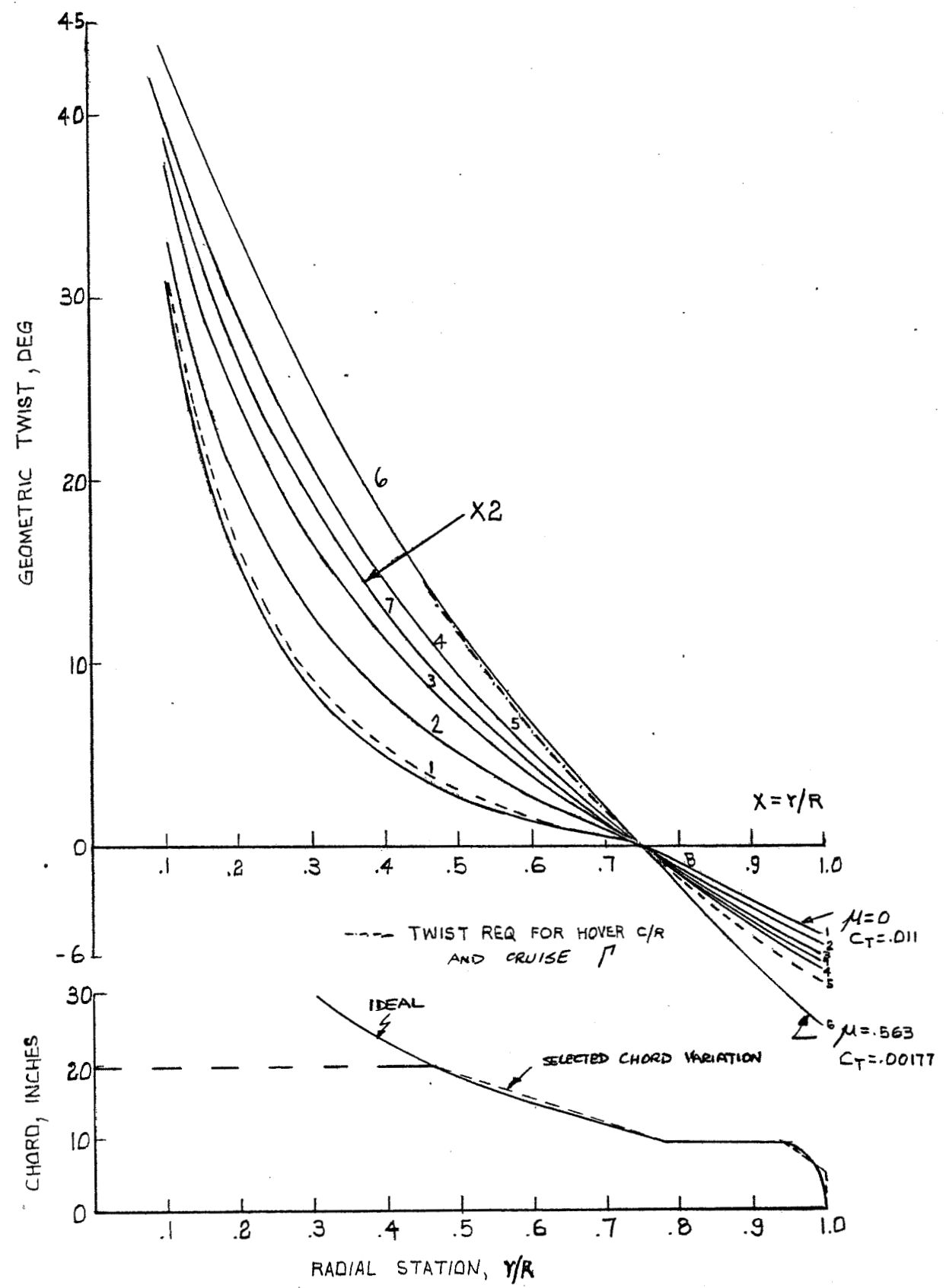


Figure A-12. Determination of Optimal Twist and Planform for the Replacement Blade  
A18

If the same optimization process is followed for the cruise condition, it is found that because of the low disc loadings occurring in cruise, the blade chords must be made very small to raise the local lift coefficients to optimal levels. These small chords are unacceptable for hover flight and hence the hover-determined planform is selected.

#### A.6.2 Twist Selection

Having fixed the chord variation it is then possible to calculate the blade twist distribution that will yield good cruise performance albeit at the expense of hover efficiency. Between the extremes of the twist distribution for best hover and that for best cruise lies a distribution of twist that will satisfy the cruise efficiency target while still yielding significant improvements in figure-of-merit compared to the existing blades.

Figure A.12 shows various twist schedules that were evaluated using the rotor performance analysis program (B92). Twist schedule 7 was selected and the blade incorporating this twist together with the hover-determined planform was designated configuration  $X_2$ . The characteristics of this blade are summarized in Figure A.13. The performance of  $X_2$  is presented in Figure A.14 and shows that a 9% increase in figure-of-merit is achieved compared to the existing blade at the design gross weight (including a 7% wing download). The cruise performance increase is very nearly achieved.

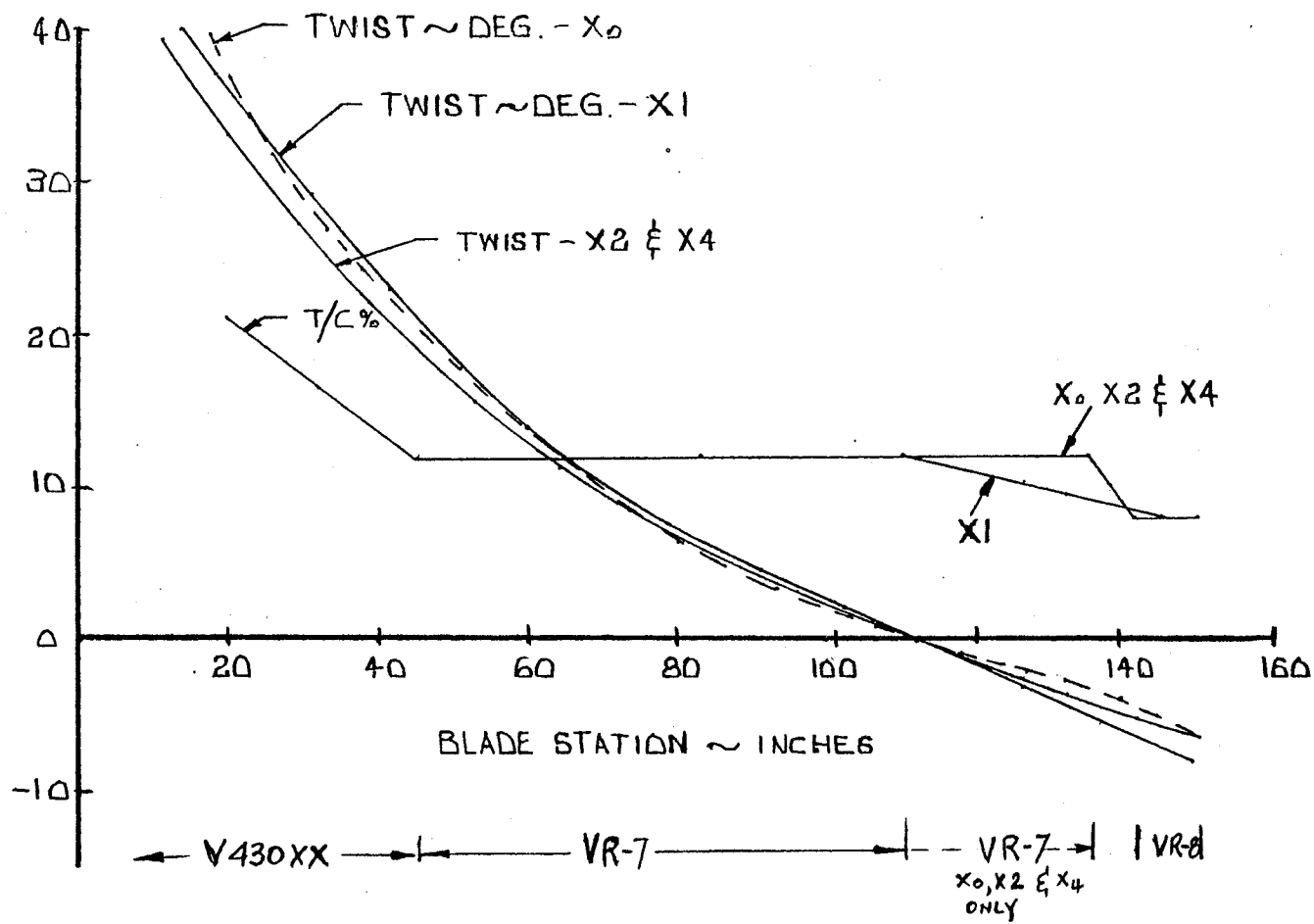


Figure 2-13. Standard propeller types

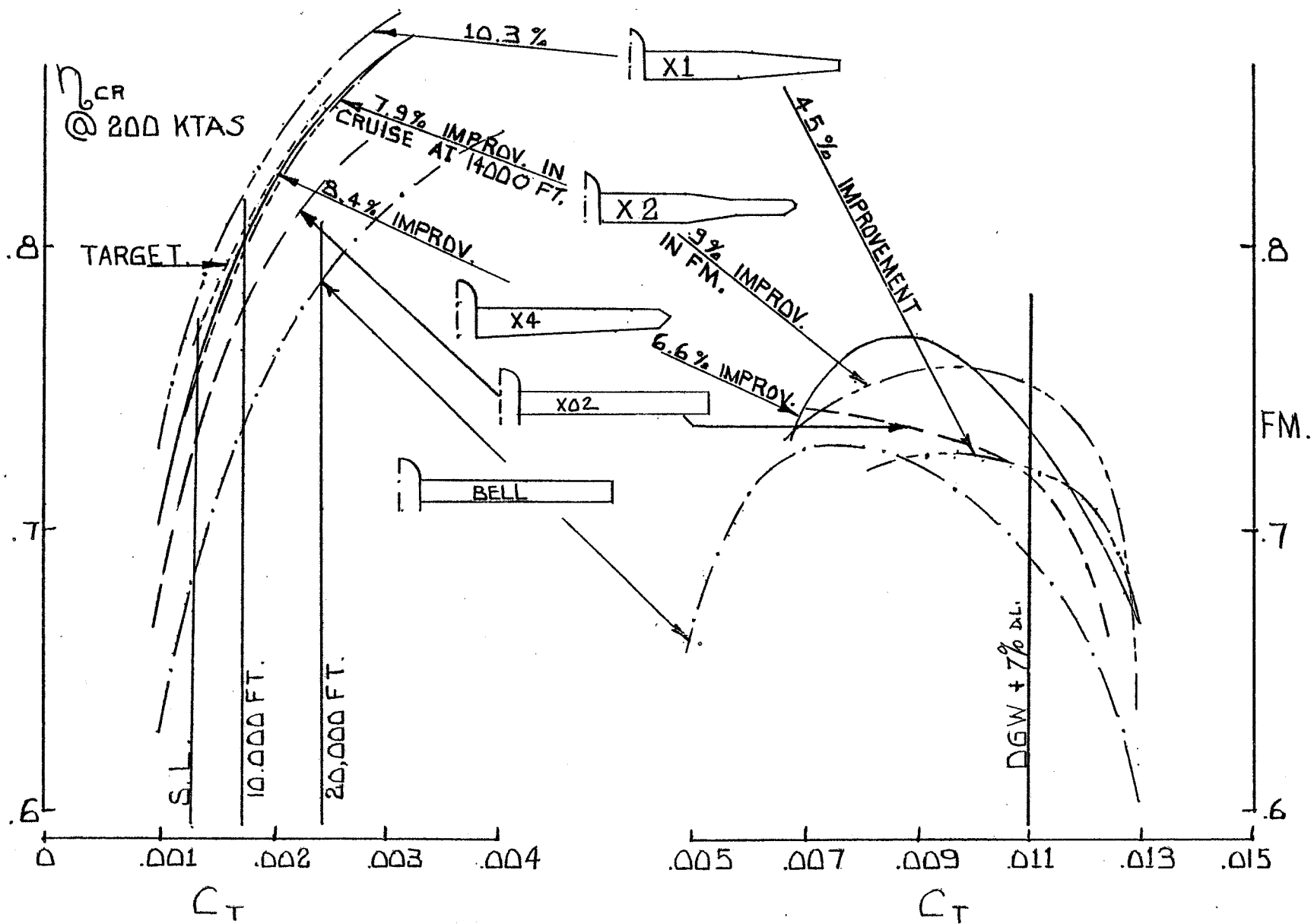


Figure A-14. Comparative Performance of Candidate Configurations

### A.7 Alternative Planforms to X<sub>2</sub>

The X<sub>2</sub> planform has both leading and trailing edge sweep (Figure 2.1) and two changes in taper ratio. It was conjectured that these features might result in manufacturing difficulties and some simpler alternatives were defined. The most promising of these, designated X<sub>4</sub>, employed linear taper from the cutout of 94% blade radius after which point the X<sub>2</sub> planform was retained. The performance of X<sub>4</sub> is presented in Figure A.14 and shows that the cruise efficiency goal is exceeded slightly with this planform but that the hover performance is reduced.

A 16" chord rectangular blade was optimized to provide reference data for a planform presenting minimum fabrication difficulty. The performance of this blade (designated X<sub>02</sub>) was evaluated and is presented in Figure A.14. As can be seen, both the hover and cruise performance fall below that of the X<sub>2</sub> and X<sub>4</sub> designs.

### A.8 Stall Margins of the Candidate Blades

The stall margins of the candidate blade X<sub>1</sub>, X<sub>2</sub>, and X<sub>4</sub> are compared with that for the existing XV-15 blades in Figure A.15. At both sea level standard and at 4000'/90°F, both the X<sub>2</sub> and X<sub>4</sub> blades achieve higher thrust coefficients at torque-limited power settings than the existing XV-15 blades.



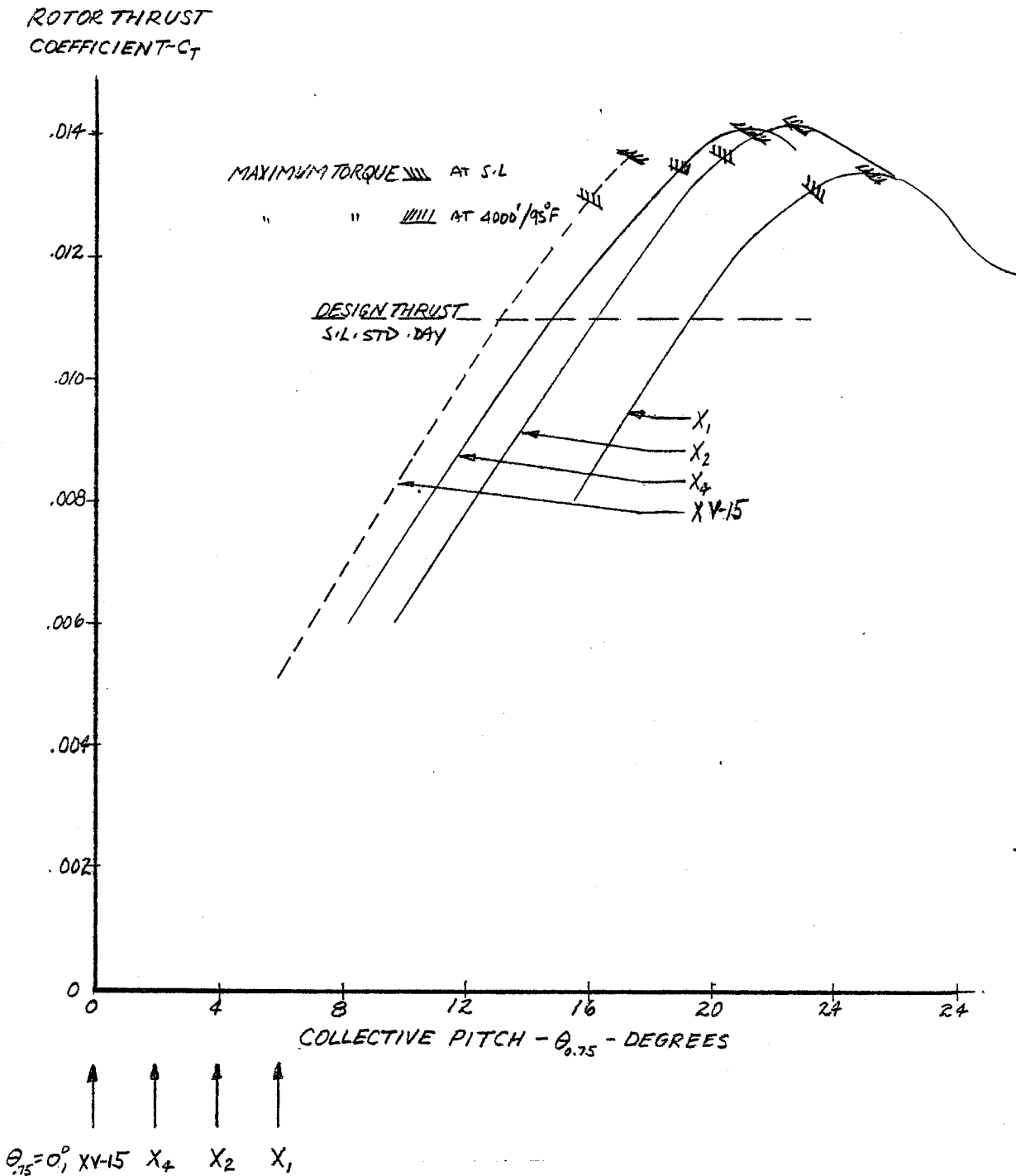


Figure A-15. Hover Stall Margin Comparison  
 A23

## REFERENCES

- A.1 Request for Proposal 2-27229(HK), "Preliminary Design Studies of Advanced Rotor Blades, Hubs, and Control Systems for the Tilt Rotor Aircraft"
- A.2 "V/STOL Tilt Rotor Research Aircraft", Volume 1, Anon, Bell Helicopter Company Report No. 301-199-001
- A.3 "Analysis of Propeller and Rotor Performance in Static and Axial Flight by an Explicit Vortex Influence Technique", Boeing Document R-372

## APPENDIX B

XV-15 FLY-BY-WIRE  
PRELIMINARY DEVELOPMENT SPECIFICATIONB.1. System Definition

The PFCS shall provide for direct pilot control of the tilt-rotor aircraft by control of rotor blade pitch via swashplates, airplane surfaces, and engine performance. The system shall modify pilot control inputs as a function of nacelle incidence angle and rotor speed. The PFCS shall accept inputs from the SCAS for aircraft stability and maneuver enhancement. The SCAS shall provide rate and attitude stabilization in pitch, roll and yaw, and provide gust alleviation signals to PFCS. PFCS and SCAS computation functions shall be housed in a single flight control processor.

B.2. PFCS Description

Pilot input shall be via conventional dual mechanically synchronized controls comprising a longitudinal/lateral control stick, directional pedals, and an engine throttle control. Signals proportional to control position shall be generated by linear transducers connected to each control. The position signals shall be conditioned in the Flight Control Processor (FCP) to generate commands for the rotor control driver actuators (two per rotor), the flaperon driver actuators (one each side), the rudder driver actuator, elevator driver actuator, and engine  $N_1$  control actuators (Figure B.1).

### B.2.1 System Functions

Major system functions shall be as shown in Figure B.2 and described in the following paragraphs.

- a. Motion Sensing - The control position transducers shall convert pilot stick and pedal motions to equivalent electrical signals for input to the Flight Control Processor.
- b. SCAS Interface - The PFCS shall accept SCAS command from the SCAS via authority and rate-limit functions. The limited signals shall be summed with the control position signals before mixing.
- c. Gain Scheduling - Axis command signals (summation of pilot control and SCAS command) shall be scheduled as a function of nacelle angle. In general, pilot inputs to the rotor shall be phased out as the nacelle is brought to the horizontal position (zero degrees).
- d. Thrust Management - Shall provide for control of rotor rpm via inputs to rotor collective pitch and engine  $N_1$  controls. The system shall respond to pilot throttle setting and rotor rpm. Direct pilot control of collective pitch shall be phased out at zero degrees nacelle incidence. Manual trim of rotor rpm and differential collective pitch shall be provided on the system control panel.
- e. Airplane Surface Control - Axis commands shall be processed via appropriate gains and actuation to position the flaperons, rudder, and elevator.

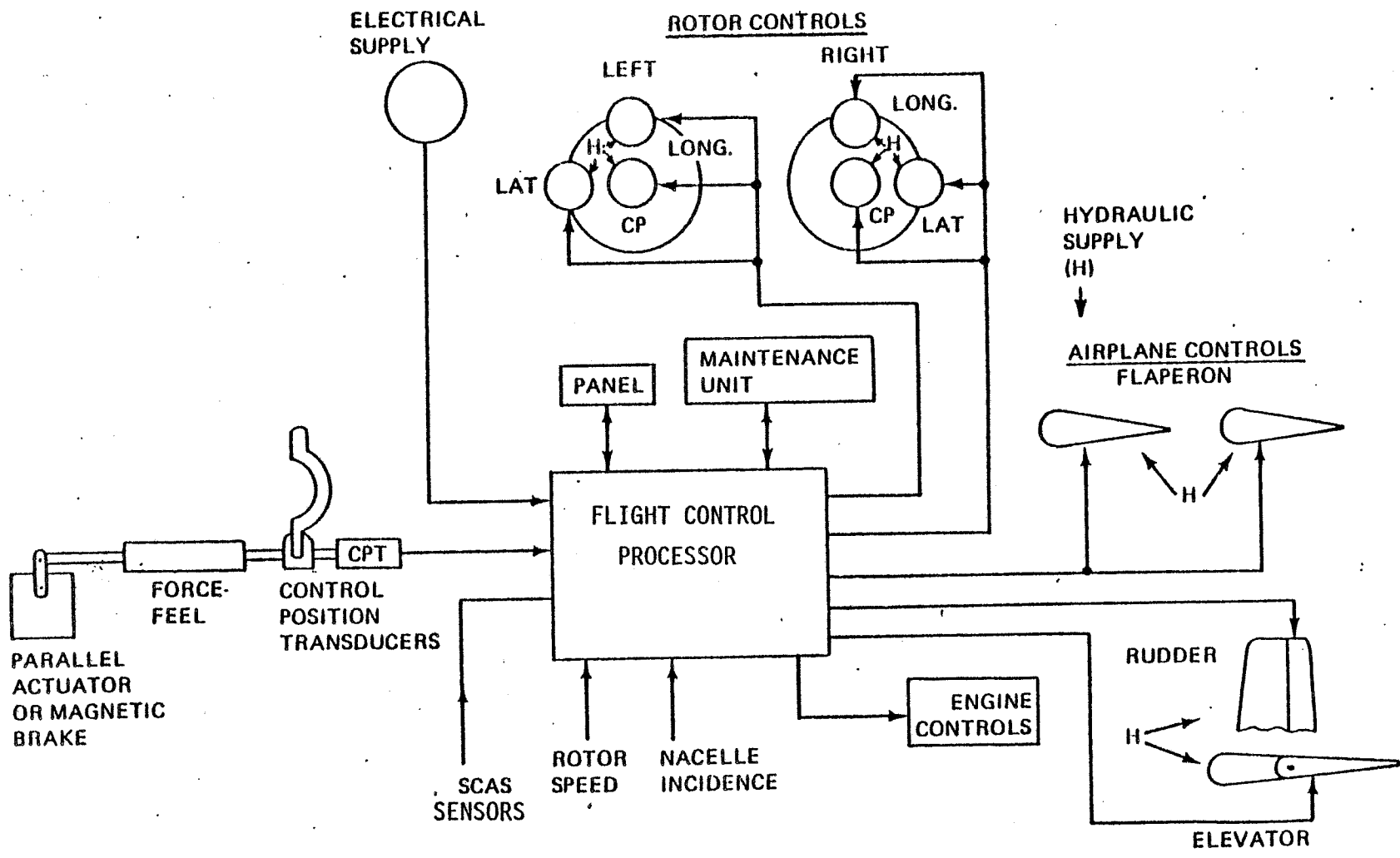
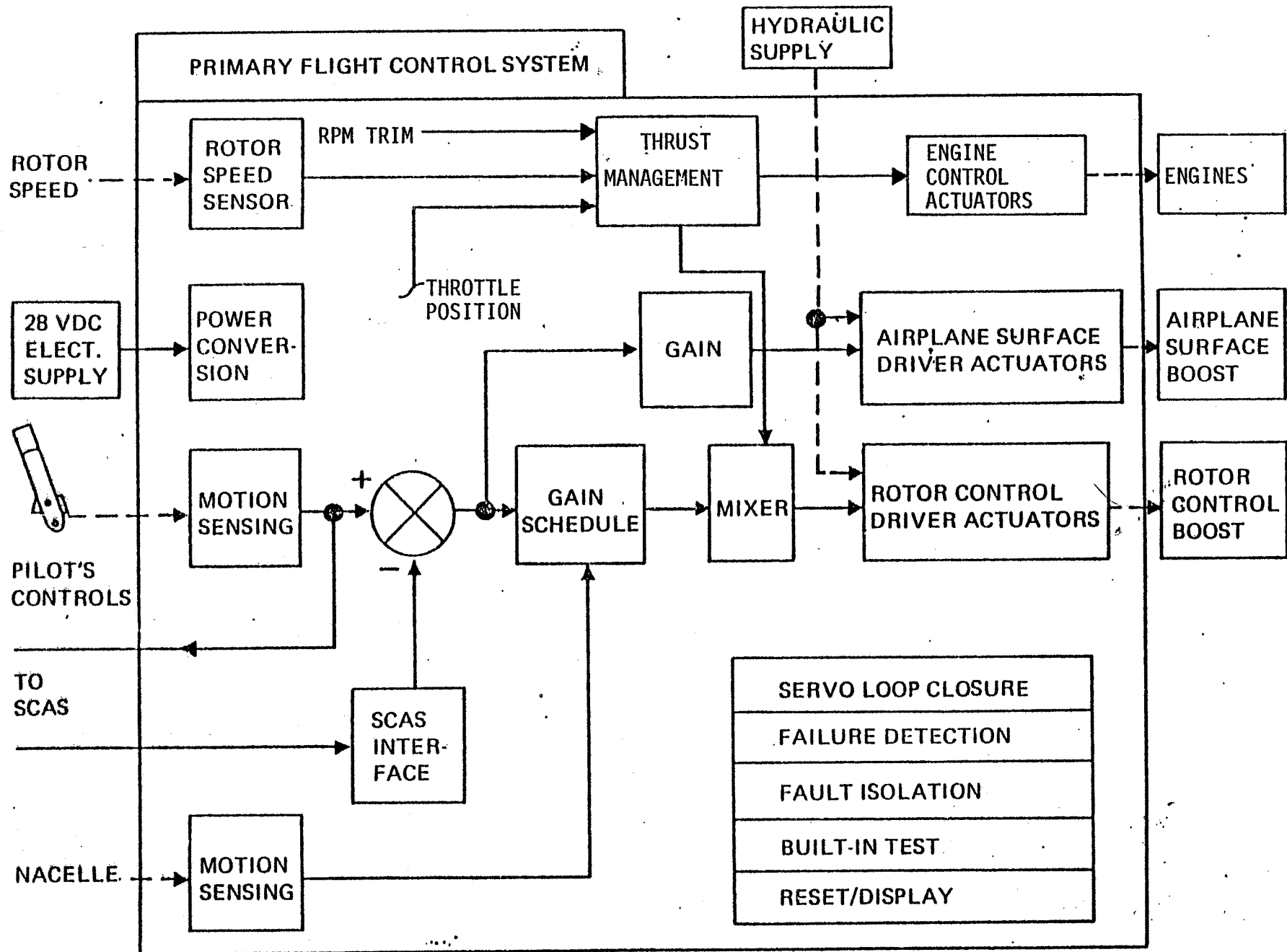


FIGURE B1 FLY-BY-WIRE FLIGHT CONTROL SYSTEM



B4

Figure B2 Primary Flight Control System Functions and Interfaces

D210-11569-1

- f. Mixing - The scheduled axis commands and governor outputs shall be mixed using appropriate gains to position the rotor control actuators.
- g. Servo Loop Closure <sup>2</sup> - Shall include the electronics to control rotor and airplane surface driver actuators which in turn control boost actuators.
- h. Rotor Actuation - The rotor control boost converts the driver outputs to equivalent rotor swashplate motion.
- i. Power Conversion - Shall convert the 28 VDC supply to AC for sensor excitation and DC supplies as needed to operate electronic devices used in the system.
- j. Failure Detection - Each Flight Control Processor shall process all failure detection within its channel and, upon detecting a failure, shall shut down the channel inputs to the affected actuators and transmit failure information to the control panel and maintenance unit.

#### B.2.2 Major Component Responsibilities

The following is a regrouping of PFCS functions by major component.

- a. Control Position Transducers
  - Motion Sensing
- b. Flight Control Processor
  - Signal Conditioning and Buffering
  - SCAS Computation and Interface
  - Gain Scheduling
  - Thrust Management
  - Mixing

- Servo Loop Closure
- Power Conversion
- Failure Detection
- c. Rotor Control Driver Actuators
  - Rotor Swashplate Actuation
- d. Airplane Surface Driver Actuators
  - Flaperon Actuation
  - Rudder Actuation
  - Elevator Actuation
- e. Control Panel
  - Fault Reset
  - Fault Display
  - Manual rpm Control
  - Manual Torque Matching (Differential Collective Pitch)
  - SCAS Mode Select/Display
- f. Maintenance Unit
  - Fault Isolation Display
  - Built-in Test Control

### B.2.3 External Interfaces

The PFCS shall be designed to interface with the following equipment and subsystems of the aircraft.

- a. Pilot's Stick, Pedals, and Throttle Lever - This is a mechanical interface with the control position transducers. The existing mechanical XV-15 controls will be adapted to achieve this interface.
- b. SCAS Sensors - This is an electrical interface with the Flight Control Processor.
- c. Nacelle Incidence - This is the mechanical interface with nacelle.



- d. Rotor Speed - This is a mechanical interface with the rotor accessory gearbox.
- e. Rotor Control Boost Actuators - This is the mechanical interface with rotor collective and longitudinal cyclic boost actuators and electrical interface with the existing lateral cyclic actuator.
- f. Airplane Surface - This is the mechanical interface with the flaperon, rudder, and elevator boost actuators.
- g. Engine - This is the mechanical interface of the linkage controlling  $N_1$  control inputs.
- h. Electrical Power Supplies - This is the electrical interface with the 28 VDC electrical power supply.
- i. Hydraulic Power Supply - This is the mechanical interface with the rotor and airplane surface control actuators.

#### B.2.4 Redundancy Management

In order to meet the reliability goals specified therein, the PFCS electronics, sensors and power supplies shall be at least dual-fail operative, which is defined to mean that the system shall withstand any two failures in the system.

Hydraulic portions of the driver actuators shall be at least single fail-operative.

Failure detection logic shall be dualized where necessary to meet reliability goals. Dual logic shall be used to drive dual-failure warning circuits.

Details on mechanization of the redundancy management shall be as specified in paragraph B.5.0, "Major Component Characteristics".

### B.2.5 Failure Detection

The PFCS shall have a self-contained capability for ground checkout.

Each channel shall identify in-flight failures independently and furnish signals to the control logic and panels for appropriate system corrective action and crew notification. Details of failure detection shall be as specified in paragraph B.5.0, "Major Component Characteristics and Requirements".

### B.3.0 System Characteristics

#### B.3.1 System Performance

B.3.1.1 Gains, Schedules, Transfer Functions - Shall be as defined in Section B.5.0 of this appendix.

B.3.1.2 Accuracy - The system electronics supplier shall be responsible for analysis and control of system tolerances so that the overall system (pilot control to control actuator) accuracy tolerances are maintained. To this end, the system electronic supplier will support definition of control position transducer (CPT) and actuator performance.

a. Static Gain Accuracy - The average gain for all FCP units shall be within 2% of the values specified in Section 5.0, the rotor speed control loops shall be within .75% of the value specified. The static gain of individual FCP units shall be within 1.5% of the average. For a given control input, the accuracy is defined as the percentage difference between the desired actuator position and the actual actuator position. These accuracies include schedule accuracies.

- b. System Null - The total steady state null associated with the PFCS (sensor to driver actuator) shall not exceed .4% of actuator full stroke.
- c. Resolution - Resolution is defined as the minimum change in control required to obtain actuator motion. The resolution (equated in actuator motion) shall not exceed .04% of actuator full stroke.
- d. System Hysteresis - Hysteresis within the PFCS shall not exceed .08% of actuator full stroke.
- e. Cross Coupling - Full motion of any axis or combination of axes shall not require more than two percent of full control displacement (in axes not in motion) to compensate.

B.3.1.3 Driver Actuator Frequency Response - The driver actuator shall exhibit a second order response with a natural frequency of 130 rad/sec and damping factor of .7. This response shall be achieved while driving a friction load of 50 pounds.

B.3.1.4 Failure Detection and Effects - The PFCS shall include the following requirements relating to system failures and effects.

- a. Failure Tolerant Performance - The PFCS shall be designed so that the aircraft meets the failure tolerance performance of FAR XX .671, subparagraph (c).

- b. Failure Detection and Isolation - Operation of the redundant channels shall be monitored to detect any failure or malfunction that could cause unsafe flight or system degradation requiring maintenance action. Unsafe flight is referred as loss of control or degradation of control (transient or steady state) that jeopardizes the pilot's ability to abort and land safely.

After the detection of failure, the failed channel shall be automatically inhibited from affecting the correctly operating channel(s). The detection and isolation time shall be compatible with paragraph 3.1.3.c.

- c. Failure Transients - Transients following first and second failures within the PFCS shall be controlled by channel locking tolerances specified in paragraph B3.1.2a of the appendix.

- d. Failure Detection Threshold - The failure detection threshold must be set low enough to detect passive failures with normal system disturbances, detect valid failures, and minimize failure transients. The threshold must be high enough to minimize nuisance trips due to normal channel tolerances and transients.

- e. Redundancy of Monitoring and Correction Circuitry - The detection, logic, and switching circuitry reliability shall be included in the channel reliability requirements. The failure or malfunction of the logic and switching circuitry shall be interpreted as a channel failure.

B.3.2 System Physical CharacteristicsB.3.2.1 Control Device and System Loads

- a. Control System Loads - The PFCS shall be designed to meet applicable portions of FAR XX .395 (considering there is no longer a linkage which can carry loads between the pilot's control and the output actuator).
- b. Limit Pilot Forces - The PFCS cockpit controls shall be designed to withstand the loads defined in FAR XX .397. The existing XV-15 controls will be adapted.
- c. Dual Control System - The PFCS cockpit controls shall be designed to meet requirements of FAR XX .415.

B.3.2.2 System Packaging - PFCS components shall be packaged so that each channel is separately contained. System panels are an exception to this requirement. Actuator sections shall be separated with respect to hydraulic supply. System electronic assemblies shall be designed to facilitate changes during the development program. System component weights shall not exceed values defined below.

COMPONENT	TOTAL WEIGHT PER AIRCRAFT (LBS)
Flight Control Processor (with mounting)	69
Dual Driver Actuator	180
Control Panel	4
Maintenance Panel	5
Engine Control Actuator N <sub>1</sub>	12

### B.3.3 Reliability

D210-11569-1

The primary flight control system, as defined in Figure B.1, including the path from transducer input to actuator output and power supplies, but excluding cockpit mechanical controls, shall exhibit a flight safety reliability of .9999999 for a two-hour mission. Flight safety reliability is defined as the probability that the system will maintain the transfer functions defined for the system. In general, loss of flight safety will result in loss of the aircraft.

### B.3.4 Environmental Conditions

B.3.4.1 Standard Condition - The following conditions shall be used to establish normal performance characteristics under standard conditions for making laboratory bench tests.

- a. Temperature - room ambient 25  $\pm$ 5°C (77°F  $\pm$ 9°F)
- b. Altitude - normal ground
- c. Humidity - room ambient up to 90% relative humidity.

B.3.4.2 Environmental Service - Components of the PFCS shall meet the requirements of this specification under the conditions listed in the following paragraphs. Electronic components shall be tested under the conditions defined in MIL-E-5400 for Class 1A equipment. Actuators shall be tested to the conditions specified. The equipment supplier shall submit a detailed procedure to be approved by Boeing.

- a. Altitude - Operation without degradation of performance throughout a pressure altitude range of -200 to +30,000 feet ASL per MIL-STD-810C.

- b. Ambient Temperature - Operation throughout an ambient temperature range of -65° to +160°F.
- c. Temperature Shock - Sudden changes in temperature of the surrounding atmosphere per MIL-STD-180C.
- d. Humidity - Operation in a warm, highly humid atmosphere such as encountered in tropical areas per MIL-STD-810C.
- e. Salt Fog - Operation in an atmosphere containing salt laden moisture per MIL-STD-810C.
- f. Rain - Operation in a rain environment per MIL-STD-810C.
- g. Sand and Dust - Operation in a dust (fine sand) laden atmosphere per MIL-STD-810C.
- h. Immersion (for hydraulic actuators only). Operation after immersion in hydraulic fluid at a temperature of +275°F per MIL-C-5503.
- i. Vibration - Operation during exposure to dynamic vibration stresses represented by those tests of MIL-STD-810C, Method 514.2, Procedure I, Part I, Equipment Category (A) to include:
- Resonance search
  - Resonance dwell
  - Cycling
- j. Mechanical Shock - Operation after exposure to a mechanical shock environment similar to that expected in handling, transportation, and service use per MIL-STD-810C.
- k. Electromagnetic Interference - Meeting per MIL-STD-461A, Notice 4.

#### B.4.0 Design and Construction

Electrical equipment shall conform with all applicable requirements of MIL-E-5400 for design, construction and workmanship except as modified herein. Hydromechanical equipment shall conform to the applicable requirements of MIL-H-5440, MIL-C-5503, and MIL-H-8775.

#### B.5.0 Major Component Characteristics and Requirements

##### B.5.1 Direct Electrical Linkage

B.5.1.1 Subsystem Description - The Direct Electrical Linkage (DEL) comprises the following units:

Flight Control Processor	3 per aircraft
Control Panel	1 per aircraft
Maintenance Unit	1 per aircraft
Control Position Transducers	4 per channel
Electrical Interconnecting Cables	To be supplied by Boeing Vertol

The DEL replaces not only the mechanical control linkages of the XV-15 aircraft, but also the five SCAS actuators, the two exciter actuators, the differential cyclic washout actuator, and the differential collective trim actuator.

B.5.1.1.1 Flight Control Processor - The synthesizes the following major flight control functions. The processor translates the cockpit control motions and the Stability and Control Augmentation (SCAS) signals into the appropriate actuator control signal inputs to provide manual and automatic flight control. Figures B.3, B.4, B.5 and B.6 provide the functional diagrams of the required control dynamics. Letters in circles adjacent to portions of the diagrams cross reference to the schedule callouts in Report CR-151950.



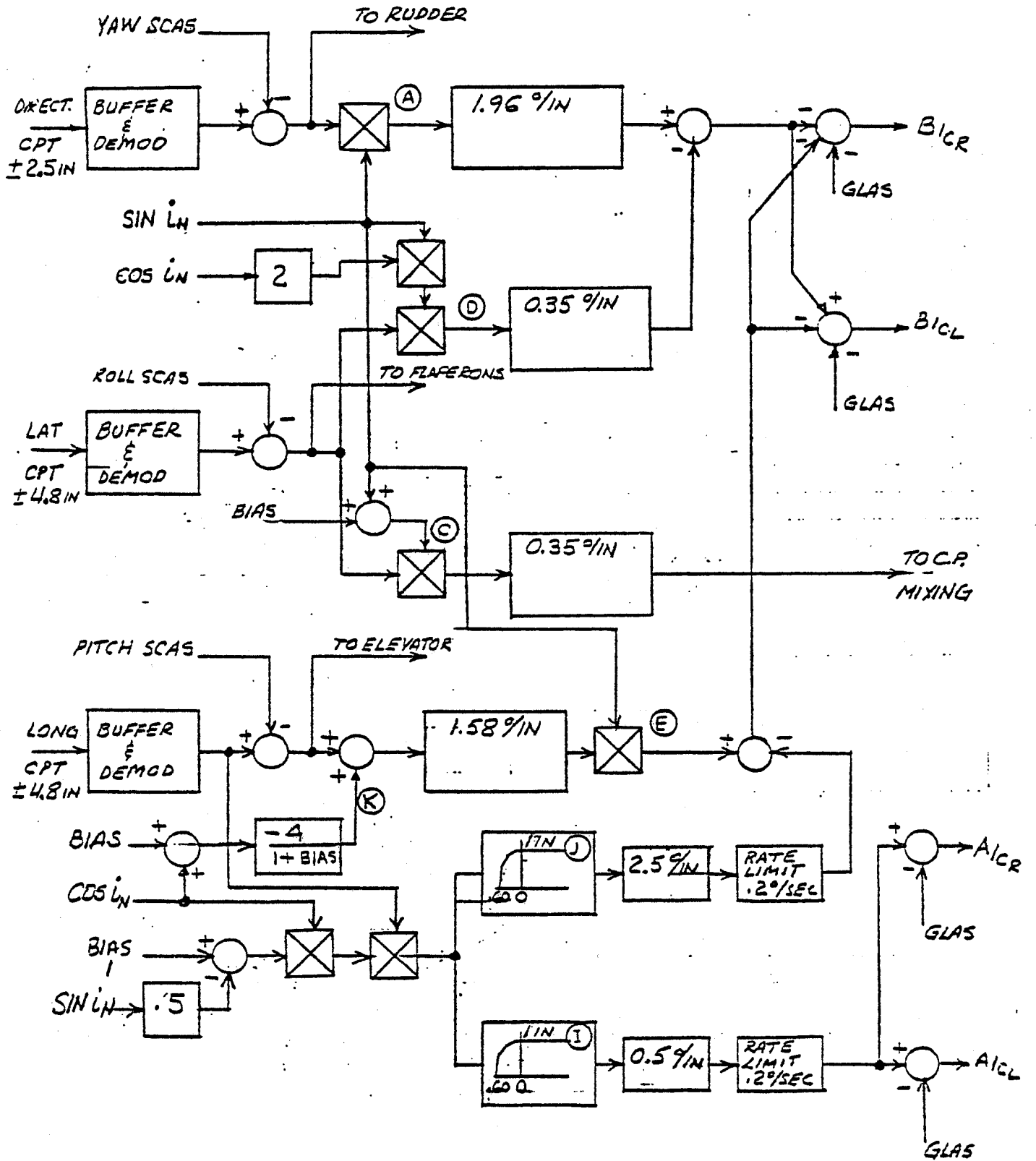
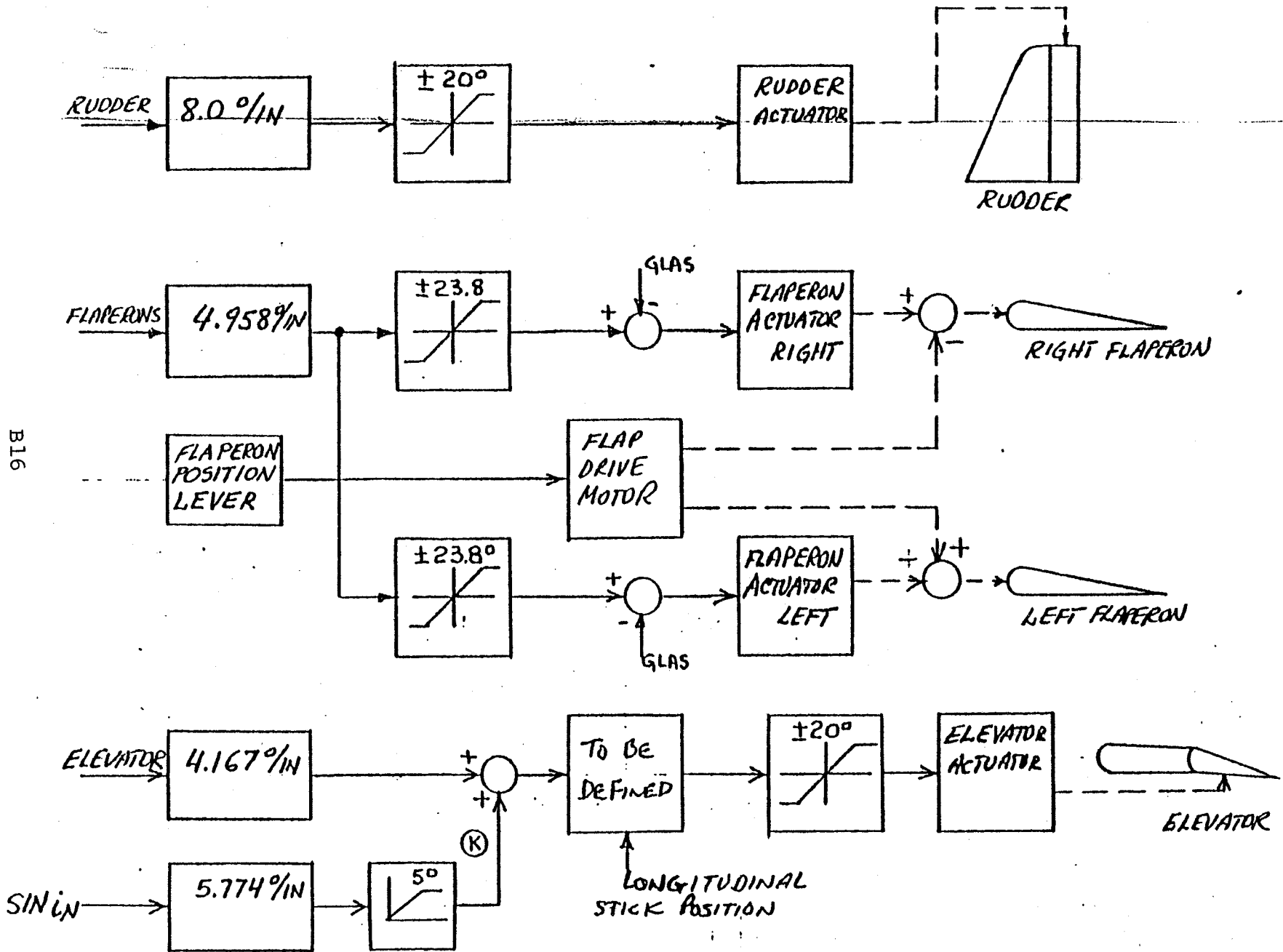


FIGURE B3 ROTOR CYCLIC CONTROLS



B16

D210-11569-1

FIGURE RA AIRPLANE SURFACE CONTROLS

B17

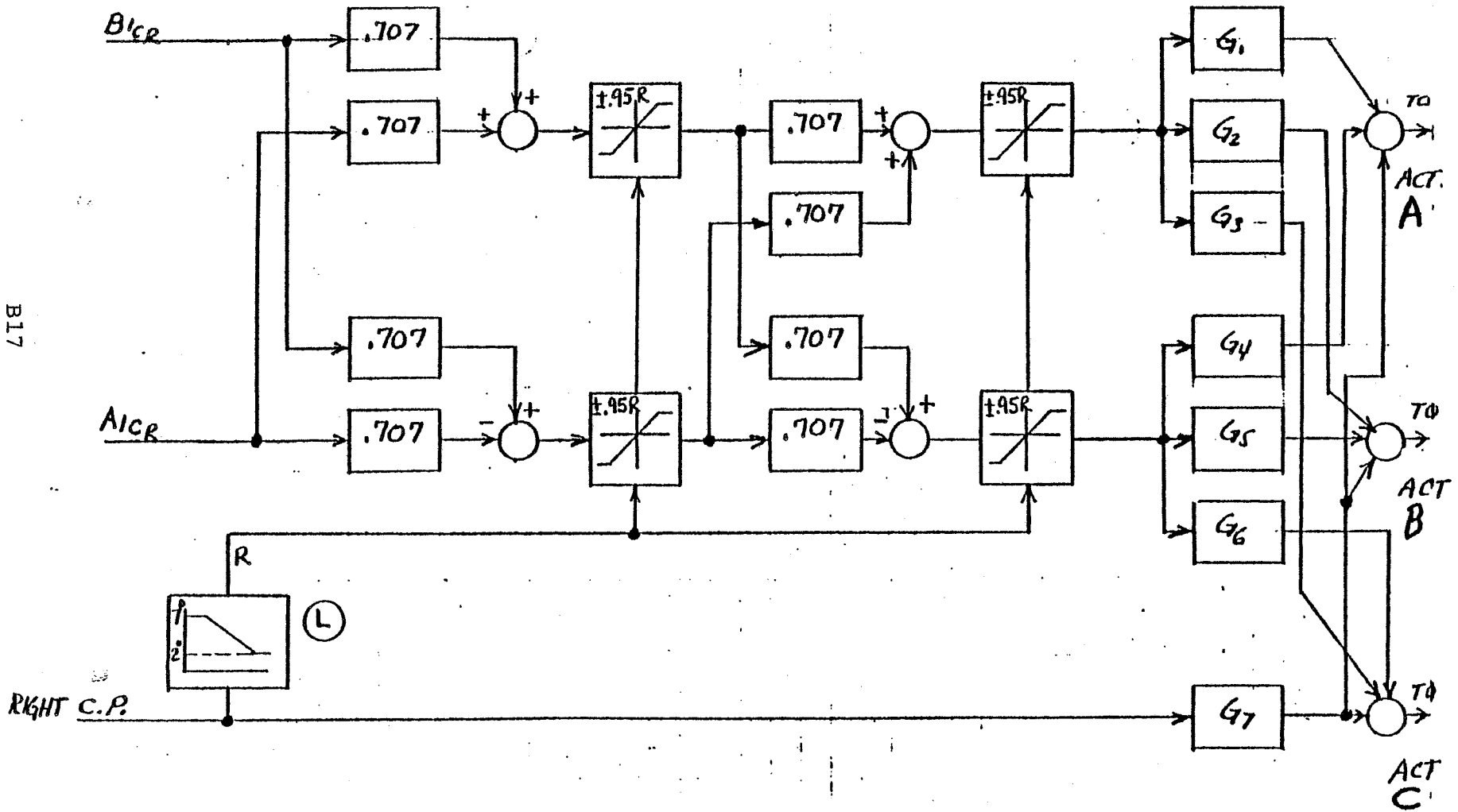


FIGURE B5 . ROTOR CYCLIC CONTROLS MIXING AND CUMULATIVE LIMITS - RIGHT ROTOR

B.5.1.1.2 Control Panel - The control panel shall provide rpm trim, differential torque trim, fault annunciation and channel reset capability for the pilot.

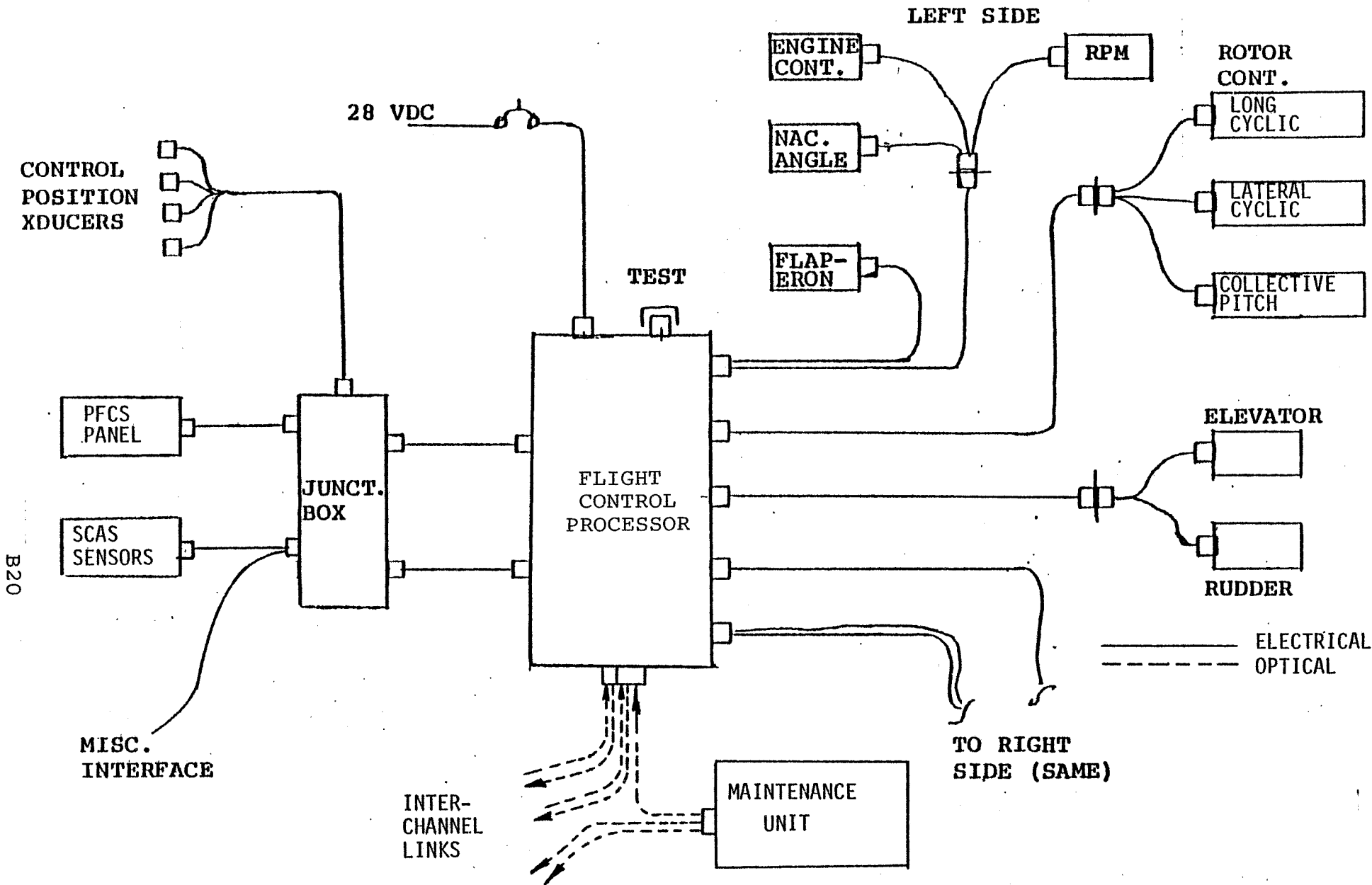
B.5.1.1.3 Maintenance Unit - The maintenance unit shall provide the following functions in conjunction with the Built-In-Test Equipment (BITE).

- Determine the operable channels within the system.
- Provide logic to drive aircraft caution/advisory panel, and control panel.
- Conduct GO/NO-GO ground tests on each channel of the system.
- Provide readouts to indicate location of system failure to assist in isolation of faults to a line replaceable unit.

B.5.1.1.4 Control Position Transducers - The control position transducers (CPTs) shall translate cockpit control motions into equivalent electrical signals which are in turn transmitted to the Processor.

B.5.1.1.5 Electrical Interconnecting Cables - The electrical interconnecting cable assemblies shall be flight control dedicated and prefabricated utilizing simple multi-conductor wires, MIL-C-83723 self-locking threaded connectors, and appropriate strain relief. The system configuration shall be designed such as to use point-to-point cables to the extent possible. Figure B7 defines a tentative interconnect for a single channel. Fiberoptic cabling shall be used for inter-channel connection.





B20

FIGURE B7 PRIMARY FLIGHT CONTROL SINGLE CHANNEL INTERCONNECT

D210-11569-1

B.5.1.1.6 Interfaces - The Direct Electrical Linkage shall interface with the following equipment and subsystems of the aircraft.

- a. Cockpit Controls - This is a mechanical interface of control position transducers with the cockpit controls. The existing XV-15 cockpit controls will be retained. The cockpit controls are longitudinal/lateral stick, the direction pedals, and the throttle lever. Figure shows the DEL interface with the cockpit controls.
- b. Actuators - This is an electrical interface with the control power actuators. The interface shall consist of the actuator command error and the actuator position electrical feedback. The following control actuators shall be interfaced with the DEL.
  - Dual Driver Actuators - Electrohydraulic
    - 2 Left Rotor
    - 2 Right Rotor
  - Airplane Surface Actuators - Electrohydraulic
    - Rudder
    - Flaperon Right
    - Flaperon Left
    - Elevator
  - Engine N<sub>1</sub> Actuator - Electromechanical
    - Right Engine
    - Left Engine
  - Existing Lateral Cyclic Actuators-Right & Left Rotor
- c. Electrical Power Supply - This is the interface with the 28 VDC supply. The supply may vary according to limits defined in MIL-STD-704A, Category B.

- d. SCAS - This is the electrical signal interface with the stability and control augmentation system sensors.
- e. Sensors Interface - This is the electrical signal interface with the nacelle incidence sensors and the rotor speed sensors. The nacelle incidence sensor shall be a synchro providing a signal proportional to the sine and to the cosine of the nacelle incidence cycle. The rotor speed sensors shall be proximity switches in the transmission providing pulses the frequency of which is proportional to rotor speed.

B.5.1.2 System Performance - System gain, schedule, and transfer function accuracies shall be met over the range of environments defined in paragraph B.3.4. Components shall be designed so that the overall system meets the requirements defined in Section B.3.1.

B.5.1.3 Redundancy

- a. The Direct Electrical Link (DEL) shall be at dual fail operative for any two electrical failures. Electrical supply failures shall be considered as failures of the DEL.
- b. All failures causing loss of one DEL channel shall be detected and immediately displayed.
- c. A failed channel shall be automatically removed from the system as soon as necessary to maintain flight control operation.



- d. Failure detection and warning/display logic shall be dualized where necessary, to meet reliability requirements.
- e. The allowable transient due to a failure shall meet the requirements of paragraph B.3.1.4.

B.5.1.4 Reliability - The overall system safety reliability of the PFCS shall be as defined in paragraph B3.3. hour flight. Reliability shall be demonstrated by analytical methods based on known failure rates of components used in the design. The required redundancy level shall be adopted to meet this reliability requirement.

B.5.1.5 Diagnostics

B.5.1.5.1 Failure Detection and Display - The DEL shall contain the capability to detect and display any malfunction causing unsafe operation or degradation of operation occurring in the primary flight control system, including actuator failures.

B.5.1.5.2 Built-In-Test Equipment (BITE) - The DEL shall have sufficient built-in test equipment to localize any failure to a line replaceable unit (LRU).

B.5.1.6.3 System Checkout - The maintenance unit, in conjunction with the BITE, shall provide the capability to check out the safe operation of each channel of the primary flight control system and isolate any failure present in the primary flight control system to a line replaceable unit. Upon initiation, the checkout shall proceed automatically until completion or until a failure has been detected.

B.5.1.5.4 Maintenance - The routing checkout and isolation of failures to an LRU shall be performable by any electronic maintenance aircraft technician. The troubleshooting and repair of an LRU after removal shall be performed by designated supplier personnel.

B.5.1.6 Test Support - Because the DEL is part of a research and development aircraft, it shall lend itself to changes of system parameters during both ground and flight tests with minimal time loss. No degraded parameters shall be acceptable. All changes of parameters shall be realized by hard-wiring and reliable workmanship in accordance with applicable military standards.

#### B.5.2 Actuators

This section establishes the performance, design, and development for the dual driver actuator assembly.

B.5.2.1 End Item Usage - The servo actuator will be used as the output element of the DELS.

B.5.2.2 Description - Two dual driver actuator assemblies are located at each rotor head. Each rotor head is independently provided with two Type II 3000 psi hydraulic systems while a third Type II 3000 psi system is common to both heads. One independent system supplies half of the dual driver actuator via a 3000/1500 psi pressure reducer; the second system supplies the other half. The third system can be selected by the pilot to backup either channel. Its engagement is also conditioned by DELS logic.

B.5.2.3 Design - The envelope of the actuator shall not exceed the dimensions given in Figure B8. The actuator shall be designed in accordance with the requirements of MIL-H-5440, MIL-H-8775, and MIL-C-5501.

The actuator shall be configured as shown schematically in Figure B9. The actuator shall consist of a two-stage jet-pipe electrohydraulic valve with second stage speed monitor LVDT. The differential pressure output of one channel shall be outputted for use in channel equalization.

The characteristics of the actuator shall be as follows:

- a. Stall output dual system 500 lbs at 1500 psid supply pressure.
- b. No-load velocity with 6 ma current command (per channel) 3 in/second.

B.5.2.4 Environmental Conditions - The actuator shall meet the requirements of this specification during and/or following exposure to any combination of the environmental conditions described below.

B.5.2.4.1 Altitude - Operation without degradation of performance throughout a pressure altitude range of -200 to +20,000 feet ASL per MIL-STD-810C.

B.5.2.4.2 Ambient Temperature - Operation throughout an ambient temperature range of -65 to +160°F.

B.5.2.4.3 Temperature Shock - Sudden changes in temperature of the surrounding atmosphere per MIL-STD-810C.

B26

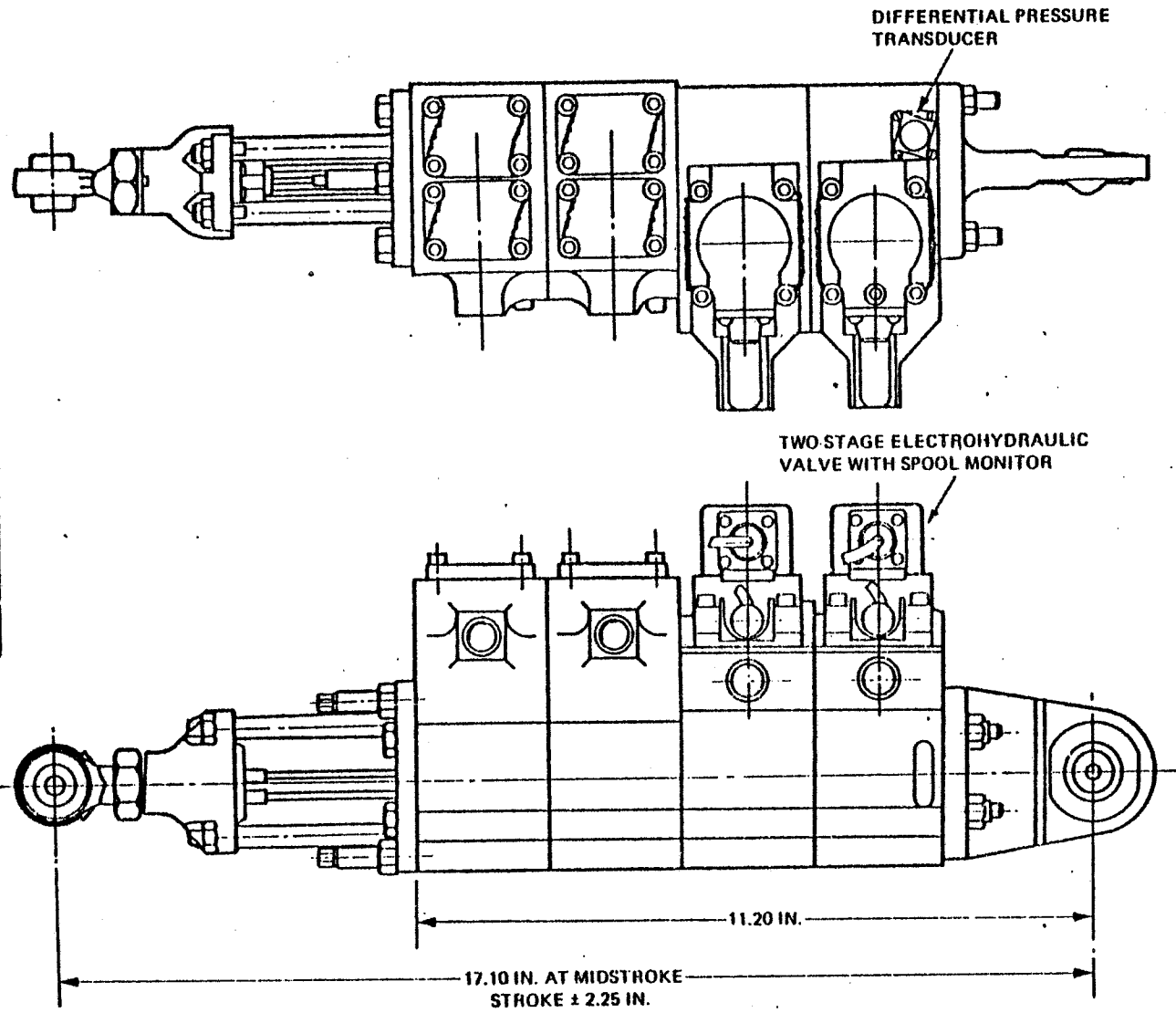
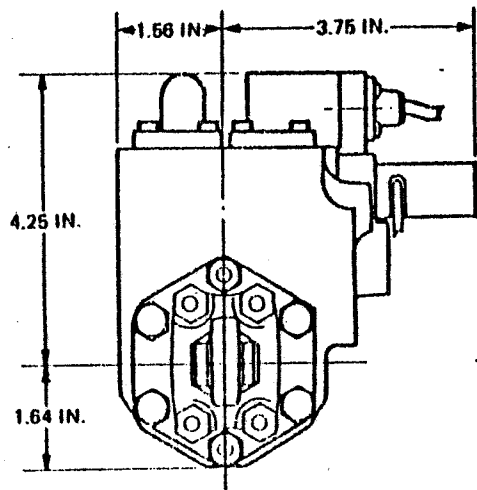


FIGURE B8 DUAL DRIVER ACTUATOR

D210-11569-1

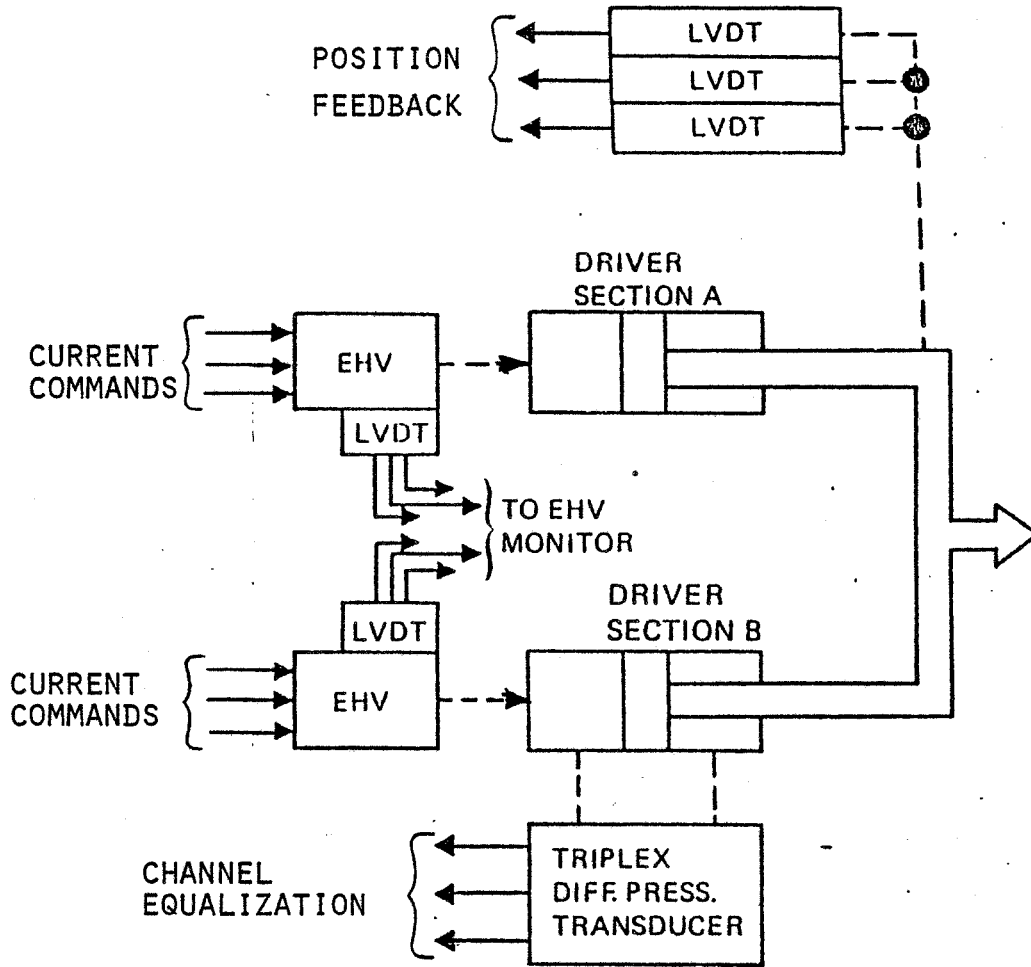


FIGURE B9. DUAL DRIVER ACTUATOR SCHEMATIC

B.5.2.4.4 Humidity - Operation in a warm, highly humid atmosphere such as encountered in tropical areas per MIL-STD-810C.

B.5.2.4.5 Salt Fog - Operation in an atmosphere containing salt laden moisture per MIL-STD-810C.

B.5.2.4.6 Sand and Dust - Operation in a dust (fine sand) laden atmosphere per MIL-STD-810C.

B.5.2.4.7 Rain - Operation in a rain environment per MIL-STD-810C.

B.5.2.4.8 Immersion - Operation after immersion in hydraulic fluid at a temperature of +275° per MIL-C-5503.

B.5.2.4.9 Vibration - Operation during exposure to dynamic vibration stresses represented by those tests of MIL-STD-810C, Method 514.2, Procedure I, Part 1, Equipment Category (A), to include:

- a. Resonance search
- b. Resonance dwell
- c. Cycling

B.5.2.4.10 Mechanical Shock - Operation after exposure to a mechanical shock environment similar to that expected in handling, transportation, and service use per MIL-STD-810C.

B.5.2.5 Reliability - The dual driver actuator shall be capable of meeting reliability requirements as follows.

B.5.2.5.1 The dual driver actuator, excluding fixed and output rod ends, shall exhibit a flight safety reliability of .99999999623, a mission reliability of .99877, and a maintenance malfunction reliability of .978 for a flight of two hours duration. Feasibility demonstration of this requirement shall consist of analytical predictions utilizing the techniques described in this section.

B.5.2.5.2 A single driver actuator includes cylinders, servo-valves, and direct auxiliary hardware required to provide control motion to a single driver actuator position. Specifically excluded are electrical and hydraulic power supplies and control/servo electronics.

B.5.2.5.3 In order to provide a complete data package necessary for proper evaluation, separate models and predictions shall be generated for the following reliability objectives:

- a. For reliability computations, a flight safety loss is defined as a failure which results in loss of a driver actuation function or damage to other aircraft equipment by actuator malfunctions (e.g., actuator on fire but still operating is considered a flight safety loss).
- b. Mission abort reliability (whenever a failure occurs such that a subsequent failure could cause a flight safety loss, a mission abort is required).
- c. Maintenance malfunction reliability (any failure which requires a maintenance action, regardless of functional effect, is a maintenance malfunction).

B.5.2.6 Maintainability - The driver actuator shall be designed for LRU replacement at the flight line. Routine checkout of the DELS shall be conducted using the DELS failure status/BITE panels.

B.5.2.6.1 Interchangeability - Interchangeability per MIL-I-8500 shall exist between all units and replaceable assemblies, subassemblies, and parts for all equipment delivered on this contract. (Not applicable to detail parts of matched assemblies).

B.5.2.6.2 Ground Support Equipment - Routine daily maintenance of the driver actuator shall be accomplished with standard hand tools available in the U.S. Army General Aircraft Mechanic's tool kit. No special tools or support equipment shall be required for work performed at organizational and direct support level maintenance.

B.5.2.6.3 Maintainability Requirements - The following maintainability requirements shall be incorporated:

- a. The driver actuator shall be interchangeable as an LRU (line replaceable unit).
- b. Driver actuator shall be removed for maintenance only "on condition". No scheduled removals shall be required.
- c. Scheduled visual inspection intervals shall be no less than 10 flight hours.
- d. No servicing shall be necessary between inspection periods.



- e. Servoactuator nameplate shall be displayed at a location as defined in envelope drawing.
- f. Driver actuators shall be prerigged; with no calibration requirement following installation.

B.5.3 Rotor Speed Sensor

Rotor speed sensing shall be accomplished by proximity switches located in the transmission gearing. The switch shall provide 40 pulses per gear revolution, which is equivalent to 174.2 pulses per rotor revolution. The pulse characteristics such as amplitude and width and source impedance shall be determined during the detail design phase of the system.

B.5.4 Nacelle Incidence Sensor

The nacelle incidence sensor shall be a synchro excited from the control unit internal A/C supply and providing an output proportional to the sine of the nacelle incidence angle. The control unit output shall be adapted to drive the existing nacelle position display and asymmetry detection system.

B.5.5 Engine N<sub>1</sub> Control Actuator

Provides control of engine power turbine in response to signals from power lever and thrust management portion of the primary flight control system. Use of existing actuator is desired. CH-47C actuator per Boeing Vertol Specification D8-2501 is a candidate.

## B.6.0 Stability and Control Augmentation System (SCAS)

### B.6.1 Description

The SCAS provides short and long term aircraft stabilization about the pitch, roll, and yaw axes and augmentation of cockpit control inputs to enhance aircraft maneuverability. It also provides for gust alleviation inputs to the primary system. SCAS computation shall be accomplished within the Flight Control Processor.

B.6.1.1 Longitudinal SCAS - The longitudinal SCAS transfer block diagram is shown in Figure B10. Pitch rate and pitch attitude are programmed as functions of airspeed to provide longitudinal stability. Cockpit control quickening in the longitudinal axis is also provided.

B.6.1.2 Lateral SCAS - The lateral SCAS transfer block diagram is shown in Figure B11. Roll rate, roll attitude, and sideslip are the parameters sensed and processed to provide lateral stabilization. Cockpit control quickening in the lateral axis is provided at low airspeeds.

B.6.1.3 Directional SCAS - The directional SCAS transfer block diagram is provided in Figure B12. Yaw rate, yaw attitude, and sideslip are the parameters used for stabilization. Turn coordination and roll into yaw cross coupling operation are also prohibited through the processing of roll bank angle and roll rate. Cockpit control quickening in the yaw axis is also provided.

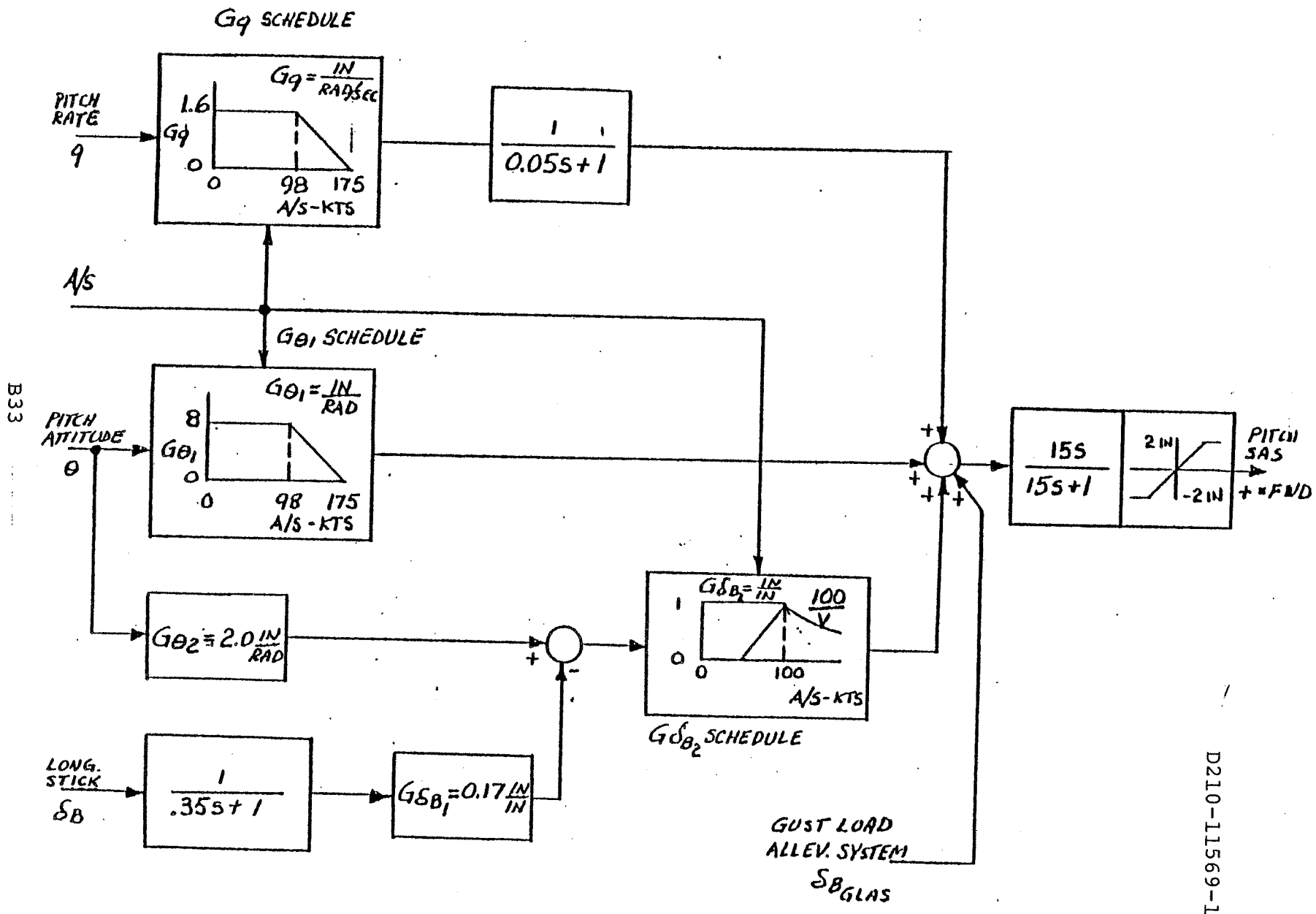
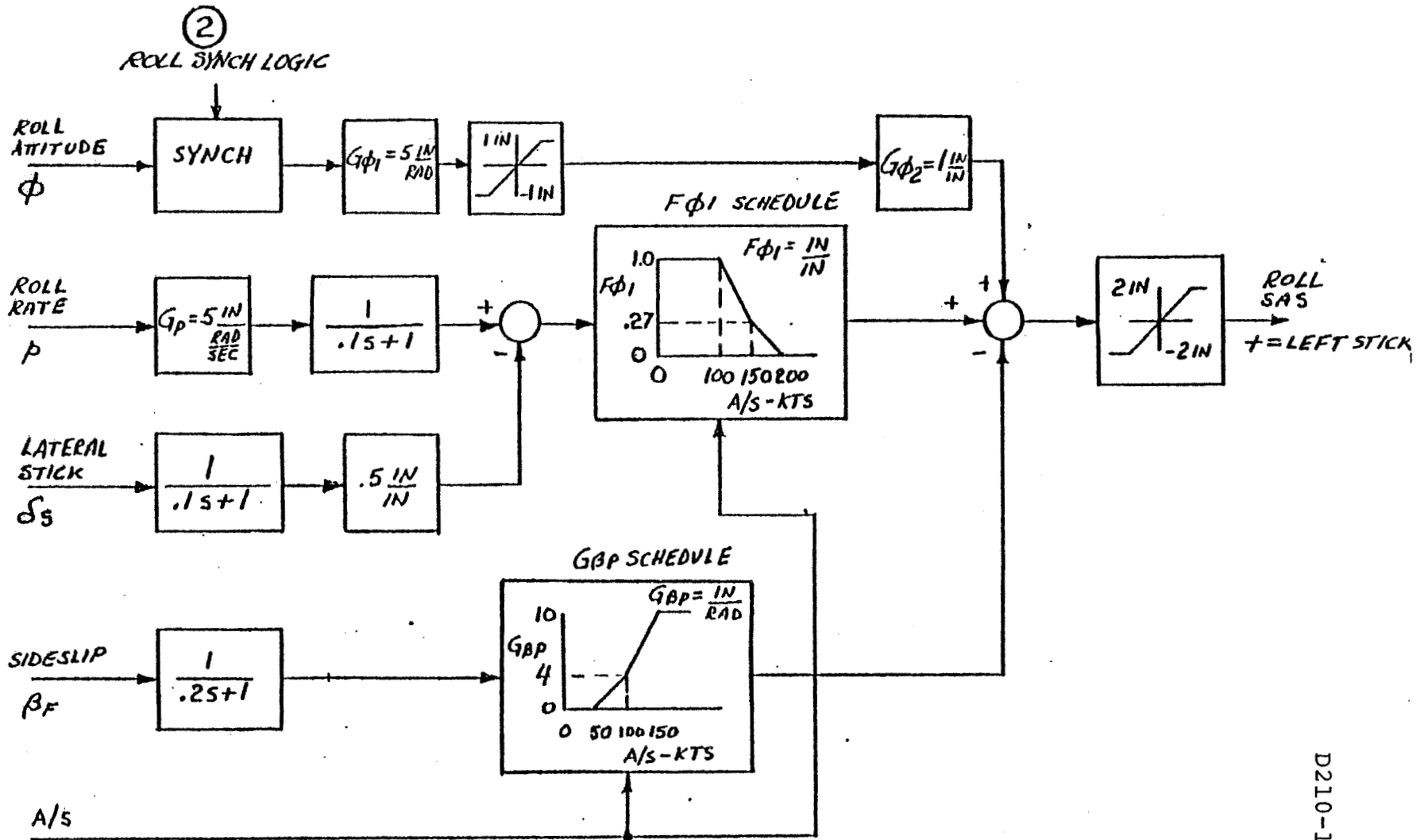


FIGURE B10. LONGITUDINAL SCAS

B34



D210-11569-1

FIGURE B11. LATERAL SCAS

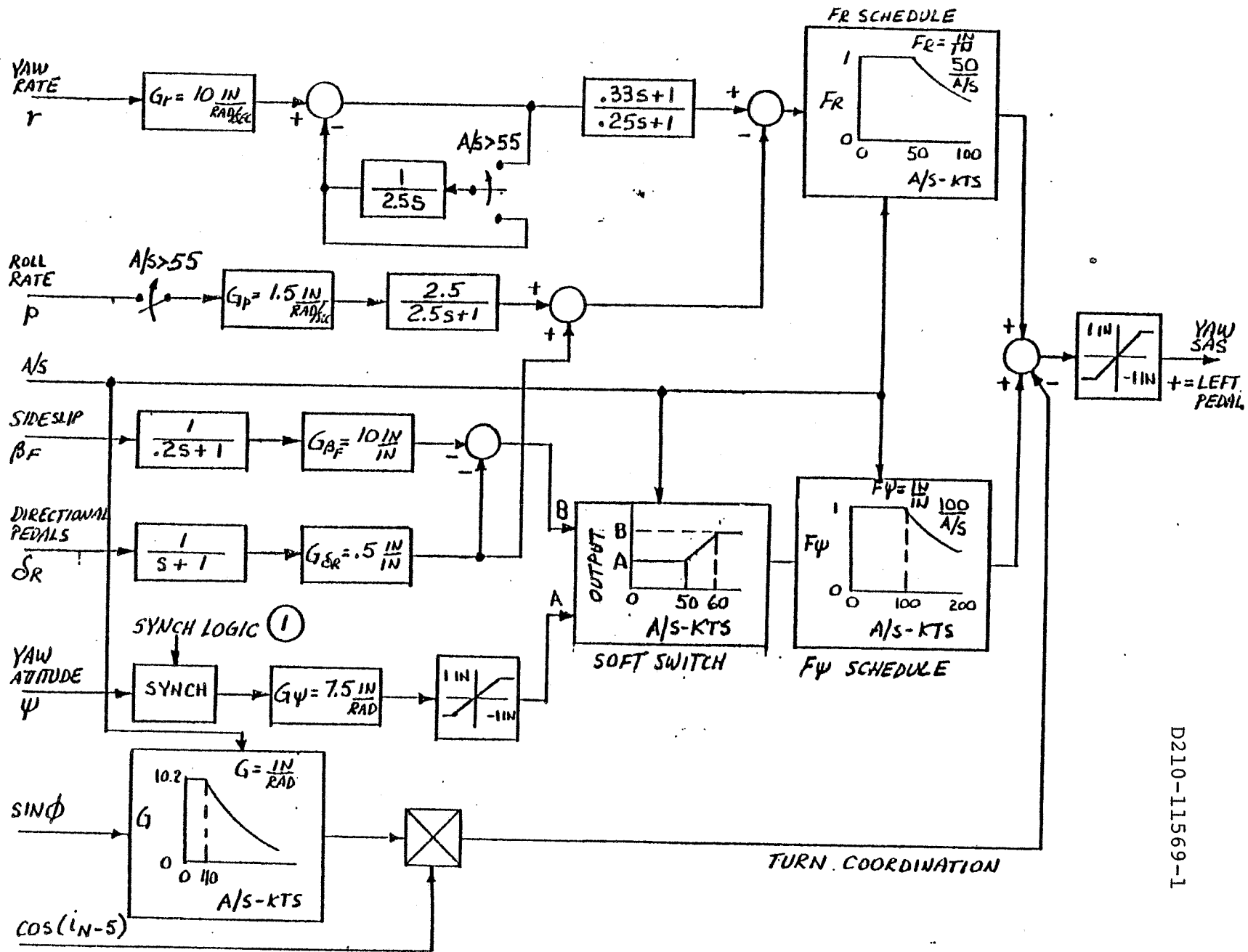


FIGURE B12. DIRECTIONAL SCAS

B.6.1.4 Logic - The logic controlling the lateral and directional SCAS functions is shown in Figure B13.

B.6.1.5 Gust Alleviation - System sensing and transfer functions are being defined. Sensing could be vertical acceleration, pitch acceleration, or angle of attack. Sensor signal to be processed through a filter such as shown in Figure B14 and input to flaps and/or elevator. Assume SCAS unit incorporates three such filters.

#### B.6.2 System Performance

B.6.2.1 System Accuracies - System gain, schedule, and transfer function accuracies shall be met over the range of environments defined in paragraph B.3.4.

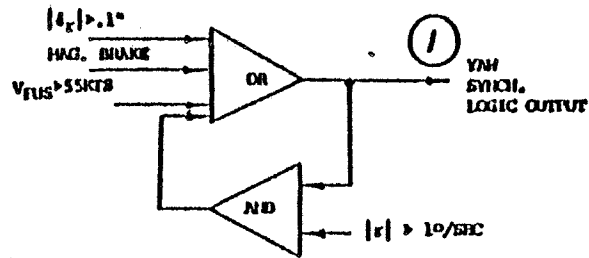
B.6.2.2 Steady State Accuracy - The steady state accuracy of SCAS shall be 5% or better. For a given control input, the accuracy is defined as the percentage between the desired actuator command voltage and the actual command voltage. The above accuracies include the schedule accuracies.

B.6.2.3 Null Accuracy - The total steady state null accuracy associated with the SCAS from sensor inputs to actuator command shall be .5% full scale.

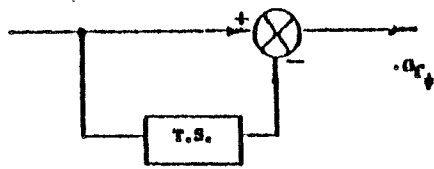
B.6.2.4 Resolution - Resolution is defined as the minimum change in control input required to obtain actuator command change. The resolution (equated to actuator command change) shall not exceed .1% full scale.

B.6.2.5 System Hysteresis - Hysteresis within the SCAS shall not exceed .1% full scale.

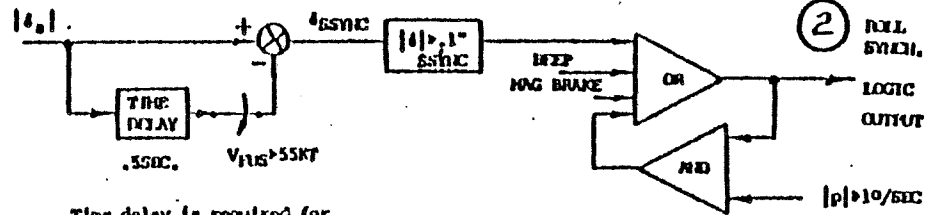
B37



YAW SYNCHRONIZER



SYNC-TRACK  
BTAD - STURE



Time delay is required for hover Lateral flight case.

ROLL SYNCHRONIZER

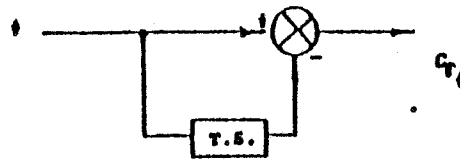
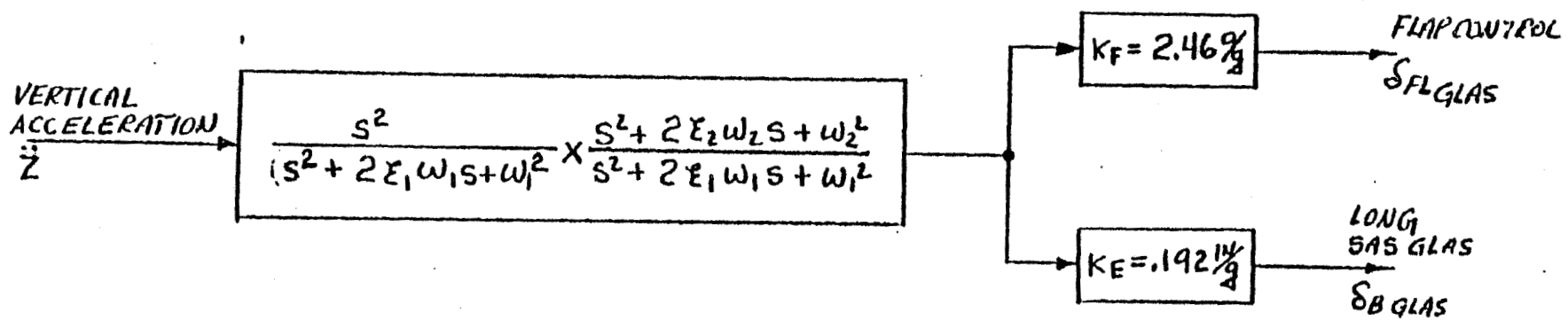


FIGURE B13. LATERAL DIRECTIONAL SCAS - SYNCHRONIZER & LOGIC

D210-11569-1



$$\omega_1 = 0.025 \text{ rad/sec}$$

$$\xi_1 = 0.6$$

$$\omega_2 = 0.5 \text{ rad/sec}$$

$$\xi_2 = 1.4274$$

FIGURE B14. TYPICAL GUST ALLEVIATION CONFIGURATION



B.6.2.6 Frequency Response - The linear range frequency response of each of the transfer paths (sensor input to actuator command) shall be flat to within  $\pm 1$  dB and within  $\pm 10^\circ$  phase shift to 5 radians per second where no filtering is required. Where filtering is required, the frequency response gain shall be within  $\pm 2$  dB and phase shift shall be within  $\pm 10^\circ$  of the theoretical value.

B.6.3 Redundancy

- a. The SCAS shall be at least single fail operative for any failure.
- b. All failures causing loss of one SCAS channel shall be detected and immediately displayed.

B.6.4 Reliability

The overall system reliability of the SCAS shall be .999 for a two-hour flight per SCAS channel. Reliability shall be demonstrated by analytical methods based on known failure rates of components used in the design. The required redundancy level shall be adopted to meet this reliability requirement.

B.7.0 Reference Specifications and Documents

FAR XX Tentative Airworthiness Standards of  
Powered Lift Transport Category Aircraft,  
August 1970.

NASA CR-151950 Preliminary Simulation of an Advanced  
Hingeless Rotor XV-15 Tilt-Rotor Air-  
craft, Boeing Vertol, December 1976.

MIL-HDBK-217A Reliability Stress and Failure Rate Data  
for Electronic Equipment

MIL-E-5400R Electronic Equipment, General Specifi-  
cations for

MIL-STD-810B Environmental Test Methods

MIL-H-5440E Hydraulic Systems Aircraft Types 1 and  
2, Design, Installation, and Data  
Requirements for

MIL-C-5503C Cylinders, Aeronautical, Hydraulics,  
Actuating, General Requirement for.

MIL-H-8775C Hydraulic System Components, Aircraft  
and Missiles, General Specification for.

D8-2501-1 Procurement Specification, Proportional  
N<sub>1</sub> Engine Control System